Thermoreversible associations between multiarm structures based on poly(trilmethylene carbonate) oligomers for materials with potential applications in the biomedical field : structure-properties relationships

Xiang Li

N°d'ordre NNT : 2019LYSES008

THESE de DOCTORAT DE L'UNIVERSITE DE LYON

opérée au sein de
l'Université Jean Monnet

Ecole Doctorale ED SIS 488
Sciences, Ingénierie, Santé

Spécialité de doctorat :
Discipline : CHIMIE ET SCIENCES DES MATERIAUX

Soutenue publiquement le 25 avril 2019, par :
Xiang LI

Thermoreversible associations between multiarm structures based on poly(trimethylene carbonate) oligomers for materials with potential applications in the biomedical field: structure-properties relationships

---

Devant le jury composé de :

BOUTEILLER, Laurent	Directeur de Recherche, Sorbonne Université	Rapporteur
LEONARDI, Frédéric	Maître de Conférences HDR, Université de Pau et des Pays de l'Adour	Rapporteur
WOISEL, Patrice	Professeur, Université Lille1	Examinateur
CHEN, Jianding	Professeur, East China University of Science and Technology	Examinatrice
BECQUART, Frédéric	Maître de Conférences HDR, Université Jean Monnet	Directeur de thèse
MIGNARD, Nathalie	Maître de Conférences HDR, Université Jean Monnet	Co-directrice de thèse
MAJESTE, Jean-Charles	Professeur, Université Jean Monnet	Co-Encadrant de thèse

To my family

Acknowledgments

First and foremost, I would like to express my sincere gratitude and appreciation to my supervisors: Prof. Frédéric BECQUART and Prof. Nathalie MIGNARD, for their patient guidance and consistent encouragement to help me complete this thesis. Their conscientious academic spirit and modest, open-minded personality inspire me both in academic study and daily life.

Besides, I would like to thank my supervisors Prof. Mohamed TAHA who retired in 2016 and Prof. Jianding CHEN in China for their support in my research.

I would like to acknowledge Prof. Jean-Charles MAJESTE for offering much help in the rheological properties analysis.

I am also indebted to all the collaborators for providing supports in experimental measurements, including: Frédéric PROCHAZKA for biodegradability tests, Carlos Fernandez-de-Alba for NMR tests, Guillaume Sudre for WAXS/SAXS tests and Laure FORT for Maldi-Tof tests.

My thanks would also go to all the colleagues and friends in the lab for their help and company during the last three years, especially Camille, Kelly, Nadège, Dara, Carine, Nelmary, Wissam, Xavier, Teddy, Shaobo, Alessandro, Benjamin, Romain and Caroline et al.

I would like to thank the financial support from China Scholarship Council (CSC). This manuscript benefits from the international cooperation between Université Jean Monnet Saint-Etienne (France) and East China University of Science and Technology (China).

Last but not least, thanks to all my family members for their everlasting support, encouragement and love.

Communications

Oral presentation: Xiang Li, Mohamed Taha, Nathalie Mignard, Jianding Chen and Frédéric Becquart, Synthesis and rheological properties of PTMC based hydrogen-bonded supramolecules, **The World Polymer Congress MACRO18**. July 1-5, 2018, Cairns, Australia

Poster: Xiang Li, Mohamed Taha, Jianding Chen, Frédéric Becquart and Nathalie Mignard, Thermal reversible PTMC based networks by Diels-Alder reaction, **Self-assembly of colloidal system**, September 20-22, 2018, Bordeaux, France

Abbreviations

AA	acrylic acid
AP	acrylamidopyridine
BDO	1,4-butanediol
BTMC	3-benzyloxytri-methylene carbonate
CEA	carboxyethylacrylate
DA	Diels-Alder
DAT	2,6-diaminotriazine
DBTL	dibutyltin dilaurate
DBU	1,8-diazabicyclo[5.4.0]-undec-7-ene
DMAP	4-N,N-dimethylaminopyridine
DMTMC	3,3-dimethoxytrimethylene carbonate
FGE	furfuryl glycidyl ether
H_{12}MDI	4,4'-methylenebis(cyclohexyl isocyanate)
HBM	hydrogen-bonding motif
HDI	hexamethylene diisocyanate
K_a	association constant
M_e	critical entanglement molar mass
PBA	poly(n-butyl acrylate)
PBL	polybutyrolactone
PCL	polycaprolactone
PDTC	poly(dimethyl trimethylene carbonate)
PGA	polyglycolide
PHA	polyhydroxyalkanoates
PHS	poly(4-hydroxystyrene)
PIB	polyisobutylenes
PLA	polylactide
PPO	poly(propylene oxide)
PTMC	poly(trimethylene carbonate)
rDA	retro-Diels-Alder
ROP	ring-opening polymerization
SBS	poly(styrene-block-butadiene-block-styrene)
$Sn(oct)_2$	tin(II) 2-ethylhexanoate or stannous octoate

TBD	1,5,7-triazabicyclo[4.4.0]dec-5-ene
THY	thymine
TMC	trimethylene carbonate
UPy	ureidopyrimidinone

Contents

General introduction

During the last several decades, dynamic associations, including noncovalent interactions and dynamic covalent bonds, have attracted tremendous attention in designing new class of materials in polymer chemistry and materials science. Due to the dynamic properties of these associations, they can not only contribute to the formation of network structures to prevent flow and creep, but also endow materials with processability and recyclability. In addition, functional materials can be created with some attractive special properties such as self-healing, shape-memory and self-adhesion.

Under such circumstances, Yiping Ni worked on the subject of "Polyurea−urethane supramolecular thermo-reversible networks" in IMP@UJM from 2007 to 2011, under the international collaboration between University Jean Monnet (UJM) in France and East China University of Science and Technology (ECUST) in China. In this study, new self-complementary hydrogen bonding motifs (HBMs), triuret and tetrauret, were found to be effective in preparing supramolecular networks.

Due to this original and successful study, it was reminded that these HBMs are also fascinating to be applied as stickers in the functionalization of biomaterials, such as poly(trimethylene carbonate) (PTMC), to enhance their properties (mechanical, thermal, etc.) by forming networks and also maintain the possibility to be processed in molten state simultaneously.

Besides, IMP@UJM has focused on the studies of dynamic covalent systems, such as Diels-Alder (DA) reaction, for more than a decade. Thanks to this thermosensitive equilibrated reaction, a variety of reversible materials have been synthesized by using various original and adapted synthetic methods, such as reactive extrusion. Current studies on DA materials are directed towards the understanding of networks structures and corresponding thermal behavior and disruption temperature.

In this case, the IMP@UJM and ECUST research groups decided to collaborate again to prepare thermoreversible networks by dynamic associations which could be further used in the biomedical field. Though triuret and tetrauret HBMs were already proved to be effective in forming transient physical networks, some scientific problems are still unclear, such as the association modes of triuret/tetrauret HBMs (form dimers or complex aggregates), the effect of polymer chains on triuret/tetrauret HBMs associations and the dynamics of triuret/tetrauret

HBMs etc. Thus, this thesis focuses on the synthesis and structure-property relationships study of PTMC-based thermoreversible networks by both triuret/tetrauret HBMs and Diels-Alder reactions.

This thesis is organized into 6 parts.

Chapter 1 aims at drawing the context of this work by three main sections. The first section reviews the ring-opening polymerization of polycarbonates and the corresponding initiation systems: organometallic initiators and metal-free catalysts. The traditional functionalization methods of polycarbonates are also shortly introduced. The second section presents the supramolecular polymers based on hydrogen bonds and their dynamic properties, especially in bulk. Besides, some applications, such as self-healing, shape memory and self-adhesion, are also presented. The third section focuses on the preparation of thermoreversible networks by Diels-Alder reactions, particularly by furan/maleimide coupling.

Chapter 2 presents the synthesis of telechelic PTMC oligomers in bulk by ring-opening polymerization (ROP) with trimethylene carbonate as monomer and 1,4-butanediol (BDO) as initiator. 1,5,7-triazabicyclo[4.4.0]dec-5-ene (TBD) organic catalyst and tin(II) bis(2-ethylhexanoate) ($Sn(Oct)_2$) organometallic initiator are chosen comparatively to study their reaction kinetics and the control over PTMC structures. The effects of TMC/BDO feed ratio, reaction time and alcohol/carbonate exchange reactions on the PTMC structures are studied as well. Through the selection of optimized synthesis conditions, the PTMC structures are preciously controlled.

Chapter 3 describes the preparation of PTMC-based multiarm supramolecular polymers bearing self-complementary triuret and tetrauret HBMs by polycondensation between isocyanate and hydroxyl/amine groups. The association constant (K_a) of triuret and tetrauret HBM in supramolecular structures are measured. The relationships between supramolecular polymers structures (functionality, HBM type and HBM concentration which is adjusted by PTMC chain length) and their thermal properties, dimensional stability, tensile mechanical properties and aerobic biodegradability are studied.

Though the synthesis and macroscopic properties of PTMC-based supramolecular polymers are presented in Chapter 3, their dynamic properties are still unclear. Thus, Chapter 4 aims at the morphology and dynamics study in order to reveal the association and relaxation modes of triuret and tetrauret HBMs in supramolecular polymers. Wide-angle X-ray scattering (WAXS)

and small-angle X-ray scattering (SAXS) are used to verify their morphologies. PTMC oligomers and a multiarm structure without any HBMs are firstly studied by rheology to reveal the relaxations of PTMC chains and hydrogen bonding between urethane bonds. In this case, the dynamics of triuret and tetrauret HBMs are isolated in the supramolecular polymers. The influences of functionality, HBM type and PTMC chain length on the dynamics of supramolecular polymers are studied in detail through the attempt to build master curves by time-temperature principle (TTS). Significantly, this chapter will reveal the effects of functionality, HBM type and PTMC chain length on the triuret and tetrauret association modes and their corresponding dynamics.

Chapter 5 makes an attempt to study the association dynamics of a bifunctional linear PTMC-based supramolecular polymer bearing triuret HBMs. This system is expected to follow a polycondensation model by dimerization between triuret HBMs in short cooling time from molten state. WAXS and SAXS are used to reveal its morphology. Thermal stability of this system at different temperatures will be studied to check if secondary interactions and dynamics have effects on material in time. A snapshot where only dimerization of triuret HBMs occurs will be selected to study its dynamic properties and to calculate K_a and activation energy by applying polycondensation theory. The rheological properties after long time of annealing will also be studied to illustrate the dynamics of triuret HBMs associations at equilibrated state.

Chapter 6 is devoted to the preparation of thermoreversible networks by Diels-Alder reactions. The furan functionalized PTMC (PTMC-F) precursors are synthesized by the polycondensation between hydroxyl and isocyanate groups. The networks are then obtained through the addition of bi-functionalized bismaleimide to PTMC-F precursors. The effects of functionality on the network density, thermal, tensile mechanical and rheological properties are studied.

Chapter 2, Chapter 3, Chapter 4, Chapter 5 and Chapter 6 are written respecting the forms for publication.

Introduction générale

Au cours des dernières décennies, les associations dynamiques, comprenant des interactions non covalentes et des liaisons covalentes dynamiques, ont suscité une forte attention pour concevoir une nouvelle classe de matériaux fondée sur cette chimie. En raison des propriétés dynamiques de ces associations, elles peuvent non seulement contribuer à la formation de structures de réseaux pour limiter ou supprimer les écoulements et le fluage, mais également conférer aux matériaux une aptitude à la mise œuvre par les procédés usuels et au recyclage. De plus, des matériaux fonctionnels peuvent être créés avec des propriétés particulières telles que l'autoréparation, la mémoire de forme ou l'auto-adhésion.

Dans ce contexte, Yiping Ni a travaillé sur le thème des «Réseaux thermo-réversibles supramoléculaires polyurée-uréthane» à IMP@UJM de 2007 à 2011, dans le cadre de la collaboration internationale entre l'Université Jean Monnet (UJM, France) et l' ECUST, Université des Sciences et Technologie de Chine orientale (ECUST, Chine). Dans cette étude, de nouveaux motifs auto-associables par liaison hydrogène (HBM), triuret et tétrauret, se sont révélés efficaces pour la préparation de réseaux supramoléculaires.

Par cette étude originale et prometteuse, ces HBM sont apparus conceptuellement intéressants pour être utilisés comme 'stickers' en vue de fonctionnaliser des biomatériaux, tels que le poly(triméthylène carbonate) (PTMC) afin d'améliorer ses propriétés (mécaniques, thermiques, etc.) en formant des réseaux tridimensionnels dans les conditions d'usage et en conservant parallèlement la possibilité d'être transformé à l'état fondu.

L'IMP@UJM s'est aussi concentré sur l'étude de systèmes covalents dynamiques, tels que la réaction de Diels-Alder (DA), pendant plus d'une décennie. Grâce à cette réaction thermosensible équilibrée, divers matériaux réversibles ont été synthétisés en utilisant diverses méthodes de synthèse originales et adaptées, telles que l'extrusion réactive. Les études en cours sur les matériaux DA visent à comprendre les structures des réseaux et le comportement thermique et la température de perturbation correspondants.

Dans ce cas, les groupes de recherche de l'IMP@UJM et l'ECUST ont décidé de collaborer à nouveau pour préparer des réseaux thermoréversibles par des associations dynamiques qui pourraient être davantage utilisées dans le domaine biomédical. Bien que les HBM triuret et tétrauret se soient déjà révélés efficaces pour la formation de réseaux physiques transitoires,

certains problèmes scientifiques restent en suspens, tels que les modes d'association des HBM triuret/tétrauret (dimères de forme ou agrégats complexes), l'effet des chaînes polymères sur les associations entre triuret/tétrauret et leurs dynamiques rendant complexes leur compréhension. Cette thèse porte donc sur l'étude de la synthèse et des relations structure-propriété des réseaux thermoréversibles à base de PTMC, à la fois par les réactions HBM triuret/tétrauret et par les réactions de Diels-Alder.

Cette thèse est organisée en 6 parties.

Le chapitre 1 vise à dessiner le contexte de ce travail en trois sections bibliographiques principales. La première section examine la polymérisation par ouverture de cycles polycarbonate et les systèmes d'initiation/amorçage correspondants: initiateurs organométalliques et catalyseurs sans métaux. Les méthodes traditionnelles de fonctionnalisation des polycarbonates sont également présentées. La deuxième partie présente les polymères supramoléculaires assemblés par liaisons hydrogène et leurs propriétés dynamiques, notamment en masse. En outre, certaines applications, telles que l'auto-cicatrisation, la mémoire de forme et l'auto-adhésion, sont également présentées. La troisième section est consacrée à la préparation de réseaux thermoréversibles par la réaction de Diels-Alder, en particulier par couplage furanne/maléimide.

Le chapitre 2 présente la synthèse en masse d'oligomères de PTMC téléchéliques par polymérisation par ouverture de cycle (ROP) avec du triméthylène carbonate de comme monomère et du butane-1,4-diol (BDO) comme co-initiateur. Le catalyseur organique 1,5,7-triazabicyclo [4.4.0]déc-5-ène (TBD) et l'initiateur organométallique, le bis(2-éthylhexanoate) d'étain ($Sn(Oct)_2$) ont été choisis et étudiés par leur cinétique de réaction et leur impact sur le contrôle des structures PTMC. Les effets du rapport molaire TMC/BDO, du temps de réaction et des réactions d'échange alcool/carbonate sur les structures de PTMC ont été également étudiées. Grâce au choix des conditions de synthèse optimisées, les structures de PTMC pourront être correctement contrôlées.

Le chapitre 3 décrit la préparation de polymères supramoléculaires à bras multiples à base de PTMC portant des HBM auto-complémentaires triuret et tétrauret par polycondensation entre des groupes isocyanate et hydroxyle/amine. Les constantes d'association (K_a) du triuret et du tétrauret HBM des structures supramoléculaires élaborées seron mesurée. Les relations entre les structures des polymères supramoléculaires (fonctionnalité, type HBM et concentration en

HBM ajustée en fonction de la longueur de la chaîne PTMC) et leurs propriétés thermiques, leur stabilité dimensionnelle, leurs propriétés mécaniques en traction et leur biodégradabilité aérobie seront étudiées.

Bien que la synthèse et les propriétés macroscopiques des polymères supramoléculaires à base de PTMC soient présentées au chapitre 3, leurs propriétés dynamiques ne sont toujours pas claires. Ainsi, le chapitre 4 porte sur l'étude de la morphologie et de la dynamique afin de mettre en évidence les modes d'association et de relaxation des HBM triuret et tétrauret dans les polymères supramoléculaires. La diffusion de rayons X à grand angle (WAXS) et la diffusion de rayons X aux petits angles (SAXS) permettent de vérifier leur morphologie. Les oligomères de PTMC avec une structure multi-bras sans HBM sont d'abord étudiés par rhéologie pour révéler les relaxations des chaînes de PTMC et des liaisons hydrogène entre les liaisons uréthane. Dans ce cas, la dynamique des HBM triuret et tétrauret est isolée des polymères supramoléculaires. Les influences de la fonctionnalité, du type d'HBM et de la longueur des chaînes PTMC sur la dynamique des structures supramoléculaires sont étudiées en détail par des essais de réalisation de courbes maîtresses fondées sur le principe temps-température (TTS). Ce chapitre révèle les effets de la fonctionnalité, du type HBM et de la longueur de la chaîne PTMC sur les modes d'association triuret et tétraure et leur dynamique correspondante.

Le chapitre 5 tente d'étudier la dynamique d'association d'un HBM triuret HBM à base de polymère supramoléculaire linéaire à base de PTMC. Ce système devrait suivre un modèle de polycondensation par dimérisation des HBM triuret après un court temps de refroidissement à partir de l'état fondu. WAXS et SAXS sont utilisés pour révéler les morphologies. La stabilité thermique de ce système à différentes températures sera étudiée pour vérifier si les interactions et dynamiques secondaires ont des effets sur le matériau dans le temps. Un instantané où seule la dimérisation des HBM triuret sera sélectionnée sera étudié afin d'en étudier les propriétés dynamiques et de calculer K_a et l'énergie d'activation en appliquant la théorie de la polycondensation. Les propriétés rhéologiques après un long recuit seront également étudiées pour illustrer la dynamique des associations de triuret HBM à l'état équilibré.

Le chapitre 6 est consacré à la préparation de réseaux thermoréversibles par réactions de Diels-Alder. Les précurseurs de PTMC fonctionnalisés au furanne (PTMC-F) sont synthétisés par la polycondensation entre des groupes hydroxyle et isocyanate. Les réseaux sont ensuite obtenus par addition de bismaléimide bi-fonctionnalisé à des précurseurs de PTMC-F. Les effets de la

fonctionnalité sur la densité du réseau, les propriétés thermiques, mécaniques de traction et rhéologiques sont étudiés.

Les chapitres 2, 3, 4, 5 et 6 sont rédigés dans le respect des formulaires de publication.

Chapter 1. Bibliography

Introduction

In the last several decades, the biodegradable (hydrolytically and enzymatically) and biocompatible materials which have extensive applications in the medical and related domains, such as tissue engineering[1,2], drug delivery[3,4] and regenerative medicine[5], have gained more and more attention[6]. Though the natural occurring proteins[7,8], polysaccharides[9] and polyhydroxyalkanoates (PHA)[10] have been used as biomaterials, the synthesis of novel biomaterials still have unique advantages because of their non-immunogenic responses, easy purification, homogeneity and good processability[11].

Nowadays, aliphatic polyesters and polycarbonates are the most broadly used biomaterials due to their synthetic versatility and various properties[12]. These aliphatic polyesters and polycarbonates include polyglycolide (PGA), polylactide (PLA)[13-15], polycaprolactone (PCL)[16,17], polybutyrolactone (PBL)[18], poly(trimethylene carbonate) (PTMC)[19] and poly(dimethyl trimethylene carbonate) (PDTC). All these biomaterials have their own merits and disadvantages which have been described in several reviews[20,21]. For example, the degradation of aliphatic polyesters usually generates the accumulation of acidic products, leading to the rapid loss of structural integrity and then mechanical stability along with the possibility to cause inflammatory responses[12]. Advantageously, aliphatic polycarbonates have a unique surface erosion degradation mechanism, avoiding the accumulation of byproducts and inducing the maintenance of mechanical properties during a long period of time. Besides, unlike polyesters, aliphatic polycarbonates generate no acidic microenvironment upon degradation, preventing potential inflammatory responses. Due to these merits, aliphatic polycarbonates are extremely suitable to be applied in *vivo* applications[12,22]. However, the weak mechanical strength of polycarbonates usually discourages the further applications in the medical field, bringing about the necessity of functionalization. The traditional functionalization methods include copolymerization, crosslinking, end-functionalization and incorporation of functional side chains[19]. Nevertheless, the incorporation of thermoreversible associations is hardly seen in the literature.

1. Ring-opening polymerization (ROP) and functionalization of polycarbonates

1.1 Ring-opening polymerization (ROP) of polycarbonates

The synthesis of aliphatic polyesters and polycarbonates includes various of methods, such as ring-opening polymerization (ROP) of cyclic monomers, self-condensation of hydroxyacids (AB monomer), condensation between diacids/diacid chlorides and diols (A + B), transesterification, dehydrogenation polymerization of diols and copolymerization of carbon dioxide with epoxide[12,23]. Among all these methods, the ROP of cyclic monomers is the most widely used one because of its mild reaction conditions and the excellent capability to control the molecular weight and keep low dispersity at the same time[24]. In particular, thanks to its mild reaction conditions and versatility, many thermosensitive biomaterials can be potentially synthesized easily[23]. As seen in Figure 1.1, the commonly used cyclic monomers include cyclic diesters, cyclic lactones, carbonates and O-carboxyanhydrides (OCA) as well as their derivatives.

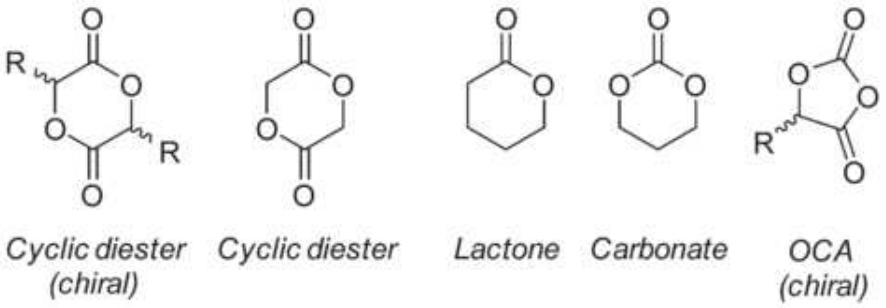

Figure 1.1 Cyclic monomers for the synthesis of polyesters and polycarbonates by ROP[12].

In the ROP of aliphatic polyesters and polycarbonates, alcohols are usually used as co-initiators. Depending on the structure of these co-initiators, the structures of polymers can be easily tailored by the adjustment of alcohol functionality. For example, through the use of mono-alcohol or diol, linear[25,26] polymer chains will be obtained. Star-shaped[25,27], combed or branched structures[28,29] can be synthesized with multi-ols as co-initiators. If polyvinyl alcohol[30] and polysaccharides[29] are used, highly hydroxylated polymers or oligomers can also potentially be obtained.

1.2 Initiation systems of ROP

Numerous researchers have worked extensively to find good initiation systems of ROP which can not only control the polymer structures precisely but also possess fast kinetics. The commonly used catalysts include organometallic initiators, enzymes and metal-free catalysts[23]. However, owing to the attention spotted on biomedical and environmental concerns, the research of new green catalysts has been focused in recent years.

1.2.1 Organometallic initiators

Organometallic initiators have been used in the ROP of lactone and lactide for decades[31-33], such as tin(II) alkoxide[34-36], aluminum alkoxides[37,38], zinc catalysts[39], calcium alkoxide[40,41], yttrium alkoxides[38] and lanthanum isopropoxide[42] (Figure 1.2). Among them, tin(II) 2-ethylhexanoate or stannous octoate ($Sn(oct)_2$) catalyst is undoubtedly the most widely commercially used one with high activity in bulk at 140-180 °C[43].

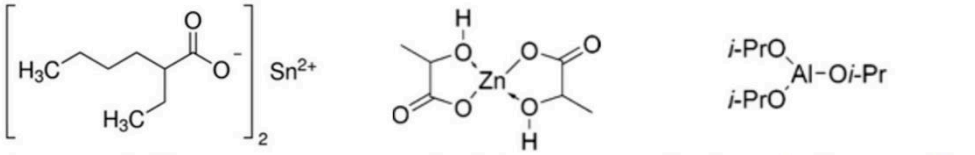

tin(II) 2-ethylhexanoate, $Sn(oct)_2$ | zinc(II) lactate, $Zn(Lact)_2$ | aluminum(III) isopropoxide, $Al(Oi\text{-}Pr)_3$

Figure 1.2 Structure of several organometallic initiators.

For metal-catalyzed ROP, the reaction happens through a coordination-insertion mechanism[34,36,44,45], which occurs via coordination of the monomer to the metal and then insertion into metal-alkoxides. This mechanism is featured by the fact that a covalent bond is shared by the charged propagating species (alkoxides) and their counterions[45].

For example, when $Sn(oct)_2$ is used as initiator[36], the exchange reaction between $Sn(oct)_2$ and alcohol leads to the formation of tin alkoxide firstly (Eq.(1.1)). Then, the active tin alkoxide can react with one monomer to obtain the first actively propagating chain end which contains both the initiating alcohol fragment and the active propagating center (Eq.(1.2)).

$$RC(O)OSnO(O)CR + R'OH \longrightarrow RC(O)OSnOR' + HO(O)CR \qquad \text{Eq.(1.1)}$$

$$RC(O)OSnOR' + M \longrightarrow RC(O)OSn-m-OR' \qquad \text{Eq.(1.2)}$$

where *R* is $C_4H_9(C_2H_5)CH$ and *R'* is the alkyl or H group. *M* and *m* are the cyclic monomer and the repeating unit of *M* respectively.

The first actively propagating chain end can lead to the chain propagation with monomers (Eq.(1.3)) or intermolecular exchange of the stannous alkoxide moiety (Eq.(1.4)).

$$RC(O)OSn-m-OR'+(n-1)M \longrightarrow RC(O)OSn-(m)_n-OR' \qquad \text{Eq.(1.3)}$$

$$RC(O)OSn-m-OR'+R'OH \longrightarrow HO-m-OR'+RC(O)OSnOR' \qquad \text{Eq.(1.4)}$$

This competing between chain propagation and intermolecular exchange between stannous alkoxide and protons results in a dynamic equilibrium between the activated and inactivated chains.

During the polymerization, a similar reaction can also happen to produce the dormant polymer chain:

$$RC(O)OSn-(m)_n-OR'+RC(O)OH \longrightarrow HO-(m)_n-OR'+RC(O)OSnO(O)CR \qquad \text{Eq.(1.5)}$$

where *HO-(m)$_n$-OR'* is the dormant chain.

Furthermore, Storey et al.[34] revealed that with stannous octoate as initiator, the induction of polymerization results from the formation of more stable and less reactive stannous alkoxides between stannous octoate and alcohol, other than stannous alkoxides derived from polymer chains. In this case, if the molar number of stannous octoate is higher than that of alcohol initiators, all the alcohol molecules will be consumed to start the chain propagation (intermediate formed between one monomer and one co-initiator) before chain propagation starts at the normal rate.

Though organometallic initiators are used widely for the ROP of lactides and lactones, the difficulties to remove initiator rests and their transition metals are major issues because of the potential toxicity of some elements (such as tin) and evermore severe rules prohibiting their use. Besides, side effects such as decarboxylation and back-biting reactions, which may cause the discrepancy of experimental and theoretical molecular weights are also inevitable[23].

1.2.2 Metal-free catalysts

In recent years, the nontoxic metal-free catalysts have developed rapidly with their successful application in ROP of lactides and lactones, overcoming the disadvantages of metal catalysts by avoiding the residual of metal in final products. These metal-free catalysts[45] include enzymes[46], Lewis and Brønsted acids[47,48], Brønsted and Lewis bases[49,50] as shown in Figure 1.3.

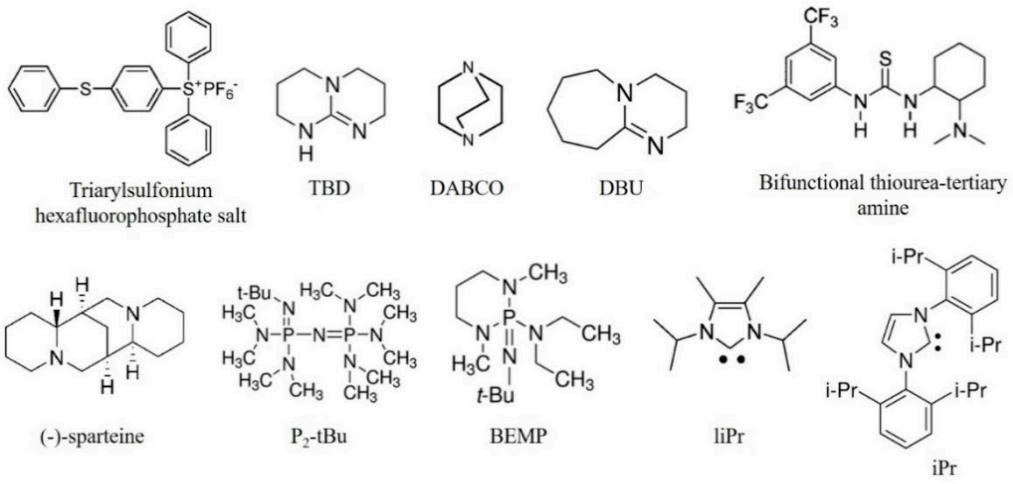

Figure 1.3 Structures of metal-free catalysts.

Brønsted bases guanidines, such as 1,5,7-triazabicyclo[4.4.0]dec-5-ene (TBD)[18,51], are the most effective and efficient among metal-free catalysts, which can also avoid some side effects such as decarboxylation[23]. For example, Helou et al.[50] compared several metal-free catalysts, including TBD, 4-N,N-dimethylaminopyridine (DMAP) and 2-tert-butylimino-2-diethyl-amino-1,3-dimethylperhydro-1,3,2diazaphosphorine (BEMP) in the ROP of six-membered cyclic carbonates (trimethylene carbonate (TMC), 3,3-dimethoxytrimethylene carbonate (DMTMC) and 3-benzyloxytri-methylene carbonate (BTMC)) under mild operation conditions (60-150 °C) in bulk, revealing that TBD exhibited the highest reactivity. Guillaume et al.[18] also compared three catalysts TBD, amidine (1,8-diazabicyclo[5.4.0]-undec-7-ene, DBU), and phosphazene BEMP in the reactivity and structure control of β-butyrolactone ROP. It was proved that TBD leads to good agreement between the theoretical and practical molar masses along with narrower molar-mass-dispersity.

In the TBD-catalyzed ROP, two mechanisms have already been proposed, namely a nucleophilic acylation mechanism and a hydrogen-bonded mechanism. In the acylation mechanism[52], nucleophilic attack of the TBD imine nitrogen at the carbonyl carbon will lead

to the formation of an acyl-TBD intermediate. The adjacent protonated nitrogen in this intermediate is suited for proton transfer to alkoxide to generate TBD amide as shown in Figure 1.4. Waymouth et al.[51] revealed that the high basicity and nucleophilicity of TBD as well as the high reactivity of the acyl-TBD intermediate account for the high reactivity of TBD.

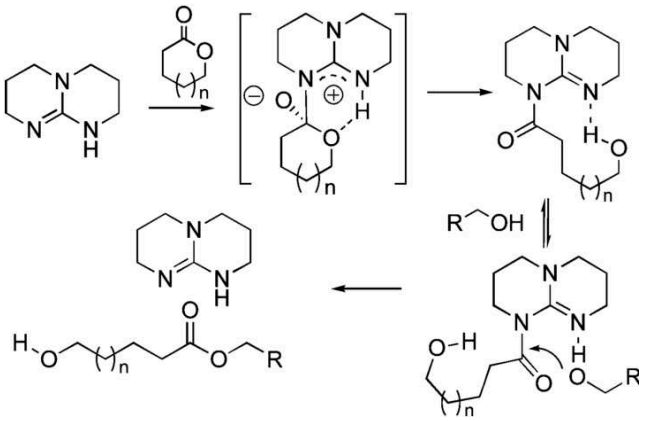

Figure 1.4 The nucleophilic acylation mechanism of TBD[52].

However, by computational chemistry and experimental observations, Chuma et al.[53] found that the hydrogen-bonded mechanism has a lower barrier transesterification reactions, indicating its preference over the acetyl transfer pathway. In this mechanism[53,54] (Figure 1.5), the alcohol firstly attacks the carbonyl group to form an intermediate. The followed rearrangement leads to the hydrogen bonding between TBD intermediate and the oxygen adjacent to carbonyl group, as well as the carbonyl oxygen. This rearranged intermediate structure would facilitate the ring opening.

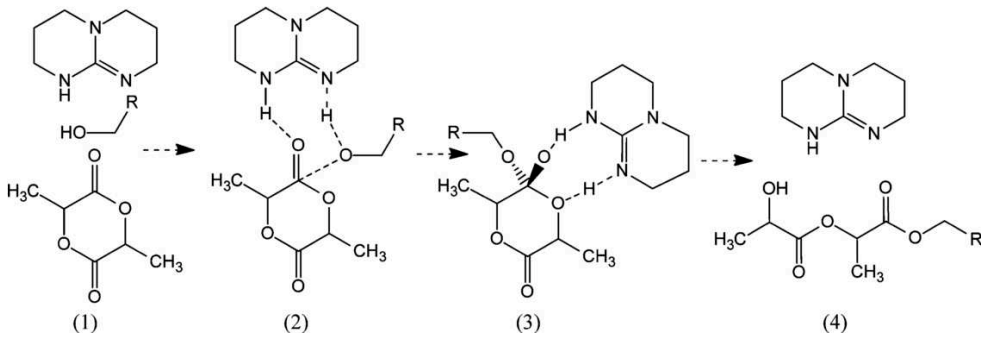

Figure 1.5 The hydrogen-bonded mechanism of TBD[53,54].

1.3 Functionalization of polycarbonates

Though polycarbonates are widely applicable, the functionality of these materials is often required in advanced biomedical applications[55]. As shown widely in the literature, the traditional functionalization methods, such as copolymerization[56], crosslinking[57-59], incorporating functional side chains[60,61] and end functionalization[62], can indeed modify their mechanical properties and even control the biodegradability or extend chemical/biological properties[19,63].

For example, Zhang et al.[64] synthesized Y-shaped (AB2-type) poly(ethylene glycol)-poly(trimethylene carbonate) (PTMC) copolymers by ROP. It was found that these copolymers are able to self-assemble into micelles in aqueous medium, with controlled drug release properties.

Yang et al.[65] synthesized PTMC-based networks through the ROP of trimethylene carbonate and ε-caprolactone with 2,20-bis(trimethylene carbonate-5-yl)-butylether (BTB) as crosslinking agent (Figure 1.6). It was found that the obtained networks have high decomposition temperature and good mechanical properties. Besides, the swelling degree of networks can be easily tuned by the change of crosslinking agent BTB or ε-caprolactone content. For example, increasing the BTB feed percentage can lead to the decrease of swelling degree. This feature endows the networks with great potentiality to be applied in drug delivery.

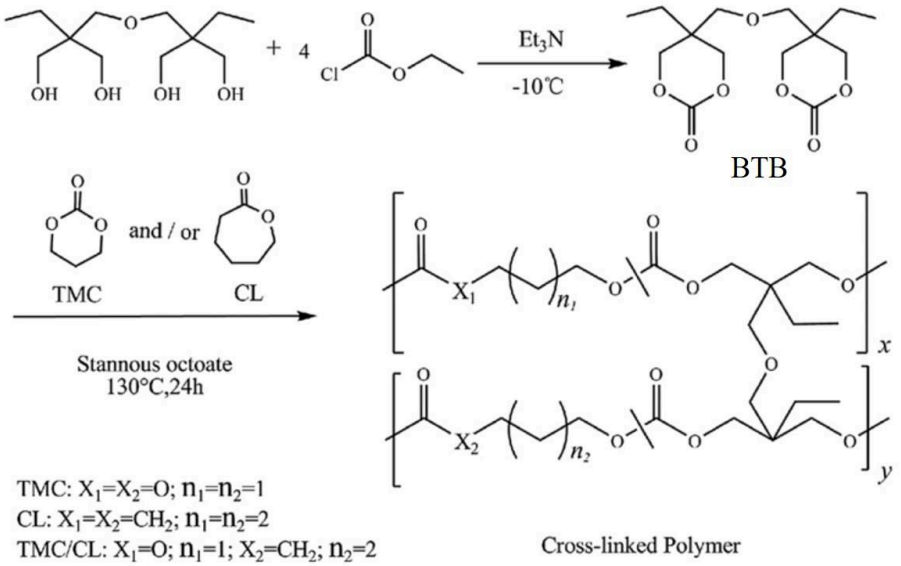

Figure 1.6 The synthesis of PTMC-based networks by ROP.

Venkataraman et al.[66] used poly(ethylene glycol) as macro-initiators to initiate fluorene-functionalize cyclic carbonate monomer to obtain amphiphilic diblock copolymers. These copolymers are able to self-assembled to form special nanostructures such as tapes, elongated micelles and spherical micelles. In addition, the existences of fluorene moieties endow the copolymer with the capability for encapsulation and release of active ingredients.

In the recent years, however, the introduction of reversible links, namely noncovalent interactions[67] and covalent bonds[68], gain more and more attention due to not only the ability to enhance mechanical properties but also the potentiality to introduce some special properties[69,70].

1.4 Conclusions

Polycarbonates have broad applications in the medical and related domains. Their syntheses are usually fulfilled by the ring-opening polymerization of corresponding cyclic monomers. Organometallic initiators and metal-free catalysts are usually used to initiate the ROP of cyclic monomers. However, the difficulties to remove metal rests which are potentially toxic in organometallic initiators and the side effects make the demand to develop green catalysts. Among all the metal-free catalysts, a guanidine TBD is the most effective and efficient one. The traditional functionalization methods of polycarbonates are copolymerization, crosslinking, incorporating functional side chains and end functionalization. Nowadays, incorporating noncovalent interactions and reversible covalent bonds to functionalize polycarbonates has attracted more and more attention.

2. Supramolecular polymers by hydrogen bonds

2.1 Supramolecular chemistry

The concept of "supramolecular chemistry" was firstly founded by Jean-Marie Lehn[71], Donald J. Cram[72] and Charles J. Pedersen[73] who received the Nobel Prize in Chemistry in 1987 for their discovery. Since then, supramolecular chemistry develops rapidly and expands into a significant, broad and active research field now[74,75]. As described by Jean-Marie Lehn et al.[71], "Supramolecular chemistry is the chemistry of the intermolecular bond, covering the structures and functions of the entities formed by association of two or more chemical species". According to this concept, many noncovalent interactions can be accounted[67], including hydrogen bonds[76,77], ionic bonds[78], halogen bonds[79,80], metal coordination[81,82], host–guest

interactions[83-87] and π-π stacking[88,89]. Compared to covalent bonds, the binding energies of these noncovalent bonds[90] are relatively low as shown in Figure 2.1.

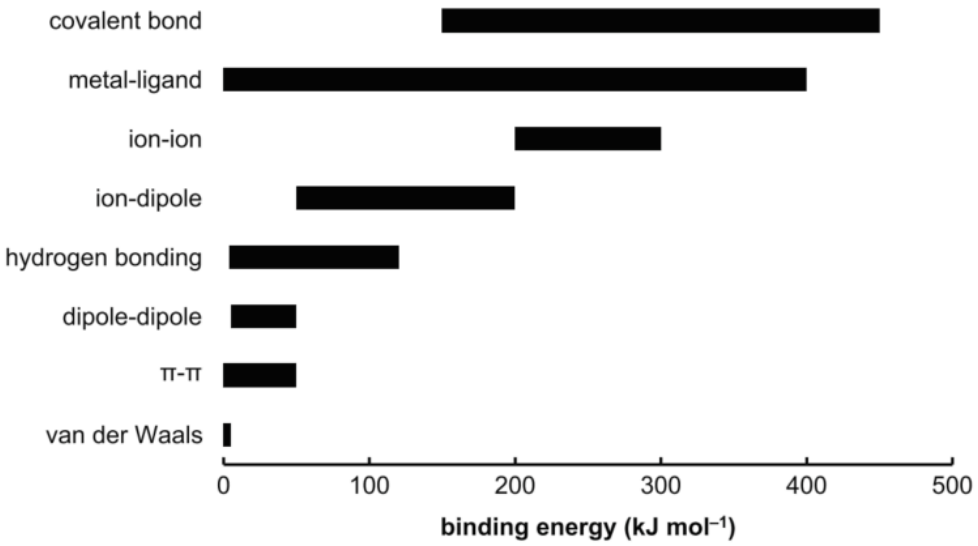

Figure 2.1 The most important noncovalent interactions and their typical range of binding strength, in comparison with covalent bonds[90].

2.2 Hydrogen bonding

Among all the supramolecular interactions, though hydrogen-bonding interaction is not the strongest one as shown previously, its strong directionality and versatility make it the most widely focused one in the supramolecular chemistry field[91,92].

2.2.1 Single hydrogen bond

A single hydrogen bond is formed between a hydrogen atom of H–A (hydrogen donor) where A is electronegative and an electronegative atom B (hydrogen acceptor) which possesses a lone pair of electrons or polarizable π electrons.

Basically, the strength of one single hydrogen bond depends on the nature of hydrogen donor and acceptor. Different hydrogen bonds possess different lengths, strengths and geometries as shown in Table 2.1, varying from strong to weak. The hydrogen bond energies cover more than two orders of magnitude, from 4 to 120 kJ.mol^{-1}[93].

Table 2.1 Properties of hydrogen bonds[93].

	Strong	Moderate	Weak
A–H···B	Partially covalent	Mostly electrostatic	Electrostatic
Energy	60–120 kJ mol^{-1}	16–60 kJ mol^{-1}	<12 kJ mol^{-1}
Lengths (Å)	A–H ~ H···B	A–H < H···B	A–H ≪ H···B
H···B	1.2–1.5	1.5–2.2	2.2–3.2
A···B	2.2–2.5	2.5–3.2	3.2–4.0
Angles (°)	175–180	130–180	90–150
Examples	Strong acids/bases; proton sponge; HF complexes	Acids; alcohols; biological molecules	Minor components of bifurcated bonds; C–H ···O, O–H ··· π

2.2.2 Multiple hydrogen-bonding arrays

Due to the limit of single hydrogen bond, multiple hydrogen-bonding arrays are then created to form stronger interactions and also improve their directionality. However, the energies of hydrogen bonds are not additive because of σ-bond cooperativity, π-bond cooperativity and also anti-cooperativity[94]. To incorporate both synergy and cooperativity[95], the structures of multiple hydrogen-bonding arrays must be considered discreetly because the intrinsic structures indeed have striking effect on their strength. Besides the number of hydrogen bonds, the secondary electrostatic interactions, preorganization of the recognition unit and the competing tautomers are also not to be neglected for deciding the strength of multiple hydrogen-bonding motif[96].

2.2.2.1 Effect of secondary electrostatic interactions

Jorgenson et al.[97,98] revealed the importance of intrinsic structures on the strength of hydrogen-bonding arrays by studying hydrogen bonded complexes of nucleotide bases. In a multiple hydrogen-bonding array, there are positive charged hydrogen bond donors (D) and negative charged hydrogen bond acceptors (A). Based on the order of donors and acceptors, plenty of modules[99,100] have already been studied by researchers in the 1990s for hetero-complementary arrays, including DAD-ADA, DDA-AAD or DDD-AAA for triple and DAAD-ADDA or AADDAA-DDAADD for quadruple hydrogen-bonding arrays. As to self-complementary modules, ADAD and DDAA modules are also studied. Due to the repulsive and attractive secondary interactions between hydrogen bond donors and acceptors, the association constant (K_a)[101], which describes the strength of hydrogen bonds indirectly, can vary in a large scale.

Triple hydrogen-bonding system can be taken as an example. Based on the initial study of triple hydrogen bond complexes by Jorgenson et al.[97], the AAD-DDA complex ($K_a \sim 10^4$ M^{-1}) was found to have higher K_a than ADA-DAD system ($K_a = 1.7\times10^2$ M^{-1}) because of the additional attractive secondary interactions (as shown in Figure 2.2 with red arrows for repulsive electrostatic interactions and black arrows for attractive electrostatic interactions). For AAA-DDD system which has all hydrogen bond donors on one component and all hydrogen bond acceptor on the other, there are only attractive interactions in the complex and the K_a is highest with $>10^5$ M^{-1} in $CDCl_3$[102].

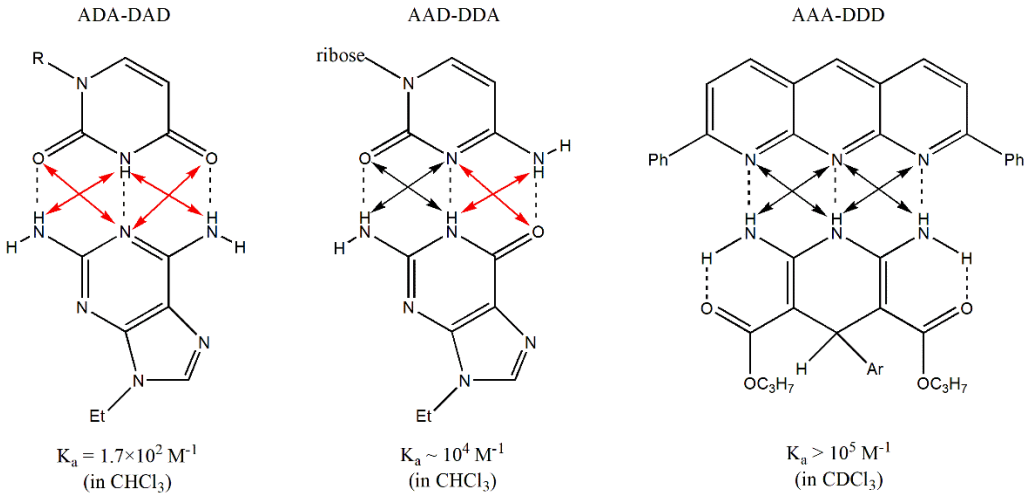

Figure 2.2 Hydrogen-bonding pairs with triple hydrogen bonds (red arrows for repulsive electrostatic interactions and black arrows for attractive electrostatic interactions)[97,102].

Similar effects of the donors and acceptors order are also shown in quadruple hydrogen bonding systems[96]. Beijer et al.[103] synthesized self-complementary quadruple hydrogen-bonding array with ADAD-DADA module (Figure 2.3, A) with the measured K_a of 1.5×10^4 M^{-1} in $CDCl_3$. Besides, the same group[104,105] proved that stronger AADD-DDAA self-complementary quadruple hydrogen-bonding complex (Figure 2.3, B) with the $K_a > 10^6$ M^{-1} (in $CHCl_3$) can be obtained by changing the order of donors and acceptors. Moreover, Zimmerman et al.[106] synthesized highly stable quadruple hydrogen-bonding complexes (Figure 2.3, C) with ADDA-DAAD module with $K_a = 3.0 \times 10^8$ M^{-1}. An AAAA-DDDD quadruple hydrogen-bonding complex synthesized by Blight et al.[107] with hydrogen bond donors and acceptors on two independent components (Figure 2.3, D) shows exceptional stability with $K_a > 10^{12}$ M^{-1}, resulting from all the 6 repulsive electrostatic interactions.

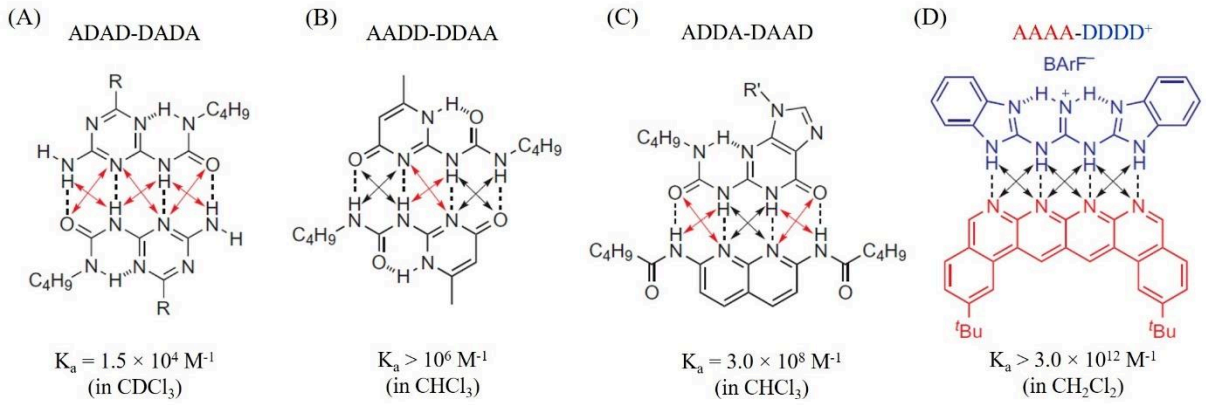

Figure 2.3 Examples of quadruple hydrogen-bonding arrays with (A) ADAD-DADA[103], (B) AADD-DDAA[104,105], (C) ADDA-DAAD[106] and (D) AAAA-DDDD$^+$[107] hydrogen bond complexes (red arrows for repulsive electrostatic interactions and black arrows for attractive electrostatic interactions).

Hamilton et al.[108] synthesized diaminopyridine-substituted isophthalamide (referred to as Hamilton receptor) which can form sextuple hydrogen bonds with barbiturate ($K_a = 1.37 \times 10^6$ M^{-1}, Figure 2.4, A). Zeng et al.[109] synthesized an extremely stable self-complementary sextuple hydrogen bonding complex as well. Though there are six repulsive interactions, the relatively far distance between repulsive interactions make its K_a (> 10^9 M^{-1} in $CHCl_3$, Figure 2.4, B) higher than Hamilton receptor and barbiturate duplex.

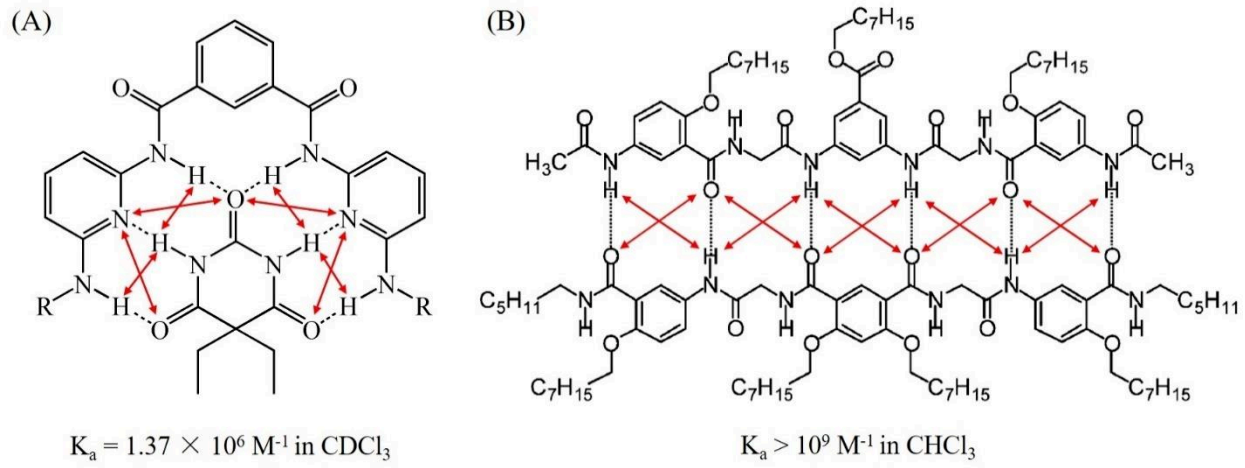

Figure 2.4 Hydrogen-bonding pairs with sextuple hydrogen bonds (red arrows for repulsive electrostatic interactions)[108,109].

2.2.2.2 Effect of steric interactions

Through the study of DAAD and ADDA hydrogen-bonding motifs with different substituents, Lüning et al.[110] found that the discrepancy of different groups can display different association

constants. For example, the replacement of a methyl group (Figure 2.5, A) by a hydrogen atom (Figure 2.5, B) will result in the increase of K_a from 160 to 2000 M^{-1}, accounting for the decreased effect of steric interactions.

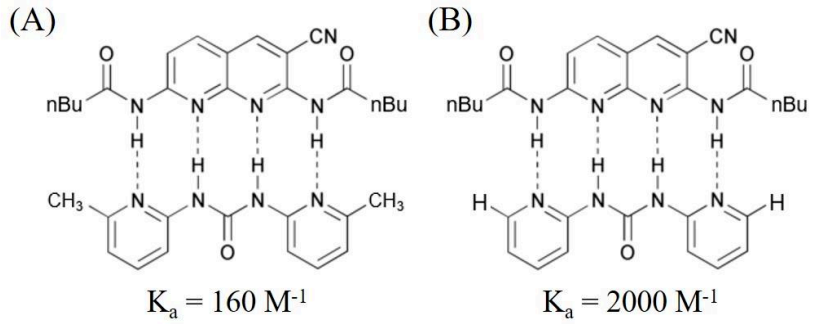

Figure 2.5 Effect of steric interactions on K_a[110].

2.2.2.3 Effect of preorganization

Meijer et al.[103] revealed that the preorganization has significant influence on K_a as well. As shown in Figure 2.6, K_a is 530 M^{-1} for monoacylated diaminotriazine dimers (Figure 2.6, A) but is much stronger (2×10^4 M^{-1}) for the preorganized ureidotriazine (Figure 2.6, B). The increase of hydrogen-bonding strength is due to the intramolecular hydrogen bond formed in the ureidotriazine molecules. Other examples[96] of dimers including amido and ureido pyrimidines are shown in Figure 2.6 (C) and (D). The presence of intramolecular hydrogen bonds in Figure 2.6 (D) increases K_a from 170 M^{-1} to higher than 2×10^5 M^{-1}.

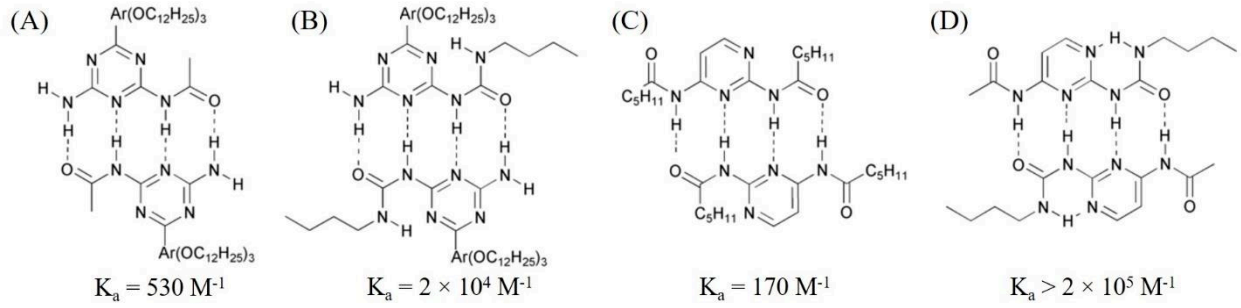

Figure 2.6 Effect of preorganization on K_a[96,103].

Apart from the effect of secondary electrostatic interactions, steric interactions and reorganization discussed above, the competing tautomers[96,111], which are unfavorable for hydrogen bonds dimerization, were also found to have great influence on the strength of hydrogen-bonding motifs.

2.3 Hydrogen-bonded supramolecular polymers and their dynamic properties

Introducing reversible noncovalent interactions into oligomers/polymers to construct supramolecular polymers can bring new opportunities in material science. Because these supramolecular structures have not only traditional polymeric characteristics but also some fascinating new properties which cannot be realized by classical polymers, contributing to the enrichment of functional materials fields[112]. The most important characters of supramolecular polymers lie in the tunability of their microstructures and then the characteristic relaxations, which are dependent on many parameters, such as temperature, intrinsic structures of hydrogen-bonding motifs and polymer chain architectures[113]. According to the study of Craig and coworkers[114,115], it was revealed that it is the dynamics of molecular links, other than the cross-linking thermodynamics, that has a crucial impact on the dynamic properties of the supramolecular networks. This phenomenon can be summarized as "strong means slow".

2.3.1 Effects of supramolecular bond lifetime and chain relaxations on supramolecular polymers dynamic properties

Supramolecular bond lifetime (τ_b) is considered as a crucial characteristic to describe the dynamic nature of supramolecular interactions[116,117]. As presented by Aide et al.[118], when the τ_b is shorter than 1 μs, no robust assembly can be generated between noncovalent interactions to form more sophisticated structures. However, if the τ_b is too long, the supramolecular polymers will lose the dynamic behaviors. Only within the τ_b range from 1 μs to 1 min, the supramolecular polymers can behave interesting tunable dynamic properties, such as adaptability, responsiveness and self-healing. Then, for certain supramolecular polymer, its dynamics are usually governed by at least two timescales: (i) the timescale of classic polymer chains and (ii) the timescale of supramolecular interactions which associate each other to form specific supramolecular architectures[119,120]. Depending on the relative values of supramolecular bond lifetime and polymer chains relaxation time, the properties of supramolecular polymers also vary. For example, when τ_b is much higher than polymer chains relaxation time, supramolecular polymers usually behave like conventional elastomers. On the contrary, only a minor retardation of terminal relaxation can be observed with τ_b much lower than polymer chains relaxation time[113].

Lots of efforts have been made to build the relation between supramolecular timescales and macroscopic properties of materials. For example, Krutyeva et al.[121] revealed that the short

lifetime between thymine and diaminotriazine hydrogen-bonding associations can make the telechelically modified linear poly(ethylene glycol) behave simple Rouse dynamics, though its molecular weight is much larger than the entanglement mass M_e. Lewis et al.[122] synthesized poly(n-butyl acrylate) (PBA) supramolecular polymers with different hydrogen-bonding side groups (Figure 2.7, A), namely acrylamidopyridine (AP), acrylic acid (AA), carboxyethylacrylate (CEA) and ureidopyrimidinone acrylate (UPy) with different number of hydrogen bonds. For polymers containing weaker hydrogen-bonding side groups (AA, AP, CEA), their Rouse-like behavior indicates the characteristics of unentangled melts (Figure 2.7, B), accounting for the fast hydrogen bond exchange compared to experimental timescale and the dominant role of free volume effects. As to strong UPy system, the observation of a plateau region at intermediate frequencies shows the behavior of viscoelastic solid and indicates the network structures, resulting from the long lifetime of UPy dimers.

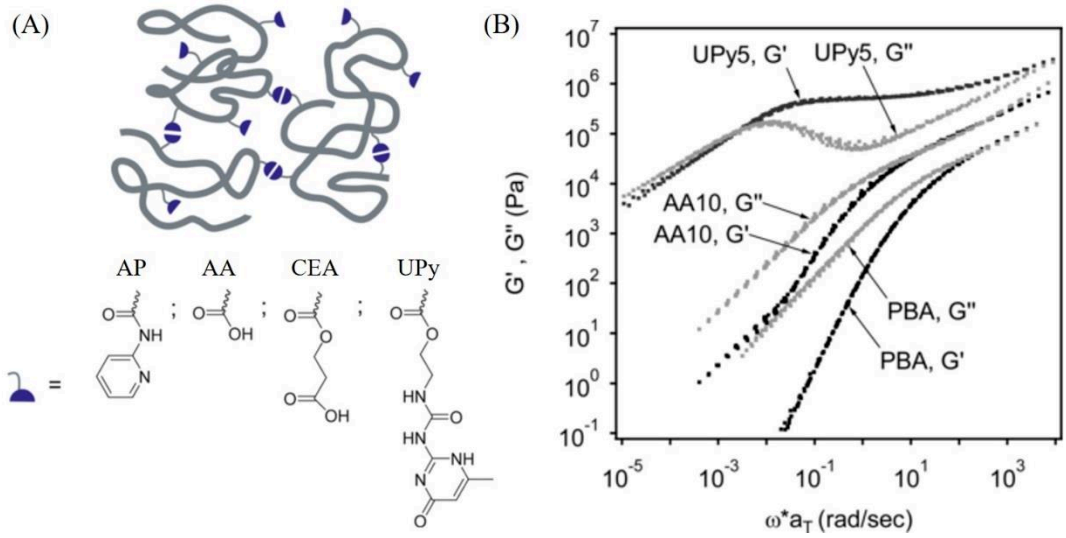

Figure 2.7 (A) Poly(n-butyl acrylate) (PBA) supramolecular networks with different hydrogen-bonding side groups: acrylamidopyridine (AP), acrylic acid (AA), carboxyethylacrylate (CEA) and ureidopyrimidinone acrylate (UPy); (B) Master curves of pure PBA, AA10 and UPy5 samples at 25 °C[122].

Zhang et al.[123] studied the effect of steric hindrance on the properties of poly(alkylurea-urethane) networks (Figure 2.8, A). The onset flow temperatures (T_{flow}, marked in Figure 2.8, B) and the relaxation times of the dynamic networks decrease with the bulkiness of hindered alkyl urea bonds. It was also found that the relaxation mechanisms differ for dynamic networks with different steric hindrances. For networks with larger steric hindrance, the network strand

diffusion mechanism dominants, while the dynamic bond lifetime is more prominent for networks with lower steric hindrance.

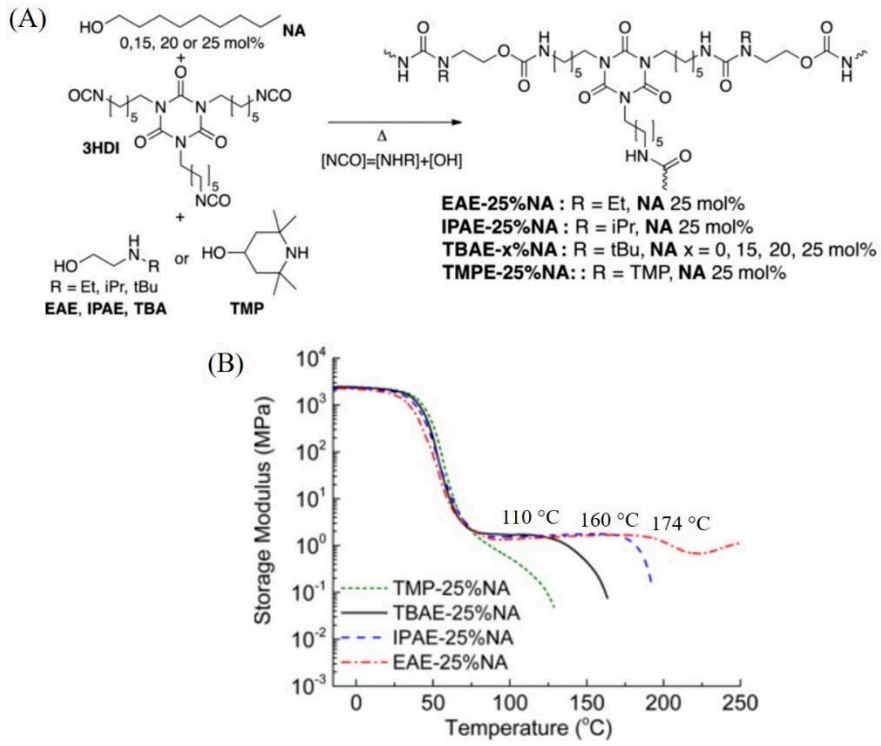

Figure 2.8 (A) Poly(alkylurea−urethane) networks with different hindered alkyl urea moiety, (B) Storage modulus of networks with a heating rate of 3 °C/min at 1 Hz[123].

Van Beek et al.[124] introduced UPy multiple hydrogen-bonding arrays into PCLs to study their effects on the rheological properties (Figure 2.9). By the comparison of pure PCLs and UPy-telechelic PCLs, it was found that the supramolecular PCLs have higher activation energies and temperature dependence on the horizontal shift factors. The UPy-telechelic PCL **1** ($\overline{M}_{n\ PCL}$= 2.9 kg/mol) complies the single Maxwell element with a relaxation time of 1.6 ms, demonstrating the unidirectionality of dimerization of UPy groups and the faster reversible chain scission than reptation. For UPy-telechelic PCLs (**2a**, **2b**, **2c**) with only the difference of PCL molar masses, it was found that the lower PCL molar masses (higher concentration of UPy groups) can enhance the formation of networks and extend G' plateau to higher frequencies. If the UPy groups are modified with bulky adamantyl groups which can hinder the stacking of UPy moieties, the corresponding **3** has a relaxation time of 18.3 ms similar to PCL 80K ($\overline{M}_n$ = 80 kg/mol) with 14.6 ms, revealing the structural requirements to obtain G' plateau at low frequencies.

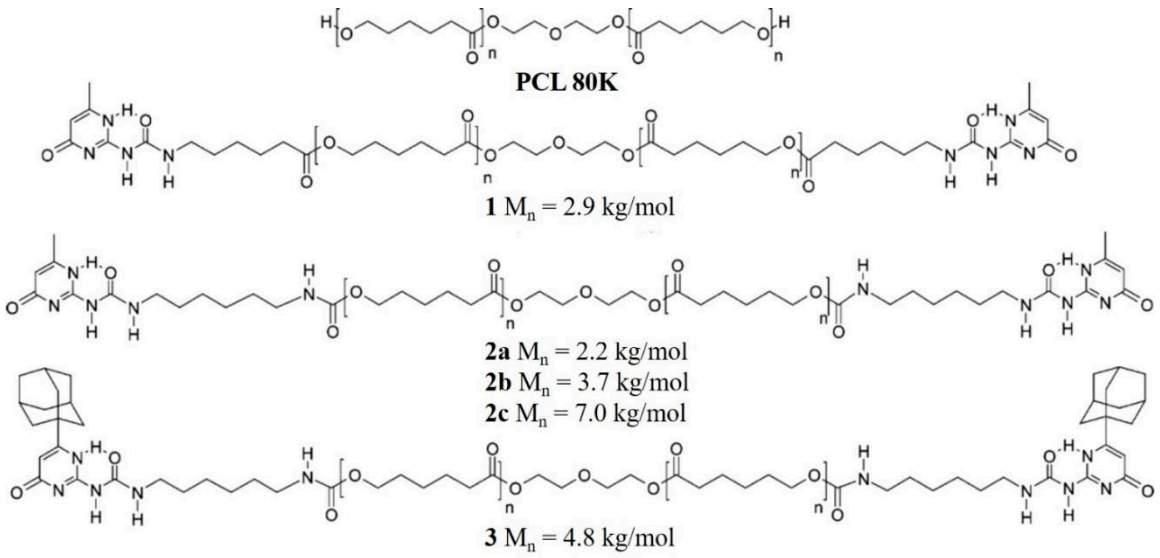

Figure 2.9 Structures of UPy-telechelic PCLs[124].

The dynamics of supramolecular polymers are directly related to the mobility of polymer chains and the hydrogen-bonding moieties. Liu et al.[125] synthesized polyesters with different pendant secondary amide groups to study the effect of chain flexibility on their rheological properties (Figure 2.10). It was revealed that the introduction of one amide group (P1AP) can indeed increase the brittleness and zero-shear rate viscosity of polyesters, resulting from the physical crosslinkers. However, with two amide groups (P2AP), the polyesters show the shortest relaxation time and the lowest zero-shear rate viscosity, which is in contrast to the expectation that more hydrogen bonds bring about slower relaxations and higher viscosity. τ of P(2AP) was measured to be the shortest with 6.1×10^{-2} s, compared to P(1AP) which has the longest τ of 1.21 s. This can be explained by the long inherently flexible side-chain of P2AP which can decrease the backbone rotation energy and increase the free volume at high temperature.

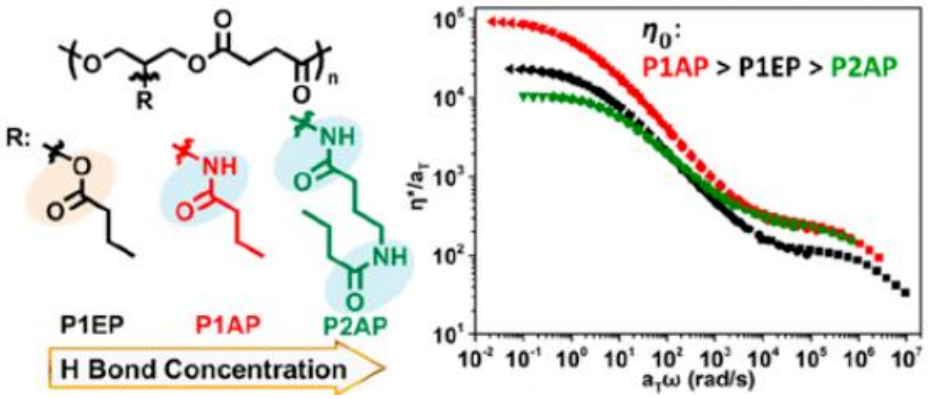

Figure 2.10 Structure of polyester with different pendant secondary amide groups and their complex viscosity at the reference temperature of $T_r = T_g + 50$ °C[125].

For unentangled supramolecular polymers, since the polymer chains usually relax rapidly, the relaxation time often relates to the supramolecular interaction lifetime (sticky Rouse model)[126]. However, in entangled systems, the relaxations of entangles can play significant role in the dynamic properties on supramolecular polymers. Jangizehi et al.[127] studied the entanglement of polymer chains on the relaxation time of UPy supramolecular interactions. When the molar mass is lower than entanglement molar mass M_e, the τ decreases with molar mass. In contrast, the τ increases with molar mass when molar mass is above M_e. It was revealed that the presence of entanglements has greater influence than transient associative interactions on the dynamics of supramolecular polymers.

Callies et al.[128,129] combined poly(butyl acrylate) (PnBA) which has an average molecular weight between entanglements M_e of 20-30 kg/mol with weak bisurea stickers and strong triurea stickers respectively. In the weak sticker system (Figure 2.11, A), there exists a critical molar mass (M_e, 20 kg/mol) of PnBA, below which the rheology properties are controlled by the size of supramolecular aggregates; while above this molar mass, the good superposition of the master curve (Figure 2.11, B) at high frequency and the similarities of shift factors a_T with those of pure PnBA suggest that molecular size and entanglement dominate.

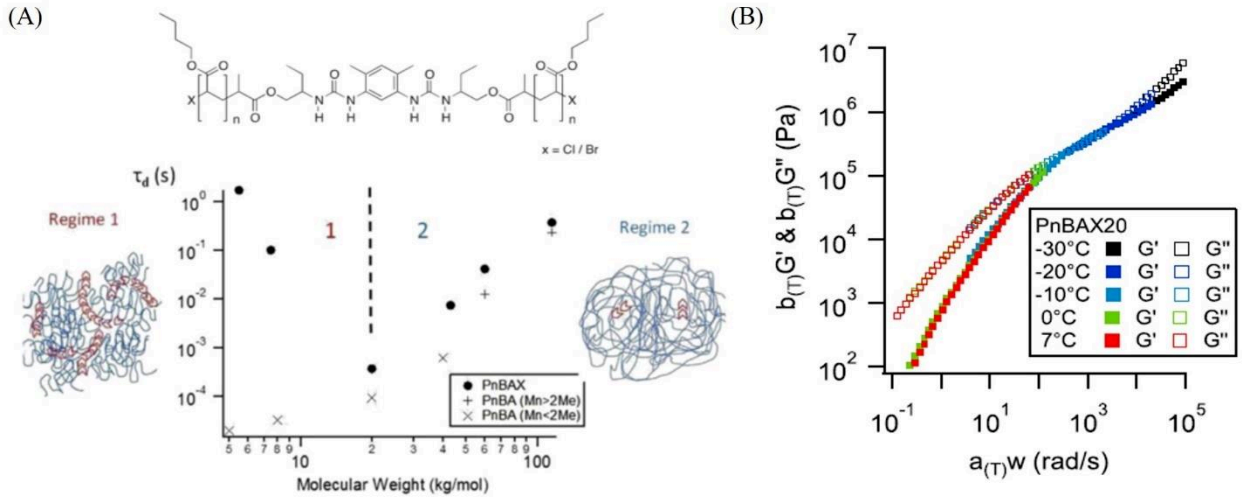

Figure 2.11 (A) τ_d (T = 20°C) vs M_w for PnBAX (circle) and unfunctionalized PnBA (cross). The dashed line materializes the sticker regime at low M_w and the side chains regime at high M_w. (B) Master Curves for PnBAX20 T_{ref} =7 °C. G': filled markers; G'': void markers[128].

In strong sticker systems[129], when the molar mass of PnBA is below the critical value 40 kg/mol, large bundles of parallel rods which do not exist in weak stickers were formed. These colloidal objects relax slow and make the material behave as elastomer at low frequencies. When the molar mass of PnBA is above 40 kg/mol, smaller and randomly oriented rods are formed and the viscoelastic properties are mainly governed by the side chains relaxations (Figure 2.12).

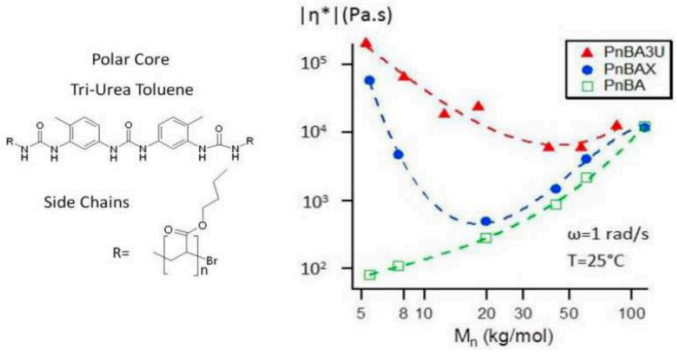

Figure 2.12 Variation of magnitude of the complex viscosity |η*| (at ω =1 rad/s, 25 °C) with $\overline{M}_n$ for triurea functionalized poly(butyl acrylate) (PnBA3U), bisurea functionalized poly(butyl acrylate) (PnBAX) and unfunctionalized PnBA[129].

2.3.2 Effects of hydrogen-bonding clusters on supramolecular polymers dynamic properties

Goldansaz et al.[113] studied the dynamics of entangled poly(n-butyl acrylate)-poly(acrylic acid) (PnBA-PAA) with AA groups which can self-assemble to have binary assemblies or to form nanodomains. It was revealed that the relatively weak binary associations of AA groups have great effect on the segmental dynamics at low temperatures while the strong hydrogen-bonding domains dominate at any temperature. As described in Figure 2.13, binary assemblies and nanodomains are phase separated by an interlayer from the matrix with polymer chains distributed inside the nanodomains and the interlayer. The lifetime of these binary assemblies and nanodomains are revealed to be longer than the longest relaxation of entangled chains, leading to the increased rheological plateau modulus.

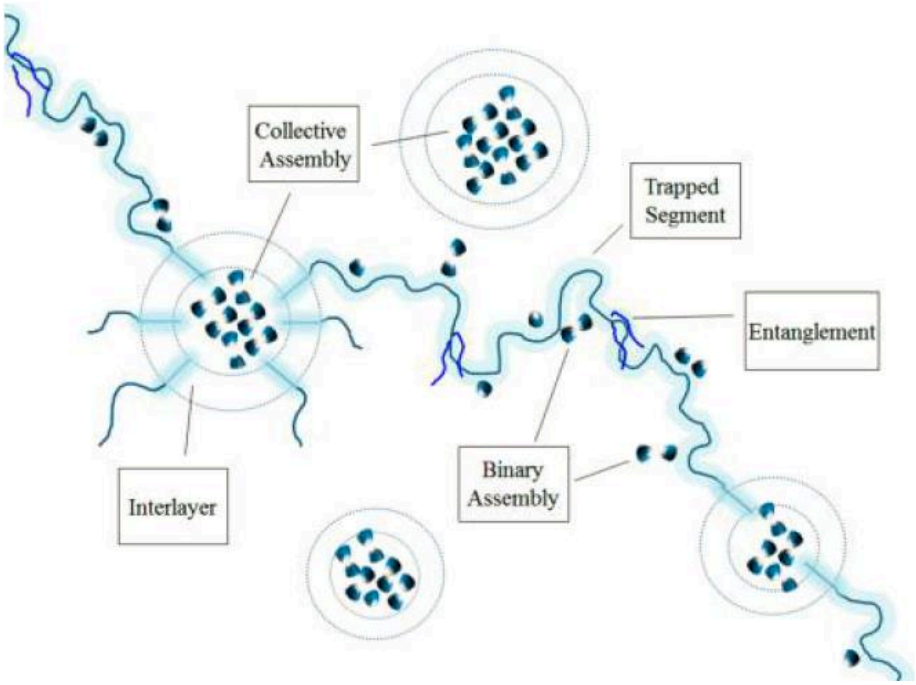

Figure 2.13 Schematic representation of the proposed microstructure of PnBA-AAs[113].

Noro et al.[130,131] synthesized supramolecular ion gels by poly(2-vinylpyridine)-b-poly(ethyl acrylate)-b-poly(2-vinylpyridine)) (P2VP-PEA-P2VP) and a poly(4-hydroxystyrene) (PHS) which are connected by hydrogen bonds. It was revealed that when the temperature is decreased below gelation temperature, the number of physical crosslinks will not be changed with only the increase of hydrogen bond numbers in each crosslink (Figure 2.14, A and B). Good master curves were obtained with upturns of G'' at high frequency for each temperature, accounting for the solvent viscosity (Figure 2.14, C). Through the Arrhenius plot of corrected FTIR absorbance and temperature, the activation energy of one hydrogen bonds was calculated to be 13 ± 2.5 kJ/mol. The hydrogen bond acceptors on P2VP blocks and hydrogen bond donors on PHS chains are not fully connected, resulting from the steric effects.

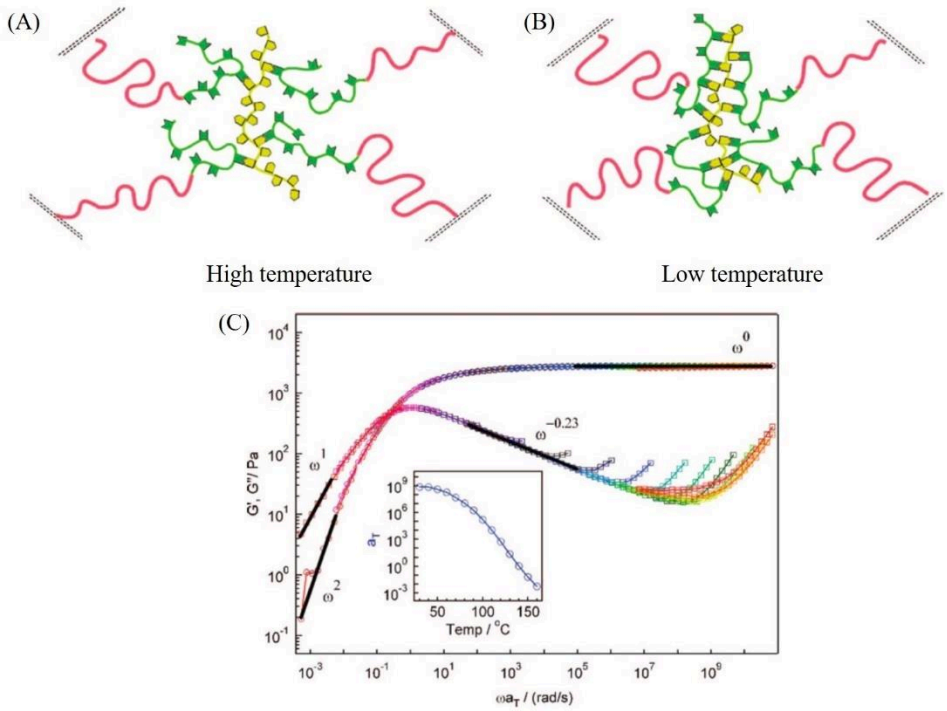

Figure 2.14 Association between P2VP blocks (green) and a PHS chain (yellow) at (A) high T and (B) low T. (C) master curve of supramolecular ion gels with a reference temperature of 140 °C. The circles are G' and the squares are G''[130].

Herbst et al.[132] studied hydrogen bonded supramolecular polymers based on polyisobutylenes (PIBs) by self-associated thymine and/or 2,6-diaminotriazine groups (Scheme 2.1). Though the association constant for thymine (K_a = 3.8 M^{-1}) and 2,6-diaminotriazine (K_a = 1.7 M^{-1}) are comparable, their viscoelastic properties differ, resulting from the formation of different aggregates. For example, when the PIB molar mass is 3500 g/mol (M_e is 16 020 or 17 000 $g.mol^{-1}$ for PIB), the supramolecular aggregates (Scheme 2.2, (a)) formed by weak hydrogen-bonding interactions in thymine telechelic PIBs lead to the increase of melt viscosity by a factor of ~5.3 at 20 °C compared to pure PIB. However, for 2,6-diaminotriazine telechelic PIBs, the formed strong and larger aggregates which are nondynamic and stable until 90 °C (Scheme 2.2, (b)) lead to the increase of viscosity by a factor of ~33. When the thymine and 2,6-diaminotriazine telechelic PIBs are mixed in equimolar quantities, though the specific interaction between thymine and 2,6-diaminotriazine moieties (Scheme 2.2, (b)) can suppress the formation of self-aggregates, aggregates by more than two chains are still formed with an increase of viscosity by a factor of ~39.5. In the study of bifunctional PIBs, it was revealed that the undirected supramolecular interaction between thymine (or 2,6-diaminotriazine) groups can favor the formation of aggregations as shown in Scheme 2.2 (e), while the more directed

interaction between thymine and 2,6-diaminotriazine lead to linear (-A-B-)$_n$ chains. In this case, the plateau value of thymine and 2,6-diaminotriazine linear (-A-B-)$_n$ chains is lower than thymine-functionalized PIBs.

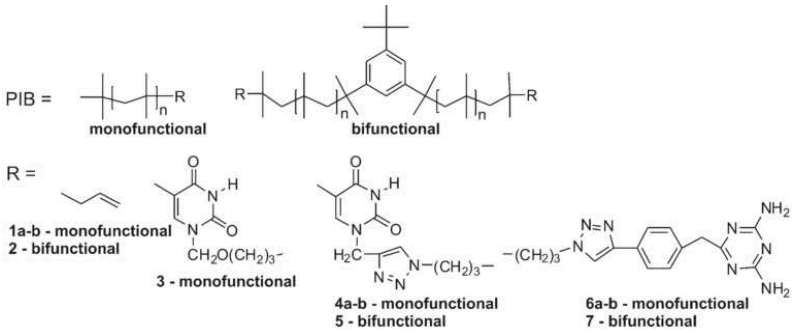

Scheme 2.1 Chemical structure of the supramolecular polyisobutylenes (PIBs) bearing thymine or 2,6-diaminotriazine moieties[132].

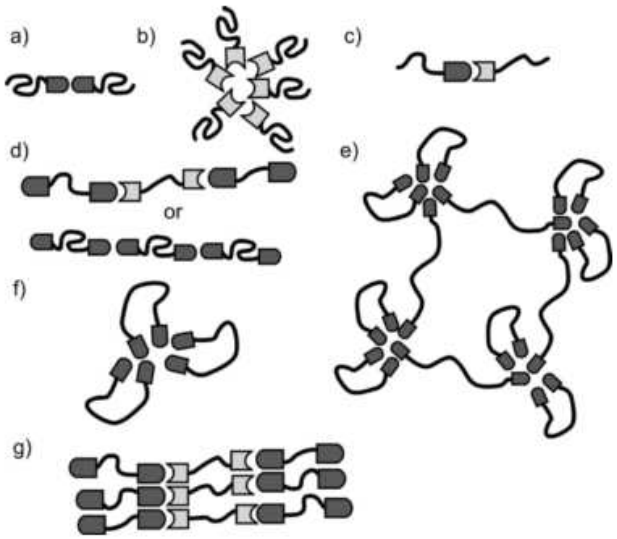

Scheme 2.2 Possible aggregation structures formed by hydrogen bonds of monofunctional (a-c) and bifunctional polymers (d-g)[132].

Afterwards, they[133] also studied mono- and bifunctional supramolecular poly(isobutylene)s (PIBs) with barbituric acid (7) or a Hamilton wedge (8) motifs (Scheme 2.3, A). It was found that the barbituric acid-functionalized PIBs 4a can form dynamic junction points of different barbituric acid groups (Scheme 2.3, B) with long lifetime at high frequencies, making the material behave like rubber. At low frequencies, these aggregates can transfer to a ‘‘semi-closed’’ or ‘‘open’’ state and make material flow. When the molecular weight of PIB is increased, the change of rheology properties was found to be negligible. Considering the same

strength of the interaction and decreased mobility of the chain, the only explanation is that the aggregate size decreases with molecular weight of PIB.

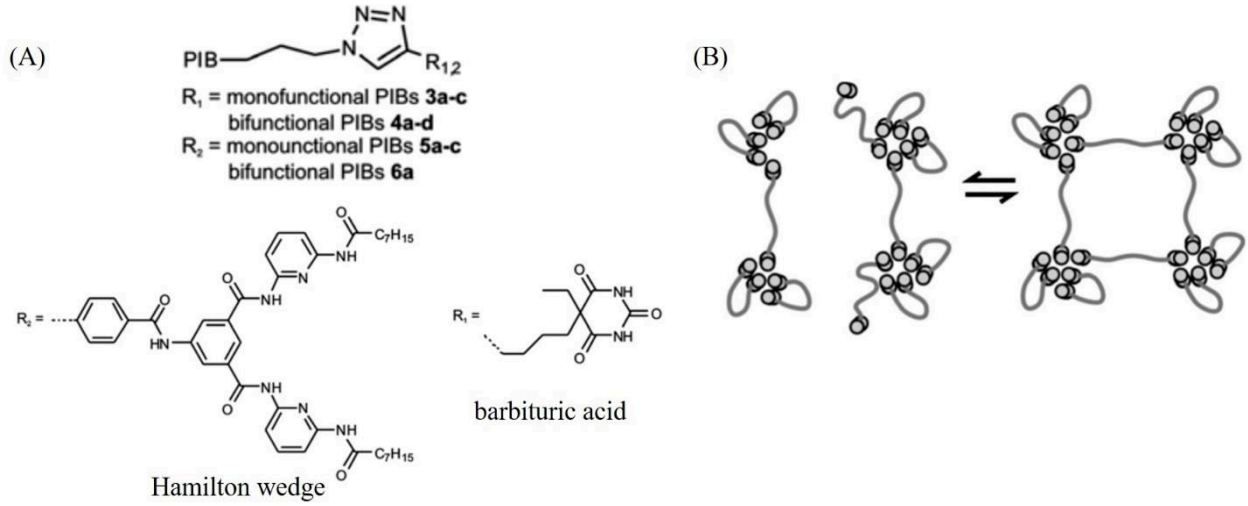

Scheme 2.3 (A) Chemical structure of supramolecular mono- and bifunctional PIBs bearing either Hamilton wedge or barbituric acid moieties. (B) Formation of a dynamic supramolecular network by aggregates[133].

2.4 Applications of hydrogen-bonded supramolecular polymers

Due to the existence of dynamic and reversible interactions, the hydrogen-bonded supramolecular polymers can then be used for recyclable, stimulus-responsive, self-healable, shape memorable and self-adhesive materials.

2.4.1 Self-healing materials

In polymer materials, it is common to have microcracks which may cause the failure of the material. The traditional ways to repair these microcracks are heating the defected area or exposing the material to a plasticizing solvent. However, these ways are usually inefficient for high molecular weight polymers because it is usually slow to diffuse and entangle chains[134]. One of the major advantages of hydrogen bonded supramolecular polymers with self-healing properties is that there is no necessity to add external agent in the material[135]. Several studies have reported the possibility to form self-healing materials when highly dynamic hydrogen bonds (high association constant) are used, though sometimes the mechanical strength and stiffness are relatively low[70,136,137]. According to the study of Bose et al.[116,117], when the relaxation time of supramolecular polymer is between 10 s and 100 s, a good surface scratch self-healing for the material and good mechanical robustness are reached simultaneously. In

addition, to design a supramolecular polymer with self-healing properties, it's necessary to compromise between the strength of secondary interactions and the mobility of polymer network.

Chino and Ashiura[138] are among the first reporters to study self-healing materials. Through introducing hydrogen-bonding moieties into rubber, they succeeded to prepare healable supramolecular polymers which can withstand several reprocessing cycles. Later, Cordier et al.[139] prepared rubber which shows recoverable extensibility up to several hundred percent and little creep under load. Due to the hydrogen bonds in this system, the material can be easily repaired at room temperature. Nevertheless, there is a maximum waiting time after which self-healing is no longer possible because during this time thermal equilibrium is reached and the quantity of free groups are not enough for repairing. Herbst et al.[133] prepared poly(isobutylene)s based self-healing materials by hydrogen bonds between barbituric acid groups. As shown in Figure 2.15, the crack between two pieces can be healed completely after 48 hours without external forces applied.

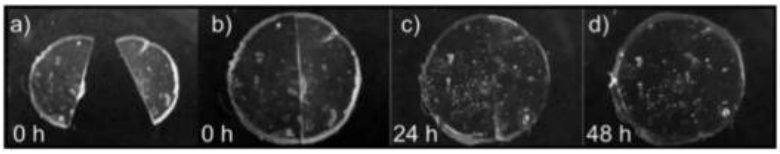

Figure 2.15 Self-healing process (a) cut parts, (b) cut parts were just brought into contact, (c) partially healed crack after 24 h and (d) completely healed crack after 48 h[133].

Yang et al.[140] synthesized self-healable supramolecular elastomers through carboxyl-terminated polydimethylsiloxane oligomers with diethylenetriamine and urea. They found that the self-healing ability of the material is dependent on the mobility of the non-associated groups on the fracture surface. The shorter of polydimethylsiloxane chains, the higher temperature needed to heal. Chen et al.[141] combined high modulus and toughness with spontaneous healing capability by designing a new hydrogen-bonding brush polymers (Figure 2.16). This supramolecular polymer can self-assemble into a hard-soft microphase-separated system. The existing nanocomposites endow the material with enhanced stiffness and toughness, but the dynamic supramolecular assemblies can bring about self-healing capability. This new system can self-heal as a single-component solid material at ambient conditions, without healing agent, plasticizer or solvent.

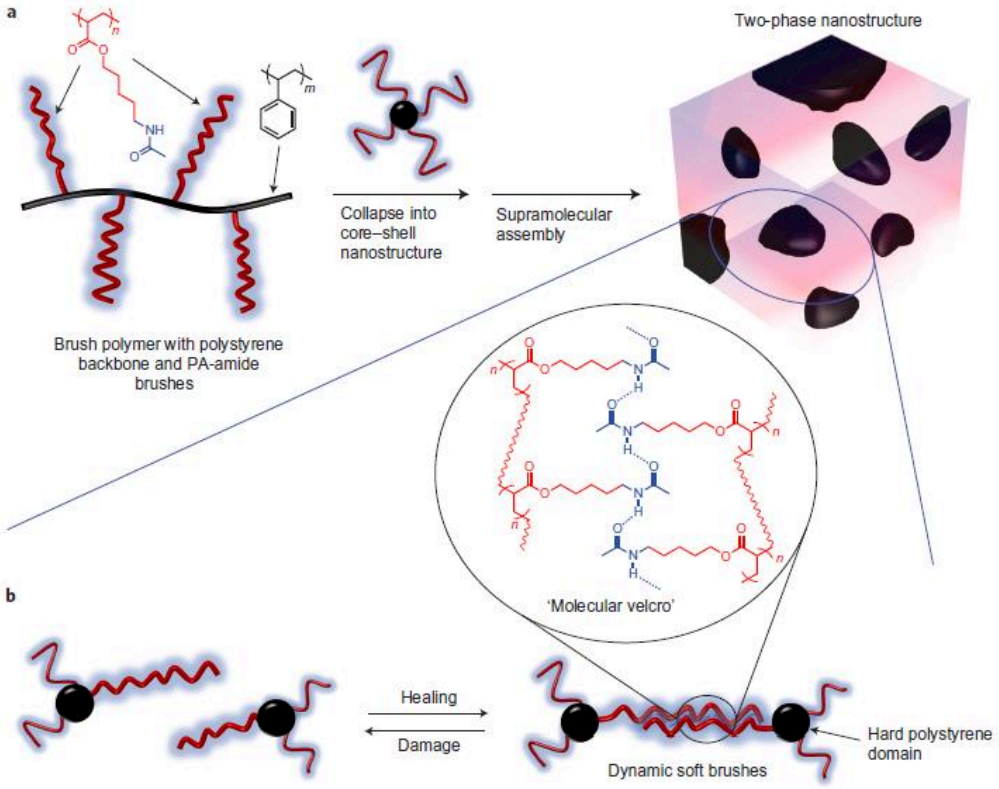

Figure 2.16 Design concept for the multiphase self-healing brush polymer system[141].

2.4.2 Shape memory materials

Shape-memory materials can be obtained by combining cross-links (physical or chemical) and supramolecular interactions together[142]. The easy adjustment of interaction strength as well as the straightforward design of multifunctional structures makes hydrogen bond the most applied one in shape-memory materials[143]. At high temperature, where hydrogen bonds can be broken, only the crosslinks respond to external deformation. If this deformation is kept with the immediate decrease of temperature, supramolecular interactions can be frozen at low temperature. After the reheating of the material, these interactions can associate again and release the stored elastic response, endowing the material with shape memory properties.

Chen et al.[144] synthesized supramolecular polyurethanes with pendant pyridine groups. It was revealed that with the decrease of pyridine content, the hydrogen bonds in urethane bonds get stronger while those in pyridine rings become weaker. Moreover, the hydrogen bonds in urethane bonds can lead to the formation of phase-separated hard phase from the soft matrix, acting as physical crosslinks, while the hydrogen bonds in pyridine can only act as molecular switch. A lowest limit content 30 wt% of isonicotinamide was found to have good shape

memory effect for supramolecular polyurethane. When the isonicotinamide content is increased, higher shape fixity, higher shape recovery and better strain stability are reached.

Ware et al.[69] synthesized triple-shape memory polymers which contain both strong hydrogen-bonding associations and covalent crosslinks. Besides keeping the permanent shape, the material can also change shapes twice and fix two metastable shapes (Figure 2.17), accounting for the glass

transition of polymer matrix and the dissociation of UPy moieties. As shown in Figure 2.17 (B), the material is in a bent and textured temporary shape at 20 °C. When the temperature is increased, the material can be transferred to twisted and textured shape at 37 °C, and flat and smooth finally at 90 °C.

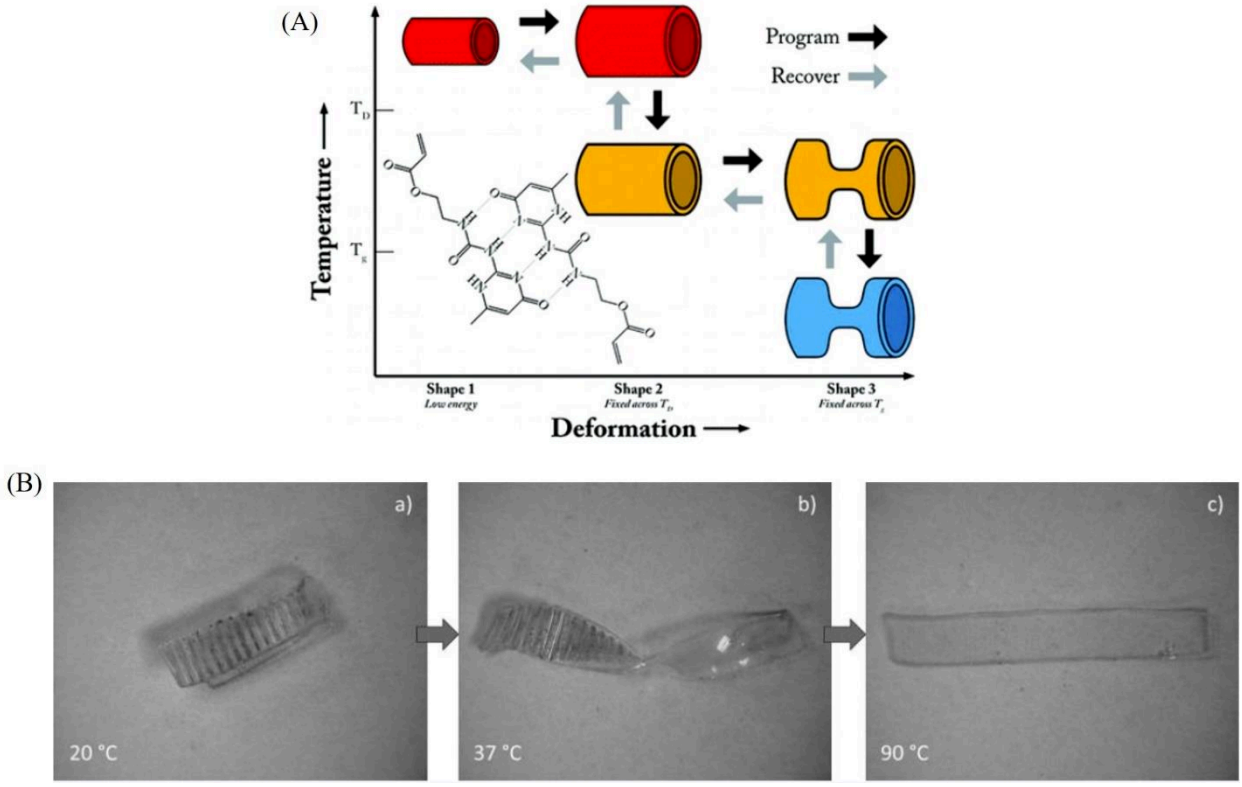

Figure 2.17 (A) Schematic of a triple-shape memory polymer programming and recovery cycles and (B) Triple-shape memory properties of triple shape memory polymer. Recovery proceeded from (a) the first temporary shape (bent and textured) to (b) the second temporary shape (twisted and textured) and to (c) the permanent shape (flat and smooth)[69].

Later, Wei et al.[145] also obtained triple-shape memory dynamic networks by the mixture of UPy-telechelic poly(tetremethylene ether) glycol (PTMEG) and four-arm star-shaped poly(ε-caprolactone) precursors. In these networks, the crystalline PTMEG and PCL act as switch

domains with different melting temperatures. While UPy dimer aggregates can function as netpoints with higher dissociation temperature. As shown in Figure 2.18, when the material was deformed at 60 °C, the UPy aggregates act as crosslinks in the melted PTMEG and PCL matrix. After cooling to 35 °C and -10 °C, the crystals of PCL and PTMEG were generated respectively. In the recovery period, if the temperature was increased to 35 °C and 60 °C in sequence, a triple-shape memory effect will be observed. In addition, due to the reversibility of UPy associations, these networks can be self-healed at 40 °C for 48 hours.

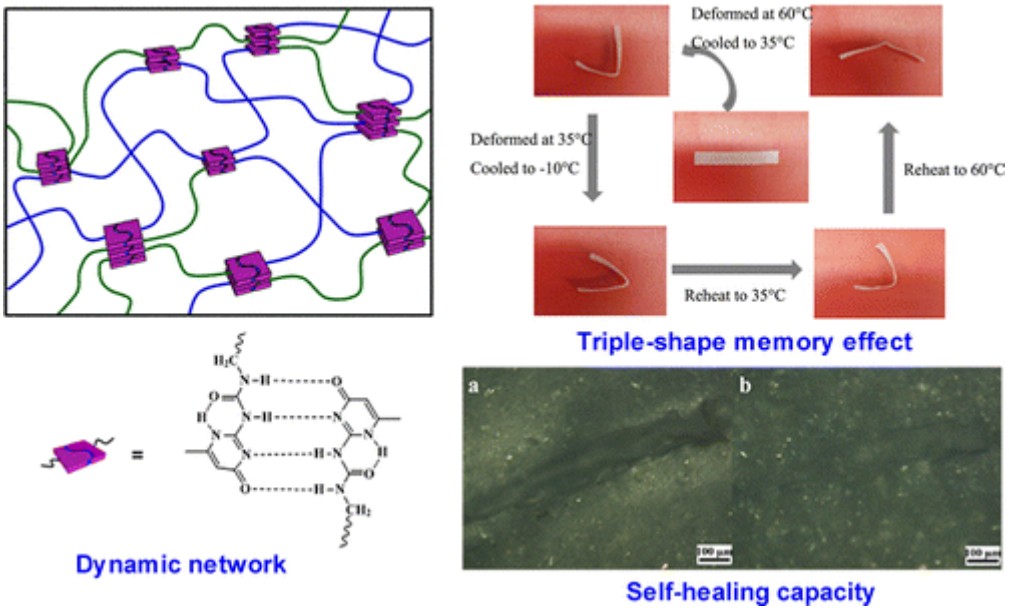

Figure 2.18 Triple-shape memory effect and self-healing capacity of PTMEG-PCL based dynamic networks[145].

2.4.3 Self-adhesive materials

Self-adhesive materials, which is also called pressure-sensitive adhesives (PSAs) are widely used in the area where only weak mechanical bond is needed. Conventionally, the combination of a small amount of polymer crosslinking networks and a low glass transition temperature is used to obtain weak adhesive materials[146]. However, in some cases, such as surfaces with high molecular mobility and low surface tension, weak van der Waals interactions are insufficient to allow adhesive layer deformation and energy dissipation, proposing the necessity to develop new materials with enhanced energy dissipation and retained flow resistance[147].

Creton et al.[147] synthesized bis-urea functionalized low-molecular-weight polyisobutylenes with adhesive properties. The slow self-association of hydrogen bonds in the material can last several days at room temperature, endowing the material with a highly dissipative nature upon

deformation. After combining the slow dynamics with strong bis-urea moieties, the material shows very fascinating adhesive properties on typical low adhesion surfaces such as silicone through the formation of fibril structures. Afterwards, the same group[148] combined a strong self-complementary sextuple tri-urea sticker with poly(butylacrylate) to obtain supramolecular networks. When the $\overline{M}_n$ of material is lower than 40 kg/mol, the rod-like aggregates can be induced to bundles and show the behavior of soft elastic material at room temperature. This material can be softened strikingly at large deformation, accounting for the low adhesion energies of these viscoelastic gels. The highest debonding energy of these materials is around 37 J/m^2, lower than the commercial PSAs with the usual values between 100 and 1000 J/m^2 in same conditions. At the same time, they[149] also synthesized low molar mass PSAs by the combination of poly(butyl acrylate-co-glycidyl methacrylate) copolymers and quadruple hydrogen-bonding bis-urea stickers. It was revealed that the formation of network structures by hydrogen bonds can facilitate the dissipative properties at both small and large deformations. Through the change of hydrogen-bonding stickers strength and polymer chain length or branching lever, the adhesive performance can be easily adjusted.

2.5 Conclusions

Hydrogen bond is one of the most widely used supramolecular interactions with high directionality and versatility. Though the strength of one single hydrogen bond is not high enough, the development of multiple hydrogen-bonding arrays allows the creation of stronger hydrogen-bonding arrays. The strength of multiple hydrogen-bonding arrays is not only dependent on the number of hydrogen bonds but also related to the secondary electrostatic interactions, steric interactions and preorganization. For supramolecular polymers, their dynamics properties are dependent on the supramolecular lifetime, chain relaxation time and the possibility to form clusters. These hydrogen-bonded supramolecular polymers are potentially to be applied in self-healing, shape memory and self-adhesion.

3. Thermoreversible networks by “click” Diels-Alder reactions

3.1 Click chemistry

In 2001, Sharpless et al.[150] fully described the concept of “click chemistry” as a set of powerful, highly reliable and selective reactions to synthesize new compounds by heteroatom links (C-X-C). Due to its superior merits, including high yields, simple reaction conditions, high selectivity, fast reaction times, inoffensive by-products and insensitivity to oxygen and

water[151], the applications of click chemistry have been extended in almost all fields, especially in bioconjugation, materials science and drug discovery[152]. According to the recent studies in click chemistry, six kinds of click reactions are noteworthy particularly, namely Diels-Alder (DA) reaction, alkyne-azide reaction, thiol-ene reaction, Michael addition, epoxy-amine/thiol reaction and imine formation[153]. Among these click reactions, the Diels-Alder reaction is a member of the most attractive ones due to its temperature-controlled reversibility without the need of catalyst, making it environmentally benign[68].

3.2 Diels-Alder reaction

Since Otto Diels and Kurt Alder invented Diels-Alder cycloaddition reaction in the 1920s, it has been studied extensively in organic chemistry. The Diels-Alder reaction generally occurs between an electron-rich diene and an electron-poor dienophile ([4+2] cycloaddition)[154] to form six-membered rings. This dynamic covalent reaction is thermoreversible within different temperature ranges, depending on the diene and dienophile structures[155]. Compared to supramolecular bonds which are combined by weak noncovalent interactions, Diels-Alder reaction combines the reversibility property and the strength of covalent bonding[68].

For Diels-Alder [4 + 2] cycloadditions, two stereoisomers of *endo* and *exo* DA adducts can be generated[156]. As shown in Figure 3.1, both *endo* and *exo* stereoisomers exist in DA adducts formed by furan and maleimide[157-160]. Since *exo* isomers have higher thermodynamic stability than *endo* isomers with the retro-Diels-Alder (rDA) temperature of *endo* adducts 20-40 °C lower than *exo* counterparts, *exo* adducts dominate in most situations[156,157].

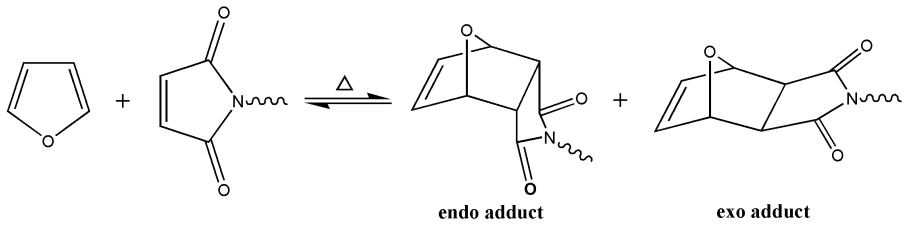

Figure 3.1 *Exo* and *endo* DA adducts formed by furan and maleimide groups.

However, the ratios between *endo* and *exo* adducts are also influenced by the reaction temperature, substituents on furan and maleimide, and the existence of nucleophile as well[161]. For example, Froidevaux et al.[161] found that the electron withdrawing substituents on furan and maleimide groups can favor the formation of *endo* adducts. On the contrary, Pearson et

al.[162] revealed that the existence of complementary hydrogen bonding can lead to the formation of 100% *exo* adducts, resulting from the stabilization of the transition state.

3.3 Furan/maleimide coupling and thermoreversible networks

The widely studied Diels-Alder reactions include furan/maleimide[163], anthracene/maleimide[164], tetrazine/cyclooctene[165] and dithioester/diene[166]. Among these reactions, the furan/maleimide coupling[163,167,168] attracts the most attention due to its relatively mild association and dissociation temperature around 60-70 °C and 100 °C respectively[163]. For this reason, it can be applied as a potential functionalization method for polymers and opens the way to some special properties[163]. Moreover, no additives are needed and no small molecules are released[169]. The renewable resources of furan derivatives also satisfy more and more serious environmentally friendly requirements[163].

3.3.1 Structure effect on reactivity and reversibility of furan/maleimide DA reaction

The reactivity and reversibility of Diels-Alder reactions are extremely important to decide the materials properties. As described by Boutelle et al.[170], the reactivity and reversibility can be easily adjusted by furan and maleimide substitution. For example, the change of substituent on furan from -OCH_3 at 3-position to -CHO at 2-position can extremely change its reactivity with maleimide from irreversible to reversible, resulting from the discrepancy of electronic properties of substituents. At the same time, Ishida et. al[171] studied the substituent effect of amide, ester and urethane on the physical properties of DA networks, indicating the great effect of electron density in furan rings as well as the hydrogen bonds between maleimide C=O and amide/urethane N-H. It was confirmed that the higher electron density of furan ring, the more favorable to react with maleimide. The equilibrium of DA reaction follows the substituent effect order of amide > urethane > ester. Moreover, Froidevaux et al.[161] revealed that the reversibility between furan and maleimide can be accelerated by far electron withdrawing substituents and electron attracting mesomeric substituent on furan and maleimide respectively. As mentioned previously, the existence of complementary hydrogen bonding can not only control the *exo* stereoisomers of DA adducts but also accelerate the DA reaction[162].

3.3.2 Thermoreversible networks by furan/maleimide DA reactions

The utilization of thermoreversible DA reactions to synthesize networks attracts more and more attention due to not only its capability to enhance mechanical properties but also its possibility

to introduce some special properties, such as self-healing[172-175] and shape memory[176,177]. Generally, three synthetic methods are used to obtain networks by DA reactions, including (i) DA cycloaddition with multifunctional monomers, such as furan (maleimide) derivatives (functionality > 2) and bismaleimide (bisfuran); (ii) DA cycloaddition between linear polymers which contain furan and/or maleimide groups; (iii) the polymerization involving DA linkages[154].

For the first method, Raquez et al.[178] synthesized poly(ε-caprolactone)-based polyesterurethane via condensation among diisocyanate, PCL and furfuryl alcohol. The bismaleimide N,N'-1,3-phenylenedimaleimide was used as DA crosslinker. DA and rDA reactions are capable of enhancing the molecular motion of the polyesterurethane and then the crystallization ability of PCL, leading to the formation of semicrystalline crosslinked polymers. The melting temperature 45 °C was revealed to be the switching temperature for shape-memory properties. Yu et al.[179] synthesized linear segmented polyurethane with pendant maleimide groups through diisocyanate, poly(tetramethylene ether glycol) and chain extender which contains maleimide groups. The thermoreversible networks were then obtained by furan crosslinker (FHF) (Figure 3.2). The increase of furan crosslinker concentration can enhance the networks mechanical properties remarkably with highest Young's modulus of 230 MPa and tensile stress of 50 MPa at the strain of 300%, attributed to not only the DA reactions but also the hydrogen bonds. The overlap of endothermic and exothermic transition in different DSC heating and cooling cycles in short time indicates the seldom fast DA reaction kinetics. Finally, these networks were proved to have excellent recyclability and remending ability at the temperature range from 140 °C to 180 °C.

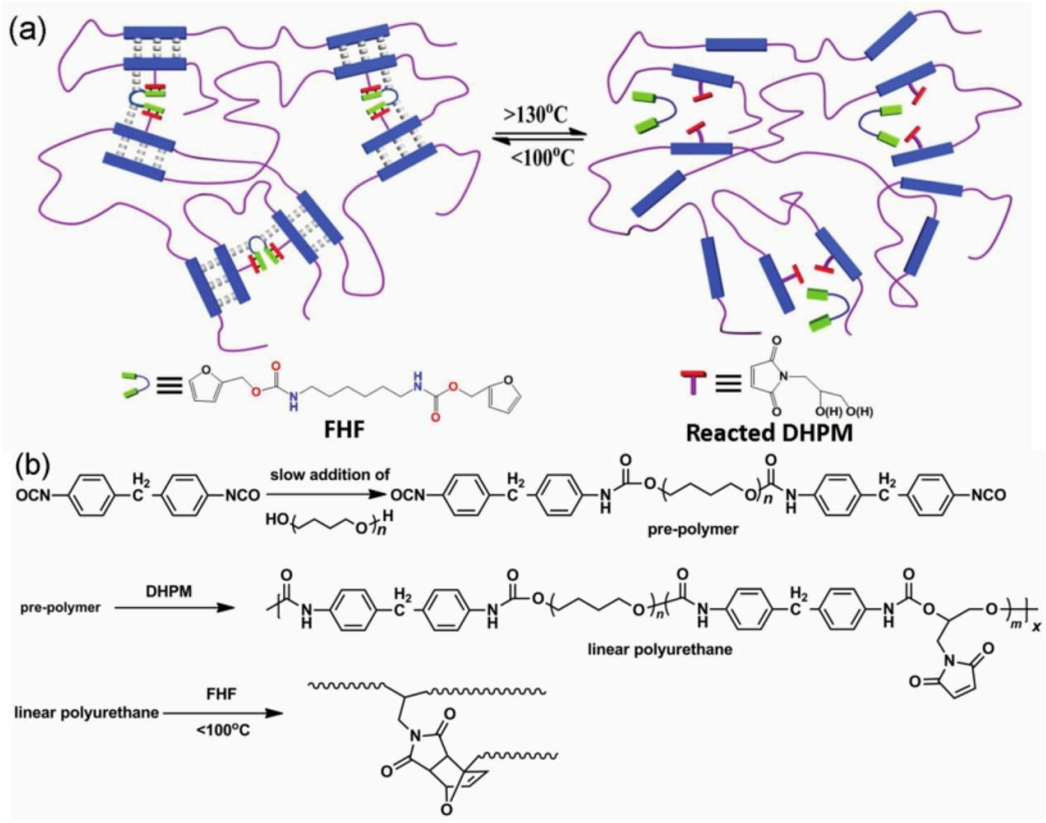

Figure 3.2 (a) Schematic depiction of reversible crosslinked network by DA reaction and hydrogen bonds; (b) Synthesis of crosslinked networks by DA reactions[179].

Trovatti et al.[180] synthesized furan grafted polybutadiene (PB) through thiol-ene reaction between furfuryl thiol and double bonds in PB. Aromatic bismaleimide was then used as crosslinker to obtain thermoreversible networks with the reverse DA reaction at temperature of 110 °C. The success in getting thermoreversible PB indicates the possibility to obtain recycling tires through furan and maleimide DA reactions. Similarly, Berto et al.[181] also synthesized thermoreversible crosslinked PB networks by furan telechelic polybutadienes (functionality of 4) and a bis-maleimide. Network structures were adjusted through the addition of different concentrations of bis-maleimide as well as the adjustment of various chain lengths which changes the furan telechelic group concentration. The obtained material possesses recycling ability and can be used from −70 to 80 °C without properties loss. Bai et al.[182] synthesized furan grafted PB through thiol−ene reaction between PB and furfuryl mercaptan with the addition of bismaleimide to get thermally recyclable polybutadiene elastomers (Figure 3.3). Through the adjustment of attached furan amount on PB chains and the bismaleimide content, the mechanical properties of polybutadiene elastomers could be tailored easily. These elastomers also have good solvent resistance from room temperature to 100 °C as well as thermally remolded and self-healing behaviors.

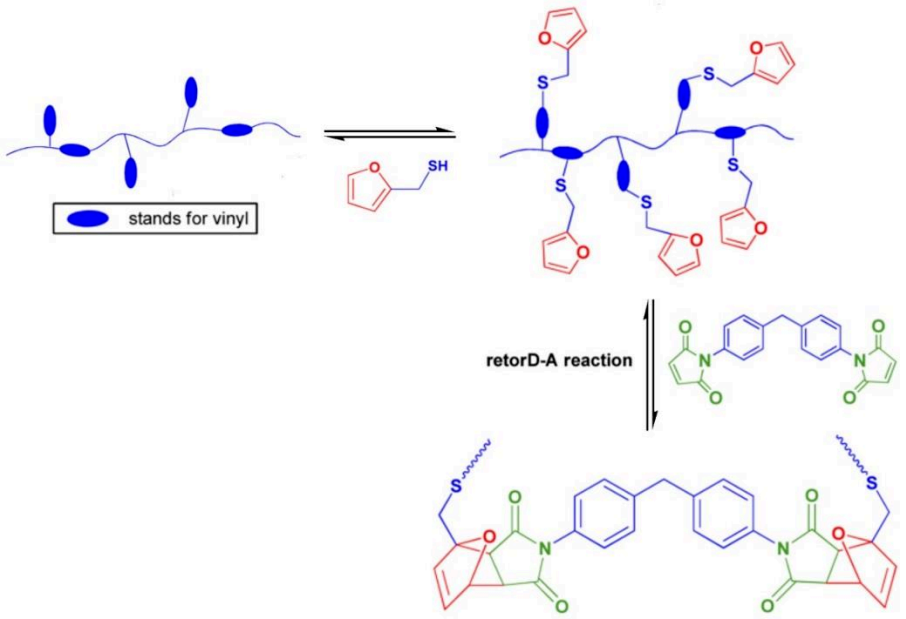

Figure 3.3 The preparation of recyclable polybutadiene elastomer by DA reactions[182].

They[183] also synthesized furan functionalized poly(styrene-block-butadiene-block-styrene) (SBS) through the same method between SBS and furfuryl mercaptan. With bismaleimide as crosslinker, dynamic crosslinked thermal plastic elastomers were obtained (Figure 3.4). The mechanical properties and solvent resistance are enhanced while keeping the thermal plastic remolding ability. The maximum tensile strength of the modified SBS was as high as 14.96 MPa, almost 8 times higher as compared to pure SBS, and keep the strain above 800% at the same time. After 3 generations of remolding, this thermal plastic elastomer can still maintain almost the same mechanical properties.

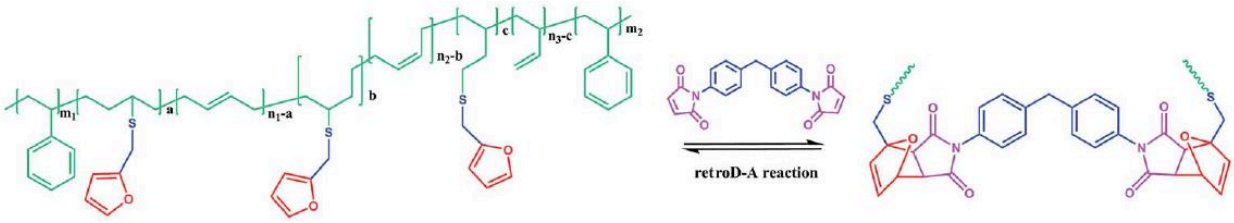

Figure 3.4 The crosslinking/decrosslinking reaction scheme of the films via DA and rDA reactions[183].

Duval et al.[184] obtained thermoreversible networks by furan-bearing tannins and bismaleimide terminated poly(propylene oxide) and poly(propylene oxide)-b-poly(ethylene oxide)-b-poly(propylene oxide) oligomers. The network structures can be broken upon heating at 120 °C.

For the second method, Wei et al.[185] established a facile method to obtain thermosensitive poly(N-isopropylacrylamide)-based hydrogels through furan functionalized poly(N-isopropylacrylamide) and poly(ethylene glycol) (PEG) based bismaleimide (Figure 3.5). The swelling behavior of these hydrogels can be adjusted by the temperature and crosslinking density. At the same time, they[186] synthesized N-vinyl-2-pyrrolidone-based hydrogels via furan functionalized poly(furfuryl methacrylate-co-N-vinyl-2-pyrrolidone) copolymers and PEG based bismaleimide. The dependence of swelling behavior on temperature and crosslinking density endows the material with potential applications as biomaterials.

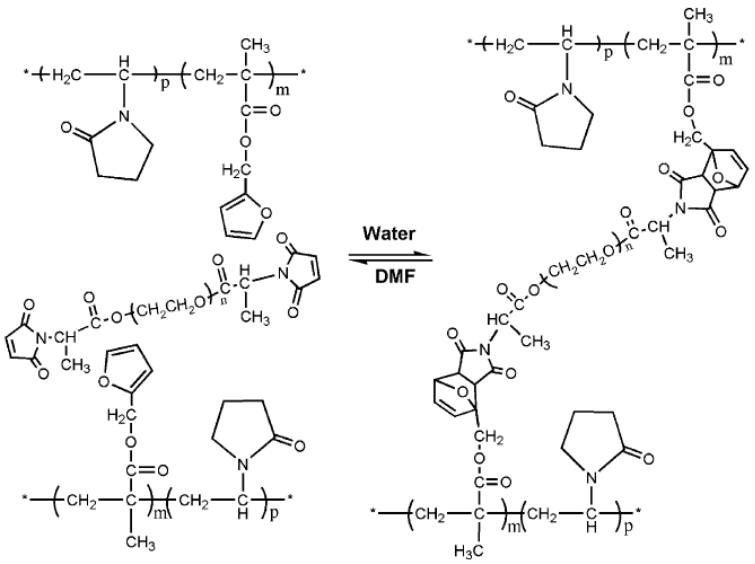

Figure 3.5 Chemical structure of poly(N-isopropylacrylamide)-based hydrogels by DA reaction[185].

Defize et al.[187,188] obtained recyclable shape-memory PCL by the mixture of tetra-furan and tetra-maleimide functionalized PCLs (Figure 3.6). Due to the existence of DA reactions, these networks are processable but still keep good mechanical properties below melting point. Through Raman spectroscopy, the DA reaction was revealed to reach 60% at 65 °C and the rDA temperature was determined to be 125 °C. In rheological isotherm studies, a plateau in moduli was observed after 10 min at 125 °C, indicating a faster rDA process as compared to DA reaction where the moduli were still increasing at 60 °C even after 120min, resulting from the less efficient contact of furan and maleimide groups and the decreased diffusion rate during the formation of the network. The reversibility of networks was confirmed by the similar rheological curves during several heating and cooling cycles between 65 and 125 °C.

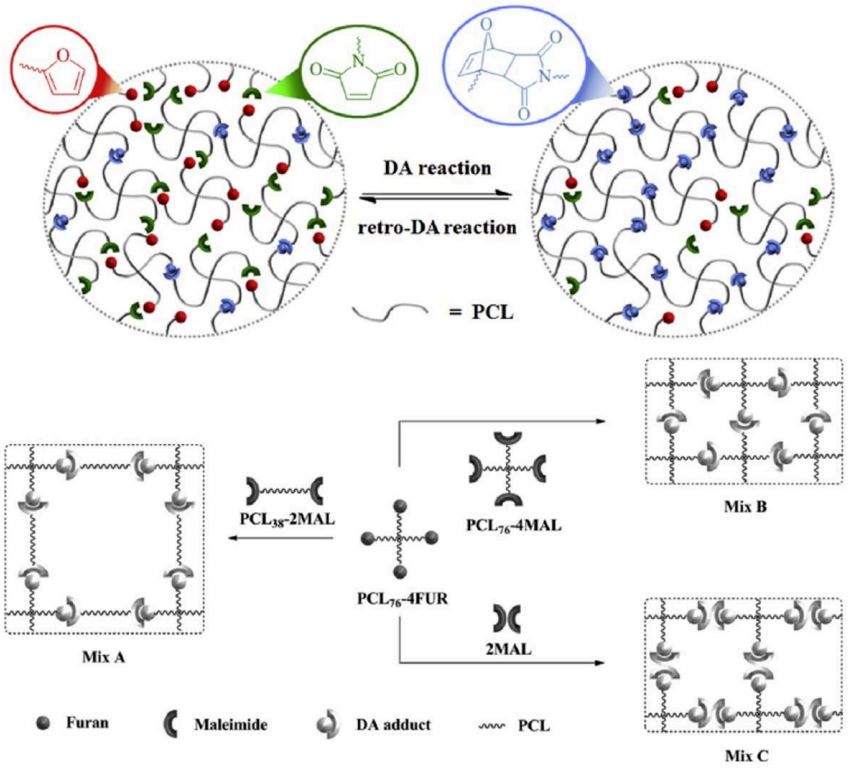

Figure 3.6 The formation of DA-based thermoreversible PCL networks[188].

Stewart et al.[189] prepared hydrogels by furan and maleimide-functionalized poly(methyl vinyl ether-alt-maleic acid) which can be used as controlled-release delivery vectors (Figure 3.7). The gelation time of these hydrogels in water varies from 15 min to 18 h, depending on the degree of functionalization of furan and maleimide and the polymer concentration as well. The elastic moduli of hydrogels increase with the density of DA crosslinkers and through the appropriate adjustment of functionalization degree, they can bear the elastic moduli similar to fat, muscle and cartilage and precalcified bone. Besides, they are also highly responsive to Ca^{2+} ions, showing a slow and persistent release of dextran drug during one week for Ca^{2+} treated hydrogels.

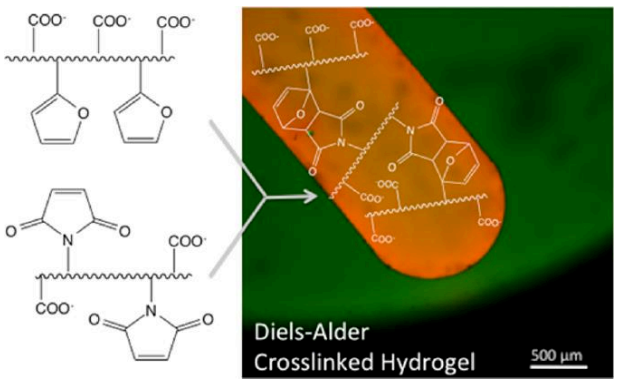

Figure 3.7 Poly(methyl vinyl ether-alt-maleic acid) hydrogels by Diels-Alder reactions[189].

For the third strategy, Magana et al.[190] synthesized DA adducts by 11-maleimido-undecanoic acid and commercial 3-(2-furyl) propanoic acid firstly. Through the reaction between epoxy groups in poly(ethylene-co-glycidyl methacrylate) and carboxyl groups in DA adducts, the networks structures were obtained as shown in Figure 3.8. The DA and rDA processes were traced by FTIR with the variation of temperature from 40 to 140 °C by several circles to confirm the thermoreversibility. After 20 cycles of heating and cooling procedures, a small reactivity loss was found, indicating good properties of remendability.

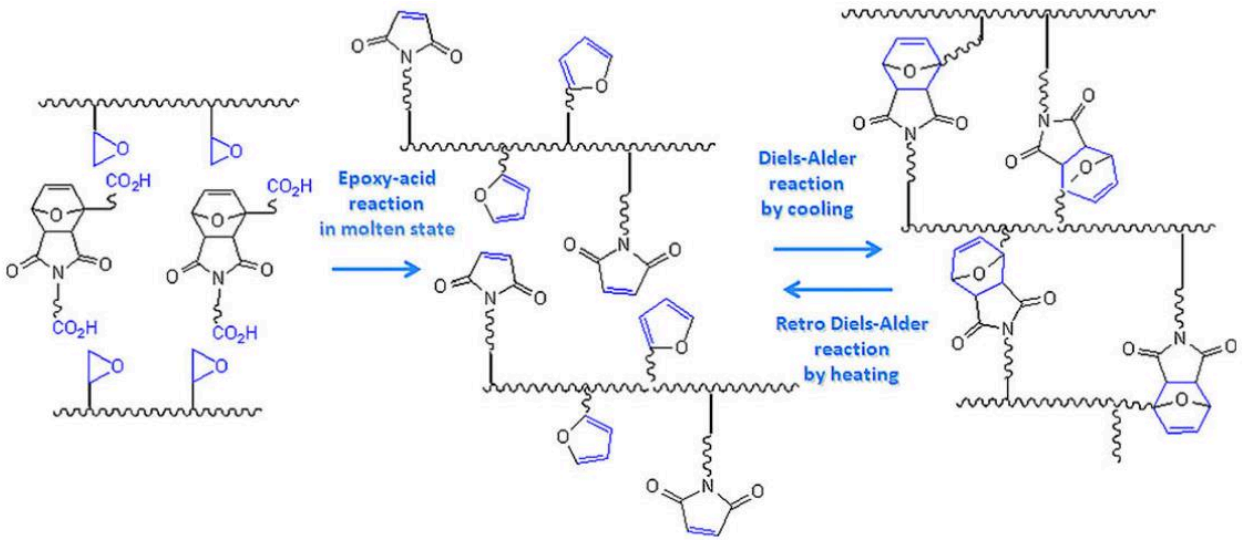

Figure 3.8 The formation of poly(ethylene-co-glycidyl methacrylate)-based networks by Diels-Alder reactions[190].

Gaina et al.[191] synthesized poly(tetrahydrofuran) based thermoreversible epoxy-urethane networks through diamines and diepoxy monomers which contain Diels–Alder adducts (Figure 3.9). Two T_g values were observed for the material, corresponding to soft and hard segments respectively. The exothermic peak at 101°C in DSC curves showed the formation of DA adduct between furan and maleimide groups. The repeatable results in second and third heating cycles confirmed the thermoreversibility of the networks and the rDA reaction was revealed to occur above 116 °C.

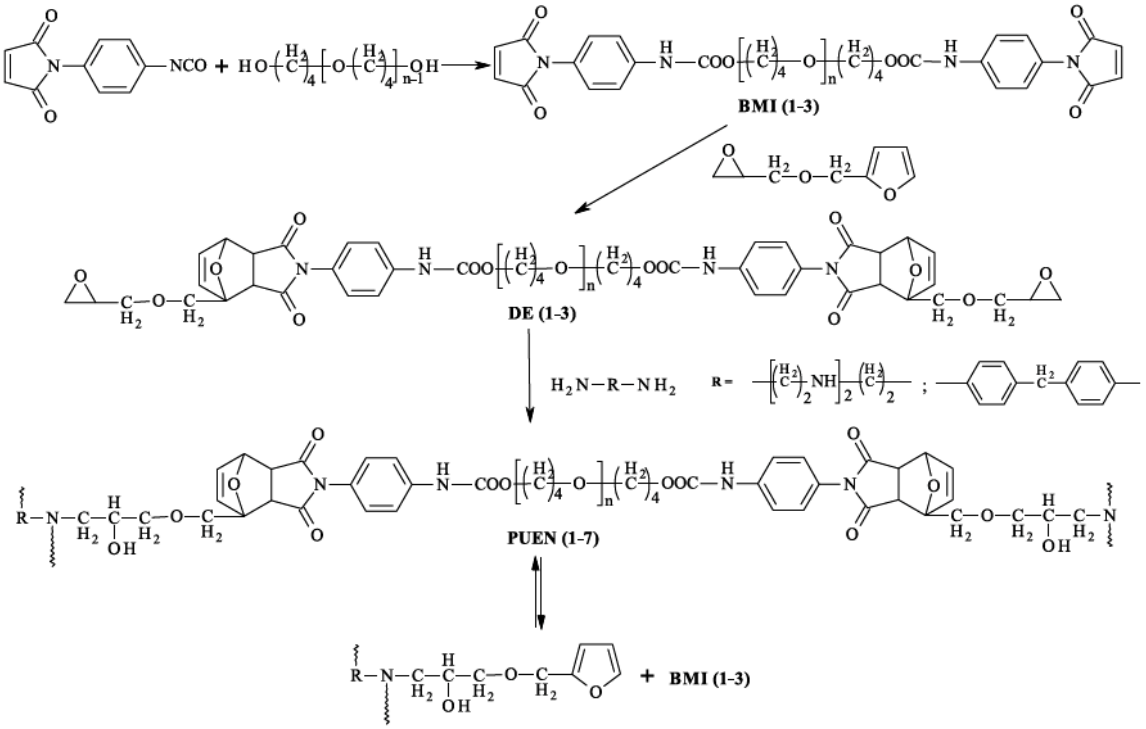

Figure 3.9 Synthetic route of thermoreversible epoxy-urethane networks by Diels-Alder reactions[191].

In the recent work of our lab, Djidi et al[192] used hydroxyl telechelic furan/maleimide DA adduct as reagents to synthesize thermosensitive polylactic acid PLA based networks via condensation with diisocyanates. The temperature to disrupt network structures varies from 40 to 130 °C depending on the node concentration of networks. Mhiri et al.[193] also used bifunctional DA adducts as reagents in one-shot method to obtain polyglycolic acid based networks involving polyglycolic acid-diol, glycerol and diisocyanate (Figure 3.10). The thermoreversible properties were verified by the repeatability of DA and rDA processes during heating-cooling cycle. When the functionality of furan functionalized polyglycolic acid was increased, denser networks were formed.

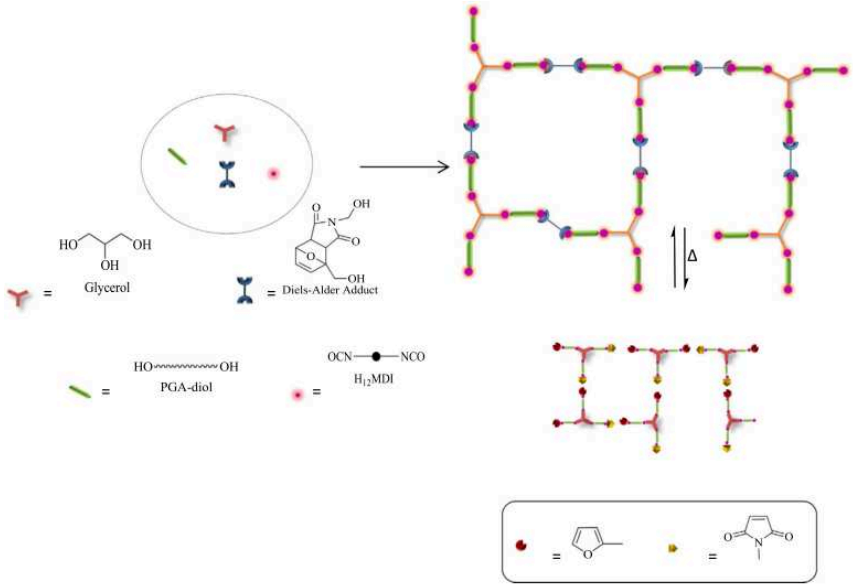

Figure 3.10 Schematic depiction of the synthesis of polyglycolic acid (PGA) based networks by Diels-Alder reactions[193].

3.4 Conclusions

In this section, one of the most widely used click reactions, Diels-Alder reaction, was introduced. Among various DA reactions, furan/maleimide coupling attracts the most attention due to their mild DA/rDA temperatures. The substituents on furan and maleimide rings can not only control the DA adducts stereoisomers of *exo* and *endo* but also change the reactivity and reversibility of DA reactions. Three main methods are generally used to construct networks by DA reactions, namely, (i) DA cycloaddition with multifunctional monomers, such as furan (maleimide) derivatives and bismaleimide (bisfuran); (ii) DA cycloaddition between linear polymers containing grafted furan and/or maleimide groups; (iii) polymerization involving DA linkages.

References

[1] B. Jiang, B. Akar, T.M. Waller, J.C. Larson, A.A. Appel, E.M. Brey, Design of a composite biomaterial system for tissue engineering applications, Acta Biomaterialia 10(3) (2014) 1177-1186.

[2] J.L. Ifkovits, J.A. Burdick, Review: Photopolymerizable and degradable biomaterials for tissue engineering applications, Tissue Engineering 13(10) (2007) 2369-2385.

[3] Y. Tang, C.L. Heaysman, S. Willis, A.L. Lewis, Physical hydrogels with self-assembled nanostructures as drug delivery systems, Expert opinion on drug delivery 8(9) (2011) 1141-59.

[4] C.T. Schwall, I.A. Banerjee, Micro- and Nanoscale Hydrogel Systems for Drug Delivery and Tissue Engineering, Materials 2(2) (2009) 577-612.

[5] J.J. Rice, M.M. Martino, L. De Laporte, F. Tortelli, P.S. Briquez, J.A. Hubbell, Engineering the Regenerative Microenvironment with Biomaterials, Advanced Healthcare Materials 2(1) (2013) 57-71.

[6] L.S. Nair, C.T. Laurencin, Biodegradable polymers as biomaterials, Progress in Polymer Science 32(8–9) (2007) 762-798.

[7] C.H. Lee, A. Singla, Y. Lee, Biomedical applications of collagen, International Journal of Pharmaceutics 221(1) (2001) 1-22.

[8] B. Kundu, R. Rajkhowa, S.C. Kundu, X. Wang, Silk fibroin biomaterials for tissue regenerations, Advanced Drug Delivery Reviews 65(4) (2013) 457-470.

[9] J.K. Francis Suh, H.W.T. Matthew, Application of chitosan-based polysaccharide biomaterials in cartilage tissue engineering: a review, Biomaterials 21(24) (2000) 2589-2598.

[10] G.-Q. Chen, Q. Wu, The application of polyhydroxyalkanoates as tissue engineering materials, Biomaterials 26(33) (2005) 6565-6578.

[11] N. Goonoo, A. Bhaw-Luximon, G.L. Bowlin, D. Jhurry, An assessment of biopolymer- and synthetic polymer-based scaffolds for bone and vascular tissue engineering, Polymer International 62(4) (2013) 523-533.

[12] R.P. Brannigan, A.P. Dove, Synthesis, properties and biomedical applications of hydrolytically degradable materials based on aliphatic polyesters and polycarbonates, Biomaterials science 5(1) (2017) 9-21.

[13] J. Kratsch, M. Kuzdrowska, M. Schmid, N. Kazeminejad, C. Kaub, P. Oña-Burgos, S.M. Guillaume, P.W. Roesky, Chiral Rare Earth Borohydride Complexes Supported by Amidinate Ligands: Synthesis, Structure, and Catalytic Activity in the Ring-Opening Polymerization of rac-Lactide, Organometallics 32(5) (2013) 1230-1238.

[14] H.A. Brown, A.G. De Crisci, J.L. Hedrick, R.M. Waymouth, Amidine-Mediated Zwitterionic Polymerization of Lactide, ACS Macro Letters 1(9) (2012) 1113-1115.

[15] J.M. Becker, S. Tempelaar, M.J. Stanford, R.J. Pounder, J.A. Covington, A.P. Dove, Development of Amino–Oxazoline and Amino–Thiazoline Organic Catalysts for the Ring-Opening Polymerisation of Lactide, Chemistry – A European Journal 16(20) (2010) 6099-6105.

[16] N.E. Kamber, W. Jeong, S. Gonzalez, J.L. Hedrick, R.M. Waymouth, N-Heterocyclic Carbenes for the Organocatalytic Ring-Opening Polymerization of ε-Caprolactone, Macromolecules 42(5) (2009) 1634-1639.

[17] K. Makiguchi, T. Satoh, T. Kakuchi, Diphenyl Phosphate as an Efficient Cationic Organocatalyst for Controlled/Living Ring-Opening Polymerization of δ-Valerolactone and ε-Caprolactone, Macromolecules 44(7) (2011) 1999-2005.

[18] C.G. Jaffredo, J.F. Carpentier, S.M. Guillaume, Controlled ROP of beta-butyrolactone simply mediated by amidine, guanidine, and phosphazene organocatalysts, Macromolecular rapid communications 33(22) (2012) 1938-44.

[19] K. Fukushima, Poly(trimethylene carbonate)-based polymers engineered for biodegradable functional biomaterials, Biomaterials science 4(1) (2016) 9-24.

[20] Y. Zhu, C. Romain, C.K. Williams, Sustainable polymers from renewable resources, Nature 540 (2016) 354.
[21] B. Guo, P.X. Ma, Synthetic biodegradable functional polymers for tissue engineering: a brief review, Science China Chemistry 57(4) (2014) 490-500.
[22] Z. Zhang, R. Kuijer, S.K. Bulstra, D.W. Grijpma, J. Feijen, The in vivo and in vitro degradation behavior of poly(trimethylene carbonate), Biomaterials 27(9) (2006) 1741-1748.
[23] L. Mespouille, O. Coulembier, M. Kawalec, A.P. Dove, P. Dubois, Implementation of metal-free ring-opening polymerization in the preparation of aliphatic polycarbonate materials, Progress in Polymer Science 39(6) (2014) 1144-1164.
[24] S.M. Guillaume, Recent advances in ring-opening polymerization strategies toward α,ω-hydroxy telechelic polyesters and resulting copolymers, European Polymer Journal 49(4) (2013) 768-779.
[25] H. Wu, Y. Ji, Z. Li, X. Wang, Q. Zhang, S. Cui, W. Wu, J. Liu, K. Guo, Cationic ring-opening polymerization of trimethylene carbonate to α,ω-dihydroxy telechelic and star-shaped polycarbonates catalyzed by reusable o-benzenedisulfonimide, Journal of Polymer Science Part A: Polymer Chemistry 53(6) (2015) 729-736.
[26] X. Wang, S. Cui, Z. Li, S. Kan, Q. Zhang, C. Zhao, H. Wu, J. Liu, W. Wu, K. Guo, A base–conjugate-acid pair for living/controlled ring-opening polymerization of trimethylene carbonate through hydrogen-bonding bifunctional synergistic catalysis, Polym. Chem. 5(20) (2014) 6051-6059.
[27] H.R. Kricheldorf, K. Ahrensdorf, S. Rost, Polylactones, 68 - Star-shaped homo- and copolyesters derived from epsilon-caprolactone, L,L-lactide and trimethylene carbonate, Macromolecular Chemistry and Physics 205(12) (2004) 1602-1610.
[28] A. Smola, P. Dobrzynski, M. Cristea, J. Kasperczyk, M. Sobota, K. Gebarowska, H. Janeczek, Bioresorbable terpolymers based on l-lactide, glycolide and trimethylene carbonate with shape memory behaviour, Polymer Chemistry 5(7) (2014) 2442-2452.
[29] C. Samuel, Y. Chalamet, F. Boisson, J.-C. Majesté, F. Becquart, E. Fleury, Highly efficient metal-free organic catalysts to design new Environmentally-friendly starch-based blends, Journal of Polymer Science Part A: Polymer Chemistry 52(4) (2014) 493-503.
[30] F. Becquart, Y. Chalamet, J. Chen, Y. Zhao, M. Taha, Poly[ethylene-co-(vinyl alcohol)]-graft-poly(ε-caprolactone) Synthesis by Reactive Extrusion, 1 - Structural and Kinetic Study, Macromolecular Materials and Engineering 294(10) (2009) 643-650.
[31] B.J. O'Keefe, M.A. Hillmyer, W.B. Tolman, Polymerization of lactide and related cyclic esters by discrete metal complexes, Journal of the Chemical Society, Dalton Transactions (15) (2001) 2215-2224.
[32] J. Matsuo, K. Aoki, F. Sanda, T. Endo, Substituent Effect on the Anionic Equilibrium Polymerization of Six-Membered Cyclic Carbonates, Macromolecules 31(14) (1998) 4432-4438.
[33] H.R. Kricheldorf, J. Jenssen, Polylactones. 16. Cationic Polymerization of Trimethylene Carbonate and Other Cyclic Carbonates, Journal of Macromolecular Science: Part A - Chemistry 26(4) (1989) 631-644.
[34] R.F. Storey, J.W. Sherman, Kinetics and Mechanism of the Stannous Octoate-Catalyzed Bulk Polymerization of ε-Caprolactone, Macromolecules 35(5) (2002) 1504-1512.
[35] A. Kowalski, A. Duda, S. Penczek, Kinetics and Mechanism of Cyclic Esters Polymerization Initiated with Tin(II) Octoate. 3. Polymerization of l,l-Dilactide, Macromolecules 33(20) (2000) 7359-7370.
[36] A. Kowalski, A. Duda, S. Penczek, Mechanism of Cyclic Ester Polymerization Initiated with Tin(II) Octoate. 2. Macromolecules Fitted with Tin(II) Alkoxide Species Observed Directly in MALDI−TOF Spectra, Macromolecules 33(3) (2000) 689-695.

[37] P. Dubois, R. Jérŏme, P. Teyssié, Aluminium alkoxides: A family of versatile initiators for the ring-opening polymerization of lactones and lactides, Makromolekulare Chemie. Macromolecular Symposia 42-43(1) (1991) 103-116.
[38] T.M. Ovitt, G.W. Coates, Stereoselective Ring-Opening Polymerization of meso-Lactide: Synthesis of Syndiotactic Poly(lactic acid), Journal of the American Chemical Society 121(16) (1999) 4072-4073.
[39] D.J. Darensbourg, O. Karroonnirun, Ring-Opening Polymerization of l-Lactide and ε-Caprolactone Utilizing Biocompatible Zinc Catalysts. Random Copolymerization of l-Lactide and ε-Caprolactone, Macromolecules 43(21) (2010) 8880-8886.
[40] M.H. Chisholm, J.C. Gallucci, K. Phomphrai, Well-Defined Calcium Initiators for Lactide Polymerization, Inorganic Chemistry 43(21) (2004) 6717-6725.
[41] D.J. Darensbourg, W. Choi, O. Karroonnirun, N. Bhuvanesh, Ring-Opening Polymerization of Cyclic Monomers by Complexes Derived from Biocompatible Metals. Production of Poly(lactide), Poly(trimethylene carbonate), and Their Copolymers, Macromolecules 41(10) (2008) 3493-3502.
[42] M. Save, M. Schappacher, A. Soum, Controlled Ring-Opening Polymerization of Lactones and Lactides Initiated by Lanthanum Isopropoxide, 1. General Aspects and Kinetics, Macromolecular Chemistry and Physics 203(5-6) (2002) 889-899.
[43] O. Dechy-Cabaret, B. Martin-Vaca, D. Bourissou, Controlled Ring-Opening Polymerization of Lactide and Glycolide, Chemical reviews 104(12) (2004) 6147-6176.
[44] C.M. Thomas, Stereocontrolled ring-opening polymerization of cyclic esters: synthesis of new polyester microstructures, Chemical Society reviews 39(1) (2010) 165-173.
[45] N.E. Kamber, W. Jeong, R.M. Waymouth, R.C. Pratt, B.G.G. Lohmeijer, J.L. Hedrick, Organocatalytic Ring-Opening Polymerization, Chemical Reviews 107(12) (2007) 5813-5840.
[46] K.S. Bisht, Y.Y. Svirkin, L.A. Henderson, R.A. Gross, D.L. Kaplan, G. Swift, Lipase-Catalyzed Ring-Opening Polymerization of Trimethylene Carbonate, Macromolecules 30(25) (1997) 7735-7742.
[47] H. Hyun, M.S. Kim, G. Khang, H.B. Lee, Ring-opening polymerization of trimethylene carbonate by poly(ethylene glycol) in the presence of HCl·Et2O as a monomer activator, Journal of Polymer Science Part A: Polymer Chemistry 44(13) (2006) 4235-4241.
[48] D. Delcroix, B. Martín-Vaca, D. Bourissou, C. Navarro, Ring-Opening Polymerization of Trimethylene Carbonate Catalyzed by Methanesulfonic Acid: Activated Monomer versus Active Chain End Mechanisms, Macromolecules 43(21) (2010) 8828-8835.
[49] F. Nederberg, B.G.G. Lohmeijer, F. Leibfarth, R.C. Pratt, J. Choi, A.P. Dove, R.M. Waymouth, J.L. Hedrick, Organocatalytic Ring Opening Polymerization of Trimethylene Carbonate, Biomacromolecules 8(1) (2007) 153-160.
[50] M. Helou, O. Miserque, J.-M. Brusson, J.-F. Carpentier, S.M. Guillaume, Organocatalysts for the Controlled "Immortal" Ring-Opening Polymerization of Six-Membered-Ring Cyclic Carbonates: A Metal-Free, Green Process, Chemistry – A European Journal 16(46) (2010) 13805-13813.
[51] M.K. Kiesewetter, M.D. Scholten, N. Kirn, R.L. Weber, J.L. Hedrick, R.M. Waymouth, Cyclic guanidine organic catalysts: what is magic about triazabicyclodecene?, The Journal of Organic Chemistry 74(24) (2009) 9490-6.
[52] R.C. Pratt, B.G.G. Lohmeijer, D.A. Long, R.M. Waymouth, J.L. Hedrick, Triazabicyclodecene: A Simple Bifunctional Organocatalyst for Acyl Transfer and Ring-Opening Polymerization of Cyclic Esters, Journal of the American Chemical Society 128(14) (2006) 4556-4557.
[53] A. Chuma, H.W. Horn, W.C. Swope, R.C. Pratt, L. Zhang, B.G.G. Lohmeijer, C.G. Wade, R.M. Waymouth, J.L. Hedrick, J.E. Rice, The Reaction Mechanism for the Organocatalytic Ring-Opening Polymerization of l-Lactide Using a Guanidine-Based Catalyst: Hydrogen-

Bonded or Covalently Bound?, Journal of the American Chemical Society 130(21) (2008) 6749-6754.
[54] L. Simón, J.M. Goodman, The Mechanism of TBD-Catalyzed Ring-Opening Polymerization of Cyclic Esters, The Journal of Organic Chemistry 72(25) (2007) 9656-9662.
[55] G. Becker, F.R. Wurm, Functional biodegradable polymers via ring-opening polymerization of monomers without protective groups, Chemical Society reviews 47(20) (2018) 7739-7782.
[56] M. Abubekerov, J. Wei, K.R. Swartz, Z. Xie, Q. Pei, P.L. Diaconescu, Preparation of multiblock copolymers via step-wise addition of l-lactide and trimethylene carbonate, Chemical Science 9(8) (2018) 2168-2178.
[57] S. Pandini, D. Dioni, K. Paderni, M. Messori, M. Toselli, E. Bontempi, T. Riccò, The two-way shape memory behaviour of crosslinked poly(ε-caprolactone) systems with largely varied network density, Journal of Intelligent Material Systems and Structures 27(10) (2016) 1388-1403.
[58] E. Bat, B.H.M. Kothman, G.A. Higuera, C.A. van Blitterswijk, J. Feijen, D.W. Grijpma, Ultraviolet light crosslinking of poly(trimethylene carbonate) for elastomeric tissue engineering scaffolds, Biomaterials 31(33) (2010) 8696-8705.
[59] D.M. Stevens, A. Rahalkar, B. Spears, K. Gilmore, E. Douglas, M. Muthukumar, E. Harth, Semibranched polyglycidols as “fillers” in polycarbonate hydrogels to tune hydrophobic drug release, Polymer Chemistry 6(7) (2015) 1096-1102.
[60] R.C. Pratt, F. Nederberg, R.M. Waymouth, J.L. Hedrick, Tagging alcohols with cyclic carbonate: a versatile equivalent of (meth)acrylate for ring-opening polymerization, Chemical communications (1) (2008) 114-116.
[61] M. Wang, J. Sun, Y. Zhai, H. Lian, C. Luo, L. Li, Y. Du, D. Zhang, W. Ding, S. Qiu, Y. Liu, L. Kou, X. Han, R. Xiang, Y. Wang, Z. He, Enteric Polymer Based on pH-Responsive Aliphatic Polycarbonate Functionalized with Vitamin E To Facilitate Oral Delivery of Tacrolimus, Biomacromolecules 16(4) (2015) 1179-1190.
[62] M. Helou, J.-F. Carpentier, S.M. Guillaume, Poly(carbonate-urethane): an isocyanate-free procedure from α, ω-di(cyclic carbonate) telechelic poly(trimethylene carbonate)s, Green Chemistry 13(2) (2011) 266-271.
[63] K. Fukushima, Biodegradable functional biomaterials exploiting substituted trimethylene carbonates and organocatalytic transesterification, Polym J 48(12) (2016) 1103-1114.
[64] H.-H. Zhang, Z.-Q. Huang, B.-W. Sun, J.-X. Guo, J.-L. Wang, Y.-Q. Chen, Y-Shaped Poly(ethylene glycol) and Poly(trimethylene carbonate) Amphiphilic Copolymer: Synthesis and for Drug Delivery, Journal Of Polymer Science Part a-Polymer Chemistry 46(24) (2008) 8131-8140.
[65] L.-Q. Yang, B. He, S. Meng, J.-Z. Zhang, M. Li, J. Guo, Y.-M. Guan, J.-X. Li, Z.-W. Gu, Biodegradable cross-linked poly(trimethylene carbonate) networks for implant applications: Synthesis and properties, Polymer 54(11) (2013) 2668-2675.
[66] S. Venkataraman, J.L. Hedrick, Y.Y. Yang, Fluorene-functionalized aliphatic polycarbonates: design, synthesis and aqueous self-assembly of amphiphilic block copolymers, Polymer Chemistry 5(6) (2014) 2035-2040.
[67] L. Yang, X. Tan, Z. Wang, X. Zhang, Supramolecular Polymers: Historical Development, Preparation, Characterization, and Functions, Chemical Reviews 115(15) (2015) 7196-7239.
[68] Y. Jin, C. Yu, R.J. Denman, W. Zhang, Recent advances in dynamic covalent chemistry, Chemical Society Reviews 42(16) (2013) 6634-6654.
[69] T. Ware, K. Hearon, A. Lonnecker, K.L. Wooley, D.J. Maitland, W. Voit, Triple-Shape Memory Polymers Based on Self-Complementary Hydrogen Bonding, Macromolecules 45(2) (2012) 1062-1069.

[70] A. Campanella, D. Döhler, W.H. Binder, Self-Healing in Supramolecular Polymers, Macromolecular Rapid Communications 39(17) (2018) 1700739.
[71] J.-M. Lehn, Supramolecular Chemistry—Scope and Perspectives Molecules, Supermolecules, and Molecular Devices (Nobel Lecture), Angewandte Chemie International Edition in English 27(1) (1988) 89-112.
[72] D.J. Cram, The Design of Molecular Hosts, Guests, and Their Complexes (Nobel Lecture), Angewandte Chemie International Edition in English 27(8) (1988) 1009-1020.
[73] C.J. Pedersen, The Discovery of Crown Ethers (Noble Lecture), Angewandte Chemie International Edition in English 27(8) (1988) 1021-1027.
[74] J.-M. Lehn, Supramolecular polymer chemistry—scope and perspectives, Polymer International 51(10) (2002) 825-839.
[75] J.-M. Lehn, Perspectives in Chemistry—Aspects of Adaptive Chemistry and Materials, Angewandte Chemie International Edition 54(11) (2015) 3276-3289.
[76] D.C. Sherrington, K.A. Taskinen, Self-assembly in synthetic macromolecular systems multiple hydrogen bonding interactions, Chemical Society Reviews 30(2) (2001) 83-93.
[77] L. Brunsveld, B.J.B. Folmer, E.W. Meijer, R.P. Sijbesma, Supramolecular Polymers, Chemical reviews 101(12) (2001) 4071-4098.
[78] M. Wathier, M.W. Grinstaff, Synthesis and Properties of Supramolecular Ionic Networks, Journal of the American Chemical Society 130(30) (2008) 9648-9649.
[79] G. Cavallo, P. Metrangolo, R. Milani, T. Pilati, A. Priimagi, G. Resnati, G. Terraneo, The Halogen Bond, Chemical reviews 116(4) (2016) 2478-601.
[80] L.C. Gilday, S.W. Robinson, T.A. Barendt, M.J. Langton, B.R. Mullaney, P.D. Beer, Halogen Bonding in Supramolecular Chemistry, Chemical reviews 115(15) (2015) 7118-95.
[81] T.R. Cook, Y.-R. Zheng, P.J. Stang, Metal–Organic Frameworks and Self-Assembled Supramolecular Coordination Complexes: Comparing and Contrasting the Design, Synthesis, and Functionality of Metal–Organic Materials, Chemical Reviews 113(1) (2013) 734-777.
[82] B.J. Holliday, C.A. Mirkin, Strategies for the Construction of Supramolecular Compounds through Coordination Chemistry, Angewandte Chemie International Edition 40(11) (2001) 2022-2043.
[83] J. Szejtli, Introduction and General Overview of Cyclodextrin Chemistry, Chemical Reviews 98(5) (1998) 1743-1754.
[84] A. Harada, A. Hashidzume, H. Yamaguchi, Y. Takashima, Polymeric Rotaxanes, Chemical Reviews 109(11) (2009) 5974-6023.
[85] G. Yu, K. Jie, F. Huang, Supramolecular Amphiphiles Based on Host–Guest Molecular Recognition Motifs, Chemical Reviews 115(15) (2015) 7240-7303.
[86] X. Ma, Y. Zhao, Biomedical Applications of Supramolecular Systems Based on Host–Guest Interactions, Chemical Reviews 115(15) (2015) 7794-7839.
[87] Y. Takashima, Y. Sawa, K. Iwaso, M. Nakahata, H. Yamaguchi, A. Harada, Supramolecular Materials Cross-Linked by Host–Guest Inclusion Complexes: The Effect of Side Chain Molecules on Mechanical Properties, Macromolecules 50(8) (2017) 3254-3261.
[88] S. Grimme, Do Special Noncovalent π–π Stacking Interactions Really Exist?, Angewandte Chemie International Edition 47(18) (2008) 3430-3434.
[89] F.J.M. Hoeben, P. Jonkheijm, E.W. Meijer, A.P.H.J. Schenning, About Supramolecular Assemblies of π-Conjugated Systems, Chemical Reviews 105(4) (2005) 1491-1546.
[90] T. Rossow, S. Seiffert, Supramolecular Polymer Networks: Preparation, Properties, and Potential, in: Supramolecular Polymer Networks and Gels, S. Seiffert (Ed.), Springer International Publishing, Cham, 2015, Vol., pp. 1-46.
[91] M.J. Krische, J.-M. Lehn, The Utilization of Persistent H-Bonding Motifs in the Self-Assembly of Supramolecular Architectures, in: Molecular Self-Assembly Organic Versus

Inorganic Approaches, M. Fuiita (Ed.), Springer Berlin Heidelberg, Berlin, Heidelberg, 2000, Vol., pp. 3-29.
[92] R.P. Sijbesma, E.W. Meijer, Self-assembly of well-defined structures by hydrogen bonding, Current Opinion in Colloid & Interface Science 4(1) (1999) 24-32.
[93] D.B. Varshey, J.R.G. Sander, Tomislav Friˇsˇci´c, L.R. MacGillivray, Supramolecular Chemistry: From Molecules to Nanomaterials, John Wiley & Sons, Ltd., NewYork, 2012.
[94] T. Steiner, The Hydrogen Bond in the Solid State, Angewandte Chemie International Edition 41(1) (2002) 48-76.
[95] B. Perlmutter-Hayman, Cooperative binding to macromolecules. A formal approach, Accounts of Chemical Research 19(3) (1986) 90-96.
[96] R.P. Sijbesma, E.W. Meijer, Quadruple hydrogen bonded systems, Chemical Communications (1) (2003) 5-16.
[97] J.P. WL Jorgensen, Importance of Secondary Interactions in Triply Hydrogen Bonded Complexes: Guanine-Cytosine vs Uracil-2,6-Diaminopyridine, Journal of the American Chemical Society 112 (1990) 2008-2010.
[98] J. Pranata, S.G. Wierschke, W.L. Jorgensen, OPLS potential functions for nucleotide bases. Relative association constants of hydrogen-bonded base pairs in chloroform, Journal of the American Chemical Society 113(8) (1991) 2810-2819.
[99] S.C. Zimmerman, P.S. Corbin, Heteroaromatic Modules for Self-Assembly Using Multiple Hydrogen Bonds, in: Molecular Self-Assembly Organic Versus Inorganic Approaches, M. Fuiita (Ed.), Springer Berlin Heidelberg, Berlin, Heidelberg, 2000, Vol., pp. 63-94.
[100] Y.S. Kyung, Z.S. C., Hydrogen Bonding Modules for Use in Supramolecular Polymers, Israel Journal of Chemistry 53(8) (2013) 511-520.
[101] V. Brandani, A continuous linear association model for determining the enthalpy of hydrogen-bond formation and the equilibrium association constant for pure hydrogen-bonded liquids, Fluid Phase Equilibria 12(1) (1983) 87-104.
[102] T.J. Murray, S.C. Zimmerman, New triply hydrogen bonded complexes with highly variable stabilities, Journal of the American Chemical Society 114(10) (1992) 4010-4011.
[103] F.H. Beijer, H. Kooijman, A.L. Spek, R.P. Sijbesma, E.W. Meijer, Self-Complementarity Achieved through Quadruple Hydrogen Bonding, Angewandte Chemie International Edition 37(1-2) (1998) 75-78.
[104] R.P. Sijbesma, F.H. Beijer, L. Brunsveld, B.J.B. Folmer, J.H.K.K. Hirschberg, R.F.M. Lange, J.K.L. Lowe, E.W. Meijer, Reversible Polymers Formed from Self-Complementary Monomers Using Quadruple Hydrogen Bonding, Science 278(5343) (1997) 1601-1604.
[105] G.B.W.L. Ligthart, H. Ohkawa, R.P. Sijbesma, E.W. Meijer, Complementary Quadruple Hydrogen Bonding in Supramolecular Copolymers, Journal of the American Chemical Society 127(3) (2005) 810-811.
[106] T. Park, S.C. Zimmerman, S. Nakashima, A Highly Stable Quadruply Hydrogen-Bonded Heterocomplex Useful for Supramolecular Polymer Blends, Journal of the American Chemical Society 127(18) (2005) 6520-6521.
[107] B.A. Blight, C.A. Hunter, D.A. Leigh, H. McNab, P.I.T. Thomson, An AAAA–DDDD quadruple hydrogen-bond array, Nature Chemistry 3(3) (2011) 244-248.
[108] S.K. Chang, A.D. Hamilton, Molecular recognition of biologically interesting substrates: synthesis of an artificial receptor for barbiturates employing six hydrogen bonds, Journal of the American Chemical Society 110(4) (1988) 1318-1319.
[109] H. Zeng, X. Yang, A.L. Brown, S. Martinovic, R.D. Smith, B. Gong, An extremely stable, self-complementary hydrogen-bonded duplex, Chemical Communications (13) (2003) 1556-1557.

[110] U. Lüning, C. Kühl, A. Uphoff, Four Hydrogen Bonds − DDAA, DADA, DAAD and ADDA Hydrogen Bond Motifs, European Journal of Organic Chemistry 2002(23) (2002) 4063-4070.
[111] S.H.M. Söntjens, R.P. Sijbesma, M.H.P. van Genderen, E.W. Meijer, Stability and Lifetime of Quadruply Hydrogen Bonded 2-Ureido-4[1H]-pyrimidinone Dimers, Journal of the American Chemical Society 122(31) (2000) 7487-7493.
[112] K. Liu, Y. Kang, Z. Kang, X. Zhang, 25th Anniversary Article: Reversible and Adaptive Functional Supramolecular Materials: "Noncovalent Interaction" Matters, Advanced Materials 25(39) (2013) 5530-5548.
[113] H. Goldansaz, C.-A. Fustin, M. Wübbenhorst, E. van Ruymbeke, How Supramolecular Assemblies Control Dynamics of Associative Polymers: Toward a General Picture, Macromolecules 49(5) (2016) 1890-1902.
[114] W.C. Yount, D.M. Loveless, S.L. Craig, Strong Means Slow: Dynamic Contributions to the Bulk Mechanical Properties of Supramolecular Networks, Angewandte Chemie International Edition 44(18) (2005) 2746-2748.
[115] W.C. Yount, D.M. Loveless, S.L. Craig, Small-Molecule Dynamics and Mechanisms Underlying the Macroscopic Mechanical Properties of Coordinatively Cross-Linked Polymer Networks, Journal of the American Chemical Society 127(41) (2005) 14488-14496.
[116] R.K. Bose, N. Hohlbein, S.J. Garcia, A.M. Schmidt, S. van der Zwaag, Relationship between the network dynamics, supramolecular relaxation time and healing kinetics of cobalt poly(butyl acrylate) ionomers, Polymer 69 (2015) 228-232.
[117] R.K. Bose, N. Hohlbein, S.J. Garcia, A.M. Schmidt, S. van der Zwaag, Connecting supramolecular bond lifetime and network mobility for scratch healing in poly(butyl acrylate) ionomers containing sodium, zinc and cobalt, Physical Chemistry Chemical Physics 17(3) (2015) 1697-1704.
[118] T. Aida, E.W. Meijer, S.I. Stupp, Functional Supramolecular Polymers, Science 335(6070) (2012) 813-817.
[119] M.E. Cates, Reptation of living polymers: dynamics of entangled polymers in the presence of reversible chain-scission reactions, Macromolecules 20(9) (1987) 2289-2296.
[120] S. Seiffert, J. Sprakel, Physical chemistry of supramolecular polymer networks, Chemical Society Reviews 41(2) (2012) 909-930.
[121] M. Krutyeva, A.R. Brás, W. Antonius, C.H. Hövelmann, A.S. Poulos, J. Allgaier, A. Radulescu, P. Lindner, W. Pyckhout-Hintzen, A. Wischnewski, D. Richter, Association Behavior, Diffusion, and Viscosity of End-Functionalized Supramolecular Poly(ethylene glycol) in the Melt State, Macromolecules 48(24) (2015) 8933-8946.
[122] C.L. Lewis, K. Stewart, M. Anthamatten, The Influence of Hydrogen Bonding Side-Groups on Viscoelastic Behavior of Linear and Network Polymers, Macromolecules 47(2) (2014) 729-740.
[123] L. Zhang, S.J. Rowan, Effect of Sterics and Degree of Cross-Linking on the Mechanical Properties of Dynamic Poly(alkylurea–urethane) Networks, Macromolecules 50(13) (2017) 5051-5060.
[124] D.J.M. van Beek, A.J.H. Spiering, G.W.M. Peters, K. te Nijenhuis, R.P. Sijbesma, Unidirectional Dimerization and Stacking of Ureidopyrimidinone End Groups in Polycaprolactone Supramolecular Polymers, Macromolecules 40(23) (2007) 8464-8475.
[125] Q. Liu, C. Wang, Y. Guo, C. Peng, A. Narayanan, S. Kaur, Y. Xu, R.A. Weiss, A. Joy, Opposing Effects of Side-Chain Flexibility and Hydrogen Bonding on the Thermal, Mechanical, and Rheological Properties of Supramolecularly Cross-Linked Polyesters, Macromolecules 51(22) (2018) 9294-9305.
[126] Q. Chen, G.J. Tudryn, R.H. Colby, Ionomer dynamics and the sticky Rouse model, Journal of Rheology 57(5) (2013) 1441-1462.

[127] A. Jangizehi, S.R. Ghaffarian, W. Schmolke, S. Seiffert, Dominance of Chain Entanglement over Transient Sticking on Chain Dynamics in Hydrogen-Bonded Supramolecular Polymer Networks in the Melt, Macromolecules 51(8) (2018) 2859-2871.
[128] X. Callies, C. Fonteneau, C. Véchambre, S. Pensec, J.M. Chenal, L. Chazeau, L. Bouteiller, G. Ducouret, C. Creton, Linear rheology of bis-urea functionalized supramolecular poly(butylacrylate)s: Part I – weak stickers, Polymer 69 (2015) 233-240.
[129] X. Callies, C. Véchambre, C. Fonteneau, S. Pensec, J.M. Chenal, L. Chazeau, L. Bouteiller, G. Ducouret, C. Creton, Linear Rheology of Supramolecular Polymers Center-Functionalized with Strong Stickers, Macromolecules 48(19) (2015) 7320-7326.
[130] A. Noro, Y. Matsushita, T.P. Lodge, Thermoreversible Supramacromolecular Ion Gels via Hydrogen Bonding, Macromolecules 41(15) (2008) 5839-5844.
[131] A. Noro, Y. Matsushita, T.P. Lodge, Gelation Mechanism of Thermoreversible Supramacromolecular Ion Gels via Hydrogen Bonding, Macromolecules 42(15) (2009) 5802-5810.
[132] F. Herbst, K. Schröter, I. Gunkel, S. Gröger, T. Thurn-Albrecht, J. Balbach, W.H. Binder, Aggregation and Chain Dynamics in Supramolecular Polymers by Dynamic Rheology: Cluster Formation and Self-Aggregation, Macromolecules 43(23) (2010) 10006-10016.
[133] F. Herbst, S. Seiffert, W.H. Binder, Dynamic supramolecular poly(isobutylene)s for self-healing materials, Polymer Chemistry 3(11) (2012) 3084-3092.
[134] K. Jud, H.H. Kausch, J.G. Williams, Fracture mechanics studies of crack healing and welding of polymers, Journal of Materials Science 16(1) (1981) 204-210.
[135] N. Roy, E. Buhler, J.-M. Lehn, The Tris-Urea Motif and Its Incorporation into Polydimethylsiloxane-Based Supramolecular Materials Presenting Self-Healing Features, Chemistry – A European Journal 19(27) (2013) 8814-8820.
[136] L.M. de Espinosa, G.L. Fiore, C. Weder, E. Johan Foster, Y.C. Simon, Healable supramolecular polymer solids, Progress in Polymer Science 49-50 (2015) 60-78.
[137] R.J. Wojtecki, M.A. Meador, S.J. Rowan, Using the dynamic bond to access macroscopically responsive structurally dynamic polymers, Nat Mater 10(1) (2011) 14-27.
[138] K. Chino, M. Ashiura, Themoreversible Cross-Linking Rubber Using Supramolecular Hydrogen-Bonding Networks, Macromolecules 34(26) (2001) 9201-9204.
[139] P. Cordier, F. Tournilhac, C. Soulie-Ziakovic, L. Leibler, Self-healing and thermoreversible rubber from supramolecular assembly, Nature 451(7181) (2008) 977-980.
[140] L. Yang, Y. Lin, L. Wang, A. Zhang, The synthesis and characterization of supramolecular elastomers based on linear carboxyl-terminated polydimethylsiloxane oligomers, Polymer Chemistry 5(1) (2014) 153-160.
[141] Y. Chen, A.M. Kushner, G.A. Williams, Z. Guan, Multiphase design of autonomic self-healing thermoplastic elastomers, Nat Chem 4(6) (2012) 467-472.
[142] Z.-C. Jiang, Y.-Y. Xiao, Y. Kang, M. Pan, B.-J. Li, S. Zhang, Shape Memory Polymers Based on Supramolecular Interactions, ACS Applied Materials & Interfaces 9(24) (2017) 20276-20293.
[143] M.D. Hager, S. Bode, C. Weber, U.S. Schubert, Shape memory polymers: Past, present and future developments, Progress in Polymer Science 49–50 (2015) 3-33.
[144] S. Chen, J. Hu, H. Zhuo, C. Yuen, L. Chan, Study on the thermal-induced shape memory effect of pyridine containing supramolecular polyurethane, Polymer 51(1) (2010) 240-248.
[145] M. Wei, M. Zhan, D. Yu, H. Xie, M. He, K. Yang, Y. Wang, Novel Poly(tetramethylene ether)glycol and Poly(ε-caprolactone) Based Dynamic Network via Quadruple Hydrogen Bonding with Triple-Shape Effect and Self-Healing Capacity, ACS Applied Materials & Interfaces 7(4) (2015) 2585-2596.
[146] C. Creton, Pressure-Sensitive Adhesives: An Introductory Course, MRS Bulletin 28(6) (2011) 434-439.

[147] J. Courtois, I. Baroudi, N. Nouvel, E. Degrandi, S. Pensec, G. Ducouret, C. Chanéac, L. Bouteiller, C. Creton, Supramolecular Soft Adhesive Materials, Advanced Functional Materials 20(11) (2010) 1803-1811.
[148] X. Callies, C. Fonteneau, S. Pensec, L. Bouteiller, G. Ducouret, C. Creton, Adhesion and non-linear rheology of adhesives with supramolecular crosslinking points, Soft Matter 12(34) (2016) 7174-7185.
[149] X. Callies, O. Herscher, C. Fonteneau, A. Robert, S. Pensec, L. Bouteiller, G. Ducouret, C. Creton, Combined Effect of Chain Extension and Supramolecular Interactions on Rheological and Adhesive Properties of Acrylic Pressure-Sensitive Adhesives, ACS Applied Materials & Interfaces 8(48) (2016) 33307-33315.
[150] H.C. Kolb, M.G. Finn, K.B. Sharpless, Click Chemistry: Diverse Chemical Function from a Few Good Reactions, Angewandte Chemie International Edition 40(11) (2001) 2004-2021.
[151] W.H. Binder, R. Sachsenhofer, 'Click' Chemistry in Polymer and Materials Science, Macromolecular Rapid Communications 28(1) (2007) 15-54.
[152] J.E. Moses, A.D. Moorhouse, The growing applications of click chemistry, Chemical Society Reviews 36(8) (2007) 1249-1262.
[153] Y. Dai, X. Zhang, F. Xia, Click Chemistry in Functional Aliphatic Polycarbonates, Macromolecular Rapid Communications 38(19) (2017) 1700357.
[154] M.A. Tasdelen, Diels–Alder "click" reactions: recent applications in polymer and material science, Polymer Chemistry 2(10) (2011) 2133.
[155] A.J. Inglis, L. Nebhani, O. Altintas, F.G. Schmidt, C. Barner-Kowollik, Rapid Bonding/Debonding on Demand: Reversibly Cross-Linked Functional Polymers via Diels−Alder Chemistry, Macromolecules 43(13) (2010) 5515-5520.
[156] L. Rulíšek, P. Šebek, Z. Havlas, R. Hrabal, P. Čapek, A. Svatoš, An Experimental and Theoretical Study of Stereoselectivity of Furan−Maleic Anhydride and Furan−Maleimide Diels−Alder Reactions, The Journal of Organic Chemistry 70(16) (2005) 6295-6302.
[157] C. Judit, F. Hartmut, D.W. Gijsbertus, v.B.R.A.T. M., Stereoisomeric effects in thermo-remendable polymer networks based on Diels–Alder crosslink reactions, Journal of Polymer Science Part A: Polymer Chemistry 48(15) (2010) 3456-3467.
[158] E.H. Discekici, A.H. St. Amant, S.N. Nguyen, I.-H. Lee, C.J. Hawker, J. Read de Alaniz, Endo and Exo Diels–Alder Adducts: Temperature-Tunable Building Blocks for Selective Chemical Functionalization, Journal of the American Chemical Society 140(15) (2018) 5009-5013.
[159] J.R. McElhanon, D.R. Wheeler, Thermally Responsive Dendrons and Dendrimers Based on Reversible Furan-Maleimide Diels−Alder Adducts, Organic Letters 3(17) (2001) 2681-2683.
[160] A. Gandini, D. Coelho, A.J.D. Silvestre, Reversible click chemistry at the service of macromolecular materials. Part 1: Kinetics of the Diels–Alder reaction applied to furan–maleimide model compounds and linear polymerizations, European Polymer Journal 44(12) (2008) 4029-4036.
[161] V. Froidevaux, M. Borne, E. Laborbe, R. Auvergne, A. Gandini, B. Boutevin, Study of the Diels-Alder and retro-Diels-Alder reaction between furan derivatives and maleimide for the creation of new materials, RSC Advances 5(47) (2015) 37742-37754.
[162] R.J. Pearson, E. Kassianidis, D. Philp, A completely selective and strongly accelerated Diels–Alder reaction mediated by hydrogen bonding, Tetrahedron Letters 45(24) (2004) 4777-4780.
[163] A. Gandini, The furan/maleimide Diels–Alder reaction: A versatile click–unclick tool in macromolecular synthesis, Progress in Polymer Science 38(1) (2013) 1-29.
[164] B. Gacal, H. Durmaz, M.A. Tasdelen, G. Hizal, U. Tunca, Y. Yagci, A.L. Demirel, Anthracene−Maleimide-Based Diels−Alder "Click Chemistry" as a Novel Route to Graft Copolymers, Macromolecules 39(16) (2006) 5330-5336.

[165] M. Wiessler, W. Waldeck, C. Kliem, R. Pipkorn, K. Braun, The Diels-Alder-reaction with inverse-electron-demand, a very efficient versatile click-reaction concept for proper ligation of variable molecular partners, International journal of medical sciences 7(1) (2009) 19-28.
[166] A.J. Inglis, S. Sinnwell, M.H. Stenzel, C. Barner-Kowollik, Ultrafast Click Conjugation of Macromolecular Building Blocks at Ambient Temperature, Angewandte Chemie International Edition 48(13) (2009) 2411-2414.
[167] Y.N. Yuksekdag, T.N. Gevrek, A. Sanyal, Diels-Alder "Clickable" Polymer Brushes: A Versatile Catalyst-Free Conjugation Platform, ACS Macro Letters 6(4) (2017) 415-420.
[168] A. Duval, H. Lange, M. Lawoko, C. Crestini, Reversible crosslinking of lignin via the furan-maleimide Diels-Alder reaction, Green Chemistry 17(11) (2015) 4991-5000.
[169] M. Watanabe, N. Yoshie, Synthesis and properties of readily recyclable polymers from bisfuranic terminated poly(ethylene adipate) and multi-maleimide linkers, Polymer 47(14) (2006) 4946-4952.
[170] R.C. Boutelle, B.H. Northrop, Substituent Effects on the Reversibility of Furan–Maleimide Cycloadditions, The Journal of Organic Chemistry 76(19) (2011) 7994-8002.
[171] K. Ishida, V. Weibel, N. Yoshie, Substituent effect on structure and physical properties of semicrystalline Diels–Alder network polymers, Polymer 52(13) (2011) 2877-2882.
[172] J. Kötteritzsch, S. Stumpf, S. Hoeppener, J. Vitz, M.D. Hager, U.S. Schubert, One-Component Intrinsic Self-Healing Coatings Based on Reversible Crosslinking by Diels–Alder Cycloadditions, Macromolecular Chemistry and Physics 214(14) (2013) 1636-1649.
[173] L. Feng, Z. Yu, Y. Bian, J. Lu, X. Shi, C. Chai, Self-healing behavior of polyurethanes based on dual actions of thermo-reversible Diels-Alder reaction and thermal movement of molecular chains, Polymer 124 (2017) 48-59.
[174] P. Du, X. Liu, Z. Zheng, X. Wang, T. Joncheray, Y. Zhang, Synthesis and characterization of linear self-healing polyurethane based on thermally reversible Diels-Alder reaction, RSC Advances 3(35) (2013) 15475-15482.
[175] L. Yuan, Z. Wang, M.S. Ganewatta, M.A. Rahman, M.E. Lamm, C. Tang, A biomass approach to mendable bio-elastomers, Soft Matter 13(6) (2017) 1306-1313.
[176] G. Zhang, Q. Zhao, L. Yang, W. Zou, X. Xi, T. Xie, Exploring Dynamic Equilibrium of Diels–Alder Reaction for Solid State Plasticity in Remoldable Shape Memory Polymer Network, ACS Macro Letters 5(7) (2016) 805-808.
[177] X. Kuang, G. Liu, X. Dong, D. Wang, Triple-shape memory epoxy based on Diels–Alder adduct molecular switch, Polymer 84 (2016) 1-9.
[178] J.M. Raquez, S. Vanderstappen, F. Meyer, P. Verge, M. Alexandre, J.M. Thomassin, C. Jérôme, P. Dubois, Design of Cross-Linked Semicrystalline Poly(ε-caprolactone)-Based Networks with One-Way and Two-Way Shape-Memory Properties through Diels–Alder Reactions, Chemistry – A European Journal 17(36) (2011) 10135-10143.
[179] S. Yu, R. Zhang, Q. Wu, T. Chen, P. Sun, Bio-Inspired High-Performance and Recyclable Cross-Linked Polymers, Advanced Materials 25(35) (2013) 4912-4917.
[180] T. Eliane, L.T. M., C.A.J. F., G. Alessandro, Recycling Tires? Reversible Crosslinking of Poly(butadiene), Advanced Materials 27(13) (2015) 2242-2245.
[181] P. Berto, A. Pointet, C. Le Coz, S. Grelier, F. Peruch, Recyclable Telechelic Cross-Linked Polybutadiene Based on Reversible Diels–Alder Chemistry, Macromolecules 51(3) (2018) 651-659.
[182] J. Bai, H. Li, Z. Shi, J. Yin, An Eco-Friendly Scheme for the Cross-Linked Polybutadiene Elastomer via Thiol–Ene and Diels–Alder Click Chemistry, Macromolecules 48(11) (2015) 3539-3546.
[183] J. Bai, H. Li, Z. Shi, M. Tian, J. Yin, Dynamic crosslinked poly(styrene-block-butadiene-block-styrene) via Diels-Alder chemistry: an ideal method to improve solvent resistance and

mechanical properties without losing its thermal plastic behavior, RSC Advances 5(56) (2015) 45376-45383.
[184] A. Duval, G. Couture, S. Caillol, L. Avérous, Biobased and Aromatic Reversible Thermoset Networks from Condensed Tannins via the Diels−Alder Reaction, ACS Sustainable Chemistry & Engineering 5(1) (2017) 1199-1207.
[185] H.-L. Wei, Z. Yang, Y. Chen, H.-J. Chu, J. Zhu, Z.-C. Li, Characterisation of N-vinyl-2-pyrrolidone-based hydrogels prepared by a Diels–Alder click reaction in water, European Polymer Journal 46(5) (2010) 1032-1039.
[186] H.-L. Wei, Z. Yang, H.-J. Chu, J. Zhu, Z.-C. Li, J.-S. Cui, Facile preparation of poly(N-isopropylacrylamide)-based hydrogels via aqueous Diels–Alder click reaction, Polymer 51(8) (2010) 1694-1702.
[187] T. Defize, R. Riva, J.-M. Raquez, P. Dubois, C. Jérôme, M. Alexandre, Thermoreversibly Crosslinked Poly(ε-caprolactone) as Recyclable Shape-Memory Polymer Network, Macromolecular Rapid Communications 32(16) (2011) 1264-1269.
[188] T. Defize, J.-M. Thomassin, M. Alexandre, B. Gilbert, R. Riva, C. Jérôme, Comprehensive study of the thermo-reversibility of Diels–Alder based PCL polymer networks, Polymer 84 (2016) 234-242.
[189] S.A. Stewart, M. Backholm, N.A.D. Burke, H.D.H. Stöver, Cross-Linked Hydrogels Formed through Diels–Alder Coupling of Furan- and Maleimide-Modified Poly(methyl vinyl ether-alt-maleic acid), Langmuir 32(7) (2016) 1863-1870.
[190] S. Magana, A. Zerroukhi, C. Jegat, N. Mignard, Thermally reversible crosslinked polyethylene using Diels–Alder reaction in molten state, Reactive and Functional Polymers 70(7) (2010) 442-448.
[191] V. Gaina, O. Ursache, C. Gaina, E. Buruiana, Novel Thermally-Reversible Epoxy-Urethane Networks, Designed Monomers and Polymers 15(1) (2012) 63-73.
[192] D. Djidi, N. Mignard, M. Taha, Thermosensitive polylactic-acid-based networks, Industrial Crops and Products 72 (2015) 220-230.
[193] S. Mhiri, N. Mignard, M. Abid, F. Prochazka, J.-C. Majeste, M. Taha, Thermally reversible and biodegradable polyglycolic-acid-based networks, European Polymer Journal 88 (2017) 292-310.

Chapter 2. Synthesis of poly(trimethylene carbonate) (PTMC) oligomers by ring-opening polymerization in bulk

Xiang Li[a,b,c], Nathalie Mignard[a,b,c], Mohamed Taha[a,b,c], Carlos Fernandez-de-Alba[a,b,d], Jianding Chen[e], Shengmiao Zhang[e] and Frédéric Becquart[a,b,c,*]

[a]Université de Lyon, F-42023 Saint-Etienne, France

[b]CNRS, UMR 5223, Ingénierie des Matériaux Polymères, F-42023 Saint-Etienne, France

[c]Université Jean Monnet, F-42023 Saint-Etienne, France

[d]INSA-Lyon, Ingénierie des Matériaux Polymères, F-69621 Villeurbanne, France

[e]Laboratory of Advanced Materials Processing, East China University of Science and Technology, 200237 Shanghai, China

[*]Corresponding Author. E-mail: Frederic.Becquart@univ-st-etienne.fr

Abstract

Poly(trimethylene carbonate) (PTMC) is a biocompatible and biodegradable polymer but studies about PTMC oligomer syntheses and characterizations remain rare. In this work, telechelic PTMC oligomers were synthesized with targeted low molar masses between 300 and 5000 g/mol in bulk by ring-opening polymerization (ROP) with 1,3-dioxan-2-one (trimethylene carbonate or TMC) as monomer and 1,4-butanediol (BDO) as co-initiator to start ROP from its hydroxyl functions. The 1,5,7-triazabicyclo[4.4.0]dec-5-ene organic catalyst (TBD) and tin(II) bis(2-ethylhexanoate) ($Sn(Oct)_2$) organometallic initiator were chosen comparatively. Due to the bi-functionality of BDO and relatively low TMC/BDO ratios, it was proved that PTMC chains were elaborated from one and both the BDO alcohol functions which consequently produce two coexisting kinds of PTMC chains with a BDO radical at the chain end or in the backbone when it is bifunctional. Additionally, PTMC chains were able to bear permanent and fast exchange reactions, leading to a dynamic redistribution of chains with possibly up to five BDO radicals in PTMC chains as well as chains without the BDO pattern. Longer reaction times and lower TMC/BDO molar ratios showed more predominant alcohol/carbonate exchange reactions. Surprisingly, these redistributions were intense at 100 °C and proved by coupling NMR and Maldi-Tof spectroscopies. Better average molar masses control and narrower distributions were obtained with TBD as compared to $Sn(Oct)_2$ and molar masses could be predicted simply with the TMC/BDO feed ratio. Kinetically, TBD was also more

efficient than $Sn(Oct)_2$. Finally, the complex viscosity and modulus were studied to show their increment with PTMC molar masses at 30°C with no chain entanglements. Then, the glass transition temperature T_g and onset decomposition temperature T_{onset} were found to raise by increasing PTMC oligomer molar mass.

Keywords: Poly(trimethylene carbonate), ring-opening polymerization, TBD, exchange reaction

1. Introduction

Nowadays, bio-based polyesters are widely used materials in the biomedical field, among which poly(lactide acid) (PLA) is certainly the most promising at the moment[1]. However, the drastic decrease of its mechanical properties during biological degradation as well as the generated acetic and propanoic acids, which may induce inflammatory responses, limit its applications in drug delivery formulations and temporary implants[2,3]. At the same time, another biodegradable material, poly(trimethylene carbonate) (PTMC), seems interesting as a substitute for PLA in the biomedical field, although its characteristics are somewhat different, such as its thermal and viscoelastic properties. Among its advantages, 1,3-dioxan-2-one (trimethylene carbonate or TMC) monomers can be bio-based because their synthetic raw materials 1,3-propanediol and dialkyl carbonates can derive respectively from renewable resources and carbon dioxide[4]. Furthermore, PTMC degradation has unique characteristics compared to a majority of aliphatic polyesters, namely the material's resistance to non-enzymatic hydrolysis. Moreover, its decomposition products contain no organic acids, preventing potential inflammatory responses. Good mechanical properties can also be maintained sustainably due to a degradation process occurring only via slow surface erosion[5,6].

Ring-opening polymerization (ROP) is now the most frequently used method to synthesize aliphatic polyesters and polycarbonates thanks to its mild reaction conditions and versatility[7]. Organometallic initiators have greatly contributed to this success for decades[8,9], especially for lactone and lactide polymerizations. However, well-described coordination-insertion mechanisms[10,11] can also cause side effects such as decarboxylation and back-biting reactions[7]. Moreover, the removal of initiator rests and their transition metals is a major issue because of their possible toxicity and ever stricter rules, such as REACH, increasingly prohibit their use[7].

In this context, metal-free catalysts have a great advantage in ROP by excluding the potential toxic problems of organometallic initiators. These metal-free catalysts[11] include enzymes[12], Lewis and Brønsted acids[13,14], Brønsted bases[15,16] and Lewis bases[15]. Guanidines, such as 1,5,7-triazabicyclo[4.4.0]dec-5-ene (TBD)[17,18], are among the most effective and certainly the most efficient ones in numerous cases.

R-OH, molecules with an alcohol function, are always required as co-initiators to engage ROP efficiently in excess of organometallic initiators[19] or very recommended with organic-based catalysts[11], where the radical R is retrieved at the starting chain. The ROP mechanism is now well defined with stannous octanoate as reminded by Slomkowski et al.[2] whereas intense discussions which started one decade ago about ROP mechanisms with TBD are still under way[11,20,21]. A dual discussion continues with two possible co-initiations via hydrogen-bonds or covalent bonds[7]. Equivalent structural results are obtained with both TBD and stannous octanoate. The end chain is terminated by an alcohol function coming from the last opened repeat unit if the reactive system is hydrolyzed at the end with stannous octanoate. Depending on the structure and functionality of the hydroxylated co-initiator, PTMC can be easily synthesized with different kinds of structures: linear[22,23] with a mono-alcohol or diol, star-like[22,24], combed or branched structures[25,26] with multi-ols or highly hydroxylated polymers or oligomers such as polyvinyl alcohol[27] and polysaccharides[26]. The obtained linear PTMC oligomers functionalized by alcohol functions at each side could offer an opportunity to use them for the further construction of specific multi-branched and multiarmed architectures, for instance, by condensation with diisocyanates[28]. PTMCs were already used as intermediates to be tailored for specific applications by functionalizations[29] including crosslinking[30], end functionalization[31] and incorporation of functional side chains[32], to endow materials with improved or specific properties. Besides, block and random copolymerizations[24,25] of TMC with other cyclic esters are also commonly used methods to obtain bio-based materials.

Free alcohol functions, in co-initiated ROP with metal alkoxides, metal carboxylates as well as strong organic bases such as guanidine, are generally in excess compared to the initiator and then fully involved in active sites for monomer insertion[33,34]. Additionally, a kinetic competition occurs where these active sites for chain propagation are continuously transferred to the remaining free alcohol sites, generating continuously “dormant” and “active” species, and favoring in time a number of polymer chains obtained by ROP equal to the number of the initial and accessible alcohol functions. The faster the transfer reaction acts compared to the propagation, the closer the expected average polymerization degree approaches the initial

monomer/alcohol function molar ratio. On the contrary, if the propagation reaction is faster, longer polymer chains are expected with a partial co-initiation by the present alcohol functions. It appears that the balance between propagation and transfer rates in ROP clearly governs the final obtained structures but the transfer reaction generally leads this competition.

PTMC synthesis by ROP to reach high molecular weights has been studied[12,35-37], particularly in bulk by Yu et al.[37]. High enough TMC monomer/alcohol ratios were chosen and consequently all the hydroxyl groups could easily initiate polymer chains whatever the structure of the molecule, bearing one or more alcohol functions, and whatever the exact balance between propagation and transfer reactions. However, tacticity and neighboring effects, if starting hydroxyl sites are located on a polymer backbone such as PVA, can become limiting factors to reach an initiation by all the present alcohol functions[38,39].

By contrast, works dealing with the synthesis of PTMC oligomers and their controlled average molecular weights and alcohol end-capped terminal groups are rare in the literature. For such objectives where smaller conventional monomer/alcohol ratios are required, it becomes possible to observe unreacted alcohol functions from the co-initiator, even with relatively fast transfer reactions. As a consequence, if diol, triol or alcohols with even more functions are used as co-initiators to obtain multiarm structures by ROP, they could experience not only fully but also partially initiated polymerization. This is the first question to deal with in this study.

Normally, ROP conducted in solvents leads to narrower molar-mass dispersity ($Đ_M = \overline{M}_n/\overline{M}_w$) comparatively to bulk where side reactions are always more prominent[16]. For example, Nederberg et al.[15] compared the PTMC synthesis in methylene chloride ($Đ_M$ = 1.04) and in bulk ($Đ_M$ = 1.09-1.15) with 1,8-diazabicyclo[5.4.0]undec-7-ene (DBU) as a catalyst to reveal the slightly higher $Đ_M$ in bulk. However, considering faster kinetics and simplicity for further use without any purification needed as well as the non-excessive large $Đ_M$ (<1.90)[40], the study of PTMC ROP in bulk is still meaningful. Besides, the polymerization in bulk is a suitable pathway for production, leading to the significance of studying optimized reaction conditions and understanding the synthesized structures in bulk.

Therefore, in this article, a facile route to synthesize ideally controlled low molecular weights PTMC, below 5000 g/mol without solvent in bulk is presented and discussed. The ROP of PTMC will be then studied with 1,4-butanediol (BDO) as co-initiator to get telechelic PTMCs. Due to the relatively small molar ratios between TMC and BDO, it is also significant to

understand if both hydroxyl groups in BDO are efficient. The effect of possible side reactions such as exchange reactions between carbonate and alcohol functions will be taken into consideration. Reaction kinetics and structure control ($Đ_M$ and $\overline{M}_n$) will be compared to finally highlight the best initiation system between $Sn(Oct)_2$ and TBD, in terms of kinetic, molar mass and dispersity. The obtained PTMC oligomer structures will be characterized by ^1H NMR, ^{13}C NMR, Maldi-Tof spectroscopy and SEC. Furthermore, both the thermal and rheological properties of PTMC will be presented.

2. Experimental section

2.1 Materials

Trimethylene carbonate (Boehringer, Germany) was dissolved and refluxed in THF with CaH_2 as the desiccant for two days and recrystallized twice before use. 1,4-butanediol (BDO) (≥99%), 1,5,7-triazabicyclo[4.4.0]dec-5-ene (TBD) (98%) and tin(II) bis(2-ethylhexanoate) ($Sn(Oct)_2$) (92.5-100.0%) were all purchased from Sigma Aldrich and used as received.

2.2 Characterization techniques

^1H NMR, 2D ^1H-^1H COSY and ^{13}C NMR analyses

NMR analyses 1D ^1H and 2D ^1H-^1H homonuclear correlation spectroscopy (COSY) were recorded using a Bruker Advance III spectrometer (400 MHz), equipped with a 5 mm multinuclear broadband probe (BBFO+) with z-gradient coil. The samples (around 20 mg) were dissolved in DMSO-d_6 (0.7 mL) and the spectra were recorded at 298 K with 128 scans for 1D ^1H NMR and 128 increments for 2D ^1H-^1H COSY. ^{13}C NMR analyses were recorded by a Bruker Advance II spectrometer equipped with a 10 mm multinuclear broadband probe (SEX) with z-gradient coil at 100.6 MHz. The samples (around 200 mg) were dissolved in DMSO-d_6 (3 mL) with the spectra recorded at 298 K with 4000 scans. Chemical shifts (δ, in ppm) were expressed relative to the resonance of tetramethylsilane (TMS, δ = 0.00 ppm).

Maldi-Tof measurements

The matrix-assisted laser desorption/ionization time-of-flight mass spectra (Maldi-Tof) tests were performed with an AutoFlex Speed TOF/TOF spectrometer (Bruker Daltonics) equipped with a 355 nm Smartbeam II laser. Spectra were acquired in (linear or reflectron) positive mode, with an accelerating voltage of 19.5 kV for linear mode or 19 kV for reflectron mode.

PTMC and 2,5-dihydroxybenzoic acid (DHB) matrix were diluted in DMSO at the concentrations of 3 mg/mL and 20 mg/mL respectively; sodium acetate (NaAc) was dissolved in methanol at 2-10 mol/L. The mixed solution was obtained by the mixture of PTMC, matrix and NaAc solutions with a volume ratio of 2:2:1. After spotting the mixed solution onto a MALDI plate and drying at room temperature overnight, the final measurement plate was prepared for analysis.

Size-Exclusion Chromatography (SEC) tests

Number average molecular weight ($\overline{M}_n$) and molar-mass dispersity ($Đ_M = \overline{M}_n/\overline{M}_w$) were determined by SEC using a Waters 515 HPLC pump, a Waters 717 plus autosampler system with WATERS 2414 refractive index detector, a WYATT ViscoStar viscometer and a WYATT miniDAWN TREOS multi-angle light scattering detector. WATERS Styragel HR 2 THF and HR 4 THF columns were used. Tetrahydrofuran (THF, Biosolve, GPC grade) was used as the mobile phase at an elution rate of 1 mL/min and the refractive index increment *dn/dC* was calculated directly from the signal. Polystyrene standards with narrow dispersity were used for calibration and all tests were conducted at 30 °C. Since no satisfying results were obtained by viscometric and scattering detections, only the refractive index detector was used.

Thermal analysis

Thermal characterizations were performed with a TA Q10 Differential Scanning Calorimeter (DSC). All the analyses were tested in hermetically sealed pans with heating and cooling rates at 10 °C/min from -70 °C to 100 °C in a nitrogen atmosphere (50 mL/min). The thermal transitions were measured during the second ramp.

Thermal Gravimetric Analysis (TGA) experiments were performed by a Mettler Toledo TGA/DSC 1 Star system from 25 to 500 °C in nitrogen atmosphere (80 mL/min) with a heating rate of 10 °C/min.

Dynamical rheology tests

The viscoelastic properties of PTMC were performed with an ARES-G2 (TA Instruments) rheometer with 40 mm diameter parallel plates geometry. Strain tests were firstly performed to determine a linear viscoelastic region (LVR) and then to conduct frequency sweep tests in it at a constant strain of 1% with angular frequencies varying from 100 to 0.1 rad/s at 30 °C.

2.3 Synthesis of PTMC in bulk

The synthesis of PTMC was conducted with a 250 mL custom glass reactor system. A stainless steel anchor was used as mixer at 60 rpm. The cover with three cylindrical openings on the top was equipped with a stirrer bearing, a cooler and a nitrogen gas feeding. Stirring was performed by a RW 28W IKA motor to record the torque of mixture at a constant rate. The heating system consisted of a DT 70 (SETARAM) thermocouple temperature controller and a silicon oil bath.

Syntheses with TBD

TMC monomer and BDO as co-initiator were firstly mixed at a chosen ratio in the reactor and heated at 100 °C until a homogeneous state and a constant temperature were reached. Then, the weighed catalyst TBD was added to start the reaction for a fixed reaction time. Conditions and formulations for PTMC preparation in bulk with TBD as catalyst are shown in Table 1.

Table 1. Conditions and formulations to synthesize PTMC in bulk with TBD as catalyst

Run	Temperature (°C)	Reaction time	TMC/TBD (mol/mol)	TMC/BDO (mol/mol)	BDO/TBD (mol/mol)
1	100	1 h	1000:1	2:1	500:1
2	100	1 h	1000:1	4:1	250:1
3	100	1 h	1000:1	6:1	167:1
4	100	1 h	1000:1	12:1	83:1
5	100	1 h	1000:1	19:1	53:1
6	100	1 h	1000:1	30:1	33:1
7	100	1 h	1000:1	50:1	20:1
8	100	10 min	1000:1	4:1	250:1
9	100	30 min	1000:1	4:1	250:1
10	100	2 h	1000:1	4:1	250:1
11	100	3 h	1000:1	4:1	250:1
12	100	4 h	1000:1	4:1	250:1

Syntheses with $Sn(Oct)_2$

TMC and BDO were first mixed with a molar ratio of 4:1 in a 100 °C reactor. Once homogeneity was reached, $Sn(Oct)_2$ was then added to initiate polymerization. PTMC samples were collected at different reaction times within 24 h. The reaction conditions and formulations with $Sn(Oct)_2$ as initiator are given in Table 2.

Table 2. Conditions and formulations to synthesize PTMC in bulk with $Sn(Oct)_2$ as initiator

Run	Temperature (°C)	Reaction time	TMC/$Sn(Oct)_2$ (mol/mol)	TMC/BDO (mol/mol)	BDO/$Sn(Oct)_2$ (mol/mol)
13	100	30 min	1000:1	4:1	250:1
14	100	1 h	1000:1	4:1	250:1
15	100	2 h	1000:1	4:1	250:1
16	100	3 h	1000:1	4:1	250:1
17	100	4 h	1000:1	4:1	250:1
18	100	24 h	1000:1	4:1	250:1

3. Results and discussions

3.1 Reagent ratio effects and main expected PTMC structures

When high TMC monomer/alcohol ratios are used with 1,4-butanediol as co-initiator, both its hydroxyl groups are possibly and statistically efficient to initiate chain propagation in the presence of $Sn(Oct)_2$ or TBD. Average polymerization degrees are expected to be equal to the initial Monomer/Alcohol molar ratios when alcohol is in excess with respect to the initiator. With stannous octanoate, the effects of these ratios are now perfectly explained by a preliminary step of tin alkoxide formation by an equilibrium[33,34] shown as follows:

$$Sn(Oct)_2 + ROH \rightleftarrows OctSnOR + OctH \qquad \text{Eq. (1)}$$

2-ethylhexanoic acid (OctH) provokes a shift of this equilibrium to the left side, limiting the formation of tin alkoxides which act as the efficient species for ROP initiation. By contrast, the excess of alcohol is in favor of the shift towards the right side. This balance between alcohol and acid is very important, taking into account that all present alcohol functions will be able to start a ROP thanks to the transfer reaction that occurs and that the residual OctH promotes a decrease of kinetics as shown by Kowalski et al.[33,34]. OctH is not only formed by the equilibrium but also naturally and commonly present in $Sn(Oct)_2$ bottles when purchased from manufacturers. In this study, with the objective to find a facile route to produce PTMC oligomers from BDO, stannous octanoate was used as received without quantifying its exact purity, knowing that an important impact on kinetics was possible[33,34]. With TBD, no carboxylic acid is present but the presence of acid protons in the media could provoke the reaction with TBD, impacting the mechanism and kinetics. In the present study, TBD was also used as received in a white and dry powder form and used under a nitrogen atmosphere.

When PTMC oligomer synthesis is targeted with low monomer/alcohol ratios but respecting high monomer/initiator ratios (Table 1 and Table 2), only one BDO alcohol function could initiate the ROP rather than both as systematically observed with large amounts of monomer. This possibility is induced here by the fact that transfer reactions with low TMC contents could not be fast enough to favor a complete initiation by all the BDO hydroxyl sites. Steric hindrance around BDO containing a firstly formed PTMC chain at one side could also explain why both sides of BDO could not be grafted. Thus, two possible basic structures may first exist as shown in scheme 1 with form (a) showing the structure where only one hydroxyl group initiates propagation and form (b) where both alcohol functions are active.

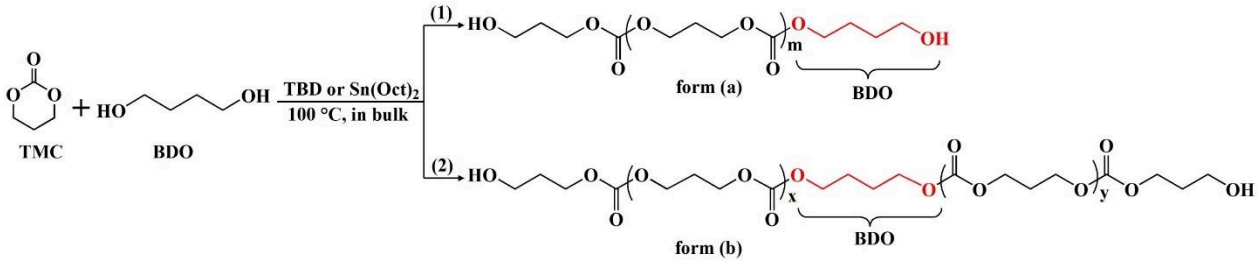

Scheme 1. PTMC structures synthesized by ROP in bulk with 1,4-butanediol (BDO) as co-initiator with (1) one hydroxyl group in BDO functions as initiator to get PTMC form (a); (2) both hydroxyl groups in BDO function as initiators to get PTMC form (b).

3.2 Exchange reactions with carbonate functions

Alcohol radical R (HO-R-OH with R = butylene for BDO) is firstly and exclusively located either at the starting chain (as form (a) in Scheme 1) or in the polymer backbone (as form (b) in Scheme 1) if ROP occurs with asymmetric functions in the monomer such as esters from lactones or lactides, even if transesterification and alcoholysis occur simultaneously during ROP[41].

Nevertheless, with symmetrical functions in cyclic monomers, such as cyclic carbonates -O-C(=O)-O-, this radical R may be located several times in one polymer backbone by competitive exchange reactions occurring at each side of the symmetric carbonate function. Consequently, the tacticity of the carbonate function, in terms of dyad, must be taken into consideration. Indeed, the result of an exchange reaction with a carbonate function is determined by its surroundings. A carbonate can belong to three possible dyads, namely (TMC, TMC), (TMC, BDO) and (BDO, BDO). Considering three dyads and two attack sides for exchange reactions, numerous possibilities have to be considered. As shown in Table 3, all the potential structures

obtained by exchange reactions between form (a) chains and/or form (b) chains were established and displayed by their structures in Figure 1.

Table 3. Newly generated PTMC structures by exchange reactions between form (a) chains and/or form (b) chains

Types of C=O / Forms after exchange / Types of -OH	(TMC, TMC) carbonyl dyad of form (a)	(BDO, TMC) carbonyl dyad of form (a)	(TMC, TMC) carbonyl dyad of form (b)	(BDO, TMC) carbonyl dyad of form (b)
BDO -OH of form (a)	form (c'), form (d), form (b), BDO	form (a), form (b), form (c'), form (d)	form (a), form (b), form (c), form (d)	form (b), form (c), form (d)
TMC -OH of form (a)	form (c″), form (d), form (a), BDO	form (a), form (c″), form (d)	form (a), form (c'), form (d)	form (a), form (b), form (c'), form (d)
TMC -OH of form (b)	form (b), BDO, form (c'), form (d)	form (a), form (b), form (c'), form (d)	form (a), form (b), form (c), form (d)	form (b), form (c), form (d)

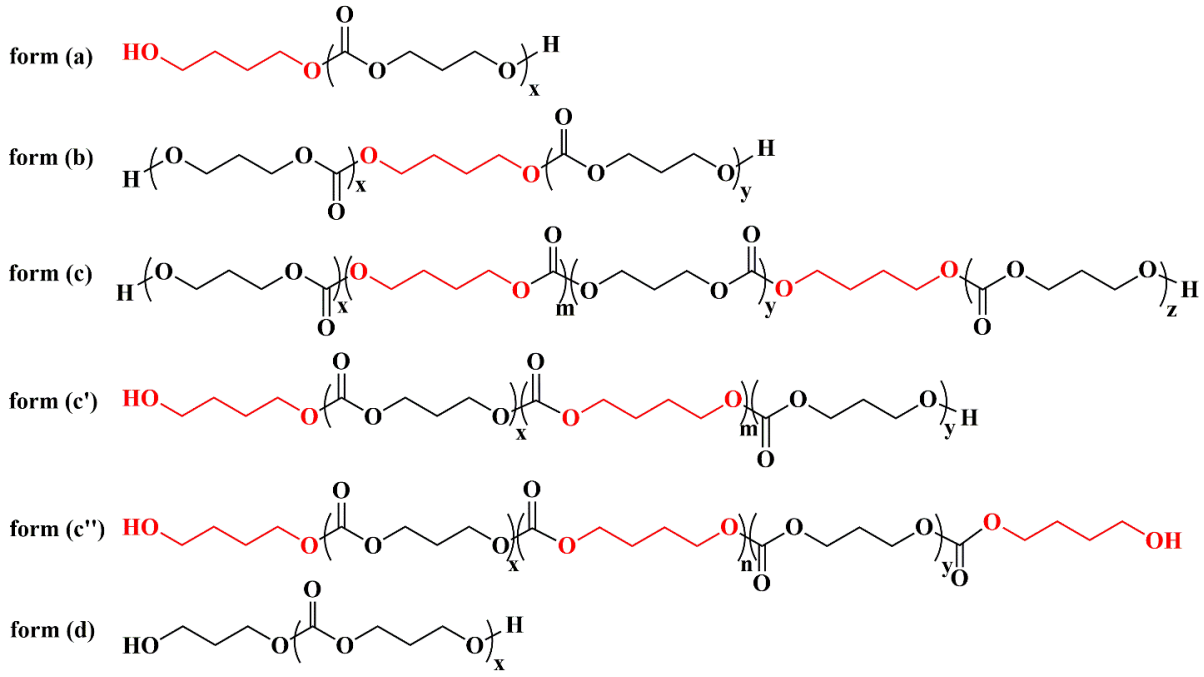

Figure 1. All the possible PTMC structures with exchange reactions between form (a) chains and/or form (b) chains ($m \geq 1$, $n \geq 0$).

For example, an exchange reaction between form (a) and form (b) is described in Figure 2. As shown, the first possible way (numbered (3)) of alcohol/carbonate exchange will lead to the increase of form (b) numbers and the decrease of form (a) numbers. In addition, it is also possible to provide new structures: form (c) containing at least two BDO radicals and two TMC hydroxyl groups at the chain end and form (d) with no BDO radicals. Indeed, such new

structures are retrieved from exchange reactions (numbered (4) here) between a BDO hydroxyl group at the chain end and a (TMC, TMC) carbonyl dyad (Figure 2).

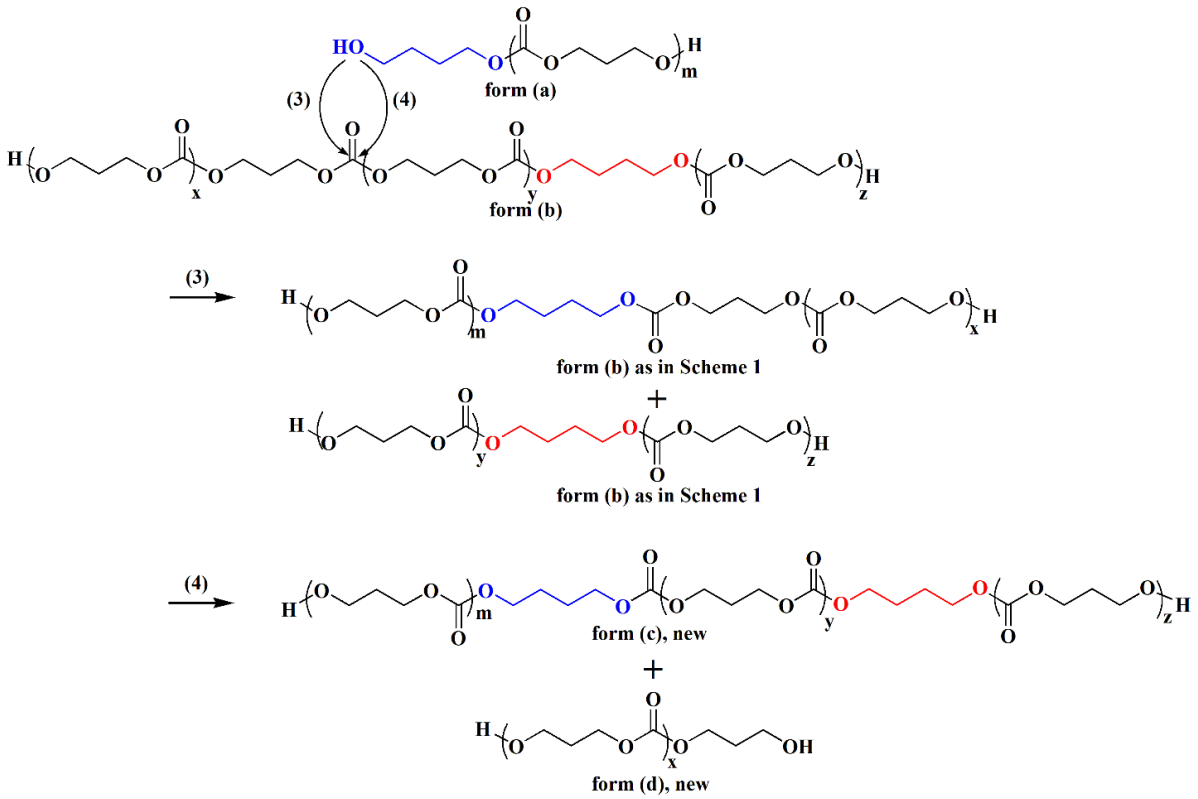

Figure 2. Structural effects of alcohol/carbonate exchange reactions taking account of the symmetric carbonate function and its dyads.

Moreover, an additional representation involving exchange reactions between two form (a) chains is shown in Figure 3 with alcohol/carbonate exchange between a free remaining BDO hydroxyl group at chain end and a (TMC, TMC) carbonyl dyad. It is obvious that this way (5) will increase the number of forms (b) and decrease that of forms (a) at the same time. Way (6) leads to the formation of new structures: form (c') (one BDO hydroxyl group and one TMC hydroxyl group at the chain end respectively), containing at least two BDO radicals, and form (d) without BDO radicals. According to these two examples, it is demonstrated that a BDO alcohol function at the chain end can be exchanged with the (TMC, TMC) carbonyl dyad to change the number of form (a) or form (b) chains and to produce new structures: forms (c), (c') and (d). Form (c″) represents the PTMC structures containing at least two BDO radicals with two BDO hydroxyl groups at the chain end simultaneously. Exchange reactions between these newly generated structures can also happen between one another but no new forms will be produced.

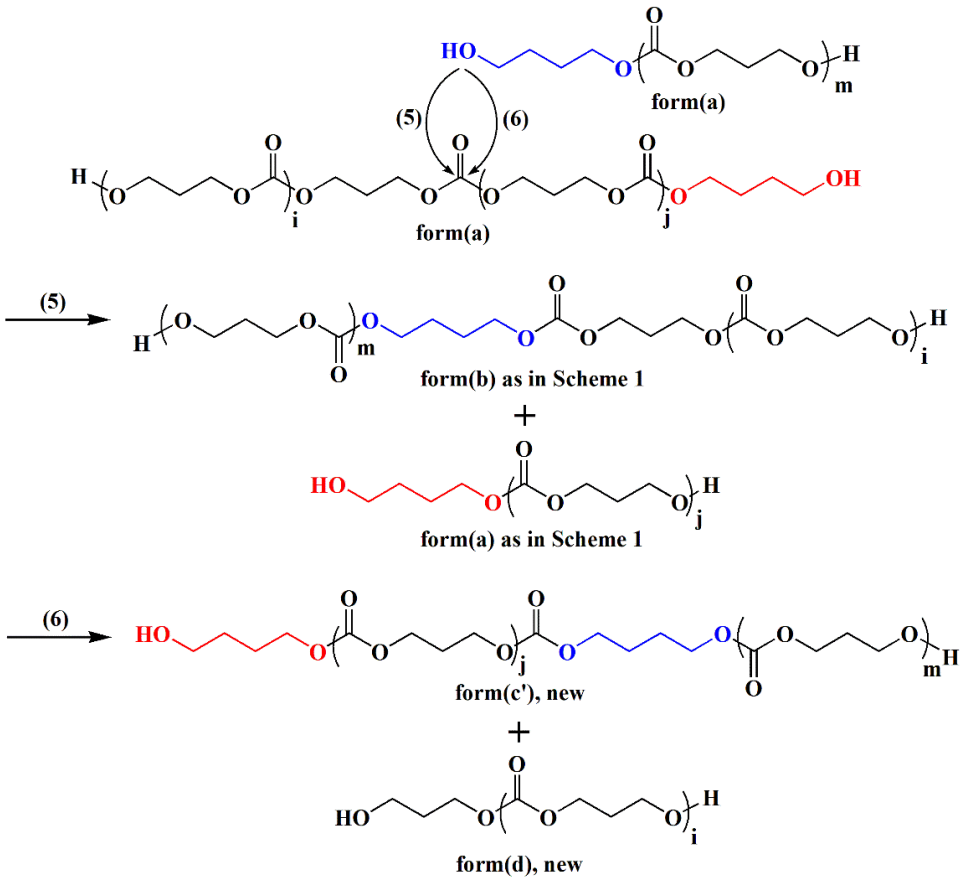

Figure 3. Examples of alcohol/carbonate exchange reaction process between two form (a) chains.

3.3 Structure determination of synthesized PTMC chains

3.3.1 ^{1}H NMR and 2D ^{1}H-^{1}H COSY characterization with TBD initiation

Considering the previous discussion where numerous PTMC structures could coexist, NMR spectroscopy was chosen to confirm their existence. The attribution of the resonances was firstly required. Then, 2D ^{1}H-^{1}H COSY spectroscopy was used to identify mutually coupled protons and overlapped resonances. A spectrum of PTMC with a TMC/BDO feed ratio of 4:1 (run 2, Table 1) is shown in Figure 4. The TMC repeating units in the backbone and at the chain end could be distinguished easily with methylene protons' resonances in the backbone (C_{β}) at 1.91-1.98 ppm and those at the chain end ($C_{\beta'}$) at 1.70-1.76 ppm respectively. Two resonance domains at 3.44-3.47 ppm and 3.39-3.40 ppm were assigned to methylene protons linked to hydroxyl groups, indicating the existence of two different types of hydroxyl groups at the chain end, belonging to either BDO or TMC repeat units. However, due to their partial overlap, it remains a challenge to distinguish or deconvolve them. Thanks to the correlation found (Figure 4) between proton resonances at 3.44-3.47 ppm and those at 1.70-1.76 ppm (H from $C_{\beta'}$), these

resonances at 3.44-3.47 ppm were then attributed to TMC methylene units at chain ends (H from $C_{\alpha'}$). The correlation between resonances at 3.39-3.40 ppm and those at 1.40-1.47 ppm (H from C_{η}) confirmed that the resonances at 3.39-3.40 ppm were assigned to methylene protons linked to BDO hydroxyl groups (H from C_{θ}), indicating the existence of BDO units at the chain end (form (a)). Besides, the resonances at 4.05-4.10 ppm (H from C_{ε}) are assigned to methylene protons of BDO in the backbone, proving the existence of form (b). In other words, the existence of at least two structures (Scheme 1), named forms (a) and (b), as a result of the PTMC ROP (run 2, Table 1) in bulk was confirmed. Moreover, the correlations between 4.12-4.15 ppm (H from C_{α}), 1.91-1.98 ppm (H from C_{β}) and 1.64-1.66 ppm (H from C_{ζ}) are found and shown in Figure 4. Proton resonances of unreacted pure BDO are differentiated from those of reacted BDO, proving that all BDO molecules reacted as co-initiator at least by one of their hydroxyl functions. The attributions of all resonances are shown in Table 4. Though the existence of form (a) and form (b) is confirmed by ^{1}H NMR, it fails to distinguish if form (c), form (c'), form (c″) or form (d) indeed exist.

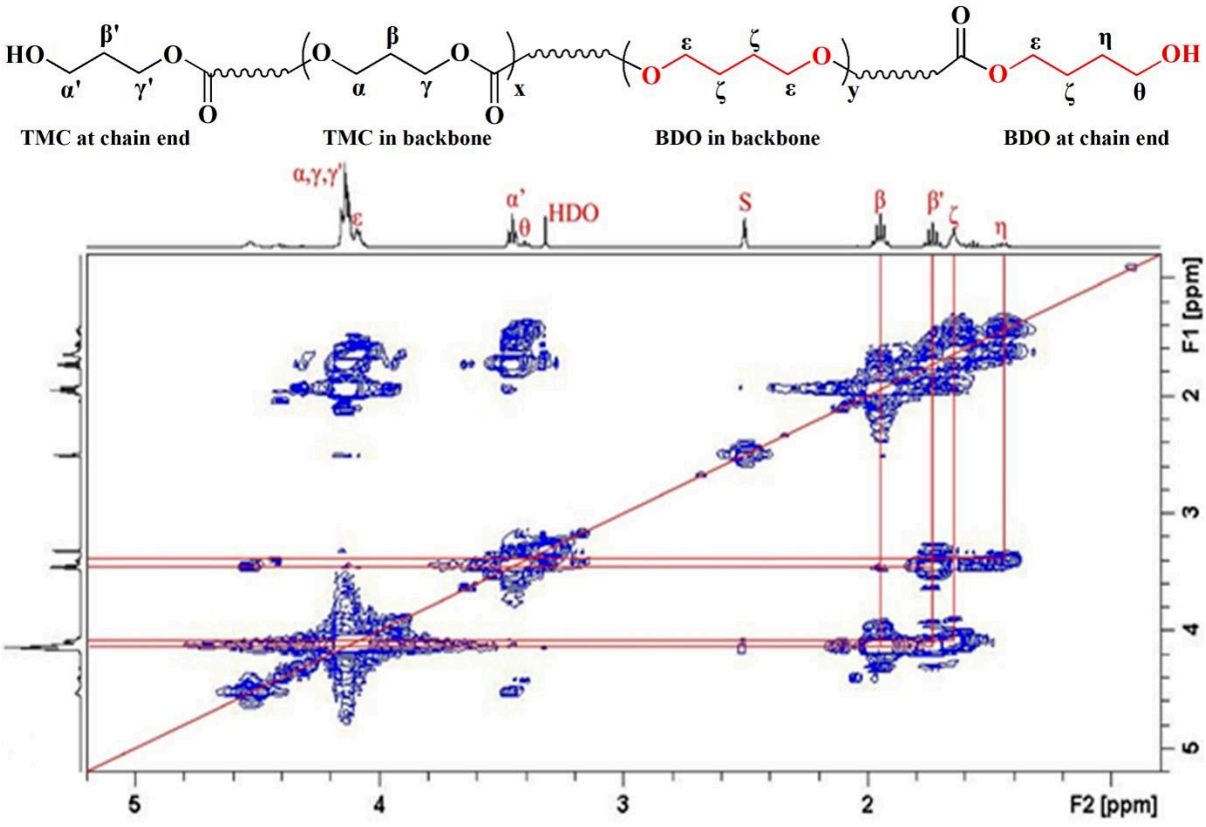

Figure 4. 2D ^{1}H-^{1}H COSY NMR spectrum of a PTMC sample (run 2, Table 1, DMSO-d_6, 400 MHz, 298 K) and the illustration of its structure.

Table 4. Resonances attribution in DMSO-d_6 at 400 MHz and 298K of PTMC polymerized with BDO in bulk from the structure described in Figure 4.

Pattern	Proton		Resonance range (ppm)
BDO	Methylene	CH_2, η	1.40-1.47
	Methylene	CH_2, ζ	1.64-1.66
	Methylene	CH_2, θ	3.39-3.40
	Methylene	CH_2, ε	4.05-4.10
	Hydroxyl	OH	4.38-4.41
TMC	Methylene	CH_2, β’	1.70-1.76
	Methylene	CH_2, β	1.91-1.98
	Methylene	CH_2, α’	3.44-3.47
	Methylene	CH_2, α, γ, γ’	4.12-4.15
	Hydroxyl	OH	4.50-4.52

After confirming the resonances attribution by 2D ^{1}H-^{1}H COSY, the average degree of polymerization ($\overline{DP}_n$) can be calculated from the integrations ($I_{\alpha'}$, I_ε, I_θ and I_β) of $C_{\alpha'}$, C_ε, C_θ and $C_{\beta'}$ proton resonances with a simple ^{1}H NMR spectrum (Figure 5).

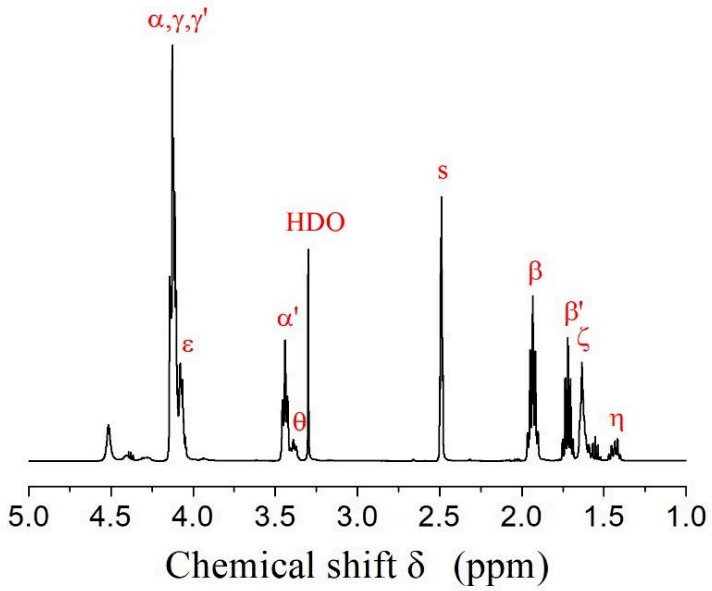

Figure 5. ^{1}H NMR spectrum in DMSO-d_6 at 400 MHz and 298 K of PTMC initiated with BDO and attributions (run 2, Table 1).

Considering that exchange reactions do not change the number of PTMC chains, they can be calculated as follows:

$$PTMC\ chain\ number = \frac{I_\theta}{2} + \frac{I_\varepsilon - I_\theta}{4} \qquad \text{Eq. (2)}$$

The TMC repeating unit number are:

$$TMC\ repeating\ unit\ number = \frac{I_{\alpha'} + I_\beta}{2} \qquad \text{Eq. (3)}$$

In this case,

$$\overline{DP_n} = \frac{TMC\ repeating\ unit\ number}{PTMC\ chain\ number} = \frac{2 \times (I_{\alpha'} + I_\beta)}{I_\theta + I_\varepsilon} \text{ Eq. (4)}$$

The different PTMC forms cannot be distinguished separately by ^{1}H NMR, therefore a BDO radical at chain end, existing in the form (a)+(c')+(c″), and TMC repeat unit at chain end, existing in the form (a)+(b)+(c)+(c')+(d), are quantified respectively by φ (BDO) and φ (TMC) (Eq. (6) and (6')). Their ratio can be calculated from the integration of H_θ and $H_{\alpha'}$ with Eq. (5):

$$\frac{\varphi\ (\text{BDO})}{\varphi\ (\text{TMC})} = \frac{I_\theta}{I_{\alpha'}} \qquad \text{Eq. (5)}$$

If φ (BDO) and φ (TMC) are expressed as percentages, then:

$$\varphi\ (\text{BDO}) = 100 \times \frac{I_\theta}{I_\theta + I_{\alpha'}} \qquad \text{Eq. (6)}$$

$$\varphi\ (\text{TMC}) = 100 \times \frac{I_{\alpha'}}{I_\theta + I_{\alpha'}} \qquad \text{Eq. (6')}$$

The theoretical number average molecular weight $\overline{M}_{\text{n theo}}$ can be calculated from Eq. (7):

$$\overline{M}_{\text{n theo}} = n_{TMC}/n_{BDO} \times M_{TMC} + M_{BDO} \qquad \text{Eq. (7)}$$

where n_{TMC}/n_{BDO} is the initial molar ratio (mol/mol) between TMC and BDO and is also equivalent to the theoretical average $\overline{DP}_{\text{n theo}}$, and M_{TMC} and M_{BDO} are respectively the molar masses equal to 102 g/mol and 90 g/mol. Results obtained for all samples are given in Table 5 and will be further discussed.

Table 5. Structure parameters of PTMC with different TMC/BDO ratios

Run	TMC/BDO (mol/mol)	TMC conversion[a] (%)	$\overline{DP}_{n\,theo}$	$\overline{DP}_n$[b]	φ (BDO) (%)	φ (TMC) (%)	$\overline{M}_{n\,theo}$ (g/mol)	$\overline{M}_n$[c] (g/mol)	$\overline{M}_n$[d] (g/mol)	$Đ_M$[d]
1	2:1	99.4	2.0	2.0	36.0	64.0	290	290	350	1.41
2	4:1	99.8	4.0	4.0	19.3	80.7	500	500	560	1.52
3	6:1	99.9	6.0	6.0	7.5	92.5	700	700	710	1.59
4	12:1	99.8	12.0	12.1	6.7	93.3	1310	1330	1330	1.58
5	19:1	99.8	19.0	18.6	1.2	98.8	2030	1990	2140	1.60
6	30:1	99.8	30.0	29.5	1.0	99.0	3100	3080	3960	1.67
7	50:1	99.8	50.0	48.8	0.8	99.2	5190	5070	6350	1.77

[a]Determined by ^{1}H NMR. [b]$\overline{DP}_n$ was determined by ^{1}H NMR with Eq. (4). [c]$\overline{M}_n$ was determined by ^{1}H NMR. [d]Determined by SEC.

3.3.2 ^{13}C NMR characterization

The newly generated PTMC structure forms (Figures 1, 2 and 3) could not be differentiated by either ^{1}H NMR or 2D 1H-1H COSY. ^{13}C NMR was then used to distinguish the different >C=O carbonyls belonging to carbonate functions in the different dyads. Therefore, “c”-like chains and “b”-like backbones are indexes introduced. According to the PTMC structures of form (a) and form (b) as shown in Scheme 1, five different carbonates, in terms of carbonyls surrounding, have to be identified by dyads: (TMC_b, TMC_b), (TMC_b, BDO_b), (TMC_b, TMC_c), (TMC_b, BDO_c) and (BDO_b, TMC_c). If exchange reactions indeed happen, two other carbonates with (BDO_b, BDO_c) and (BDO_b, BDO_b) dyads are expected. All these carbonate dyad structures are shown in Figure 6.

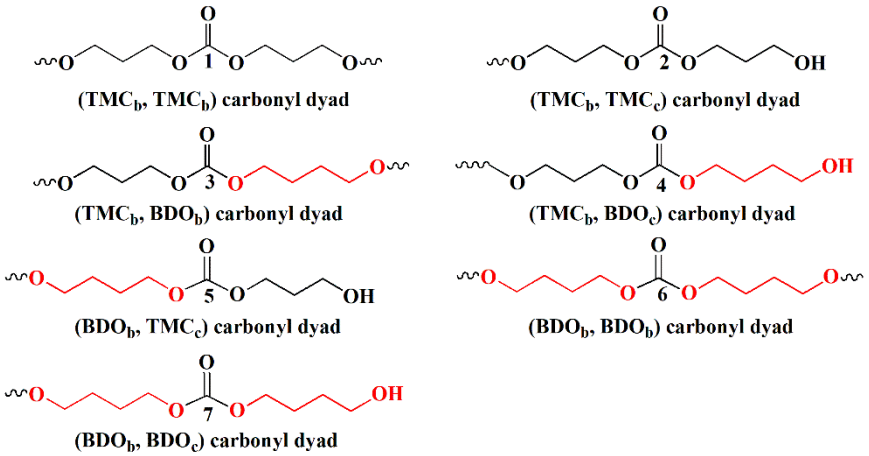

Figure 6. Structures of all the carbonate dyads in PTMC chains.

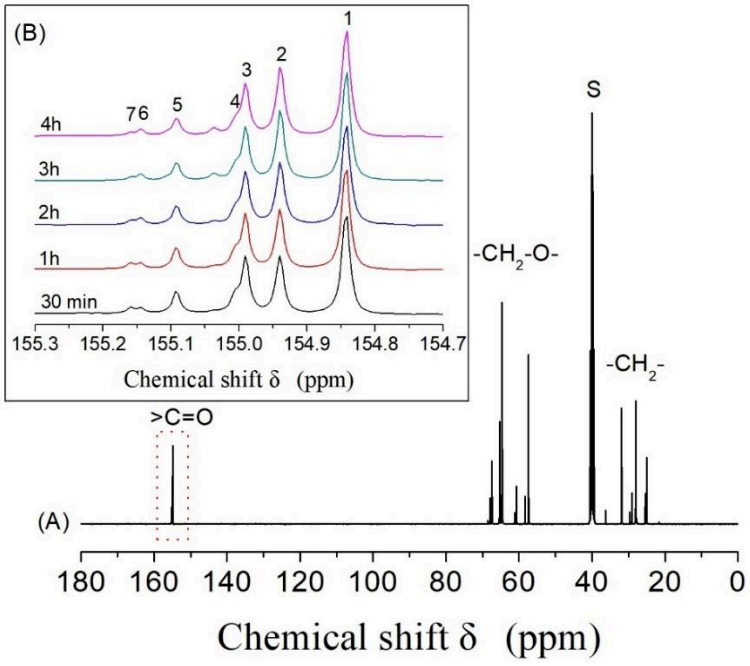

Figure 7. ^{13}C NMR spectra in DMSO-d_6 at 100.6 MHz and 298 K of (A) PTMC initiated with BDO (run 2, Table 1); (B) resonances of >C=O carbons with reaction times of 30 min (run 9), 1 h (run 2), 2 h (run 10), 3 h (run 11) and 4 h (run 12).

A ^{13}C NMR spectrum of PTMC (run 2, Table 1) is presented in Figure 7 (A). As seen, the resonances between 155.2 and 154.8 ppm are all assigned to carbonate carbonyls and more than five resonances are found in this range (Figure 7 (B)), in agreement with the effective exchange reactions. Although carbon NMR is not quantitative, a discussion from the relative intensities of carbonate carbonyls can be engaged since their relaxation times are relatively equivalent, offering the possibility to compare them qualitatively. According to the PTMC forms (a) and (b) as well as the TMC/BDO ratio, C_1, C_2 and C_3 at respectively 154.84, 154.94 and 154.99 ppm, as indexed on the structures (Figure 6), are more intense than the others. By comparison of C_1 and C_3, the change from TMC_b to BDO_b can shift the resonances toward low field by 0.15 ppm. The resonances at 155.14 ppm can be assigned to C_6 with the same resonances discrepancy (0.15 ppm) from C_3 by changing TMC_b (C_3) to BDO_b (C_6). Similarly, the resonances shift from C_2 to C_5 and C_4 to C_7 should have the same resonance shift. In this case, resonances at 155.01, 155.09 and 155.16 ppm are ascribed to C_4, C_5 and C_7 respectively. Additionally, the resonances between 25 and 38 ppm are all assigned to methylenes surrounded by other TMC methylenes and the resonances between 57 and 68 ppm are attributed to PTMC methylenes linked to the carbonate function. From the ^{13}C NMR spectra at different reaction times: 30 min, 1 h, 2 h, 3 h and 4 h (Figure 7 (B)), it is clear that by increasing the reaction time,

the intensities of C_4 (TMC_b, BDO_c) and C_7 (BDO_b, BDO_c) diminish, meaning that BDO radicals are favored to be exchanged into chain backbones.

3.3.3 Structure determination by Maldi-Tof with TBD

3.3.3.1 Confirmation of PTMC structures generated by exchange reactions

The PTMC forms (c), (c'), (c″) and (d) (Figure 1) can be confirmed by Maldi-Tof spectroscopy. As shown in Figure 8, main peaks (marked in red) corresponding to PTMC chains with one BDO of indifferently form (a) or form (b) are observed with their mass peaks retrieved by m/z values expressed as follows:

$$m/z = 90.12 + n \times 102.09 + 22.99 \qquad \text{Eq. (8)}$$

where *n* index is the DP_n and 90.12, 102.09 and 22.99 are the BDO, TMC and Na molar masses, respectively.

These m/z peaks confirm that the ROP of PTMC is in fact initiated by BDO. Meanwhile, decarboxylated structures, normally evidenced by an m/z decrease of 44 from main peaks corresponding to PTMC structures with one BDO, are never observed as expected from the literature[7], proving the absence of decarboxylation during PTMC polymerization with TBD.

Several new mass peaks are frequently observed by m/z at -14, +14, +28 and +42 additionally to the mass of the main forms (a)+(b) (marked in red in Figures 8), corresponding exactly to the structures obtained by exchange reactions between alcohol/carbonate and carbonate/carbonate functions as discussed previously in section 3.2 (Exchange reactions with carbonate functions). Precisely in way (4) (Figure 2) or way (6) (Figure 3), it can be seen that another BDO pattern is introduced in one PTMC chain to generate new chains by forms (c) and (c'), as well as the new chain form (d) without BDO as expressed by Figure 1. It is then possible to obtain two or more butanediol patterns in PTMC chains.

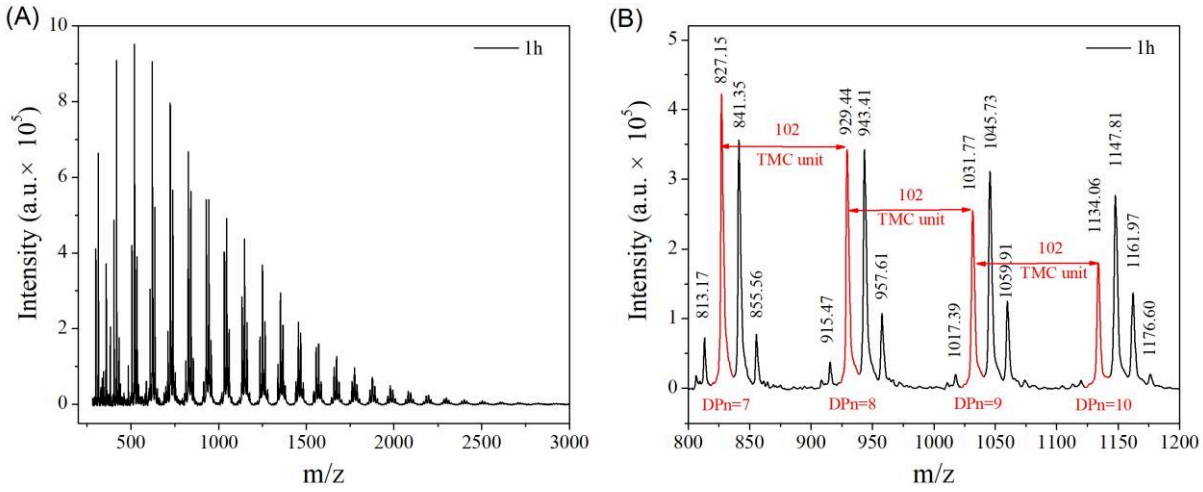

Figure 8. Maldi-Tof spectrum of PTMC with (A) run 2, Table 1; (B) enlarged area of run 2, Table 1 (the m/z gap values in (B) were all rounded up and main peaks are marked in red).

Then, the m/z of forms (c), (c') and (c″) can be calculated, with at least two BDO in the chain, by the general relation:

$$m/z = i\times 90.12 + n\times 102.09 + (i\text{-}1)\times 28.01 - (i\text{-}1)\times 2\times 1 + 22.99 \qquad \text{Eq. (9)}$$

where i (≥2) corresponds to the number of total BDO patterns, n (≥1) is the TMC DP_n of forms (c), (c') or (c″) chains.

The m/z of PTMC form (d) chains without BDO radicals can be expressed by:

$$m/z = 76.09 + n\times 102.09 + 22.99 \qquad \text{Eq. (10)}$$

where n is the DP_n and 76.09 is the molar mass of HO-CH_2-CH_2-CH_2-OH (Figure 1).

So, from Maldi-Tof spectra which are composed of very characteristic and reproducible series of peaks (Figure 8 (A) and (B)), it is then possible to model them with easy structure attributions. In a series (Figure 9), all peaks can be easily attributed from the main peak, called m/z=a, corresponding to the forms (a)+(b) (Eq. (8)) with a given DP_n of x and only one BDO radical. The a-14 peak belongs to the PTMC chains of form (d) without any BDO radicals bearing also the DP_n = x. Then, a+14, a+28, a+42 and a+56 are ascribed to the PTMC chains with DP_n of x-1, x-2, x-3 and x-4, corresponding respectively to BDO radical numbers of 2, 3, 4 and 5 (Figure 9).

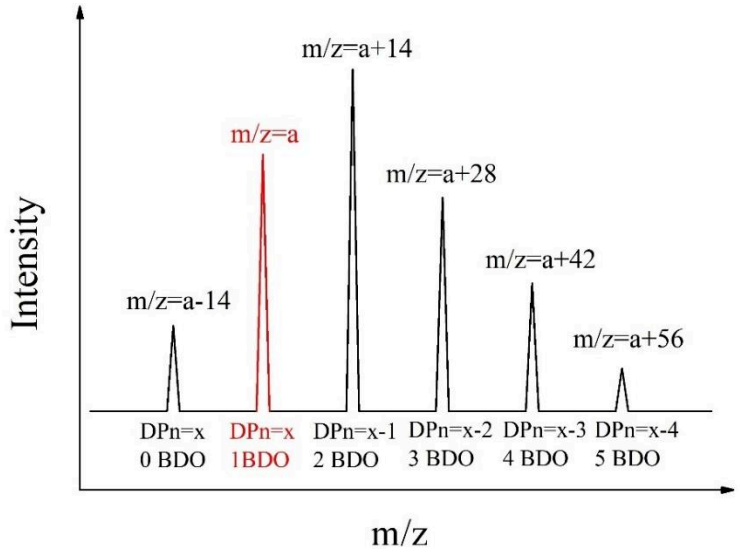

Figure 9. Maldi-Tof spectra model of one group of m/z peaks with different DP_n and number of BDO radicals in the PTMC chains (the main peak is marked in red).

Table 6. Observed m/z data of PTMC run 2, Table 1 and corresponding DP_n and number of BDO patterns in PTMC chains

m/z	316.73	419.54	521.19	623.23	725.3	827.15	929.44	1031.77	1134.06	1236.13
DP_n	2	3	4	5	6	7	8	9	10	11
n° of BDO	1	1	1	1	1	1	1	1	1	1
m/z-14	-	405.34	507.22	609.16	711.04	813.17	915.47	1017.39	-	-
DP_n	-	3	4	5	6	7	8	9	-	-
n° of BDO	-	0	0	0	0	0	0	0	-	-
m/z+14	-	-	-	637.25	739.31	841.35	943.41	1045.73	1147.81	1250.11
DP_n	-	-	-	4	5	6	7	8	9	10
n° of BDO	-	-	-	2	2	2	2	2	2	2
m/z+28	-	-	-	-	753.42	855.56	957.61	1059.91	1161.97	1264.23
DP_n	-	-	-	-	4	5	6	7	8	9
n° of BDO	-	-	-	-	3	3	3	3	3	3
m/z+42	-	-	-	-	-	-	-	-	1176.60	1278.07
DP_n	-	-	-	-	-	-	-	-	7	8
n° of BDO	-	-	-	-	-	-	-	-	4	4

Table 6 gives the observed m/z values varying from 300 to 1300 of PTMC run 2, Table 1. All the data are fully accordant to the theoretical m/z calculated by Eq. (8), Eq. (9) and Eq. (10). It can be seen that the number of breakdowns for PTMC chains which underwent exchange reactions is dependent on the DP_n. For example, m/z = 637.25 corresponds to the PTMC chains with DP_n = 4 and 2 BDO radicals (one extra BDO radical added in forms (a) or (b)) while the PTMC chains with DP_n lower than 4 and 2 BDO radicals do not exist. The peak at m/z = 1176.60 shows that three BDO patterns have been introduced in the chain forms (a) or (b) with a DP_n =

7. However, when the PTMC DP_n is lower than 7, the chains with three added BDO molecules do not exist and the maximum number of BDO radicals added is 2 with DP_n below 7 (m/z = 957.61, DP_n = 6). From these observations and statistical considerations to reach a given number of BDO patterns in one chain, both initial PTMC chain length and TMC/BDO ratio are criteria to be taken into account. As a consequence, the longer the initial PTMC chain, the higher the maximum BDO patterns number. This conclusion is well observed in Table 6. In the following paragraph, another parameter, namely the reaction time, will be introduced in the discussion.

3.3.3.2 Evolution of exchange reactions in time

With TBD as catalyst, exchange reactions are possibly more prominent by increasing reaction times at 100°C. The Maldi-Tof spectra of PTMC with different reaction times of 30 min (run 9), 1 h (run 2) and 4 h (run 12) are shown in Figure 10. According to the previous discussion, the m/z of PTMC found in these spectra can also be attributed using the same formulas established by Eq. (8), (9), (10) and the model in Figure 9. As shown, it is obvious that with the increase of reaction times, the relative intensity of peaks at low m/z decreases and that at high m/z slightly increases, also proving the formation of longer chains due to the exchange reactions between different PTMC chains as clarified previously. At short reaction times, the number of exchanged BDO in one PTMC chain is limited. When increasing reaction times, the exchange reactions happen more intensely and lead to the formation of longer PTMC chains with more transferred BDO radicals. For example, as shown in Figure 10 (B), after 4 h of reaction, new PTMC structures are observed (m/z = a+56) corresponding to 4 extra BDO radicals added in one PTMC chain. Comparatively, for the structures obtained after 1 h, only a maximum of three extra BDO radicals was observed in the same m/z range from 800 to 1200 (Figure 8 (B) and Figure 10 (B)). It is therefore proven that these newly-formed longer PTMC chains (m/z = a+56) with prolonged reaction times at 100 °C include more BDO patterns as explained in the previous paragraph. Since the total number of BDO radicals remains constant during synthesis, the number of long chains without BDO (form (d)) also increases in time as observed by a relative increase of the peaks at m/z = a-14, specifically for the highest DP_n (Figure 10 (A)).

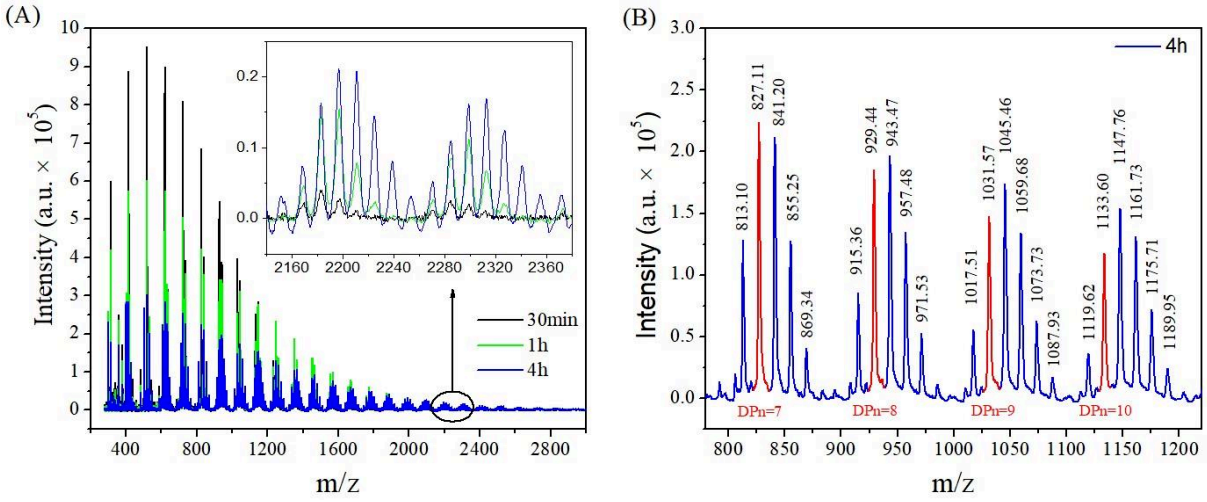

Figure 10. Maldi-Tof spectra of PTMC run 2 (Table 1) with TBD as catalyst at (A) 30 min (run 9), 1 h (run 2) and 4 h (run 12); (B) enlarged area of 4 h (run 12) (main peaks are marked in red).

3.3.3.3 Effect of TMC/BDO feed ratio on exchange reactions

Table 7 presents all the observed m/z data of forms (c), (c') or (c″) in run 2 (TMC/BDO = 4:1) and run 5 (TMC/BDO = 19:1) with DP_n of 10. The observed maximum number of BDO radicals in run 2 is then 5 when m/z = 1598.55. For run 5, the maximum BDO radicals in PTMC chains is only three, bearing the m/z = 1365.89. According to these observations, it can be inferred that higher TMC/BDO feed ratios lead to fewer exchange reactions in relation with the fact that both the concentration of free hydroxyl groups at chain end and carbonate functions in dyads involving a BDO radical decrease.

Table 7. Observed m/z data of PTMC form (c), (c') or (c″) (10 TMC repeating units) by run 2 and run 5, Table 1

Number of BDO		1	2	3	4	5	6
run 2	m/z	1134.06	1250.11	1366.36	1482.58	1598.55	-
	DP_n	10	10	10	10	10	-
run 5	m/z	1133.95	1249.90	1365.89	-	-	-
	DP_n	10	10	10	-	-	-

The observed m/z data of form (d) in run 2 and run 5 (Table 1) are picked in Table 8. The maximum DP_n is only 9 in run 2 while it reaches 15 in run 5. These results are expected since the higher TMC/BDO feed ratio of run 5 firstly leads to longer form (a) and form (b) chains, consequently resulting in the production of longer forms (d) by random exchange reactions.

Table 8. Observed m/z data of PTMC form (d) by run 2 and run 5, Table 1

DP_n		3	4	5	6	7	8	9	10	11	12	13	14	15
m/z	run 2	405.24	507.33	609.54	711.43	813.61	915.77	1017.39	-	-	-	-	-	-
	run 5	-	507.34	609.59	711.7	813.51	915.21	1017.19	1119.94	1222.15	1323.96	1426.25	1528.2	1630.32

Efficient transesterification and alcoholysis with polyesters were already observed with TBD or stannous octanoate above 200 °C in the melt state[41]. It is clear that carbonate functions in PTMC are much more active for exchange reactions than esters, occurring at 100 °C.

3.4 Polymerization kinetics and PTMC structures control with $Sn(Oct)_2$ or TBD

To compare the control of PTMC structures with $Sn(Oct)_2$ and TBD, kinetics, $\overline{M}_n$ and dispersity are now discussed.

The kinetics of PTMC polymerization was studied at 100 °C using TBD or $Sn(Oct)_2$ with a fixed TMC/BDO ratio of 4:1 as well as TMC/TBD and TMC/$Sn(Oct)_2$ ratios of 1000:1. Results are presented in Table 9. With TBD, TMC conversion was 78.9% after 10 min and 99.7% after 30 min while it was only 15.1% after 30 min with $Sn(Oct)_2$. To exceed 99.0% of conversion rate, 24 h was required at 100 °C. This poor efficiency of $Sn(Oct)_2$ can be certainly explained by its use without further purification and very possibly the presence of unexpected 2-ethylhexanoic acid as a very limiting side-product to expect fast kinetics[34]. Its effect has already been discussed previously in paragraph 3.1. Through these simple comparisons of TMC conversions between TBD and $Sn(Oct)_2$ in the same reaction conditions, it is obvious that TBD is a much more efficient catalyst.

The initiation systems are now discussed regarding their effects on the structure evolution in time to study the evolution of the chain ends. These chain ends are derived from either the last opened TMC repeat units (such as forms (a), (b), (c), (c') and (d)) or BDO patterns containing unreacted alcohol functions (such as forms (a), (c') and (c")). The percentages of both BDO (φ (BDO) from Eq. (6)) and TMC (φ (TMC) from Eq. (6')) patterns at chain end are examined from calculated results presented in Table 9 as follows: when TBD is used, φ (TMC) increases from 77.4% after ten minutes of reaction to 79.8% after 30 min and finally to 84.8% after four h. The monomer conversion is not complete until 30 minutes of reaction. In fact, it must be reminded that chain propagation sites are in competition for their transfer onto a free remaining hydroxyl function (coming from unreacted hydroxyls of co-initiator (BDO) or a terminated

PTMC chain end) to continue the propagation as has been described in the introduction. Then, before the completion of the reaction, the propagation sites may transfer continuously onto free BDO hydroxyl functions, leading to the decrease of φ (BDO). The chain end evolution is certainly and mainly due to the transfer during the monomer propagation. After total monomer conversion, in 30 minutes with TBD, φ (BDO) continues to decrease, induced exclusively by exchange reactions similar to transesterification reactions. This observation matches very well the previous ^{13}C NMR analyses where it was concluded that BDO tends to be exchanged with carbonate functions in dyads located in PTMC backbones. It must be kept in mind that such exchange reactions can correspond to either a carbonate/alcohol exchange with BDO as in form (a) or a carbonate/carbonate exchange with BDO as in form (b). Therefore, to explain the decrease of φ (BDO) over time after a total monomer conversion, only the reactivity of remaining BDO located at the chain end as presented in form (a), must be considered.

The proportion of BDO chain end (φ (BDO)) is also dependent on the TMC/BDO feed ratio. As shown in Table 5, φ (BDO) decreases logically with the increase of the TMC/BDO feed ratio. For example, when the TMC/BDO feed ratio is relatively low at 2:1, φ (BDO) is calculated to be 36.0%. When the ratio is increased to 19:1, φ (BDO) decreases to 1.2%, signifying that only 1.2% of end-capped hydroxyl groups in PTMC chains are from BDO. This clearly means that the higher the TMC/BDO feed ratio is, the more favorable it is for PTMC chains formation with both active BDO hydroxyl functions as co-initiators. In other words, increasing the TMC/BDO feed ratio favors ROP to get more forms (b) as conventionally expected, with fewer possibilities of obtaining forms (a) (Figure 1).

With $Sn(Oct)_2$ where the conversion rate is slow, φ (BDO) mainly decreases with the monomer conversion and reaches 16.0% after 24 h, which is near to the value obtained with TBD (20.2%) just after the completion of the reaction. It is very possible that exchange reactions also occur during this long reaction time in favor of the decrease of φ (BDO) but no Maldi-Tof analyses were performed to verify and quantify their competitive existence.

Table 9. Conversion rates, molecular weight and chain end composition of bulked PTMC polymerization with TBD or $Sn(Oct)_2$ as catalyst/initiator at 100 °C with TMC/BDO feed molar ratio of 4:1

Run	Initiation system	Reaction time	TMC conversion[a] (%)	$\overline{DP}_n$[b]	φ (BDO) (%)	φ (TMC) (%)	$\overline{M}_n$[c] (g/mol)	$\overline{M}_n$[d] (g/mol)	$Đ_M$[d]
8	TBD	10 min	78.9	3.5	22.6	77.4	450	240	1.81
9	TBD	30 min	99.7	4.0	20.2	79.8	500	540	1.43
2	TBD	1 h	99.8	4.0	19.3	80.7	500	560	1.52
10	TBD	2 h	99.8	4.1	16.0	84.0	510	800	1.61
11	TBD	3 h	99.8	4.1	15.4	84.6	510	880	1.64
12	TBD	4 h	99.8	4.1	15.2	84.8	510	890	1.65
13	$Sn(Oct)_2$	30 min	15.1	0.7	71.5	28.5	160	-	-
14	$Sn(Oct)_2$	1 h	23.7	1.0	58.9	41.1	190	-	-
15	$Sn(Oct)_2$	2 h	33.3	1.4	47.0	53.0	230	-	-
16	$Sn(Oct)_2$	3 h	43.4	1.8	38.0	62.0	270	-	-
17	$Sn(Oct)_2$	4 h	55.0	2.4	29.6	70.4	340	-	-
18	$Sn(Oct)_2$	24 h	99.5	3.9	16.0	84.0	490	540	1.75

[a]Determined by ^{1}H NMR. [b]$\overline{DP}_n$ was determined by ^{1}H NMR with Eq. (4). [c]$\overline{M}_n$ was determined by ^{1}H NMR. [d]Determined by SEC.

The SEC chromatograms from runs presented in Table 9 are shown in Figure 11 (A) and (B). With $Sn(Oct)_2$, elution times between 22.5 and 24 minutes belong to the unreacted monomer TMC and those between 16 and 21.7 minutes are ascribed to PTMC chains. It is obvious that the TMC monomer decreases with reaction time and disappears finally after 24 h. It also verifies the relatively slow kinetics of $Sn(Oct)_2$ which is compatible with the TMC conversion data shown in Table 9. After the complete conversion of TMC after 24 h, the measured final $\overline{M}_n$ is 540 g/mol with a $Đ_M$ of 1.75, which corresponds to $Đ_M$ values of previous studies in the range of 1.5-2.6[28] and 1.78-1.88[42] with $Sn(Oct)_2$. With TBD as catalyst, as shown in Figure 11 (B), when the reaction time is prolonged PTMC elution times become shorter in accordance with the formation of longer chains by exchange reactions as discussed and characterized by Maldi-Tof spectroscopy previously. $Đ_M$ also increase from 1.43 to 1.65 for reaction times between 30 min and 4 h after the complete conversion of the monomer. Compared to $Đ_M$ of 1.75 for $Sn(Oct)_2$ with 24-h reactions, $Đ_M$ with TBD are all narrower in ranges between 1.43 and 1.65. The obtained $\overline{M}_n$ by TBD after 1 h of reaction is 500 g/mol, also closer to the targeted theoretical value. By comparing both polymerization kinetics and structure control, it is obvious that TBD is better regarding both these criteria than $Sn(Oct)_2$ in the chosen conditions. To control PTMC synthesis with TBD and to target theoretical molecular weights, it makes sense to stop the

reactive system immediately after total monomer conversion in order to limit important and unexpected exchange reactions in time.

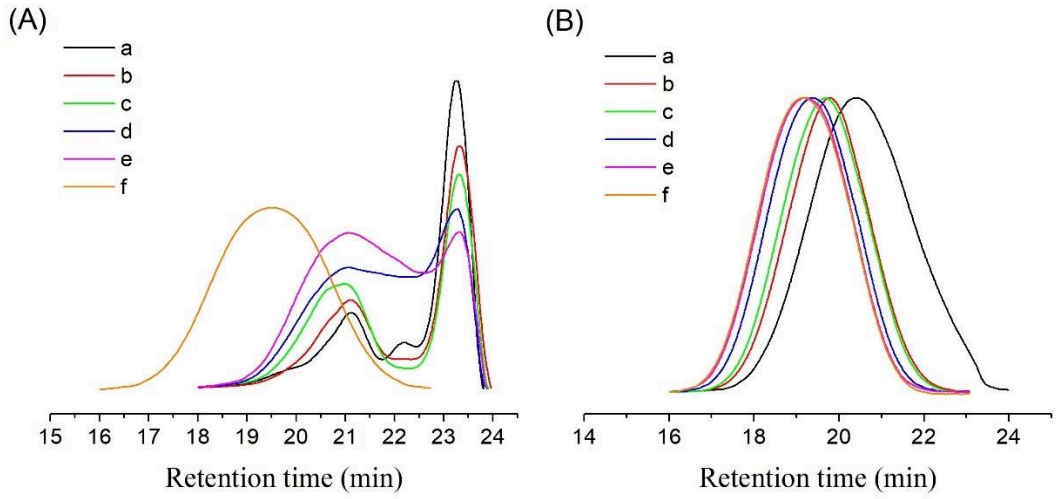

Figure 11. SEC chromatograms of PTMC synthesis with (A) $Sn(Oct)_2$ as initiator at (a) 30 min, (b) 1 h, (c) 2 h, (d) 3 h, (e) 4 h, (f) 24 h; (B) TBD as catalyst at (a) 10 min; (b) 30 min; (c) 1 h; (d) 2 h; (e) 3 h; (f) 4 h (in THF at 30 °C).

3.5 Effect of TMC/BDO feed ratio on PTMC average molecular weights with TBD

Theoretically, it is possible to obtain PTMC with different molar masses by simply changing the feed ratio between TMC and BDO[7,16,20]. As shown in Table 5 this feed ratio in fact controls the PTMC molar mass since the calculated $\overline{DP}_n$ and $\overline{M}_n$ are all close to their theoretical values. For example, with a TMC/BDO feed ratio of 4:1 and theoretical $\overline{M}_n$ of 500 g/mol, the NMR-calculated $\overline{DP}_n$ and $\overline{M}_n$ are also 4.0 and 500 g/mol respectively. When the feed ratio is increased to 19:1, the NMR-calculated PTMC $\overline{DP}_n$ is 18.6 with theoretical and measured $\overline{M}_n$ values of 2030 and 1990 g/mol respectively. It seems that the consistency between theoretical and NMR-calculated PTMC molar masses validates the feasibility of using TMC/BDO feed ratio to predict the average molar mass of PTMC.

SEC chromatograms of runs 1-7 (Table 5) are shown in Figure 12. With higher TMC/BDO feed ratios, retention times of PTMC oligomers are shifted to shorter times, corresponding to longer PTMC chains. As shown in Table 5, for a TMC/BDO ratio of 2:1, the corresponding $Đ_M$ is 1.41. Increasing the TMC/BDO ratio to 50:1, $Đ_M$ increases to 1.77. It is therefore obvious that $Đ_M$, when total monomer conversion is completed, is dependent on TMC/BDO feed ratio.

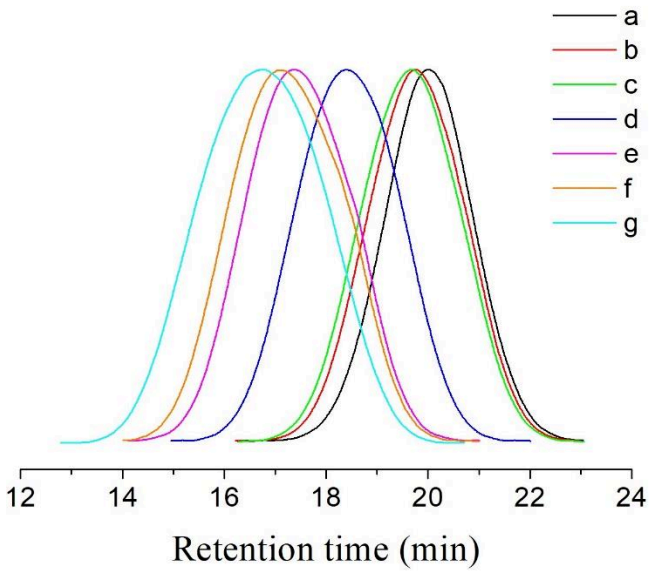

Figure 12. SEC chromatograms of PTMC by TBD with different molar masses: (a) run 1; (b) run 2; (c) run 3; (d) run 4; (e) run 5; (f) run 6; (g) run 7 (Table 1, in THF at 30 °C).

3.6 Thermal properties of PTMC oligomers

3.6.1. Glass transition

According to the study of Pêgo et al.[35], PTMC T_g is around -20 °C with $\overline{M}_n$ ranging from 57 000 to 355 000 g/mol. As seen in Table 10, T_g of PTMC oligomers obtained by DSC are dependent on $\overline{M}_n$. For example, T_g increases sharply from -76.1 to -35.4 °C with $\overline{M}_n$ increasing from 290 to 1330 g/mol. For PTMC with $\overline{M}_n$ of 5070 g/mol, T_g reaches -22.6 °C, which is near to the T_g determined by Pêgo. We can consider that exchange reactions and multiple BDO retrieved in the oligomer backbones do not affect the global T_g measured. When $\overline{M}_n$ is above 5070 g/mol, T_g will not be significantly changed by increasing $\overline{M}_n$ further since the critical molar mass of entanglement is exceeded[35]. The relation between PTMC $\overline{DP}_n$ and T_g is shown in Figure 13.

Table 10. Glass transitions and thermal degradation properties of PTMC oligomers synthesized at 100 °C

Run	TMC/BDO (mol/mol)	Reaction time (h)	$\overline{DP}_n$[a]	$\overline{M}_n$[b] (g/mol)	T_g (°C)	T_{onset} (°C)	T_{max} (°C)
1	2:1	1	2.0	290	-76.1	133.6	242.7
2	4:1	1	4.0	500	-55.8	135.7	242.5
3	6:1	1	6.0	700	-49.6	151.5	240.7
4	12:1	1	12.1	1330	-35.4	181.8	239.1
5	19:1	1	18.6	1990	-31.6	184.2	237.4
6	30:1	1	29.5	3080	-28.0	182.1	240.7
7	50:1	1	48.8	5070	-22.6	191.5	240.7

[a]$\overline{DP}_n$ was determined by ^{1}H NMR with Eq. (4). [b]$\overline{M}_n$ was determined by ^{1}H NMR.

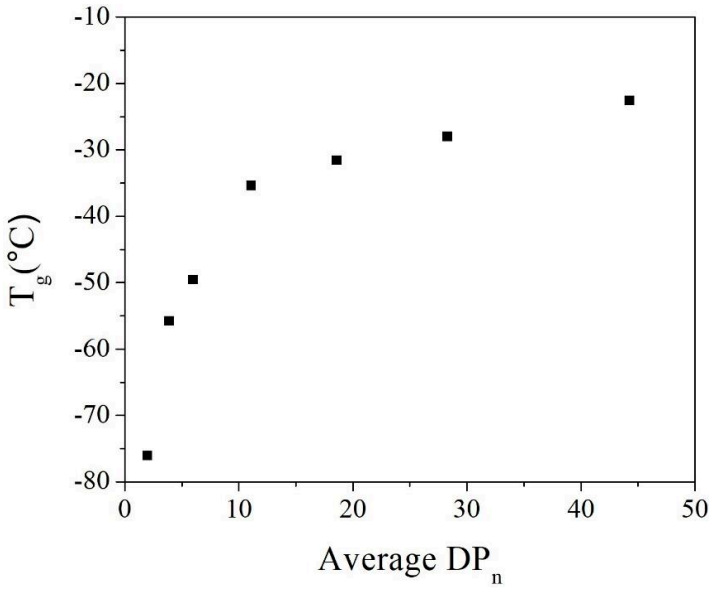

Figure 13. Influence of $\overline{DP}_n$ on T_g for PTMC oligomers.

3.6.2. Thermal degradation

The thermal stability of PTMC oligomers was evaluated by thermogravimetric analysis (TGA) and derivative thermogravimetry (DTG) at temperatures ranging from 25 to 500 °C as depicted in Figure 14. For all PTMC samples, the similar shapes of TGA thermograms indicate a unique degradation process. The onset decomposition temperature T_{onset} (5% of weight loss) is used to discuss thermal stability. As seen in Figure 15 and Table 10, it is obvious that T_{onset} increases

from 133.6 to 181.8 °C when $\overline{M}_n$ varies from 290 to 1330 g/mol. Above 1330 g/mol, T_{onset} tends to be constant around 182 °C and it reaches 191.5 °C with $\overline{M}_n$ at 5070 g/mol. In Figure 14 (B), the DTG curves show one single-stage degradation process and the fastest degradation temperature (T_{max}). It is clear that T_{max} are similar for all PTMC oligomers around 240 °C and that all PTMC oligomers bear a 100% degradation before 500 °C.

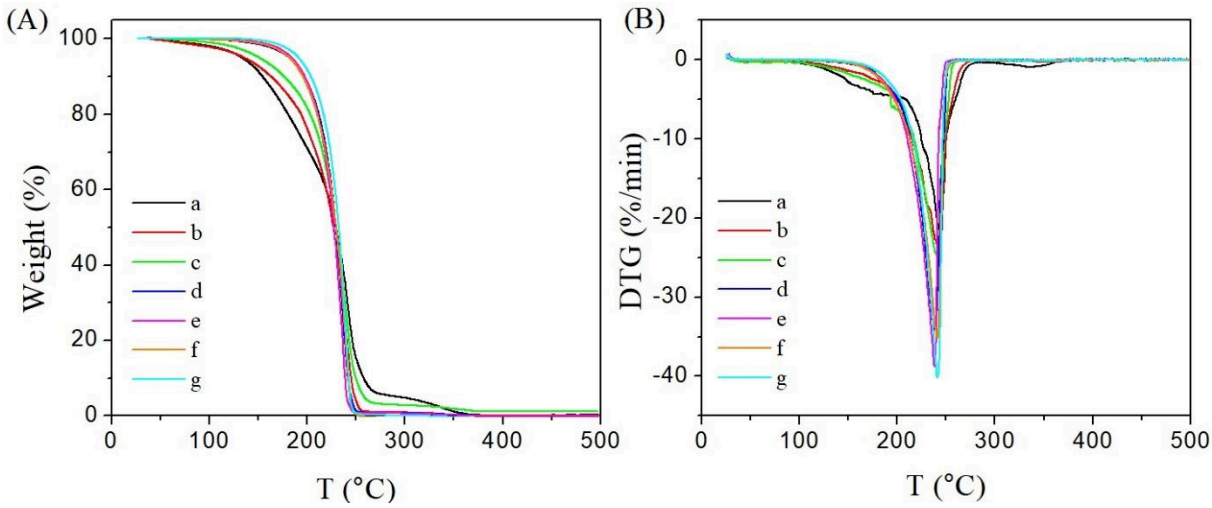

Figure 14. (A) TGA and (B) DTG derivative thermogravimetry curves of PTMC oligomers with (a) run 1; (b) run 2; (c) run 3; (d) run 4; (e) run 5; (f) run 6; (g) run 7 (Table 10, heating from 25 °C to 500 °C at 10 °C/min).

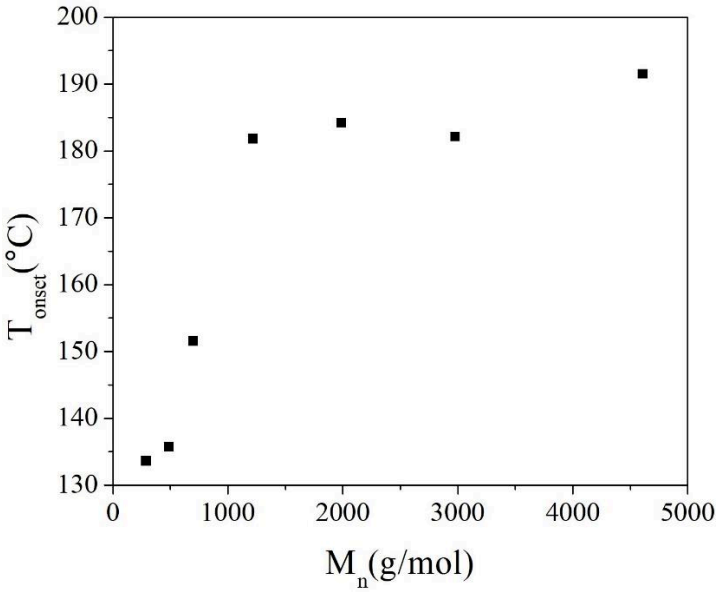

Figure 15. The effect of $\overline{M}_n$ on T_{onset} for PTMC oligomers.

3.7 Viscoelastic properties of PTMC oligomers

The rheology of the synthesized PTMC was obtained at 30 °C from frequency sweep tests (Figure 16). The loss modulus G'' increases with the PTMC molar mass within the same frequency range. Moreover, the resulting average complex viscosity η^* increases from 2 Pa.s to 320 Pa.s with molar masses ranging from 500 g/mol to 1990 g/mol (Table 5). As expected, these oligomers are viscous with no entanglements in these molecular weight ranges. T_g is below -22°C in all cases.

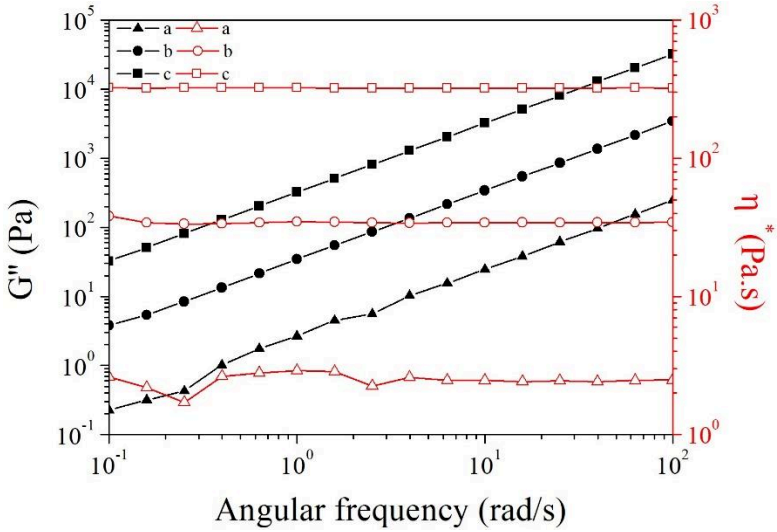

Figure 16. Rheological behaviors of loss modulus G'' (full symbols) and complex viscosity η^* (hollow symbols) for PTMC with (a) run 2; (b) run 4; (c) run 5 (Table 5, 30 °C, strain of 1%).

4. Conclusion

PTMC oligomers were synthesized in bulk at 100 °C with BDO as co-initiator through ring-opening polymerization by conventional mechanisms. Both alcohol functions of the used diol were not able to fully start the PTMC chains growing due to the specific low monomer/BDO ratios. Surprisingly, exchange reactions between carbonate and alcohol functions were found to be intense but without decarboxylation at 100 °C. Consequently, new kinds of PTMC chains were clearly characterized either without BDO or with several BDO radicals, up to five of them. Such radical from the co-initiator can be retrieved in the backbones and/or at the end chains. These exchange reactions provoked the formation of longer chains with broadened mass distributions. With TBD as catalyst, a total monomer conversion was observed after 30 minutes while $Sn(Oct)_2$ required 24 h to get a full conversion. This long reaction time with $Sn(Oct)_2$ was certainly due to its direct use associated to the existence of octanoic acid. The higher TMC/BDO

feed ratios led to fewer exchange reactions. TBD was able to get $\overline{M}_n$ closer to theoretical values as well as $Đ_M$ relatively lower than $Sn(Oct)_2$. The PTMC T_g was found to increase from -78 to -22 °C when $\overline{M}_n$ exceeded 5070 g/mol. Besides, T_{onset} also increased with molar mass and reached 191.5 °C for PTMC with $\overline{M}_n$ = 5070 g/mol. Through rheological tests, it was observed that both complex viscosity η^* and loss modulus G″ increased as a function of PTMC molar mass with no chain entanglements. Such oligomers remained in the liquid state with complex viscosities between 2 and 320 Pa.s.

Acknowledgments

The authors thank the financial support from China Scholarship Council (CSC). This work benefited from the international cooperation between Université Jean Monnet (France) and East China University of Science and Technology (China).

References

[1] I. Armentano, N. Bitinis, E. Fortunati, S. Mattioli, N. Rescignano, R. Verdejo, M.A. Lopez-Manchado, J.M. Kenny, Multifunctional nanostructured PLA materials for packaging and tissue engineering, Progress in Polymer Science 38(10) (2013) 1720-1747.

[2] S. Slomkowski, S. Penczek, A. Duda, Polylactides—an overview, Polymers for Advanced Technologies 25(5) (2014) 436-447.

[3] D. Ishii, T.H. Ying, A. Mahara, S. Murakami, T. Yamaoka, W. Lee, T. Iwata, In Vivo Tissue Response and Degradation Behavior of PLLA and Stereocomplexed PLA Nanofibers, Biomacromolecules 10(2) (2009) 237-242.

[4] D. Donald J., M. Adriana I., W. Stephanie J., Ring-Opening Polymerization of Renewable Six-Membered Cyclic Carbonates. Monomer Synthesis and Catalysis, in: Green Polymerization Methods: Renewable Starting Materials, Catalysis and Waste Reduction, Robert T. Mathers, M.A.R. Meier (Eds.), Wiley-VCH, Weinheim, 2011, Vol., pp. 165-201.

[5] Z. Zhang, R. Kuijer, S.K. Bulstra, D.W. Grijpma, J. Feijen, The in vivo and in vitro degradation behavior of poly(trimethylene carbonate), Biomaterials 27(9) (2006) 1741-1748.

[6] R.P. Brannigan, A.P. Dove, Synthesis, properties and biomedical applications of hydrolytically degradable materials based on aliphatic polyesters and polycarbonates, Biomaterials science 5(1) (2017) 9-21.

[7] L. Mespouille, O. Coulembier, M. Kawalec, A.P. Dove, P. Dubois, Implementation of metal-free ring-opening polymerization in the preparation of aliphatic polycarbonate materials, Progress in Polymer Science 39(6) (2014) 1144-1164.

[8] J. Matsuo, K. Aoki, F. Sanda, T. Endo, Substituent Effect on the Anionic Equilibrium Polymerization of Six-Membered Cyclic Carbonates, Macromolecules 31(14) (1998) 4432-4438.

[9] H.R. Kricheldorf, J. Jenssen, Polylactones. 16. Cationic Polymerization of Trimethylene Carbonate and Other Cyclic Carbonates, Journal of Macromolecular Science: Part A - Chemistry 26(4) (1989) 631-644.

[10] C.M. Thomas, Stereocontrolled ring-opening polymerization of cyclic esters: synthesis of new polyester microstructures, Chemical Society reviews 39(1) (2010) 165-173.

[11] N.E. Kamber, W. Jeong, R.M. Waymouth, R.C. Pratt, B.G.G. Lohmeijer, J.L. Hedrick, Organocatalytic Ring-Opening Polymerization, Chemical Reviews 107(12) (2007) 5813-5840.

[12] K.S. Bisht, Y.Y. Svirkin, L.A. Henderson, R.A. Gross, D.L. Kaplan, G. Swift, Lipase-Catalyzed Ring-Opening Polymerization of Trimethylene Carbonate, Macromolecules 30(25) (1997) 7735-7742.

[13] H. Hyun, M.S. Kim, G. Khang, H.B. Lee, Ring-opening polymerization of trimethylene carbonate by poly(ethylene glycol) in the presence of HCl·Et2O as a monomer activator, Journal of Polymer Science Part A: Polymer Chemistry 44(13) (2006) 4235-4241.
[14] D. Delcroix, B. Martín-Vaca, D. Bourissou, C. Navarro, Ring-Opening Polymerization of Trimethylene Carbonate Catalyzed by Methanesulfonic Acid: Activated Monomer versus Active Chain End Mechanisms, Macromolecules 43(21) (2010) 8828-8835.
[15] F. Nederberg, B.G.G. Lohmeijer, F. Leibfarth, R.C. Pratt, J. Choi, A.P. Dove, R.M. Waymouth, J.L. Hedrick, Organocatalytic Ring Opening Polymerization of Trimethylene Carbonate, Biomacromolecules 8(1) (2007) 153-160.
[16] M. Helou, O. Miserque, J.-M. Brusson, J.-F. Carpentier, S.M. Guillaume, Organocatalysts for the Controlled "Immortal" Ring-Opening Polymerization of Six-Membered-Ring Cyclic Carbonates: A Metal-Free, Green Process, Chemistry – A European Journal 16(46) (2010) 13805-13813.
[17] M.K. Kiesewetter, M.D. Scholten, N. Kirn, R.L. Weber, J.L. Hedrick, R.M. Waymouth, Cyclic guanidine organic catalysts: what is magic about triazabicyclodecene?, The Journal of Organic Chemistry 74(24) (2009) 9490-6.
[18] C.G. Jaffredo, J.F. Carpentier, S.M. Guillaume, Controlled ROP of beta-butyrolactone simply mediated by amidine, guanidine, and phosphazene organocatalysts, Macromolecular rapid communications 33(22) (2012) 1938-44.
[19] O. Dechy-Cabaret, B. Martin-Vaca, D. Bourissou, Controlled Ring-Opening Polymerization of Lactide and Glycolide, Chemical reviews 104(12) (2004) 6147-6176.
[20] A. Chuma, H.W. Horn, W.C. Swope, R.C. Pratt, L. Zhang, B.G.G. Lohmeijer, C.G. Wade, R.M. Waymouth, J.L. Hedrick, J.E. Rice, The Reaction Mechanism for the Organocatalytic Ring-Opening Polymerization of l-Lactide Using a Guanidine-Based Catalyst: Hydrogen-Bonded or Covalently Bound?, Journal of the American Chemical Society 130(21) (2008) 6749-6754.
[21] L. Simón, J.M. Goodman, The Mechanism of TBD-Catalyzed Ring-Opening Polymerization of Cyclic Esters, The Journal of Organic Chemistry 72(25) (2007) 9656-9662.
[22] H. Wu, Y. Ji, Z. Li, X. Wang, Q. Zhang, S. Cui, W. Wu, J. Liu, K. Guo, Cationic ring-opening polymerization of trimethylene carbonate to α,ω-dihydroxy telechelic and star-shaped polycarbonates catalyzed by reusable o-benzenedisulfonimide, Journal of Polymer Science Part A: Polymer Chemistry 53(6) (2015) 729-736.
[23] X. Wang, S. Cui, Z. Li, S. Kan, Q. Zhang, C. Zhao, H. Wu, J. Liu, W. Wu, K. Guo, A base–conjugate-acid pair for living/controlled ring-opening polymerization of trimethylene

carbonate through hydrogen-bonding bifunctional synergistic catalysis, Polym. Chem. 5(20) (2014) 6051-6059.
[24] H.R. Kricheldorf, K. Ahrensdorf, S. Rost, Polylactones, 68 - Star-shaped homo- and copolyesters derived from epsilon-caprolactone, L,L-lactide and trimethylene carbonate, Macromolecular Chemistry and Physics 205(12) (2004) 1602-1610.
[25] A. Smola, P. Dobrzynski, M. Cristea, J. Kasperczyk, M. Sobota, K. Gebarowska, H. Janeczek, Bioresorbable terpolymers based on l-lactide, glycolide and trimethylene carbonate with shape memory behaviour, Polymer Chemistry 5(7) (2014) 2442-2452.
[26] C. Samuel, Y. Chalamet, F. Boisson, J.-C. Majesté, F. Becquart, E. Fleury, Highly efficient metal-free organic catalysts to design new Environmentally-friendly starch-based blends, Journal of Polymer Science Part A: Polymer Chemistry 52(4) (2014) 493-503.
[27] F. Becquart, Y. Chalamet, J. Chen, Y. Zhao, M. Taha, Poly[ethylene-co-(vinyl alcohol)]-graft-poly(ε-caprolactone) Synthesis by Reactive Extrusion, 1 - Structural and Kinetic Study, Macromolecular Materials and Engineering 294(10) (2009) 643-650.
[28] P.Y.W. Dankers, Z. Zhang, E. Wisse, D.W. Grijpma, R.P. Sijbesma, J. Feijen, E.W. Meijer, Oligo(trimethylene carbonate)-Based Supramolecular Biomaterials, Macromolecules 39(25) (2006) 8763-8771.
[29] K. Fukushima, Poly(trimethylene carbonate)-based polymers engineered for biodegradable functional biomaterials, Biomaterials science 4(1) (2016) 9-24.
[30] E. Bat, B.H.M. Kothman, G.A. Higuera, C.A. van Blitterswijk, J. Feijen, D.W. Grijpma, Ultraviolet light crosslinking of poly(trimethylene carbonate) for elastomeric tissue engineering scaffolds, Biomaterials 31(33) (2010) 8696-8705.
[31] M. Helou, J.-F. Carpentier, S.M. Guillaume, Poly(carbonate-urethane): an isocyanate-free procedure from α, ω-di(cyclic carbonate) telechelic poly(trimethylene carbonate)s, Green Chemistry 13(2) (2011) 266-271.
[32] R.C. Pratt, F. Nederberg, R.M. Waymouth, J.L. Hedrick, Tagging alcohols with cyclic carbonate: a versatile equivalent of (meth)acrylate for ring-opening polymerization, Chemical communications (1) (2008) 114-116.
[33] A. Kowalski, A. Duda, S. Penczek, Mechanism of Cyclic Ester Polymerization Initiated with Tin(II) Octoate. 2. Macromolecules Fitted with Tin(II) Alkoxide Species Observed Directly in MALDI−TOF Spectra, Macromolecules 33(3) (2000) 689-695.
[34] A. Kowalski, A. Duda, S. Penczek, Kinetics and Mechanism of Cyclic Esters Polymerization Initiated with Tin(II) Octoate. 3. Polymerization of l,l-Dilactide, Macromolecules 33(20) (2000) 7359-7370.

[35] A.P. Pêgo, D.W. Grijpma, J. Feijen, Enhanced mechanical properties of 1,3-trimethylene carbonate polymers and networks, Polymer 44(21) (2003) 6495-6504.
[36] K.J. Zhu, R.W. Hendren, K. Jensen, C.G. Pitt, Synthesis, properties, and biodegradation of poly(1,3-trimethylene carbonate), Macromolecules 24(8) (1991) 1736-1740.
[37] F. Yu, R. Zhuo, Synthesis and Characterization of OH-Terminated Poly(trimethylene carbonate)s by Alcohol-Initiated Ring-Opening Polymerization in Melt Bulk without Using Any Catalyst, Polym J 36(1) (2004) 28-33.
[38] F. Becquart, M. Taha, A. Zerroukhi, J. Kaczun, M.-F. Llauro, Microstructure and properties of poly(vinyl alcohol-co-vinyl acetate)-g-ε-caprolactone, European Polymer Journal 43(4) (2007) 1549-1556.
[39] F. Becquart, M. Taha, A. Zerroukhi, Y. Chalamet, J. Kaczun, M.-F. Llauro, ε-caprolactone grafting on a poly(vinyl alcohol-co-vinyl acetate) in the melt without added initiator, Journal of Applied Polymer Science 105(5) (2007) 2525-2531.
[40] H. Marion, M. Olivier, B. Jean-Michel, C. Jean-François, G.S. M., Ultraproductive, Zinc-Mediated, Immortal Ring-Opening Polymerization of Trimethylene Carbonate, Chemistry – A European Journal 14(29) (2008) 8772-8775.
[41] S. Touhtouh., F. Becquart., M. Taha., Graft copolymers synthesis by dynamic covalent reorganization of polycaprolactone and poly(ethylene-co-vinyl alcohol), Journal of Applied Polymer Science 123(5) (2012) 3145-3153.
[42] A.-C. Albertson, M. Sjoling, Homopolymerization of 1,8Dioxan-2-one to High Molecular Weight Poly(Trimethylene Carbonate), Journal of Macromolecular Science, Part A 29(1) (1992) 43-54.

Chapter 3. Thermoreversible supramolecular networks from poly(trimethylene carbonate) synthesized by condensation with triuret and tetrauret

Xiang Li[a,b,c], Nathalie Mignard[a,b,c], Mohamed Taha[a,b,c], Frédéric Prochazka[a,b,c], Jianding Chen[d], Shengmiao Zhang[d] and Frédéric Becquart[a,b,c*]

[a]Université de Lyon, F-42023 Saint-Etienne, France

[b]CNRS, UMR 5223, Ingénierie des Matériaux Polymères, F-42023 Saint-Etienne, France

[c]Université Jean Monnet, F-42023 Saint-Etienne, France

[d]Laboratory of Advanced Materials Processing, East China University of Science and Technology, 200237 Shanghai, China

[*]Corresponding Author. E-mail: Frederic.Becquart@univ-st-etienne.fr

Abstract

Poly(trimethylene carbonate) (PTMC) is a promising biomaterial but with relatively poor dimensional stability and low tensile mechanical properties. To overcome these drawbacks, PTMC-based multiarm supramolecular polymers bearing self-complementary triuret and tetrauret hydrogen-bonding motifs (HBMs) at the chain ends were synthesized in this work with various functionalities and HBM concentrations. These supramolecular structures were elaborated through condensation between diisocyanate 4,4'-methylenebis(cyclohexyl isocyanate) (H_{12}MDI) and telechelic PTMC oligomers, urea/biuret, glycerol and 1-pentanol in three steps. The equilibrium shifts of hydrogen bonding between HBMs were traced by ^{1}H NMR in DMSO-d_6 and FT-IR in bulk at different temperatures. Association constants (K_a) of triuret and tetrauret HBMs were measured to be 0.32 M^{-1} and 1.59 M^{-1} respectively in $CDCl_3$. Compared to a previous study, PTMC chains reduced the triuret HBM K_a by 300 times. PTMC chain length was found to have the greatest effect on T_g while the functionality or HBM structure did not. Thermal stability of supramolecular polymers was enhanced by HBMs with tetrauret being more efficient than triuret. Networks structures were formed due to the transient physical crosslinks by hydrogen bonding between HBMs, evidenced by the high transient temperature from elastic state to liquid state ($T_{crossover}$) and good creep resistance. Increasing the functionality or reducing PTMC chain length can increase the $T_{crossover}$, creep resistance and Young's modulus in tensile tests. In contradiction to the measured K_a, triuret HBMs leads to

the formation of denser physical network structures than their tetrauret counterparts, causing higher $T_{crossover}$ and better dimensional stability consequently. Although the introduction of triuret or tetrauret HBMs decrease the biodegradability of supramolecular polymers, the influence of their structures is unapparent.

Keywords: PTMC, hydrogen bonds, supramolecular, urea, self-assembly

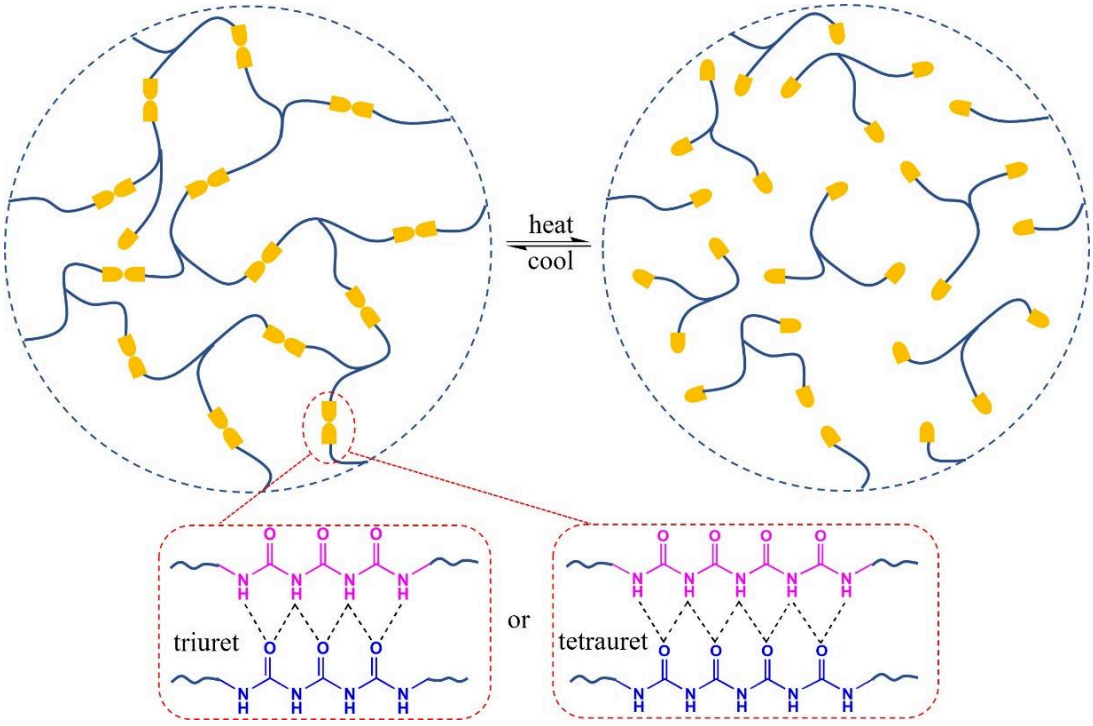

1. Introduction

In the last three decades, supramolecular chemistry has developed rapidly since Jean-Marie Lehn[1], Donald J. Cram[2] and Charles J. Pedersen[3] founded this bioinspired reversible chemistry in 1987. Hydrogen bonding attracts people the most among all supramolecular interactions because of its strong directionality and versatility[4]. Despite the possibility to simply describe a hydrogen bond as an interaction between a proton donor and an acceptor, several factors could affect its energy, such as electrostatic, polarization, transfer and dispersion[5].Besides, the nature of atoms linked to the electropositive hydrogen and the chemical environment affect the characteristics of hydrogen bond greatly as well. As to the hydrogen bonding directionality, although linear geometry is always preferred, bifurcated structures could also be formed[6,7]. In polymer science, due to the dynamic properties of hydrogen-bonding interactions, various supramolecular structures[4,8] were designed to endow the materials with certain fascinating new functions[9] such as self-healing[10-12], shape

memory[13,14], stimuli-responsiveness[15] and even some biomimetic opportunities in the biomedical field[16].

For single hydrogen bond, its strength usually varies from weak to strong in more than two orders of magnitude[17]. Thanks to the development of multiple hydrogen-bonding motifs (HBMs), K_a values extend on a larger scale[18,19]. For example, Ni et al.[20] synthesized relatively weak associations by triuret blocks with a K_a of 95 M^{-1} (in $CDCl_3$). Sijbesma et al.[21] obtained extremely strong quadruple hydrogen-bonded dimers by 2-ureido-4[1H]-pyrimidinone (UPy) groups with a corresponding K_a of 6×10^7 M^{-1} (in $CDCl_3$). It is noteworthy that the strongest systems usually resemble covalent systems and endow materials with robustness, leading to the loss of reversibility and certain properties such as recyclability[22,23].

The strength of hydrogen bonding can be evaluated by its association energy. Iogansen[24] built a direct relation between such energy and the intensification of the labile proton stretching vibration band by FT-IR. Besides, Noro et al.[25] measured the energy of hydrogen bonding between a poly(2-vinylpyridine)-b-poly(ethyl acrylate)-b-poly(2-vinylpyridine) triblock copolymer and a poly(4-hydroxystyrene) crosslinker to be 13 kJ/mol using the same way. More generally, the strengths of hydrogen bonds are determined indirectly by the association constant (K_a) which relates to the thermodynamic equilibrium of associations. Titration experiments in solutions[26] are often used to measure K_a, for example, by ^{1}H NMR[27], fluorescence[28] and UV/vis[29] with different calculation models[26,30-32]. ^{1}H NMR titration in deuterated chloroform is the most widely applied choice, imparting the possibility to compare K_a of different hydrogen-bonding interactions with $CDCl_3$ acting as an almost universal reference.

Poly(trimethylene carbonate) (PTMC) is a biodegradable and biosourced material[33-35] with a low glass transition temperature T_g of -20 °C and high flexibility in standard use conditions[36]. Due to its biocompatibility, it can be used for specific applications such as acting as hydrogels for biomedical use[37]. However, its weak mechanical strength usually discourages its further applications even as scaffolds for soft tissue regeneration[38]. For example, when PTMC molar mass is below 100 000 g/mol, it has poor dimensional stability and tensile mechanical properties[36,39].

PTMC is usually synthesized by ring-opening polymerization (ROP) with numerous activation systems[40] just as well-known lactide and lactone ROP[41]. In particular, co-initiation with monoalcohol ROH is of interest since the radical R is retrieved at polymerized starting chain

and offers functionalization opportunities consequently. If a diol (HO-R-OH) is used as co-initiator, linear PTMC chains with hydroxyl functions at both chain ends (HO-R-O-PTMC-OH) will be obtained. Thanks to the vast chemistry opportunities applied to alcohol functions, such as esterification, reactions with isocyanates, ring-opening polymerization of lactide, lactone or epoxy, it becomes possible to build more sophisticated structures from telechelic PTMC. For example, an isocyanate/alcohol reaction is attractive because it offers not only the possibility to design PTMC with different end-capped structures or functionalities but also the possibility to introduce HBMs simultaneously to elaborate supramolecular structures. This strategy was already applied to introduce triuret/tetrauret HBM by the reactions between urea or biuret and diisocyanates in a previous study in our laboratory[20]. Through the additional use of multi-ols such as glycerol, the functionality of supramolecular polymers could be adjusted, such as to obtain mutiarmed structures.

In this work, multiarm supramolecular polymers will be synthesized by condensation between isocyanates and -OH/-NH_2 functions with trifunctional glycerol as a starting point, PTMC oligomers as spacers and diisocyanates as linkers. Additionally, triuret/tetrauret HBMs will be implemented by the reaction between diisocyanates and urea/biuret. The functionality, namely number of arms will be tuned by the reagent feed ratios. Two PTMC oligomers with the molar masse of 1000 and 2000 g/mol will be used with the purpose of adjusting HBMs concentration. Through the associations between triuret or tetrauret HBMs in each arm of supramolecular polymers, crosslinked structures can be formed. K_a of triuret and tetrauret HBMs will be measured and compared to Ni's result (K_a of triuret HBMs is 95 M^{-1})[20] to reveal the effect of neighboring PTMC oligomers on the hydrogen-bonding associations. These multiarm supramolecular polymers will be studied in bulk by rheology and creep tests to verify the existence of networks structures and to establish the structure-properties relationships. The effects of HBM functionality and concentration on thermal, tensile mechanical, and biodegradable properties will be studied.

2. Experimental section

2.1 Materials

Glycerol (≥ 99.5%) and 1-pentanol (≥ 99%) were purchased from Sigma Aldrich and dried on 4 Å molecular sieves before use. Urea (98%), biuret (≥ 98%), 4,4'-methylenebis(cyclohexyl isocyanate) (H_{12}MDI, 90%, mixture of isomers), dibutyltin dilaurate (DBTL, 95%) and N,N-

dimethylformamide (DMF, anhydrous, 99.8%) were all purchased from Sigma Aldrich and used directly. DMSO-d_6 and $CDCl_3$ were purchased from Eurisotop.

PTMC oligomers were synthesized by ring-opening polymerization with trimethylene carbonate (TMC) as monomer and 1,4-butanediol (BDO) as co-initiator. 1,5,7-triazabicyclo[4.4.0]dec-5-ene (TBD) was used as catalyst. The syntheses and characterizations were studied in detail in our recent work[42]. Despite the carbonate-carbonate and carbonate-alcohol exchange reactions which lead to redistribution of TMC and BDO units, the synthesized linear oligomers are all capped by alcohol functions and have molar masses close to theoretical ones. $PTMC_{1000}$ (number average molar mass $\overline{M}_n$ = 1000 g/mol, molar-mass dispersity $Đ_M = \overline{M}_n/\overline{M}_w$ = 1.58) and $PTMC_{2000}$ ($\overline{M}_n$ =2000 g/mol, $Đ_M$ = 1.60) oligomers were used in this work.

2.2 Characterization techniques

FT-IR analyses

Fourier-transform infrared spectroscopy (FT-IR) spectra were recorded with a Nicolet Nexus FT-IR spectrometer using an ATR from 4000 cm^{-1} to 700 cm^{-1}. 64 scans were collected with a bandwidth set at 4 cm^{-1} at room temperature. The reaction of isocyanate groups was followed by peaks at 2260 cm^{-1} of samples freshly withdrawn from the reaction system.

FT-IR spectra of samples at different temperatures were recorded from thin films onto a 13 mm KBr pellet. Thin films were obtained by spreading THF diluted samples onto KBr pellets and drying in an oven at 80 °C and 0.2 mbar overnight. The temperature was controlled by an electrically heated chamber linked to a temperature controller. All spectra were recorded from 4000 cm^{-1} to 700 cm^{-1} by 64 scans.

^{1}H NMR analyses

^{1}H NMR analyses were performed by a Bruker Advance III spectrometer working at 400 MHz equipped with a 5 mm multinuclear broadband probe (BBFO+) with z-gradient coil. DMSO-d_6 and $CDCl_3$ were used as the deuterated solvents.

20-30 mg of samples were weighed and totally solubilized in 0.7 mL DMSO-d_6 to obtain transparent solutions for structural characterizations. Samples with various HBMs concentrations (0.005-0.05 mol/L) in $CDCl_3$ were obtained for K_a measurements. Spectra were

recorded by 128 scans at 298 K for $CDCl_3$ and at 298 K, 353 K, 393 K for DMSO-d_6. Tetramethylsilane (TMS) was used as reference with a chemical shift δ of 0.00 ppm.

Size-exclusion chromatography (SEC) tests

Molecular weights were obtained by SEC using Waters equipment: a 515 HPLC pump, a 717 plus autosampler, and a 2414 refractive index detector. Additionally, a Wyatt ViscoStar viscometer and a WYATT miniDAWN TREOS multi-angle light scattering detector were used with no signal detected. Styragel HR 0.5, 1 and 3 columns were used. Tetrahydrofuran (THF, Biosolve, GPC grade) was used as solvent at 30 °C with a flow rate of 1 mL/min. Refractive index increments *dn/dC* were obtained directly from peaks. Narrow dispersity polystyrene standards were used for calibration.

Thermal analysis

Analyses by differential scanning calorimetry (DSC) were performed by a TA Q10 with heating and cooling ramps at 10 °C.min^{-1}. All experiments were tested in hermetically sealed pans by two heating and one cooling ramps from -70 °C to 200 °C under nitrogen flow at 50 mL/min. The thermal transitions were measured from the second heating ramp.

Thermal gravimetric analysis (TGA) experiments were performed with a Mettler Toledo TGA/DSC 1 Star system from 25 °C to 500 °C at 10 °C.min^{-1} under nitrogen atmosphere (80 mL/min). The weight of samples was fixed around 5 mg.

Oscillatory rheology tests

Oscillatory rheology tests were performed with an ARES-G2 (TA Instruments) rheometer with parallel plates (25 mm diameter). All the samples were first annealed in an oven at 80 °C at 200 mbar for approximately 24 h prior to rheology tests. Strain sweep tests were performed to obtain the linear viscoelastic region (LVR). Temperature ramp tests were conducted with a controlled strain in LVR under oscillation mode.

Creep tests

Creep tests were carried out by a stress-controlled MCR 301 from ANTON PAAR with parallel plates (25 mm diameter) and a gap fixed between 0.5 and 0.8 mm at 80 °C or 140 °C. All the tests were performed under a controlled constant rotational stress of 100 Pa for 90 minutes

followed by a 90 minutes relaxation process. Samples were annealed at the measurement temperature in an oven for around 24 h at 200 mbar.

Tensile tests

Tensile measurements were carried out by a universal tensile tester, a Shimadzu Autograph AGS-X with 500 N load cells. Dumbbell-shaped specimens were prepared with a dimension of 50 mm × 4 mm × 0.5 mm respecting ISO 37:2005 standard (dumbbell: type 3). All samples were first maturated in an oven at 80 °C for 24 h and then tested at room temperature with a crosshead speed of 10 $mm.min^{-1}$. Young's modulus was measured from true stress versus true strain plots in a strain range between 0.2 and 0.6%.

Biodegradability tests

Biodegradability tests were conducted in 500 mL glass bottles with a carbon dioxide snare in the headspace and a cover with pressure indicator (OxiTop® Control, WTWGmbH, Weilheim, Germany) based on ISO 14851 standard. 15 mg of sample was mixed in the aqueous medium with activated sludge from a wastewater treatment station (Monistrol, France). All the samples were stirred for 28 days at 23 °C and the produced carbon dioxide during biodegradation was trapped by sodium hydroxide pellets. Biological Oxygen Demand (BOD, $mg.L^{-1}$) was calculated by the pressure in the bottle as follows:

$$Dt(\%) = \frac{BOD_{test} - BOD_{blank}}{C \times DthO_{test}} \times 100 \qquad \text{Eq. (1)}$$

where Dt is the biodegradability, BOD_{test} is the BOD of the sample, BOD_{blank} is the BOD of the activated sludge, C ($g.L^{-1}$) is the concentration of the sample and $DthO_{test}$ ($mg.g^{-1}$) is the theoretical BOD of the sample. Each sample was tested twice and the average value was reported.

2.3 Methods

Nomenclature

The obtained multiarm supramolecular polymers were named according to the main synthesis parameters. PTMC*f*L*m* denotes the material with a desired functionality of "*f*" and a PTMC molar mass of 100 × "*m*" g/mol. "L" represents the HBM, namely "B" for biuret (tetrauret motif), "U" for urea (triuret motif) and "X" for the absence of biuret or urea.

Association constant K_a determination by ^{1}H NMR chemical shifts

The K_a of HBMs were determined by a dilution titration in $CDCl_3$ (298 K) by applying labile protons from triuret or tetrauret >N-H bonds to Chen's equation[30]:

$$\delta_{obs} = \delta_m + (\delta_d - \delta_m)\frac{(1+8K_aC)^{1/2} - 1}{(1+8K_aC)^{1/2} + 1} \qquad \text{Eq. (2)}$$

Where δ_m is the >N-H chemical shift when the triuret or tetrauret HBM is fully free and not dimerized by association; δ_d is the chemical shift when all the triuret or tetrauret HBMs are dimerized; δ_{obs} is the observed chemical shift at a value between δ_m and δ_d limits; K_a and C are the association constant and the supramolecular motif concentration (mol.L^{-1}) respectively.

2.4 Synthesis of PTMC oligomers and multiarm supramolecular polymers

2.4.1 Synthesis of PTMC oligomers

The bulk syntheses and characterizations of $PTMC_{1000}$ and $PTMC_{2000}$ have already been described in detail in recent work[42]. The synthesis of $PTMC_{1000}$ oligomer is given as an example. In a 250 mL glass reactor equipped with a steel anchor, a cooler, a nitrogen gas flow and a thermostatically controlled oil bath, 60.006 g of TMC (0.588 mol) and 5.886 g of BDO (0.065 mol) were firstly mixed in the preheated reactor at 100 °C until a homogeneous state was reached. Then, 0.082 g of TBD (0.588 mmol) catalyst was added in the reactor with a stirring rate of 60 rpm. The reaction was kept for 30 min to finally get a transparent viscous material in the molten state.

2.4.2 Synthesis of multiarm supramolecular polymers with and without triuret/tetrauret HBMs

Synthesis of multiarm supramolecular polymers without HBMs

To study the influence of HBMs on the properties of multiarm supramolecular polymers, a similar structure without urea or biuret (named as PTMC3X20 in Table 1) was synthesized as a reference. 0.233 g of glycerol (2.533 mmol), 0.670 g of 1-pentanol (7.600 mmol) and 15.200 g of $PTMC_{2000}$ oligomer (7.600 mmol) were mixed in 80 mL anhydrous DMF in a preheated three-necked flask at 80 °C under a nitrogen atmosphere. After homogenization, 4.431 g of $H_{12}MDI$ (15.200 mmol) and 9.6 mg of DBTL catalyst (0.1 mol% of $H_{12}MDI$) were added. The reaction was followed up by FT-IR on withdrawn samples and stopped when the absorption of

isocyanate groups at 2260 cm^{-1} disappeared after about 3 h. After cooling down to room temperature, the material was precipitated with diethyl ether and finally dried in an oven at 80 °C for 24 h at 0.2 mbar.

Synthesis of multiarm supramolecular polymers with triuret/tetrauret HBMs

Due to the competitive reactivity of -OH and -NH_2 groups to react with isocyanates, the syntheses containing triuret/tetrauret HBMs were conducted necessarily in several steps. For the PTMC3U10 synthesis, 0.313 g of glycerol (3.395mmol) and 10.186 g of $PTMC_{1000}$ (10.186 mmol) were dissolved firstly in 80 mL of anhydrous DMF in a three-necked flask under N_2 atmosphere. After homogenization at 80 °C, 5.939 g of H_{12}MDI (20.373 mmol) and 19.3 mg of DBTL catalyst (0.1 mol% of H_{12}MDI) were added and the reaction was kept until the isocyanate carbonyl absorption at 2260 cm^{-1} became stable by FT-IR. When this first synthesis step was achieved, free isocyanate groups remained in excess at the end of the arms (scheme 1 A).

Then, the reaction temperature was increased to 110 °C along with the addition of 0.612 g of urea (10.200 mmol) and 2.969 g of H_{12}MDI (10.186 mmol). After the absorption of isocyanate groups at 2260 cm^{-1} became stable (scheme 1 B), 0.898 g of 1-pentanol (10.200 mmol) was added and the reaction was stopped when the absorption at 2260 cm^{-1} disappeared. A viscous solution was finally obtained (scheme 1 C). The solution was cooled down to room temperature and precipitated with diethyl ether. The final material was dried in an oven at 80 °C for 24 h at 0.2 mbar. The different formulations used are described in Table 1.

Table 1. Used formulations to synthesize multiarm supramolecular polymers with different functionalities in DMF at 80°C.

Sample	Glycerol:PTMC:H_{12}MDI: HBM:1-pentanol (by mol)	PTMC $\overline{M}_n$ (g/mol)	HBM type	HBM functionality
PTMC3X20	1:3:6:0:3	2000	-	0
PTMC3U20	1:3:9:3:3	2000	triuret	3
PTMC4U20	2:4:13:4:4	2000	triuret	4
PTMC3U10	1:3:9:3:3	1000	triuret	3
PTMC3B20	1:3:9:3:3	2000	tetrauret	3
PTMC3B10	1:3:9:3:3	1000	tetrauret	3

3. Results and discussions

3.1 Synthesis of multiarm supramolecular polymers

Condensation between urea/biuret and isocyanates was conducted to introduce triuret and tetrauret HBMs in final PTMC-based multiarm supramolecular polymers. In the used strategy, primary multiarm precursors were envisaged from hydroxy terminated PTMC oligomers and trifunctional glycerol as a reagent to multiply arms. Diisocyanate H_{12}MDI was chosen as linkers between these hydroxylated reagents. These multiarm precursors were all terminated by isocyanate functions to allow further reactions (scheme 1 A). To obtain the targeted supramolecular structures bearing triuret or tetrauret HBMs, urea or biuret and partial H_{12}MDI were added in a second step to induce the triuret/tetrauret formation (scheme 1 B). Finally, a monoalcohol 1-pentanol was chosen to react with the terminal isocyanate functions from H_{12}MDI (scheme 1 C).

To conduct the reaction between isocyanates and hydroxyl or amino functions, their reactivity is necessary to be considered. It is well established that the reactivity of primary aliphatic amino groups is higher than that of primary hydroxyl groups[43]. However, due to the electron-withdrawing effect of carbonyl group linked to $-NH_2$ in urea and biuret, these amino groups are less active than primary hydroxyl groups[44]. In this case, the reagents glycerol, PTMC oligomers and 1-pentanol must be introduced separately from urea and biuret to expect an exclusive reaction of amino groups with isocyanates to precisely control the supramolecular structures. The end of the first and second steps were evaluated by FT-IR following the absorbance of -NCO groups around 2260 cm^{-1} until it became stable. At this time, all -OH and $-NH_2$ groups were reacted to form urethane and urea functions respectively.

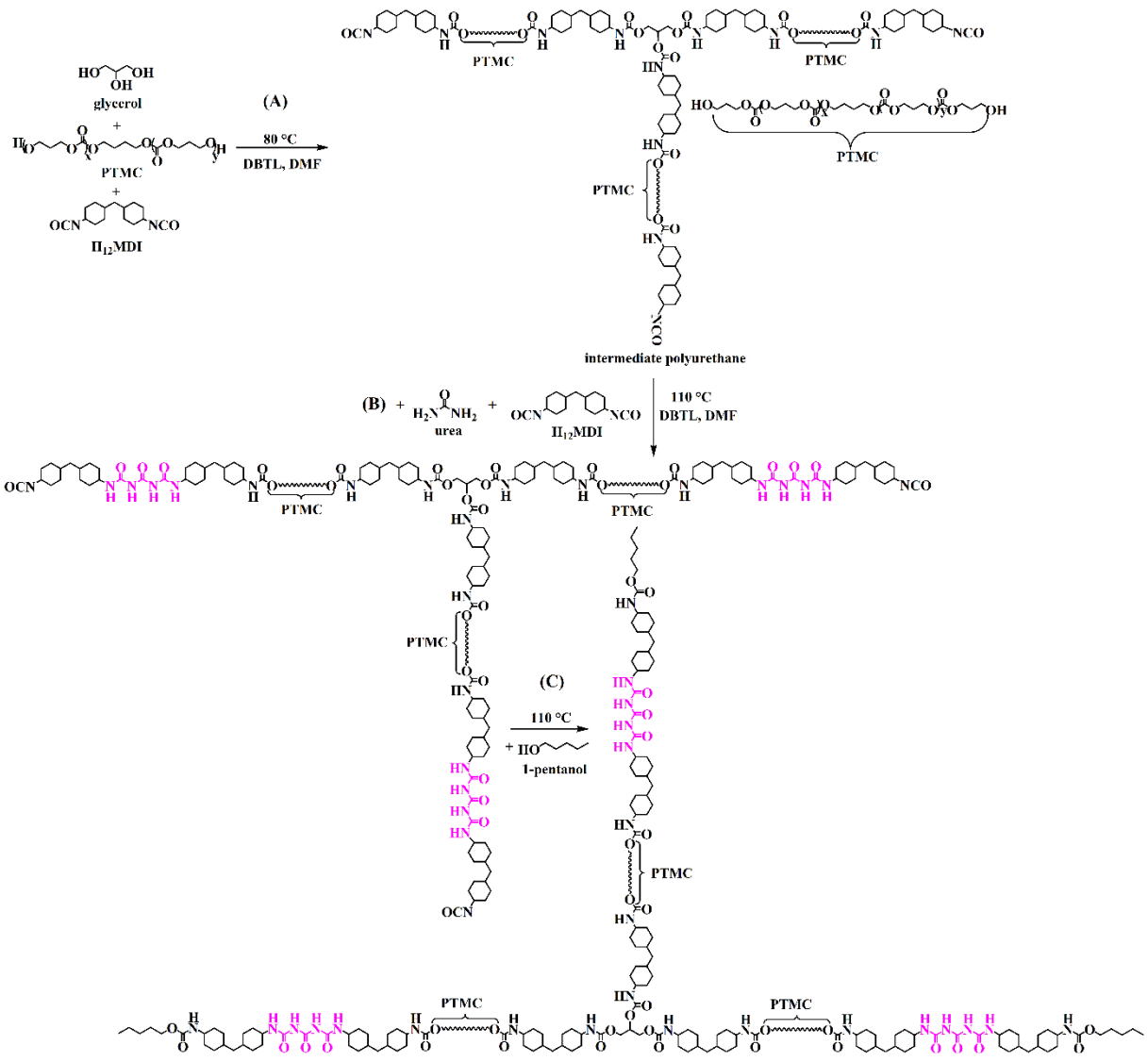

Scheme 1. Synthesis of trifunctional supramolecular PTMC3U20 with triuret HBMs.

From the formulations presented in Table 1, the final expected structures are presented in Figure 1.

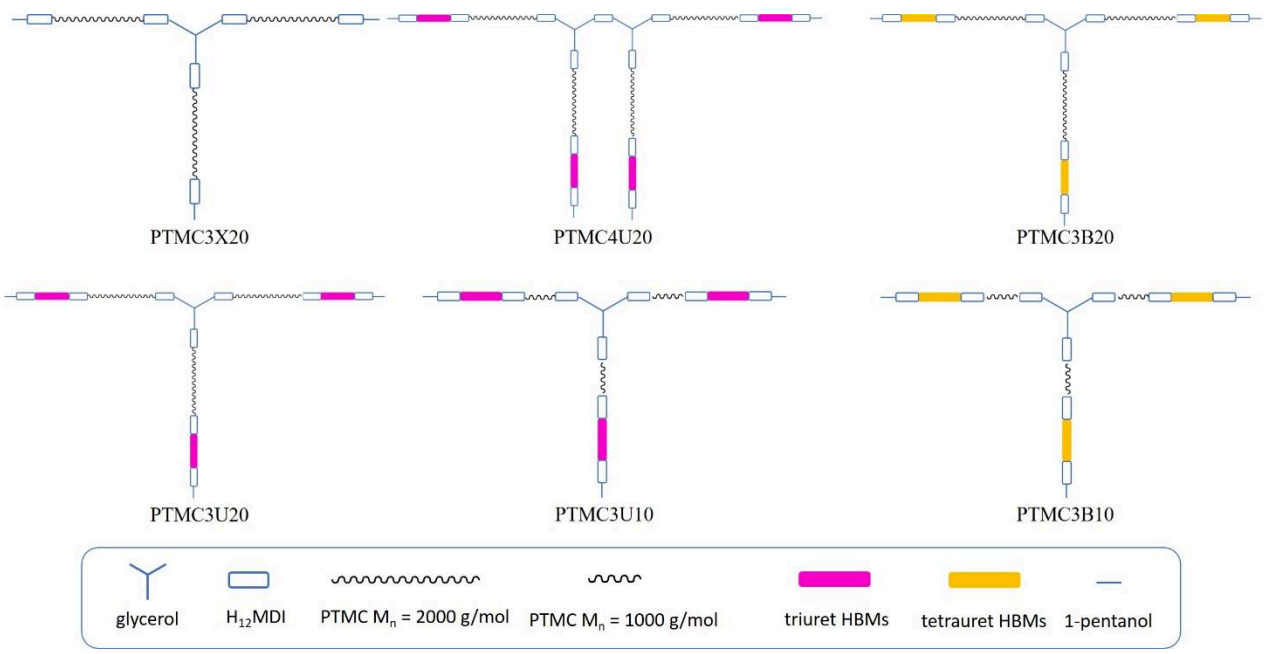

Figure 1. Schematic representation of the synthesized multiarm supramolecular polymers.

3.2 Structure characterizations of the multiarm supramolecular polymers

3.2.1 Characterization of multiarm supramolecular polymers by ^{1}H NMR

Due to the structural similarity of synthesized multiarm supramolecular polymers, all their spectra from proton resonances are very similar (Figure 2). Therefore, it is necessary to take into consideration their differences in terms of stoichiometry (Table 1). ^{1}H NMR spectrum of PTMC3U20 is presented in Figure 2 as an example. The resonances at 0.86 ppm (H_g), 1.11 ppm (H_f) and 1.45 ppm (H_e) are assigned to protons in aliphatic cyclohexyl rings, confirming the incorporation of H_{12}MDI in PTMC3U20. The complex region between 0.50 and 1.82 ppm is due to H_{12}MDI which is a mixture of three geometrical isomers trans/trans, cis/trans and cis/cis isomers[45]. The resonances near 4.13 ppm and 1.94 ppm are assigned to protons of methylene groups linked to PTMC carbonate groups (H_j) and methylene protons in TMC unit (H_k) respectively. Resonances at 3.97 and 1.87 ppm are separately attributed to $H_{j'}$ and $H_{k'}$ of the reacted TMC unit at PTMC chain end. The proton resonances of BDO units in PTMC chains are at 4.08 ppm (H_l) and 1.45 ppm (H_p) respectively. The resonances of glycerol protons are at 5.03 ppm (H_a) and 3.65 ppm (H_b). The resonances at 7.00 ppm group all labile protons from -NH- in urethane bonds (H_c, H_i and H_u) and urea bonds (H_r)[46,47]. The doublet resonances ranging from 5.86 to 5.74 ppm are assigned to -NH- protons in urea groups (H_q)[48,49]. Resonances also appear between 5.47 and 5.57 ppm. They might be due to the low hydrolysis of isocyanate groups in H_{12}MDI by moisture brought by PTMC oligomers, generating

additional alkyl amine functions[49]. After clarifying the attributions of all proton resonances, it is possible to characterize the structure of multiarm supramolecular polymers precisely.

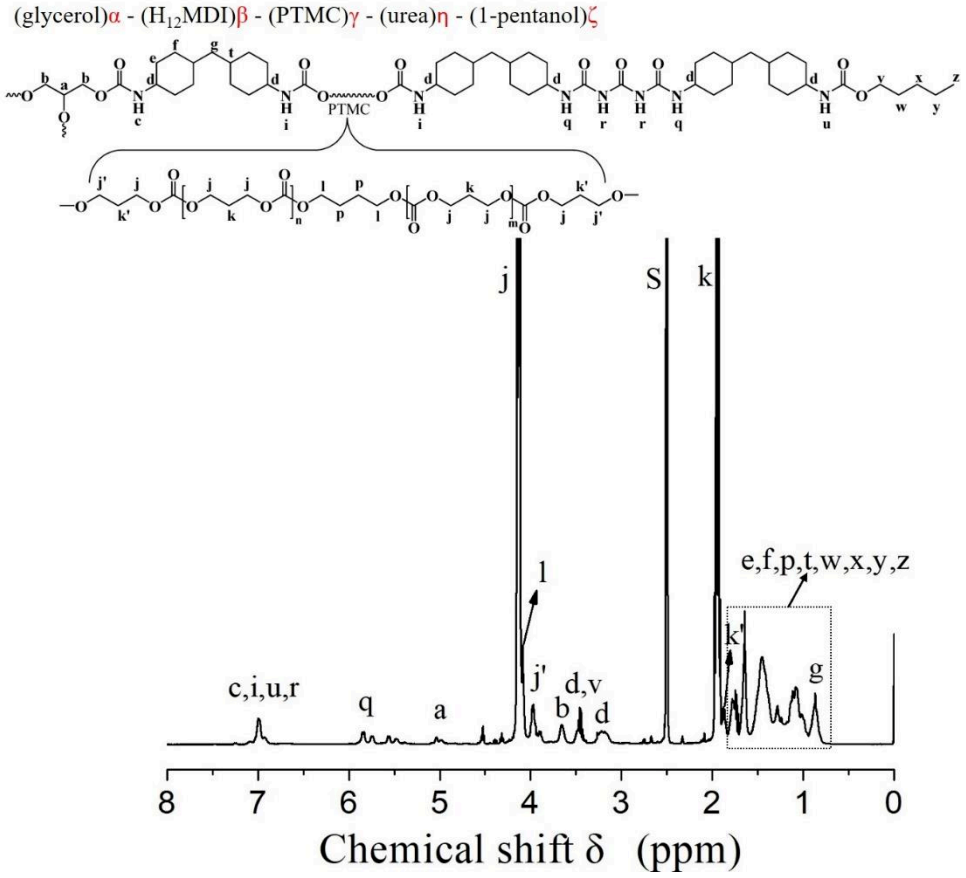

Figure 2. ^{1}H NMR spectrum of PTMC3U20 (DMSO-d_6, 400 MHz, 298 K).

The PTMC3U20 structure can be described by (glycerol)α-(H_{12}MDI)β-(PTMC)γ-(urea)η-(1-pentanol)ζ, where α, β, γ, η and ζ are the molar numbers of glycerol, H_{12}MDI, PTMC, urea and 1-pentanol reagent segments respectively. Consequently, the molar ratio of H_{12}MDI and glycerol can be calculated by the integration of H_g, H_a and H_b with:

$$\frac{n_{H_{12}MDI}}{n_{glycerol}} = \frac{\beta}{\alpha} = \frac{\frac{I_g}{2}}{\frac{(I_a + I_b)}{5}} = \frac{5I_g}{2(I_a + I_b)} \qquad \text{Eq. (3)}$$

The molar ratio of PTMC and glycerol is calculated by the integration of protons in the reacted TMC unit at PTMC chain ends ($H_{j'}$) and of glycerol protons (H_a and H_b) with:

$$\frac{n_{PTMC}}{n_{glycerol}} = \frac{\gamma}{\alpha} = \frac{\frac{I_{j'}}{2}}{\frac{(I_a + I_b)}{5}} = \frac{5I_{j'}}{2(I_a + I_b)} \qquad \text{Eq. (4)}$$

The molar ratios of urea/glycerol and 1-pentanol/glycerol are shown respectively in Eq. (5) and Eq. (6) with:

$$\frac{n_{urea}}{n_{glycerol}} = \frac{\eta}{\alpha} = \frac{\frac{I_q}{2}}{\frac{(I_a + I_b)}{5}} = \frac{5I_q}{2(I_a + I_b)} \qquad \text{Eq. (5)}$$

$$\frac{n_{pentanol}}{n_{glycerol}} = \frac{\varsigma}{\alpha} = \frac{\frac{I_g - I_d}{2}}{\frac{(I_a + I_b)}{5}} = \frac{5(I_g - I_d)}{2(I_a + I_b)} \qquad \text{Eq. (6)}$$

Thanks to Eq. (3), Eq. (4), Eq. (5) and Eq. (6), the ratios between glycerol, H_{12}MDI, PTMC, urea and 1-pentanol were calculated and retrieved closely to the chosen formulations (Table 1). The molar ratios of all the other synthesized structures were also calculated by similar methods (Table 2).

Table 2. Structure parameters of multiarm supramolecular polymers by ^{1}H NMR.

Sample	H_{12}MDI/glycerol (mol/mol)	PTMC/glycerol (mol/mol)	1-pentanol/glycerol (mol/mol)	HBM/glycerol (mol/mol)
PTMC3X20	5.93	2.62	2.52	0
PTMC3U20	8.34	2.66	2.27	2.73
PTMC4U20	6.33	1.72	1.98	2.00
PTMC3U10	8.94	2.71	2.83	2.48
PTMC3B20	8.94	2.67	2.51	2.69
PTMC3B10	8.80	2.69	2.60	2.70

Based on the ratios of α, β, γ, η and ζ, if α is normalized to 1, the $\overline{M}_n$ of PTMC3U20 can be calculated by Eq.(7):

$$\overline{M}n = 92.09 \times \alpha + 262.35 \times \beta + 2000 \times \gamma + 60.06 \times \eta + 88.15 \times \zeta \qquad \text{Eq. (7)}$$

where 92.09, 262.35, 2000, 60.06 and 88.15 are the molar masses of glycerol, H_{12}MDI, PTMC, urea and 1-pentanol respectively. The $\overline{M}_n$ of other multiarm supramolecular polymers were also calculated by the same method. As shown in Table 3, the NMR-calculated $\overline{M}_n$ of multiarm supramolecular polymers are close to their theoretical values.

Table 3. Structure parameters of multiarm supramolecular polymers.

Sample	HBM functionality	PTMC $\overline{M}_n$ (g/mol)	$\overline{M}_{n\ theo}$[a]	$\overline{M}_n$[b]	HBM content[c] (mmol/g)	Number of HBM[d]
PTMC3X20	0	2000	7900	7100	0	0
PTMC3U20	3	2000	8900	8000	0.341	2.7
PTMC4U20	4	2000	12200	11000	0.364	4.0
PTMC3U10	3	1000	5900	5500	0.447	2.5
PTMC3B20	3	2000	9000	8300	0.325	2.7
PTMC3B10	3	1000	6000	5600	0.482	2.7

[a] Theoretical $\overline{M}_n$. [b]Calculated by ^{1}H NMR (Eq. (7)). [c]HBM content is the molar fraction of urea or biuret motifs per gram of multiarm supramolecular polymers. [d]Calculated by ^{1}H NMR.

3.2.2 Characterization of multiarm supramolecular polymers by Size Exclusion Chromatography

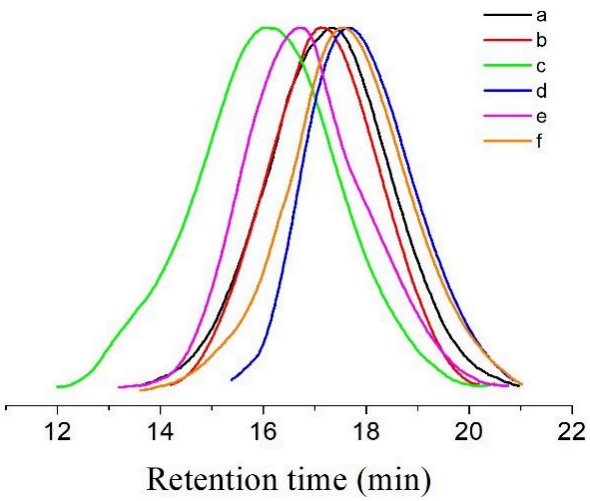

Figure 3. SEC chromatograms of multiarm supramolecular polymers with (a) PTMC3X20, (b) PTMC3U20, (c) PTMC4U20, (d) PTMC3U10, (e) PTMC3B20 and (f) PTMC3B10.

In polar and aprotic THF, multiarm supramolecular polymers are totally solubilized. Thus, their structures are all characterized by SEC. Since all the structures are branched (Figure 1), their accurate number average molecular weights ($\overline{M}_n$) and molar-mass dispersity ($Đ_M$) cannot be

calculated with linear polystyrene used as standard. Therefore, the retention times are only presented qualitatively. As shown in Figure 3, each chromatogram displays a Gaussian distribution and the retention times shift to shorter values when the sizes of structures grow (Figure 1). This phenomenon is in accordance with their corresponding number average molecular weights (Table 3).

3.3 Thermoreversibility of multiarm supramolecular polymers

3.3.1 Qualitative characterization of hydrogen bonds

3.3.1.1 Identification of hydrogen-bonding interactions by ^{1}H NMR

To study the equilibrium of hydrogen bonding in the synthesized materials, ^{1}H NMR analyses were conducted separately at 298 K, 353 K and 393 K in DMSO-d_6. As expected, an obvious temperature dependence of the labile -NH- protons is observed by their involvement in the supramolecular interaction towards a thermodependant equilibrium. PTMC3U20 is presented as an example in Figure 4. When temperature is increased, significant shifts of the labile -NH- protons resonances toward lower frequencies are observed. For example, the chemical shifts of -NH- (H_r, H_c, H_i and H_u) shift from 7.00 ppm to 6.33 ppm at 298 K and 393 K respectively. Similarly, H_q has the same shift tendency as H_r, H_c, H_i and H_u with the increase of temperature but with lower sensitivity. At higher temperatures, the breaking of hydrogen bonds leads to the increase of electron density of H proton in -NH-, consequently giving rise to shielding contributions[50,51]. This temperature dependence of chemical shifts fully confirms the shift of equilibrium of hydrogen bonding, and the dissociation of hydrogen bonds is certainly favored at high temperature.

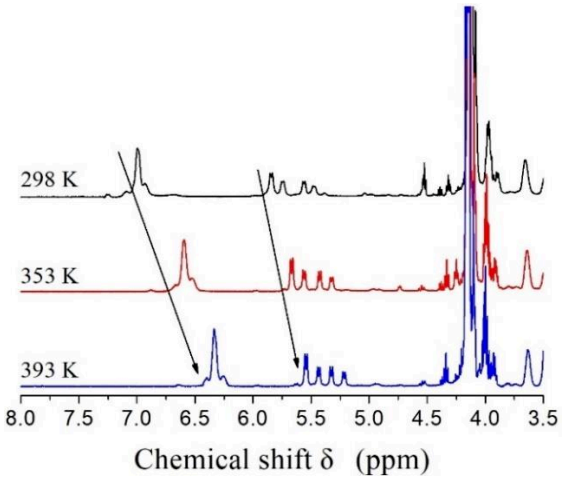

Figure 4. ^{1}H NMR spectrum of PTMC3U20 at 298 K, 353 K and 393 K (DMSO-d_6, 400 MHz).

3.3.1.2 Identification of hydrogen-bonding interactions by FT-IR

The hydrogen bonds in supramolecular materials are generated by the interaction between the >N-H donor and the >C=O acceptor in urethane functions and triuret/tetrauret HBMs. Based on the infrared absorption discrepancy of these groups in free and bonded states, FT-IR was used to probe the associations of these hydrogen-bonding interactions. The FT-IR spectra of PTMC3U20 bearing triuret HBMs collected at different temperatures are shown in Figure 5. The absorbances at 1630 cm^{-1} and 1643 cm^{-1} belong respectively to the stretching vibration of bonded and unbonded carbonyl groups[52,53]. With the increase of temperature, the bonded carbonyls tend to disappear gradually while the free ones appear at the same time. In addition, the stretching vibration of bonded >N-H groups, around 3400 cm^{-1}, shifts toward higher wavenumbers with increasing temperature as well. Conversely, the absorptions around 1520 cm^{-1}, which are ascribed to the bending vibration of free >N-H groups[54], shift to lower wavenumbers. All these wavenumber shifts of >N-H and >C=O groups confirm the dissociation of hydrogen bonds with increasing temperature. Moreover, if the samples are cooled, all these absorbances can evolve reversibly, proving the thermoreversibility of the system.

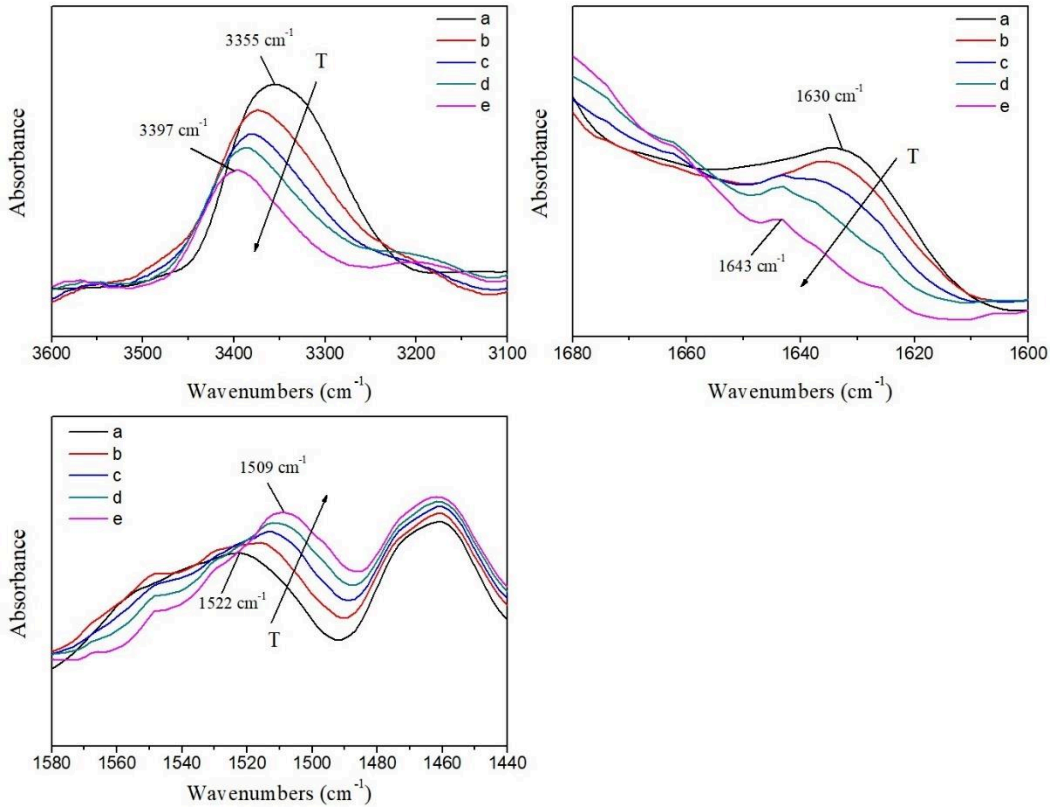

Figure 5. FT-IR spectra of PTMC3U20 at different temperatures with (a) 30 °C, (b) 60 °C, (c) 100 °C, (d) 140 °C and (e) 180 °C.

3.3.2 Association constant (K_a) calculation by Chen's model

For self-associated systems, ^{1}H NMR titration was often used to calculate the K_a by studying the chemical shifts of the labile protons belonging to supramolecular motifs. As shown in Figure 6, by increasing HBM concentrations in $CDCl_3$, >N-H labile protons resonances shift to low field. By the application of Chen's equation as given in Eq. (2), K_a of triuret and tetrauret HBMs were measured at 0.32 M^{-1} and 1.59 M^{-1} respectively. According to a previous study[20], triuret HBM is supposed to be in zigzag conformation with a K_a of 95 M^{-1} with cyclo-hexyl as backbone. This value is nearly 300 times higher than that determined in PTMC3U20. Such difference shows the impact of the chemical environment around the HBM on its ability to associate. Surely, by this observation, it is proved that the strength of HBMs cannot be generalized for all systems where they are engaged. For tetrauret HBMs, a previous study[20] revealed the impossibility to calculate K_a due to a possible folded conformation and extremely weak intermolecular interactions in $CDCl_3$. Surprisingly, their K_a was successfully calculated here to be 1.59 M^{-1} with PTMC3B20. This radical change could be explained by the supramolecular motifs surroundings. It seems that the PTMC chains, which mainly compose the supramolecular polymers, could prevent the formation of intramolecular interactions in tetrauret HBMs. In addition, it is also observed that the K_a of tetrauret HBMs is higher than that of triuret HBMs. Reasonably, tetrauret motif with 4 -NH-C(=O)- groups has a higher possibility to form intermolecular hydrogen bonds than the triuret motif with 3 -NH-C(=O)- groups, leading to stronger associations.

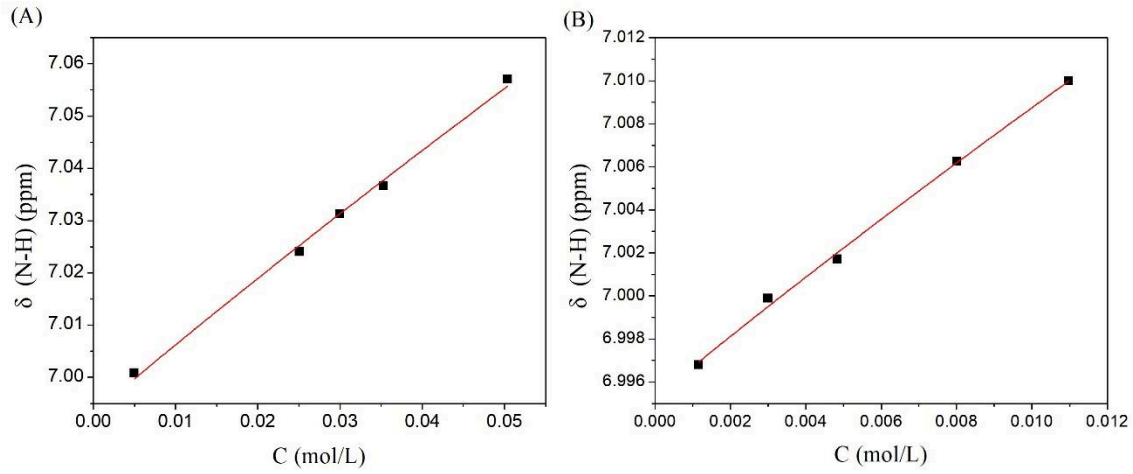

Figure 6. Association constants calculation by curve fitting of δ_{N-H} (in ppm) and HBM concentration in $CDCl_3$ (mol/L) with (A) PTMC3U20, (B) PTMC3B20; —fitting curve by Chen's model, ■ experiment data (in $CDCl_3$ at 298K, 400 MHz).

3.4 Thermal properties of multiarm supramolecular polymers

3.4.1 Glass transitions

According to a previous study[42], glass transition temperatures (T_g) of $PTMC_{1000}$ and $PTMC_{2000}$ oligomers were found relatively low at -45.2 °C and -31.6 °C respectively. In addition, when the $\overline{M}_n$ of PTMC is higher than the critical entanglement molecular weight, T_g will close to -20 °C[36].

T_g of all supramolecular polymers were determined by DSC with data given in Table 4. For triarmed PTMC3X20 which bears no HBM and a NMR-calculated molar mass of 7100 g/mol, the T_g is -19.7 °C. After introducing separately 0.341 and 0.364 mmol/g triuret HBMs in PTMC3U20 and PTMC4U20, their T_g increase to -16.1 °C and -13.9 °C respectively. These increased T_g are ascribed to the formation of relatively strong hydrogen bonds by triuret HBMs. However, the effect of the functionality in the synthesized structures can be discarded since T_g difference between PTMC3U20 and PTMC4U20 T_g is only 2.2 °C while their arm lengths are constant.

Table 4. Thermal properties of PTMC oligomers and multiarm supramolecular polymers.

Sample	T_g (°C)	T_{onset} (°C)	T_{max}[b] (°C)	$T_{crossover}$[c] (°C)
$PTMC_{1000}$[a]	-45.2	181.2	237.0	-
$PTMC_{2000}$[a]	-31.6	184.2	237.4	-
PTMC3X20	-19.7	212.5	241.7	98.4
PTMC3U20	-16.1	228.0	248.1	151.5
PTMC4U20	-13.9	228.0	245.2	158.5
PTMC3U10	0.9	268.3	279.5	198.7
PTMC3B20	-9.5	269.5	271.7	147.0
PTMC3B10	2.2	269.2	279.3	178.7

[a]Thermal properties of the used PTMC oligomers. [b]T_{max} was obtained in derivative thermogravimetry curves of PTMC oligomers and multiarm supramolecular polymers. [c]$T_{crossover}$ was obtained from the crossover point of G' and G'' in temperature ramp tests.

The PTMC chain lengths, namely molecular weights, have great influence on the T_g. It is shown that by decreasing PTMC $\overline{M}_n$, the T_g increase significantly and systematically. For example, PTMC3U20 and PTMC3B20 have T_g of -16.1 °C and -9.5 °C respectively. When the PTMC $\overline{M}_n$ is decreased to 1000 g/mol, T_g are increased to 0.9 °C and 2.2 °C for PTMC3U10 and

PTMC3B10 respectively. These T_g increases also match with the HBM contents (Table 3), which are decided by the PTMC chain length directly. By comparing triuret and tetrauret HBMs with K_a of 0.32 M^{-1} and 1.59 M^{-1} respectively in $CDCl_3$, their effect differences are not obvious on T_g. As seen, PTMC3U20 and PTMC3B20 have a T_g gap of 6.6 °C while the difference between PTMC3U10 and PTMC3B10 only reaches 1.3 °C. However, it seems that supramolecular polymers bearing tetrauret HBMs have higher T_g than their triuret counterparts. No crystalline signals were found in DSC curves for all supramolecular polymers, indicating their amorphous states.

3.4.2 Thermal stability

According to our recent work[42], the thermal stability of PTMC oligomers is relatively low with T_{onset} (the temperature of 5% weight loss) of $PTMC_{1000}$ and $PTMC_{2000}$ at 181.2 °C and 184.2 °C respectively (Table 4). The thermal stability of supramolecular polymers is significant enough to be examined prior to rheology with the purpose of excluding the effects of thermal degradation on their rheological properties which will be discussed afterward. The thermal stability assessment was therefore carried out by TGA (Figure 7). It is obvious that all the supramolecular polymers possess a T_{onset} higher than 210 °C (Table 4). Compared to PTMC oligomers, the T_{onset} of PTMC3X20 increased by nearly 30 °C to 212.5 °C. Once triuret HBM was introduced, the T_{onset} increased further to 228.0 °C for both PTMC3U20 (0.341 mmol/g) and PTMC4U20 (0.364 mmol/g), indicating the enhancement of thermal stability and the absence of functionality influence on T_{onset}. PTMC3U10 with triuret HBM possesses a high T_{onset} of 268.3 °C which indicates that the T_{onset} was enhanced with the increase of HBM concentration (0.447 mmol/g) by reducing PTMC chain length. For the samples containing tetrauret HBMs, T_{onset} are around 269.5 °C for both PTMC3B20 and PTMC3B10, which reveals better thermal stability than their triuret counterparts. This phenomenon may be induced by the stronger hydrogen bonding between tetrauret HBMs than triuret HBMs.

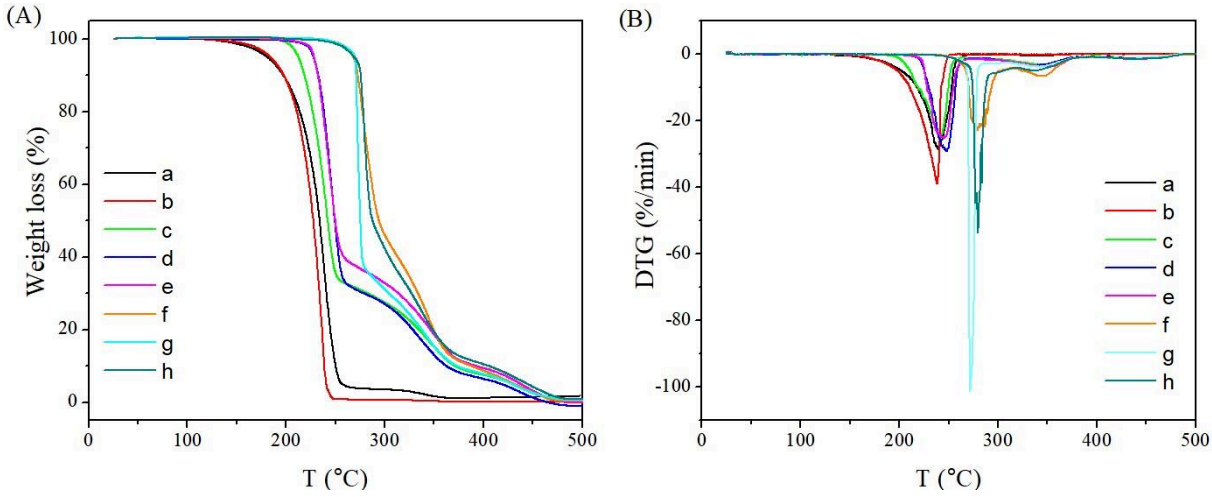

Figure 7. (A) TGA and (B) derivative thermogravimetry curves of PTMC oligomers and supramolecular polymers with (a) $PTMC_{1000}$, (b) $PTMC_{2000}$, (c) PTMC3X20, (d) PTMC3U20, (e) PTMC4U20, (f) PTMC3U10, (g) PTMC3B20 and (h) PTMC3B10.

T_{max} is the temperature at maximum decomposition rate obtained from the derivative of the TGA curves. It is also introduced to describe thermal stability. As shown in Table 4, PTMC3X20, PTMC3U20 and PTMC4U20 have T_{max} values close to that of PTMC oligomers (around 240 °C). However, the T_{max} of PTMC3B20 (271.7 °C) is 30 °C higher than that of PTMC3U20, in accordance with the better thermal stability of tetrauret-containing structures as shown previously. For PTMC3U10 and PTMC3B10, T_{max} are relatively high at 279.5 and 279.3 °C respectively, indicating the better thermal stability with higher HBM concentrations.

The derivative thermogravimetry curves (Figure 7) indicate that the thermal degradation proceeds in three steps. For example, a rapid degradation region from 228 °C to 280 °C with a weight loss of 67 wt% was observed for PTMC3U20. This weight loss value corresponds to the weight content of $PTMC_{2000}$ in PTMC3U20, indicating the first degradation of soft PTMC segments at this stage due to its low degradation activation energy (90 kJ/mol)[55]. The maximum weight loss rate is at 250 °C. This first degradation stage was also shown for PTMC3X20 and PTMC4U20 in the same temperature range. Compared to PTMC oligomers, it seems that the thermal stability of PTMC segments in supramolecular structures is enhanced by the introduction of HBMs, although the corresponding mechanism is not yet clear. The weak CO-NH bonds in urethane/urea bonds have their dissociation activation energy ranging from 100 to 130 kJ/mol[56]. It means that the degradation of triuret/tetrauret HBMs occurs between 280 and 400 °C with a maximum weight loss at 336 °C[57]. The short third stage after 400 °C with a weight loss below 10 wt% may belong to the decomposition of material residues into

volatile products[58]. For PTMC3B20, PTMC3U10 and PTMC3B10, the first step of the soft segment PTMC degradation and the second step of triuret/tetrauret HBMs degradation are increased to 250-300 °C and 320-400 °C respectively. The third degradation step is in the same temperature range as PTMC3X20, PTMC3U20 and PTMC4U20.

3.5 Characterization of supramolecular network structures

3.5.1 Viscoelastic properties of supramolecular polymers

Temperature ramp tests were conducted under controlled strains to study the viscoelastic behaviors and to prove if physical networks are indeed formed and reversible. To this end, $T_{crossover}$ corresponding to the temperature at which a crossover occurs between storage modulus G' and loss modulus G'' was chosen to highlight a nominal transition from the elastic behavior to the viscous state. It is obvious in Figure 8 that both G' and G'' decrease dramatically when temperature is above $T_{crossover}$. As shown, PTMC3X20 containing no HBMs possesses the lowest $T_{crossover}$ of 98.4 °C (Table 4). Considering the relatively low T_g of PTMC3X20 (-19.7 °C), it is reasonable to infer that the hydrogen bonding between urethane bonds accounts for its elastic state below 98.4 °C.

The incorporation of triuret and tetrauret HBMs led to an increase of $T_{crossover}$ to 151.5 and 147.0 °C for PTMC3U20 and PTMC3B20 respectively. Considering these dramatically increased $T_{crossover}$ and low T_g of PTMC3U20 and PTMC3B20, it is reasonable to infer that physical crosslinks could be formed by associations between triuret or tetrauret HBMs. Moreover, increasing the functionality by the number of multiarm can also raise the $T_{crossover}$ value to 158.5 °C for PTMC4U20 due to the increase of crosslinking density by HBM association. Once the PTMC molar mass decreased from 2000 to 1000 g/mol, PTMC3U10 and PTMC3B10 $T_{crossover}$ predominantly increased to 198.7 and 178.7 °C. This phenomenon attributes to the fact that increasing HBMs concentration by shortening PTMC chain length leads to the formation of denser networks which need higher temperature to destroy. Through the comparison of supramolecular polymers bearing triuret and tetrauret HBMs, it was also found that triuret HBMs functionalized materials have higher $T_{crossover}$ than their tetrauret counterparts, which is contrary to their K_a values measured in $CDCl_3$. It is noteworthy that $T_{crossover}$ of all materials are below 200 °C, lower than the T_{onset} (>210°C) as shown previously by TGA. Besides, all materials are transformed from tough elastic elastomers to flowing materials when the

temperature is increased around $T_{crossover}$, indicating the thermoreversibility of transient physical networks and the possible processability in the molten state before thermal degradation.

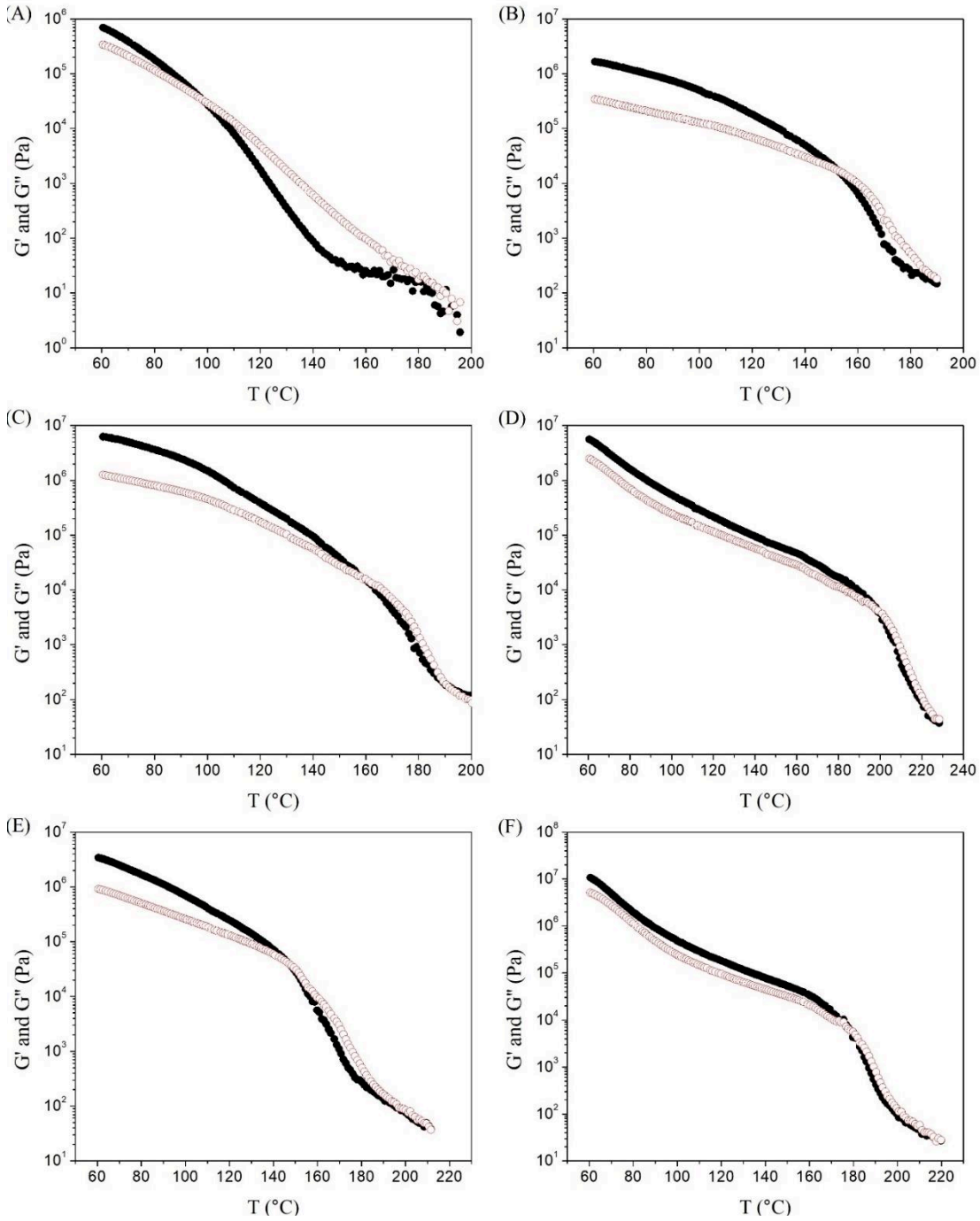

Figure 8. Temperature ramp tests of multiarm supramolecular polymers from PTMC oligomers at 5 °C/min, frequency = 1 rad/s, strain = 1% with (A) PTMC3X20, (B) PTMC3U20, (C) PTMC4U20, (D) PTMC3U10, (E) PTMC3B20 and (F) PTMC3B10. G' (●), G'' (○).

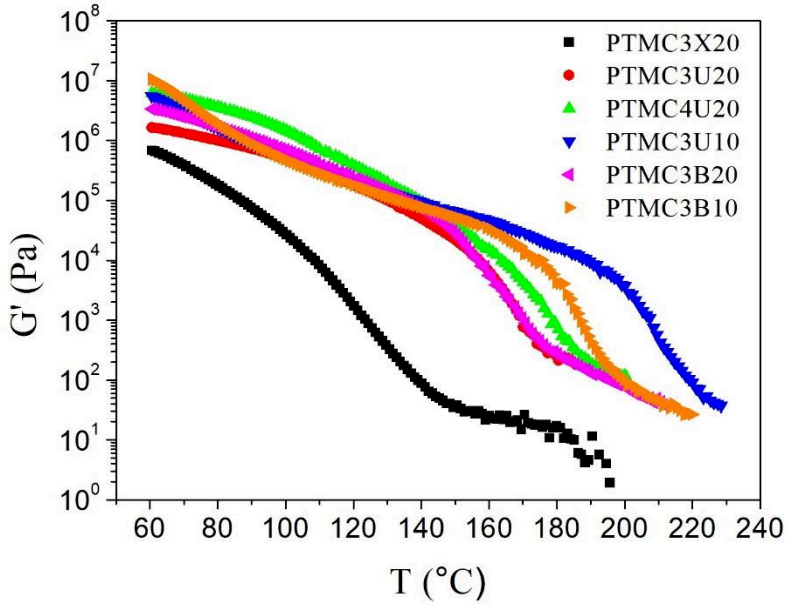

Figure 9. G' comparison of multiarm supramolecular polymers by temperature ramp tests at 5 °C/min, frequency = 1 rad/s, strain = 1%.

In all cases, the introduction of HBMs can also increase G' values between 60 °C and 220 °C predominantly. It was shown in Figure 9 that the G' of supramolecular polymers bearing HBMs have no big discrepancy before $T_{crossover}$ (60 to 150°C). However, since the crossover temperature was increased by introducing HBMs as mentioned previously, G' modulus after $T_{crossover}$ (150 to 220 °C) follows the pattern: PTMC3U10 > PTMC3B10 > PTMC4U20 > PTMC3U20 ≈ PTMC3B20 > PTMC3X20.

3.5.2 Creep properties of supramolecular polymers

The study of creep properties is common for covalently crosslinked networks due to the resistance of free flow for polymer chains in networks. However, its application in supramolecular polymers is still not extensive, even though it is a convenient method to trace the formation and break of thermoreversible physical network structures. Therefore, the creep and creep recovery tests were conducted at 80 °C and 140 °C for supramolecular polymers.

All the creep curves are shown in Figure 10 with corresponding data given in Table 5. As seen in Figure 10 (A), when 100 Pa stress was applied on PTMC3X20 at 80 °C, the strain reached 4.740% after 90 min with an increase rate of 3.16% per hour. After removing the stress, the strain began to recover slowly and reached 3.370% after 90 min and the total recovery ratio was 28.9%. At 140 °C with the same creep conditions, the maximum strain was huge, nearing 150000% along with a negligible final recovery ratio of 0.7%. According to the $T_{crossover}$ of 98.4

°C for PTMC3X20 as shown previously, it is reasonable to have no creep resistance at 140 °C because the material is mainly viscous.

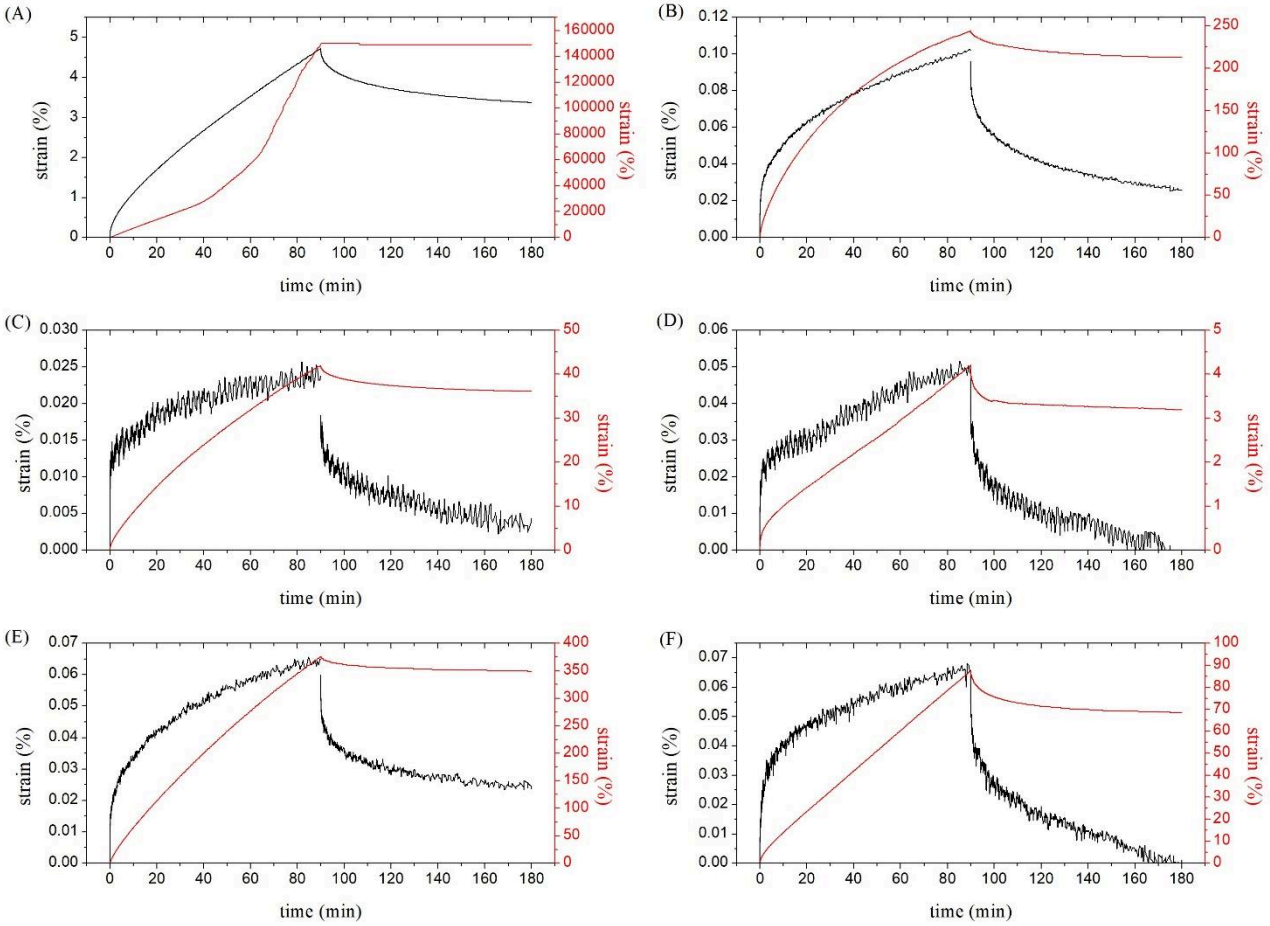

Figure 10. Creep tests of multiarm supramolecular polymers at 80 °C (—black line) and 140 °C (—red line) with (A) PTMC3X20; (B) PTMC3U20; (C) PTMC4U20; (D) PTMC3U10; (E) PTMC3B20 and (F) PTMC3B10 (90 min under 100 Pa and 90 min for relaxation).

After introducing triuret and tetrauret HBMs, the creep was strikingly reduced as shown in Figure 10 (B), (C), (D), (E) and (F). For example, the maximum strain of PTMC3U20 was reduced to 0.102% by the association between triuret HBMs. Besides, the creep rate was also decreased to 0.07% per hour which is nearly 50 times lower compared to PTMC3X20. Because of the limitation of free flow, when the applied stress was released, the unsteady state could recover up to 74.5% of its initial strain by intrinsic stress. It is important to indicate that the relaxation still carried on after 90 min. When the HBM functionality was increased from 3 to 4, the maximum strain of PTMC4U20 decreased further to 0.024% with increased recovery ratio of 87.5% at 80 °C. The better deformation resistance ability is logically owing to the denser physically crosslinked structure with the increase of HBM functionality, even though

PTMC4U20 and PTMC3U20 have similar triuret HBM concentrations. For PTMC3U10 (Figure 10, D) with shorter PTMC chains, a recovery ratio of 100% was observed at 80 °C, in accordance with the measured high $T_{crossover}$ at 198.7 °C. This complete recovery indicates the formation of complete transient physical networks by hydrogen-bonding interactions. With tetrauret HBMs, PTMC3B10 also completely recovered their dimensions at 80 °C like PTMC3U10. However, the recovery ratio at 63.1% of PTMC3B20 was lower than PTMC3U20 (74.5%), indicating less denser networks. All the supramolecular materials bearing triuret or tetrauret HBMs have very low creep strains and good abilities to retain their dimensions at 80 °C. Moreover, the maximum strain does not change significantly with the various supramolecular structures.

When the temperature was increased to 140 °C, creep resistances of all materials became unsatisfactory with higher maximum strains and creep rates but with lower recovery ratios. This is explained by the gradual dissociation of hydrogen bonds with temperature, corresponding to the lower G' and G'' at 140 °C than those at 80 °C as shown previous (Figure 8). For all supramolecular polymers bearing triuret or tetrauret HBMs, the non-zero recovery ratios mean that partial crosslinks always exist even at 140 °C. Comparatively, structures with triuret motifs appear to have better dimensional stability than those with tetrauret motifs, which is at the opposite to the K_a for triuret (0.32 M^{-1}) and tetrauret (1.59 M^{-1}) HBMs.

Table 5. Creep properties of multiarm supramolecular polymers.

Temperature	80 °C				140 °C			
Sample name	Maximum strain[a] (%)	Final ratio[b] (%)	Recovery ratio (%)	Creep rate (%/h)	Maximum strain[a] (%)	Final ratio[b] (%)	Recovery ratio (%)	Creep rate (%/h)
PTMC3X20	4.740	3.370	28.9	3.16	150000	149000	0.7	100000
PTMC3U20	0.102	0.026	74.5	0.07	244.0	213.0	12.7	162.7
PTMC4U20	0.024	0.003	87.5	0.02	42.0	36.1	14.0	28.0
PTMC3U10	0.047	0	100.0	0.03	3.9	2.8	28.2	2.6
PTMC3B20	0.065	0.024	63.1	0.04	376.0	349.0	7.2	250.7
PTMC3B10	0.066	0	100.0	0.04	87.5	68.6	21.6	58.3

[a]Maximum strain: the strain after 90 min under stress of 100 Pa. [b]Final ratio: the final ratio after 90 min of recovery.

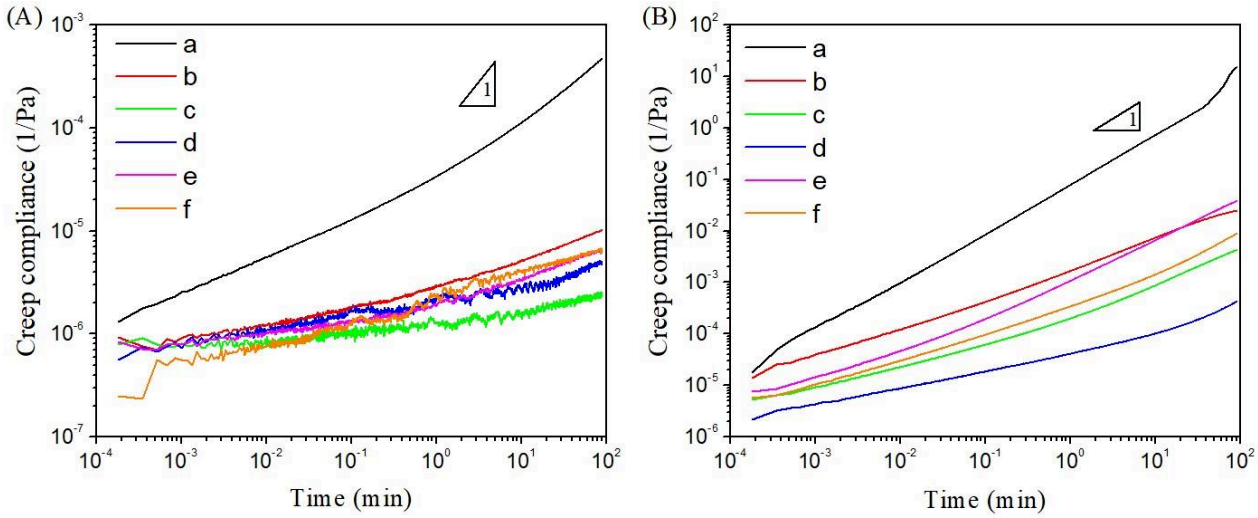

Figure 11. Creep curves of supramolecular polymers in log-log plot at (A) 80 °C and (B) 140 °C with (a) PTMC3X20; (b) PTMC3U20; (c) PTMC4U20; (d) PTMC3U10; (e) PTMC3B20 and (f) PTMC3B10 (90 min under 100 Pa).

Figure 11 shows the creep compliance[59] (the ratio between deformation and applied stress) for the synthesized materials at different temperatures. In Figure 11 (A), all the curves deviate the slope of 1 in log-log plot at 80 °C, indicating the deviation of steady flow state for all samples, corresponding to the formation of networks at this temperature. As shown in Figure 11 (B), when the temperature was increased to 140 °C, in addition to PTMC3X20, curves of all materials with triuret and tetrauret tend to approach the slope of 1 as well. It means that they all flow at 140 °C, even though partial crosslinks still exist in supramolecular polymers.

3.6 Tensile mechanical properties of multiarm supramolecular polymers

To characterize these materials in potential use conditions, mechanical properties were assessed by tensile tests. For the sake of displaying the material's response directly, true stress (σ_t) and true strain (ε_t) are calculated as follows:

$$\sigma_t = \lambda \sigma_e = \lambda \frac{P}{A_0} \qquad \text{Eq. (8)}$$

$$\varepsilon_t = \ln \lambda \qquad \text{Eq. (9)}$$

where σ_e is the engineering stress measured directly, λ is the extension ratio, P is the force, A_0 is the original specimen cross-sectional area.

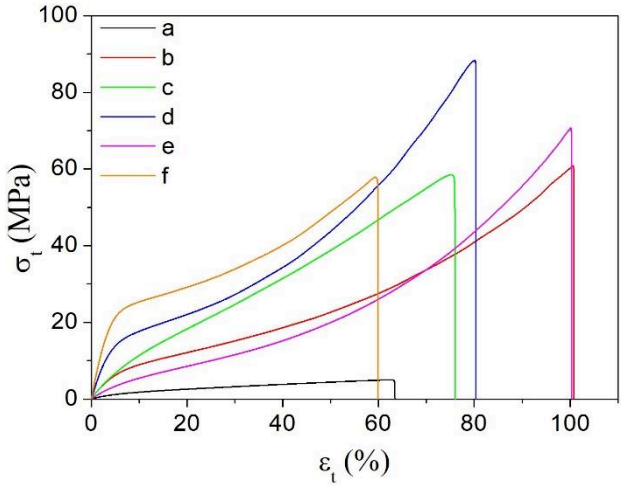

Figure 12. True stress-true strain curves of multiarm supramolecular polymers with (a) PTMC3X20, (b) PTMC3U20, (c) PTMC4U20, (d) PTMC3U10, (e) PTMC3B20 and (f) PTMC3B10 (room temperature, 10 mm/min).

The true stress-true strain curves are shown in Figure 12 with corresponding parameters summarized in Table 6. As seen obviously, PTMC3X20, which bears neither triuret nor tetrauret HBMs, possesses the lowest true strength at break σ_b and Young's modulus E with 5.0 MPa and 0.4 MPa separately. After introducing HBMs, the tensile mechanical properties become obviously superior. For PTMC3U20 with triuret HBMs, E was increased sharply by nearly 4 times to 1.5 MPa compared to PTMC3X20 (0.4 MPa). Moreover, σ_b was increased more than 10 times to 60.0 MPa while keeping a higher elongation at break (ε_b) of 101% at the same time. The augmentation of tensile mechanical properties is fully ascribed to the formed physical networks thanks to triuret HBMs[60].

Table 6. Tensile mechanical properties of multiarm supramolecular polymers.

Sample	E[a] (MPa)	σ_b[b] (MPa)	ε_b[c] (%)
PTMC3X20	0.4 ± 0.0	5.0 ± 0.5	63 ± 8
PTMC3U20	1.5 ± 0.2	60.0 ± 9.9	101 ± 9
PTMC4U20	1.7 ± 0.1	58.4 ± 9.4	76 ± 6
PTMC3U10	4.4 ± 0.2	88.3 ± 5.8	80 ± 5
PTMC3B20	0.9 ± 0.2	70.7 ± 12.4	100 ± 10
PTMC3B10	6.6 ± 0.7	58.1 ± 8.9	60 ± 7

[a]Young's modulus. [b]Ultimate strength. [c]Elongation at break.

When the HBM functionality is increased from 3 to 4 with the similar triuret HBM content (0.341 and 0.361 mmol/g for PTMC3U20 and PTMC4U20 respectively), although their E and

σ_b are similar, PTMC4U20 has higher true strength values than PTMC3U20 (Figure 12). It shows that the higher concentration of crosslinking points in PTMC4U20 could increase the rigidity of the material[61]. Compared to PTMC3U20 (ε_b = 101%), ε_b of PTMC4U20 is decreased slightly to 76 % because its extra arm (3 arms for PTMC3U20 and 4 arms for PTMC4U20) provides more chain mobility restrictions and its stretchability is then suppressed as a result. For fully elastic PTMC3U10 with 100% recovery in creep tests, E and σ_b increase to 4.4 MPa and 88.3 MPa respectively with ε_b decreasing to 80% due to the higher motif concentration. Additionally, shorter soft PTMC chains could only bear a lower deformation before the breaking of hydrogen-bonding crosslinks[62]. Similarly, for PTMC3B10, decreasing PTMC molar mass has similar effects to their triuret counterparts. Although PTMC3B10 has high E of 6.6 MPa, its ε_b is lower than that of PTMC3B20 because of the shorter PTMC chains and more denser networks. Its stretchability is then restricted to the lowest with 60%. Therefore, it is proved that the introduction of self-associable HBMs can indeed increase ultimate strength σ_b and Young's modulus. Moreover, increasing HBM concentration by decreasing PTMC chain length can enhance tensile mechanical properties extensively.

3.7 Aerobic biodegradability of multiarm supramolecular polymers

Due to the potential applications of PTMC-based multiarm supramolecular polymers in the medical field, it is significant to explore their ability to biodegrade. In that way, samples were submitted to biodegradation in aerobic conditions.

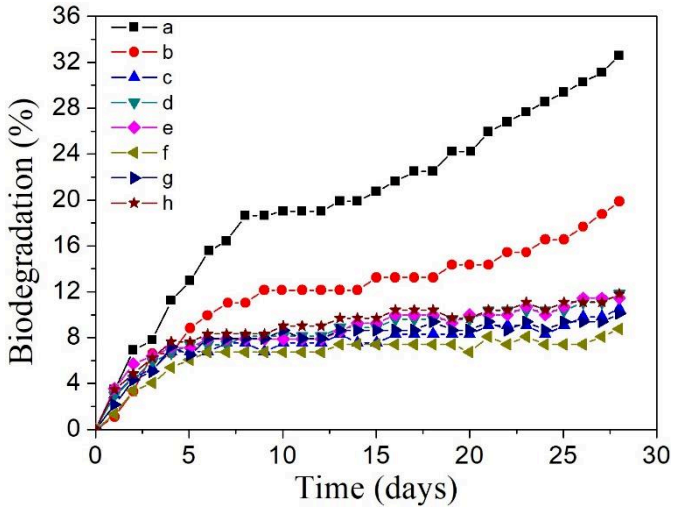

Figure 13. Aerobic biodegradability according to ISO 14851 standard using OxiTop® control measuring system with (a) $PTMC_{1000}$, (b) $PTMC_{2000}$, (c) PTMC3X20, (d) PTMC3U20, (e) PTMC4U20, (f) PTMC3U10, (g) PTMC3B20 and (h) PTMC3B10.

As shown in Figure 13, it is obvious that $PTMC_{1000}$ and $PTMC_{2000}$ oligomers have higher biodegradation ratios among all samples with nearly 33% and 20% after 28 days respectively. At the beginning, an acceleration region is observed during the first 10 days. From day 10 to day 20, the biodegradability rate keeps relatively stable followed by a second acceleration region after day 20. When triuret or tetrauret HBMs were introduced, the biodegradation was slowed down apparently. Meanwhile, the first acceleration region was reduced from days 0-10 to days 0-5 as compared to PTMC oligomers. A stable plateau was also observed after the acceleration region until day 28. The discrepancy between different structures and HBM contents are not obvious to observe.

3.8 Comparison of triuret and tetrauret HBMs in multiarm supramolecular polymers

To compare the effects of triuret and tetrauret HBMs on materials properties, it was shown firstly that tetrauret has a higher K_a value 1.59 M^{-1} than triuret with 0.32 M^{-1}. However, in rheological tests, it was seen that supramolecular materials with triuret HBMs have higher $T_{crossover}$ than tetrauret HBMs, which is accordant with the lower creep of supramolecular polymers bearing triuret motifs than those with tetrauret motifs. It signifies that triuret HBMs can form denser crosslinked structures than tetrauret. In tensile tests, PTMC3U10 with triuret HBMs also has higher stress at break 88.3 MPa compared to 58.1 MPa for PTMC3B10 with tetrauret HBMs. These results which are contradictory to the measured K_a values for triuret and tetrauret HBMs may come from their different aggregation modes in solution and in the solid state. To further understand these discrepancies, the dynamics study of supramolecular polymers will be published in another article soon.

4. Conclusion

In this work, PTMC-based thermoreversible multiarm supramolecular polymers bearing triuret and tetrauret HBMs were successfully synthesized in three steps. The shift of hydrogen bonding equilibrium was traced by ^1H NMR and FT-IR. K_a of triuret and tetrauret HBMs were determined to be 0.32 M^{-1} and 1.59 M^{-1} respectively by Chen's equation. Compared to the measured K_a of triuret HBMs (95 M^{-1}) in a previous study, PTMC strongly affects the triuret HBMs association with a K_a reduction by 300 times. T_g are mainly affected by the PTMC chain length, but not the functionality or HBM structures. Decreasing PTMC molar mass to raise HBM concentration can effectively enhance thermal stability. In addition, materials with tetrauret HBMs have better thermal stability than their triuret counterparts. Triuret and tetrauret HBMs lead to the formation of thermoreversible transient network structures, evidenced by the extremely high $T_{crossover}$ and 100% of recovery ratios in creep tests. Both increasing

functionality and decreasing PTMC chain length contribute to the increase of $T_{crossover}$, creep recovery ratios and Young's modulus in tensile tests. However, decreasing PTMC chain length is more efficient than increasing functionality, caused by the formation of denser transient physical networks by hydrogen-bonding interactions. Although K_a of tetrauret HBMs is higher than that of triuret HBMs, supramolecular polymers bearing tetrauret HBMs have worse deformation resistance and lower $T_{crossover}$ than their triuret counterparts. HBMs decrease the biodegradation ratio from 20% for PTMC oligomers to 10% for supramolecular networks, but the supramolecular structural effects are unapparent. The contradictory creep resistance, $T_{crossover}$ and tensile strength of supramolecular polymers bearing triuret and tetrauret HBMs may due to their different aggregation modes in solution and in the solid state. The dynamics of these supramolecular polymers will be studied to further understand their behaviors.

Acknowledgments

The authors thank the financial support from China Scholarship Council (CSC). This work benefited from the international cooperation between Université Jean Monnet Saint-Etienne (France) and East China University of Science and Technology (China).

References

[1] J.-M. Lehn, Supramolecular Chemistry—Scope and Perspectives Molecules, Supermolecules, and Molecular Devices (Nobel Lecture), Angewandte Chemie International Edition in English 27(1) (1988) 89-112.

[2] D.J. Cram, The Design of Molecular Hosts, Guests, and Their Complexes (Nobel Lecture), Angewandte Chemie International Edition in English 27(8) (1988) 1009-1020.

[3] C.J. Pedersen, The Discovery of Crown Ethers (Noble Lecture), Angewandte Chemie International Edition in English 27(8) (1988) 1021-1027.

[4] G. ten Brinke, J. Ruokolainen, O. Ikkala, Supramolecular Materials Based On Hydrogen-Bonded Polymers, in: Hydrogen bonded polymers, W. Binder (Ed.), Springer-Verlag, Berlin, Heidelberg, 2007, Vol. 207, pp. 113-177.

[5] K. Morokuma, Why do molecules interact? The origin of electron donor-acceptor complexes, hydrogen bonding and proton affinity, Accounts of Chemical Research 10(8) (1977) 294-300.

[6] G.A. Jeffrey, An Introduction to Hydrogen Bonding, Oxford University Press, New York, 1997.

[7] T. Steiner, The Hydrogen Bond in the Solid State, Angewandte Chemie International Edition 41(1) (2002) 48-76.

[8] S.W. Kuo, Hydrogen Bonding in Polymeric Materials, Wiley-VCH Weinheim, Germany, 2018.

[9] K. Liu, Y. Kang, Z. Kang, X. Zhang, 25th Anniversary Article: Reversible and Adaptive Functional Supramolecular Materials: “Noncovalent Interaction” Matters, Advanced Materials 25(39) (2013) 5530-5548.

[10] F. Herbst, D. Döhler, P. Michael, W.H. Binder, Self-Healing Polymers via Supramolecular Forces, Macromolecular Rapid Communications 34(3) (2013) 203-220.

[11] L.R. Hart, J.L. Harries, B.W. Greenland, H.M. Colquhoun, W. Hayes, Healable supramolecular polymers, Polymer Chemistry 4(18) (2013) 4860-4870.

[12] L. Yang, Y. Lin, L. Wang, A. Zhang, The synthesis and characterization of supramolecular elastomers based on linear carboxyl-terminated polydimethylsiloxane oligomers, Polymer Chemistry 5(1) (2014) 153-160.

[13] J. Li, J.A. Viveros, M.H. Wrue, M. Anthamatten, Shape-Memory Effects in Polymer Networks Containing Reversibly Associating Side-Groups, Advanced Materials 19(19) (2007) 2851-2855.

[14] Z.-C. Jiang, Y.-Y. Xiao, Y. Kang, M. Pan, B.-J. Li, S. Zhang, Shape Memory Polymers Based on Supramolecular Interactions, ACS Applied Materials & Interfaces 9(24) (2017) 20276-20293.

[15] X. Yan, F. Wang, B. Zheng, F. Huang, Stimuli-responsive supramolecular polymeric materials, Chemical Society Reviews 41(18) (2012) 6042-6065.

[16] T. Aida, E.W. Meijer, S.I. Stupp, Functional Supramolecular Polymers, Science 335(6070) (2012) 813-817.

[17] D.B. Varshey, J.R.G. Sander, Tomislav Friˇsˇci´c, L.R. MacGillivray, Supramolecular Chemistry: From Molecules to Nanomaterials, John Wiley & Sons, Ltd., NewYork, 2012.

[18] Y.S. Kyung, Z.S. C., Hydrogen Bonding Modules for Use in Supramolecular Polymers, Israel Journal of Chemistry 53(8) (2013) 511-520.

[19] J.P. WL Jorgensen, Importance of Secondary Interactions in Triply Hydrogen Bonded Complexes: Guanine-Cytosine vs Uracil-2,6-Diaminopyridine, Journal of the American Chemical Society 112 (1990) 2008-2010.

[20] Y. Ni, F. Becquart, J. Chen, M. Taha, Polyurea–Urethane Supramolecular Thermo-Reversible Networks, Macromolecules 46(3) (2013) 1066-1074.

[21] R.P. Sijbesma, F.H. Beijer, L. Brunsveld, B.J.B. Folmer, J.H.K.K. Hirschberg, R.F.M. Lange, J.K.L. Lowe, E.W. Meijer, Reversible Polymers Formed from Self-Complementary Monomers Using Quadruple Hydrogen Bonding, Science 278(5343) (1997) 1601-1604.

[22] H. Zeng, X. Yang, A.L. Brown, S. Martinovic, R.D. Smith, B. Gong, An extremely stable, self-complementary hydrogen-bonded duplex, Chemical Communications (13) (2003) 1556-1557.

[23] B. Rybtchinski, Adaptive Supramolecular Nanomaterials Based on Strong Noncovalent Interactions, ACS Nano 5(9) (2011) 6791-6818.

[24] A.V. Iogansen, Direct proportionality of the hydrogen bonding energy and the intensification of the stretching ν(XH) vibration in infrared spectra, Spectrochimica Acta Part A: Molecular and Biomolecular Spectroscopy 55(7) (1999) 1585-1612.

[25] A. Noro, Y. Matsushita, T.P. Lodge, Thermoreversible Supramacromolecular Ion Gels via Hydrogen Bonding, Macromolecules 41(15) (2008) 5839-5844.

[26] P. Thordarson, Determining association constants from titration experiments in supramolecular chemistry, Chemical Society Reviews 40(3) (2011) 1305-1323.

[27] L. Fielding, Determination of Association Constants (Ka) from Solution NMR Data, Tetrahedron 56(34) (2000) 6151-6170.

[28] K. Hirose, Quantitative Analysis of Binding Properties, in: Analytical Methods in Supramolecular Chemistry, C.A. Schalley (Ed.), Wiley-VCH, Weinheim, 2012, Vol., pp. 27-66.
[29] B.A. Blight, C.A. Hunter, D.A. Leigh, H. McNab, P.I.T. Thomson, An AAAA–DDDD quadruple hydrogen-bond array, Nature Chemistry 3(3) (2011) 244-248.
[30] J.-s. Chen, R. Franz, Accurate nmr data evaluation for monomer shift, dimer shift and dimerization constant in a self-associating system, Tetrahedron Letters 31(28) (1990) 3975-3978.
[31] H. Stamm, W. Lamberty, J. Stafe, Molecular complexes. 3. Nonparallel and nonlinear slopes of NMR Scatchard plots caused by additional unspecific shielding, Journal of the American Chemical Society 102(5) (1980) 1529-1531.
[32] Y.-Y. Lim, R.S. Drago, Influence of solvents on ion association. II. Proton nuclear magneticesonance of (Bu4N)(Ph3PCoBr3), Journal of the American Chemical Society 94(1) (1972) 84-90.
[33] B.D. Ulery, L.S. Nair, C.T. Laurencin, Biomedical applications of biodegradable polymers, Journal of Polymer Science Part B: Polymer Physics 49(12) (2011) 832-864.
[34] D.J. Darensbourg, A. Horn Jr, A.I. Moncada, A facile catalytic synthesis of trimethylene carbonate from trimethylene oxide and carbon dioxide, Green Chemistry 12(8) (2010) 1376-1379.
[35] K. Fukushima, Poly(trimethylene carbonate)-based polymers engineered for biodegradable functional biomaterials, Biomaterials science 4(1) (2016) 9-24.
[36] A.P. Pêgo, D.W. Grijpma, J. Feijen, Enhanced mechanical properties of 1,3-trimethylene carbonate polymers and networks, Polymer 44(21) (2003) 6495-6504.
[37] A.S. Hoffman, Hydrogels for biomedical applications, Advanced Drug Delivery Reviews 64, Supplement (2012) 18-23.
[38] K. Fukushima, Poly(trimethylene carbonate)-based polymers engineered for biodegradable functional biomaterials, Biomaterials science 4(1) (2016) 9-24.
[39] A.P. PÊGO, A.A. POOT, D.W. GRIJPMA, J. FEIJEN, Copolymers of trimethylene carbonate and e-caprolactone for porous nerve guides: Synthesis and properties, Journal of Biomaterials Science, Polymer Edition 12(1) (2001) 35–53.
[40] L. Mespouille, O. Coulembier, M. Kawalec, A.P. Dove, P. Dubois, Implementation of metal-free ring-opening polymerization in the preparation of aliphatic polycarbonate materials, Progress in Polymer Science 39(6) (2014) 1144-1164.

[41] L. Mezzasalma, A.P. Dove, O. Coulembier, Organocatalytic ring-opening polymerization of l-lactide in bulk: A long standing challenge, European Polymer Journal 95 (2017) 628-634.
[42] X. Li, N. Mignard, M. Taha, C. Fernandez-de-Alba, J. Chen, S. Zhang, F. Becquart, Synthesis of poly(trimethylene carbonate) (PTMC) oligomers by ring-opening polymerization in bulk (submitted), (2019).
[43] M. Ionescu, Chemistry and technology of polyols for polyurethanes, Rapra Technology Limited, Shawbury, Shrewsbury, United Kingdom, 2005.
[44] E. Delebecq, J.-P. Pascault, B. Boutevin, F. Ganachaud, On the Versatility of Urethane/Urea Bonds: Reversibility, Blocked Isocyanate, and Non-isocyanate Polyurethane, Chemical Reviews 113(1) (2013) 80-118.
[45] A. Saralegi, A. Etxeberria, B. Fernández-d'Arlas, I. Mondragon, A. Eceiza, M.A. Corcuera, Effect of H12MDI isomer composition on mechanical and physico-chemical properties of polyurethanes based on amorphous and semicrystalline soft segments, Polymer Bulletin 70(8) (2013) 2193-2210.
[46] O. Lamarzelle, P.-L. Durand, A.-L. Wirotius, G. Chollet, E. Grau, H. Cramail, Activated lipidic cyclic carbonates for non-isocyanate polyurethane synthesis, Polymer Chemistry 7(7) (2016) 1439-1451.
[47] S. Li, X. Kong, S. Feng, Preparation of uniform poly(urea-siloxane) microspheres through precipitation polymerization, RSC Advances 5(110) (2015) 90313-90320.
[48] L.H. Chan-Chan, G. González-García, R.F. Vargas-Coronado, J.M. Cervantes-Uc, F. Hernández-Sánchez, A. Marcos-Fernandez, J.V. Cauich-Rodríguez, Characterization of model compounds and poly(amide-urea) urethanes based on amino acids by FTIR, NMR and other analytical techniques, European Polymer Journal 92 (2017) 27-39.
[49] F.-Z. Belmokaddem, J. Dagonneau, J. Lhomme, R. Blanc, A. Garduno-Alva, C. Maliverney, A. Baceiredo, E. Maerten, E. Fleury, F. Méchin, Novel nucleophilic/basic and acidic organocatalysts for reaction between poorly reactive diisocyanate and diols, Designed Monomers and Polymers 19(4) (2016) 347-360.
[50] W.E. Stewart, T.H. Siddall, Nuclear magnetic resonance studies of amides, Chemical Reviews 70(5) (1970) 517-551.
[51] S.H. Gellman, G.P. Dado, G.B. Liang, B.R. Adams, Conformation-directing effects of a single intramolecular amide-amide hydrogen bond: variable-temperature NMR and IR studies on a homologous diamide series, Journal of the American Chemical Society 113(4) (1991) 1164-1173.

[52] A.N. Patel, M.M. Patel, A. Dighe, Influence of compositional variables on the morphological and dynamic mechanical behavior of fatty acid based self-crosslinking poly (urethane urea) anionomers, Progress in Organic Coatings 74(3) (2012) 443-452.
[53] J. Mattia, P. Painter, A Comparison of Hydrogen Bonding and Order in a Polyurethane and Poly(urethane−urea) and Their Blends with Poly(ethylene glycol), Macromolecules 40(5) (2007) 1546-1554.
[54] H. Wang, J. Yu, H. Fang, H. Wei, X. Wang, Y. Ding, Largely improved mechanical properties of a biodegradable polyurethane elastomer via polylactide stereocomplexation, Polymer 137 (2018) 1-12.
[55] I.C. McNeill, A. Rincon, Degradation studies of some polyesters and polycarbonates: Part 5—Poly(trimethylene carbonate), Polymer Degradation and Stability 24(1) (1989) 59-72.
[56] D.K. Chattopadhyay, D.C. Webster, Thermal stability and flame retardancy of polyurethanes, Progress in Polymer Science 34(10) (2009) 1068-1133.
[57] G. Montaudo, C. Puglisi, Thermal Degradation Mechanisms in Condensation Polymers, in: Developments in Polymer Degradation—7, N. Grassie (Ed.), Springer Netherlands, Dordrecht, 1987, Vol., pp. 35-80.
[58] L. Jiao, H. Xiao, Q. Wang, J. Sun, Thermal degradation characteristics of rigid polyurethane foam and the volatile products analysis with TG-FTIR-MS, Polymer Degradation and Stability 98(12) (2013) 2687-2696.
[59] C. Yan, D.J. Pochan, Rheological properties of peptide-based hydrogels for biomedical and other applications, Chemical Society Reviews 39(9) (2010) 3528-3540.
[60] D.H. Merino, A. Feula, K. Melia, A.T. Slark, I. Giannakopoulos, C.R. Siviour, C.P. Buckley, B.W. Greenland, D. Liu, Y. Gan, P.J. Harris, A.M. Chippindale, I.W. Hamley, W. Hayes, A systematic study of the effect of the hard end-group composition on the microphase separation, thermal and mechanical properties of supramolecular polyurethanes, Polymer 107 (2016) 368-378.
[61] Y. Wang, X. Liu, S. Li, T. Li, Y. Song, Z. Li, W. Zhang, J. Sun, Transparent, Healable Elastomers with High Mechanical Strength and Elasticity Derived from Hydrogen-Bonded Polymer Complexes, ACS Applied Materials & Interfaces 9(34) (2017) 29120-29129.
[62] T.A. Speckhard, K.K.S. Hwang, S.L. Cooper, V.S.C. Chang, J.P. Kennedy, Properties of polyisobutylene polyurethane block copolymers: 3. Hard segments based on 4,4′-dicyclohexylmethane diisocyanate (H12MDI) and butane diol, Polymer 26(1) (1985) 70-78.

Chapter 4. Microphase separation morphology and chain dynamics of PTMC-based hydrogen-bonded supramolecular networks in the melt state

Xiang Li[a,b,c], Nathalie Mignard[a,b,c], Jean-Charles Majesté[a,b,c], Guillaume Sudre[a,b,d], Jianding Chen[e], Shengmiao Zhang[e] and Frédéric Becquart[a,b,c,*]

[a]Université de Lyon, F-42023 Saint-Etienne, France

[b]CNRS, UMR 5223, Ingénierie des Matériaux Polymères, F-42023 Saint-Etienne, France

[c]Université Jean Monnet, F-42023 Saint-Etienne, France

[d]Université Claude Bernard Lyon 1, F-69622 Villeurbanne, France

[e]Laboratory of Advanced Materials Processing, East China University of Science and Technology, 200237 Shanghai, China

[*]Corresponding Author. E-mail: Frederic.Becquart@univ-st-etienne.fr

Abstract

The morphology and dynamics of poly(trimethylene carbonate) (PTMC) based multiarm supramolecular polymers bearing self-complementary triuret and tetrauret hydrogen-bonding motifs (HBMs) were investigated in the melt state to reveal the association and relaxation modes of HBMs. No crystallinity was observed but small-angle X-ray scattering proved the existence of two kinds of microphase-separated microdomains, induced by hydrogen bonding between urethane groups or HBMs. In supramolecular polymers, the relaxation time of PTMC chains and hydrogen bonding between urethane groups were revealed to be extremely short and 2.77 s respectively. The aggregates formed by triuret and tetrauret HBMs can increase the relaxation times of supramolecular polymers strikingly. Triuret HBM functionalized PTMC oligomers (molar mass of 2000 g/mol) has the relaxation time of 1.03×10^6 s. Through the increase of functionality or the decrease of PTMC chain length, bigger HBM aggregates with longer relaxation times can be formed. When the temperature is increased, weak hydrogen bonding between urethane groups dissociate first but stronger HBM aggregates can still maintain the physical network structures until the final collapse at higher temperature. Though the ^{1}H-NMR-determined association constant of tetrauret is higher than triuret HBM in $CDCl_3$, the formation of smaller and weaker hydrogen bonding aggregates in supramolecular polymers

containing tetrauret HBMs makes the rheological relaxation time lower than their triuret counterparts.

Keywords: supramolecular, microphase separation, rheological properties, dynamics

1. Introduction

During the last several decades, combining polymers and noncovalent interactions to obtain supramolecular polymers has become a significant strategy to design new class of materials in polymer chemistry and materials science[1-9]. Due to the dynamic properties of noncovalent interactions, these supramolecular polymers usually possess certain special and attractive properties such as stimuli responsiveness[10,11], self-healing[12,13] or shape memory[14,15]. The implemented noncovalent interactions usually include hydrogen bonds, ionic bonds, halogen bonds, host-guest interactions and π-π stacking[1]. Among them, the hydrogen bond is the most widely used because of its strong directionality and versatility[16]. Thanks to multiple hydrogen-bonding motifs (HBMs)[17], the association constant (K_a), which describes the supramolecular strength, can vary in several orders of magnitude offering extensive applications. However, besides the strength of noncovalent interactions, their dynamics are also significant to determine supramolecular polymers properties[18]. For example, Craig et al.[19-21] highlighted that crosslinking dynamics play much more prominent roles than thermodynamic equilibrium in deciding the dynamic and mechanical properties of metallo-supramolecular networks, namely "strong means slow".

In most of cases, the association of HBMs in solution is a diffusion-controlled process[22]. However, the dynamics in bulk is different, resulting from the movement restriction by polymer chains[23]. Actually, the interaction geometry (bond length and angle) of hydrogen bonds is never optimum in the solid state[24]. Due to the intrinsic structure of supramolecular polymers, their dynamics are usually composed of two main characteristic timescales[18,25]. Firstly, it is related to the inherent dynamics of noncovalent interactions which can be described by supramolecular bond lifetime (τ_b)[4,25-29], depicting the average timescale for noncovalent interactions association and dissociation. When τ_b is in the range from 1 μs to 1 min, the supramolecular polymers can have tunable properties such as adaptability, responsiveness and self-healing[30]. Moreover, the relaxations of the polymer backbones are not negligible either[18]. When the polymer chain relaxation is much longer than τ_b, only a minor retardation of terminal

relaxation can be observed[31]. On the contrary, the relaxation of supramolecular polymer is decided by τ_b and supramolecular polymers usually behave like conventional elastomers[32,33].

In addition to the individual hydrogen bonding between HBMs, complex aggregates which contains multiple moieties can also be formed, affecting the dynamic properties of supramolecular polymers significantly[34-38]. For instance, Goldansaz et al.[39] revealed that the acrylic acid groups in entangled poly(n-butyl acrylate)-poly(acrylic acid) random copolymers are able to self-assemble to form binary and collective associations. The relatively weak binary associations only have a great effect on the segmental dynamics at low temperatures while the strong collective associations dominate at any temperature. Herbst et al.[35] synthesized thymine (K_a = 3.8 M^{-1}) and/or 2,6-diaminotriazine (K_a = 1.7 M^{-1}) functionalized telechelic polyisobutylenes. Although these two moieties have comparable association constants in solution, the formation of various aggregated structures in the melt state leads to supramolecular polyisobutylenes with different viscoelastic properties. Later, they[40] found that barbituric acid-functionalized poly(isobutylene)s could form aggregates with long lifetimes at high frequency, inducing the materials to behave like rubbers. However, aggregates can dissociate and make the material flow at low frequencies.

Recently, poly(trimethylene carbonate) (PTMC) based multiarm supramolecular polymers bearing triuret and tetrauret HBMs were synthesized in our lab[41] by condensation from trifunctional glycerol, oligomeric PTMC diol, H_{12}MDI, urea or biuret, and 1-pentanol as a terminating agent. Though K_a of triuret and tetrauret HBMs were compared by ^{1}H-NMR to be 0.32 and 1.59 M^{-1} respectively, the rheological properties and relaxations of these materials in condensed phase are still unclear. Besides, it is significant to study the distribution of these supramolecular moieties in the materials and their assembly modes, for instance, to possibly form dimers or complex aggregates. In this work, the morphology of the previously synthesized supramolecular polymers will be studied by Wide-angle X-ray scattering (WAXS) and small-angle X-ray scattering (SAXS) to verify if crystalline or phase separation exist. Then, the dynamic behaviors of pure PTMC oligomers and PTMC-based multiarm elementary structures containing only urethane functions will be studied to clarify the relaxations of PTMC chains and urethane functions in the final materials respectively. Finally, the dynamics of triuret and tetrauret HBMs will be studied by temperature-dependent methods. This study makes an attempt to establish the relation between supramolecular structures and their dynamics in order to facilitate the future chemical design of supramolecular polymers in relation to their dynamic properties.

2. Experimental section

2.1 Materials

The syntheses and characterizations of all samples presented in this article have been reported in a recent study[41]. A nomenclature is chosen to name supramolecular polymers. PTMC*f*L*m* denotes the material with a desired functionality of "*f*" and a PTMC molar mass of 100 × "*m*" g/mol. "L" represents the HBM, namely "B" for biuret (tetrauret motif), "U" for urea (triuret motif) and "X" for the absence of biuret or urea. All the structures are schematically presented in Figure 1.

The synthesis method of PTMC3U10 is presented as an example. In a three-neck flask, 0.313 g glycerol (3.395 mmol) and 10.186 g $PTMC_{1000}$ (10.186 mmol) were dissolved in 80 mL anhydrous DMF at 80 °C under nitrogen atmosphere. After homogenization, 5.939 g 4,4'-methylenebis(cyclohexyl isocyanate) ($H_{12}MDI$) (20.373 mmol) and 19.3 mg dibutyltin dilaurate catalyst (0.1 mol% of $H_{12}MDI$) were added. The reaction was kept until isocyanate carbonyl absorption (2260 cm^{-1}) became stable by FT-IR; In the second step, 0.612 g urea (10.200 mmol) and 2.969 g $H_{12}MDI$ (10.186 mmol) were added after increasing the reaction temperature to 110 °C. When the absorption of isocyanate group at 2260 cm^{-1} became stable, 0.898 g 1-pentanol (10.200 mmol) was added and the reaction was stopped when the absorption at 2260 cm^{-1} disappeared in FT-IR spectrum. The obtained viscous solution was cooled to ambient temperature and precipitated in diethyl ether. The final material was dried at 80 °C for 24 h at 0.2 mbar. All the ^{1}H-NMR calculated $\overline{M}_{n,\,NMR}$ and T_g of supramolecular polymers are presented in Table 1.

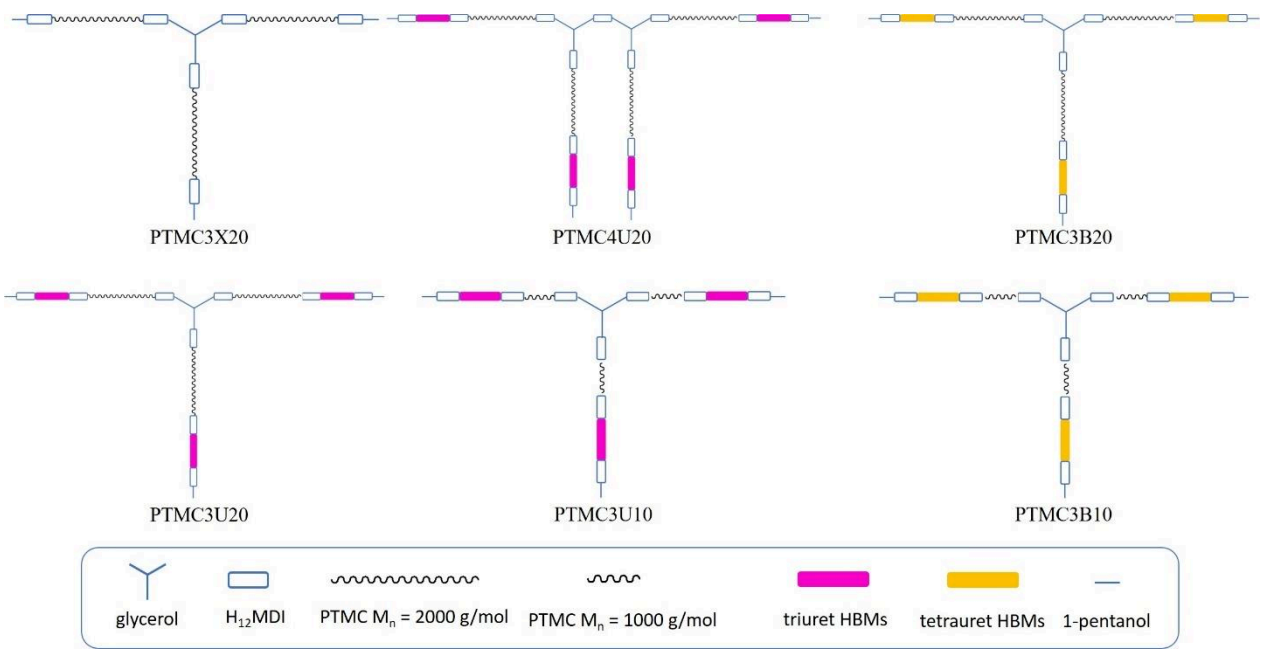

Figure 1. Schematic representation of the synthesized multiarm supramolecular polymers from PTMC.

2.2 Characterization techniques

Small-angle X-ray scattering (SAXS) and Wide-angle X-ray scattering (WAXS)

SAXS/WAXS experiments were carried out at the European Synchrotron Radiation Facility (ESRF) in Grenoble (France) on the BM2-D2AM beamline. The incident photon energy was set to 18 keV. Samples with a thickness between 800 and 1000 µm were directly placed in the beam path. The SAXS and the WAXS signals were detected simultaneously using two 2D XPad solid state detectors. For SAXS acquisition, the sample-to-detector distance was set at about 1.15 m and a beam stop with a diameter of 2 mm was used. For WAXS acquisition, the sample to detector distance was set at 10 cm. The q-calibration ($q = 4\pi\sin(\theta)/\lambda$; 2θ: scattering angle) was realized using a silver behenate powder standard for SAXS and a chromium(III) oxide (Cr_2O_3) powder standard for WAXS. The scattering contribution of air was subtracted from the scattering intensity of the samples. The image data treatments took into account the flat field response. The intensity was further normalized by the incident flux, and the sample thickness and I-calibration were realized with a glassy carbon standard. The scattering profiles of the intensity I as a function of the scattering vector q were obtained by azimuthally averaging the corrected images.

Oscillatory rheology tests

The rheology tests of PTMC oligomers and supramolecular polymers were carried out with an ARES-G2 (TA Instruments) rheometer with 40 mm and 25 mm diameter parallel plates respectively and a gap fixed between 0.5 and 0.8 mm. Strain sweep tests were performed to obtain the linear viscoelastic region (LVR). All measurements were then conducted with a controlled strain in the LVR. Frequency sweep tests were performed at a constant strain of 1% with angular frequencies from 100 to 0.1 rad/s at different temperatures in order to construct master curves. Before each experiment, samples were annealed in an oven at 80 °C at 200 mbar for 24 h. A new sample was used for each temperature. The supramolecular polymers were annealed at each temperature for approximately 2 h in the rheometer prior tests. Time-temperature superposition (TTS) principle was applied to build master curves from frequency sweep tests at different temperatures. 100 °C was chosen as the reference temperature. Horizontal shift factors (a_T) were determined by the superposition of tan δ (ω, T) and vertical shift factors (b_T) were obtained by the superposition of G' ($a_T\omega$, T) and G'' ($a_T\omega$, T) manually afterward.

3. Results and discussions

In the condensed state, crystallization[3] and microphase separation[38,42] have a great influence on the properties of supramolecular polymers. Consequently, the morphology of the synthesized multiarm supramolecular polymers must be elucidated by WAXS and SAXS. In order to reveal the assembly mode and relaxations of HBMs, the dynamics of PTMC oligomers and hydrogen bonding between urethane groups are isolated by the respectively study of PTMC oligomers and PTMC3X20 which contain urethane groups but no triuret or tetrauret HBMs yet.

3.1 Morphology of multiarm supramolecular polymers

3.1.1 Amorphous state determined by Wide-angle X-ray scattering

As reported in a previous study[41], no crystallinity was observed for supramolecular polymers by DSC. However, in some cases, the crystalline structures could not be detected by DSC. In this case, WAXS was chosen to verify if supramolecular polymers are purely amorphous. From the WAXS scattering spectra in Figure 2, only broad amorphous peaks were observed at the similar scattering vector ($q \approx 1.5$ Å^{-1}) for all samples, indicating the random distribution of intersegment distance and the absence of crystallinity[43].

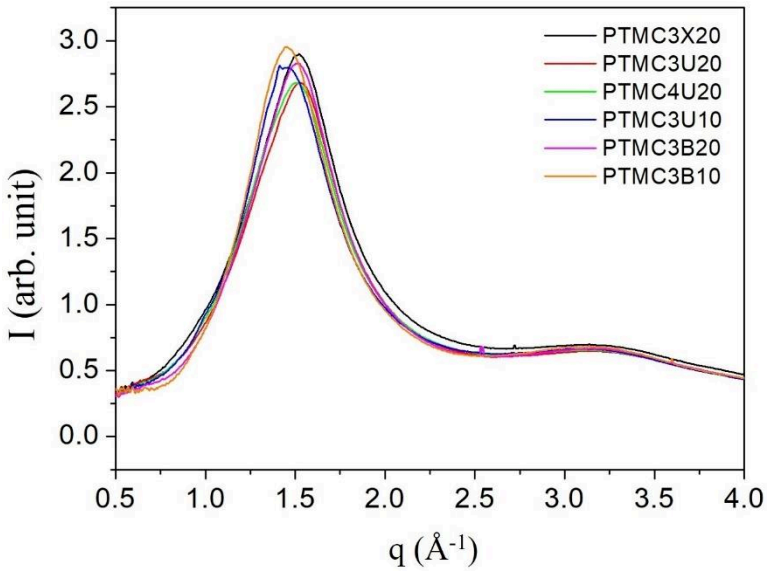

Figure 2. WAXS spectra of multiarm supramolecular polymers (room temperature). I: intensity, q: scattering angle.

3.1.2 Microphase-separated morphology by Small Angle X-ray Scattering

SAXS is usually used to detect the morphologies of materials. SAXS spectra of supramolecular polymers were collected and shown in Figure 3. It is obvious that all samples have a single scattering peak in the q-range between 0.01 and 0.1 $Å^{-1}$, indicating the microphase-separated morphologies.

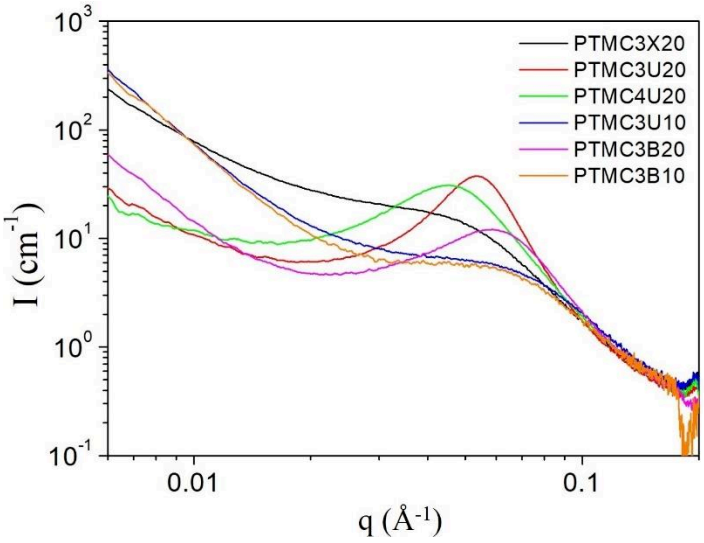

Figure 3. SAXS spectra of multiarm supramolecular polymers (room temperature).

The scattering peak abscissa is associated with the average interdomain distance, "center to center" (also called d-spacing), arising from the presence of periodic structures, at least on a short range. d-spacing can be calculated with:

$$d = \frac{2\pi}{q^*} \qquad \text{Eq. (1)}$$

where q^* is the q value corresponding to the maximum intensity. d-spacings for all samples are shown in Table 1.

Table 1. The structure parameters of multiarm supramolecular polymers.

Sample	Functionality	PTMC $\overline{M}_n$ (g/mol)	HBM	HBM content[a] (mmol/g)	$\overline{M}_{n,\,NMR}$ [b]	T_g (°C)	d-spacing (nm)
PTMC3X20	3	2000	-	0	7100	-19.7	11.5
PTMC3U20	3	2000	triuret	0.341	8000	-16.1	11.1
PTMC4U20	4	2000	triuret	0.364	11000	-13.9	12.3
PTMC3U10	3	1000	triuret	0.447	5500	0.9	8.0
PTMC3B20	3	2000	tetrauret	0.325	8300	-9.5	9.7
PTMC3B10	3	1000	tetrauret	0.482	5600	2.2	8.2

[a]HBM content is the molar fraction of urea or biuret motifs per gram of multiarm supramolecular polymers[41]. [b]Calculated by ^{1}H NMR

When aliphatic isocyanate H_{12}MDI was used, hard ordered domains were already observed in synthesized polyurethanes[44-47]. For example, Sheth et al.[46] synthesized polyurethanes from polydimethylsiloxane and H_{12}MDI with observed interdomain d-spacing between 9.6 and 12.7 nm. In addition, Kull and co-workers[47] also reported interdomain d-spacing of 4.5 nm for polycarbonate polyol ($\overline{M}_n$ = 2000 g/mol) and H_{12}MDI based polyurethanes. According to these studies, the measured d-spacing of 11.5 nm (Table 1) for PTMC3X20, which contains no HBM, is attributed to the microdomains formed by hydrogen bonding between urethane bonds. Nevertheless, it is impossible to determine the quantity of urethane functions present in each microdomain, namely, the stoichiometry of the associated urethane functions is not directly accessible. For supramolecular polymers containing HBMs, it seems that d-spacing values are independent of HBM type and functionality within the experimental uncertainty but are related to the PTMC chain length as already been observed in polyurethanes[46]. As compared in Table 1, d-spacings of all samples based on $PTMC_{2000}$ ($\overline{M}_n$ = 2000 g/mol) range from approximately

9.7 to 12.3 nm. However, when PTMC chain length are shorter ($\overline{M}_n$ = 1000 g/mol), the corresponding d-spacings are decreased to 8.0 nm and 8.2 nm for PTMC3U10 and PTMC3B10 respectively.

3.2 Rheological properties of PTMC oligomers and multiarm supramolecular polymers

The rheological properties of supramolecular polymers were studied to understand their dynamic behaviors. Generally, time-temperature superposition (TTS) principle[48] is used to study the viscoelastic properties of materials through the construction of master curves. However, TTS principle is only viable when the polymer structure remains unaltered and only the relaxation rate is dependent on temperature. Though these conditions are usually not satisfied for supramolecular polymers due to the existence of noncovalent and dynamic interactions, it is still significant to make an attempt to build master curves because they can give a clear snapshot of the viscoelastic properties over a wide frequency range[4,18,49,50].

To build master curves, horizontal shifts, which are related to frequency, are used for the attempt to superpose tan δ curves collected in frequency sweep tests at different temperatures. Because tan δ is independent of absolute modulus values, no assumption about vertical shifts is needed in the a_T shifts[48]. Then, vertical shifts, which are related to the stress magnitude dependence on temperature, are implemented to superpose reduced modulus (b_TG', b_TG'') and reduced frequency ($a_T\omega$). Before the discussion of obtained master curves, the temperature dependences of PTMC oligomers and supramolecular polymers viscoelastic properties are compared by the horizontal shift factors (a_T) to have an overview of their rheological properties.

3.2.1 Temperature dependence of viscoelastic properties by horizontal shift factors

Log a_T versus ($T-T_{ref}$) curves (Figure 4) give the temperature dependences of PTMC oligomers and supramolecular polymers viscoelastic properties directly. Two main domains were observed. $PTMC_{1000}$ and $PTMC_{2000}$ exhibit almost the same temperature dependence evidenced by the overlap of their plots. However, all plotting of supramolecular polymers deviates far from PTMC oligomers. By these comparisons, it is then proved that the viscoelastic properties of PTMC-based supramolecular polymers bearing hydrogen-bonding associations depend much more on temperature than pure PTMC oligomers. Furthermore, all supramolecular polymers have similar temperature dependences on their dynamic properties, as evidenced by the comparable a_T values. It also suggests that hydrogen bonding, no matter from urethane bonds or triuret/tetrauret HBMs, has similar effects on the relaxation models of materials.

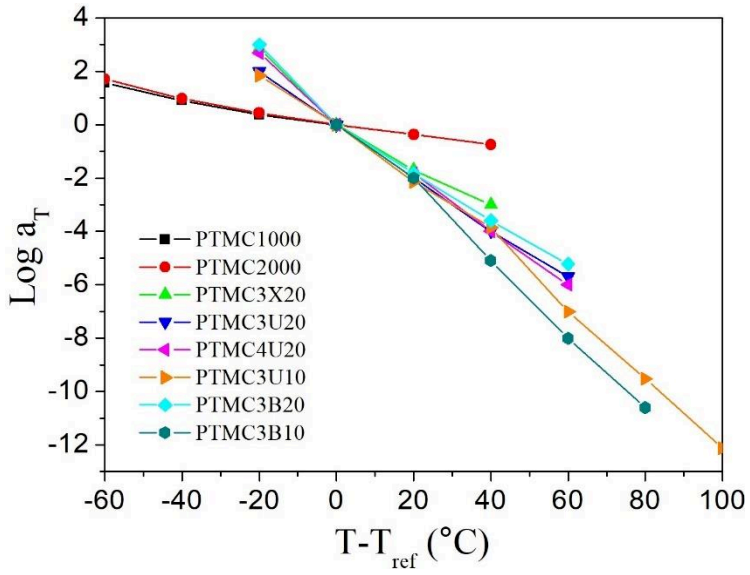

Figure 4. Temperature dependences of horizontal shift factors a_T for PTMC oligomers and supramolecular polymers. T_{ref} = 100 °C.

3.2.2 Viscoelastic properties of PTMC oligomers

To isolate the relaxations of noncovalent interactions, the rheological behaviors of pure PTMC oligomers were firstly studied. According to Pêgo et al.[51], PTMC has a critical entanglement molar mass of 2700 g/mol, which is higher than the molar mass of PTMC oligomers implemented in this article. The master curves of PTMC oligomers were obtained by plotting loss modulus G'' and reduced frequency $a_T\omega$ with only horizontal shifts at the reference temperature of 100 °C. As shown in Figure 5 (A), perfect superposition of G'' was obtained for both $PTMC_{1000}$ and $PTMC_{2000}$ with the curve slope of 1, signifying the terminal flow of PTMC chains. It is then concluded that full relaxation of PTMC chains are achieved in this range of temperatures. The scattered dots shown at low frequencies are all out of the sensitivity range of the rheometer.

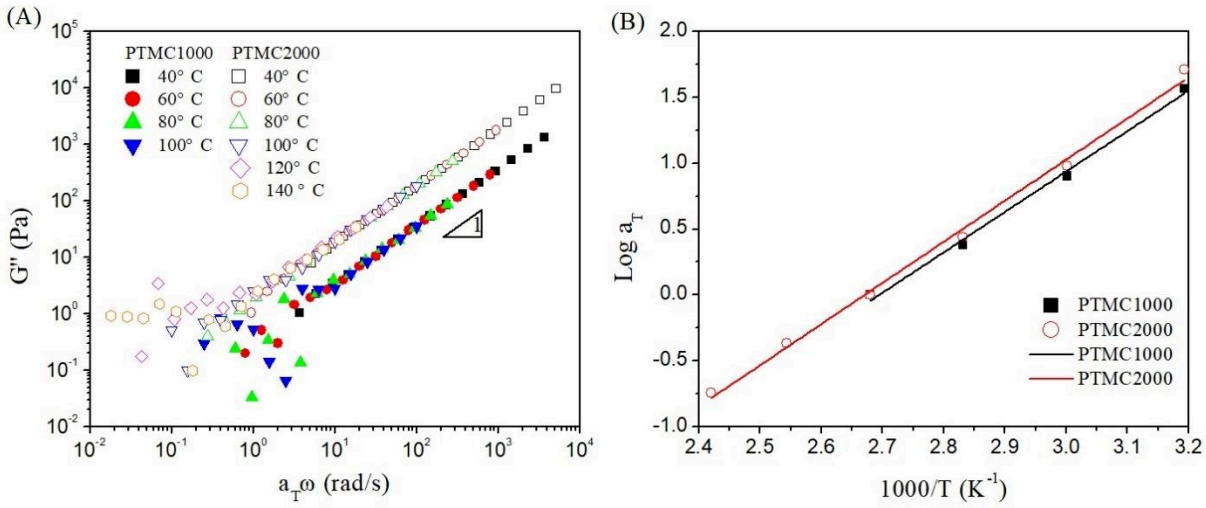

Figure 5. (A) Master curves of $PTMC_{1000}$ (filled markers) and $PTMC_{2000}$ (void markers); (B) Log a_T— 1000/T of $PTMC_{1000}$ and $PTMC_{2000}$ (markers: experimental data; line: curve-fitting result). T_{ref} = 100 °C.

The activation energy of polymer relaxation can be determined by Arrhenius law:

$$a_T = A\exp(E_a / RT) \qquad \text{Eq. (2)}$$

where A is a constant, E_a is the activation energy, R is the universal gas constant.

As shown in Figure 5 (B), E_a of $PTMC_{1000}$ and $PTMC_{2000}$ can be obtained directly by the plotted log a_T–1000/T curves with close values of 58.7 and 59.8 kJ/mol respectively. These low E_a and the undetectability of storage modulus G' signify the extremely short relaxation times for PTMC oligomers chains at 100 °C.

3.2.3 Dynamics of urethane groups in supramolecular polymers

Due to the existence of hydrogen bonding between urethane groups deriving from reactions between H_{12}MDI and alcohol functions, the dynamics of urethane groups must be determined in the purpose of separating them from the relaxations of triuret and tetrauret HBMs.

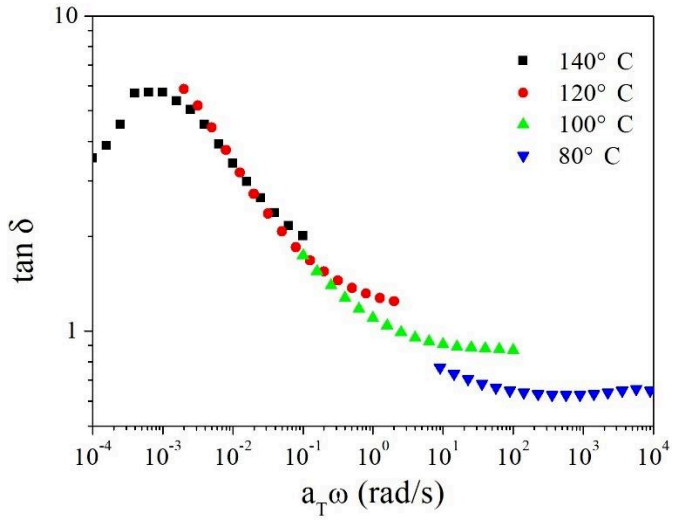

Figure 6. Attempts to superpose the tan δ (ω, T) curves for PTMC3X20. T_{ref} = 100 °C.

The superposition of tan δ curves for PTMC3X20 by horizontal shifts at T_{ref} = 100 °C is shown in Figure 6. The systematically failed superposition indicates the dependence of intrinsic structure or the relaxation mechanism on temperature and a rheological complex behavior. Segmental relaxations observed at higher frequencies do not have the same activation energy which seems to be distributed over the range of relaxation mechanisms. However, when possible, it was decided to superimpose all the tan δ curves on one master envelop for the longest relaxation mechanisms. The corresponding inferred activation energy will then be used for comparison purpose between all the systems.

At 100 °C, the crossover of G' and G'' (tan δ = 1) defines one characteristic relaxation time τ_{rheo} which can be calculated by the reciprocal of this crossover frequency with $\tau_{rheo} = 2\pi/\omega$[4,25,40]. On account of the extremely short relaxation time of PTMC oligomers, the obtained τ_{rheo} of 2.77 s (Table 2) for PTMC3X20 reveals the formation of complex structures by functionalized PTMC association with larger width of relaxation time distribution as shown in the terminal zone of PTMC3X20 at low frequencies (temperature range above 100 °C, Figure 7, A). This phenomenon is definitely induced by the hydrogen bonding between urethane groups. By Arrhenius law, the E_a can be calculated by the log a_T–1000/T curve (Figure 7, B) to be 231.9 kJ/mol, much higher than the values of PTMC oligomers.

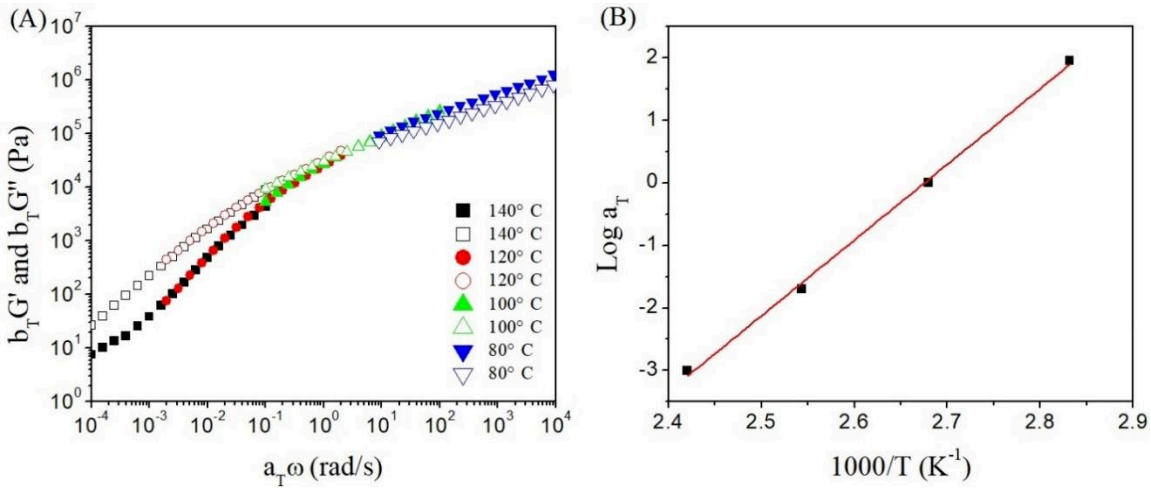

Figure 7. (A) Master curve of PTMC3X20 (G': filled markers; G'': open markers); (B) Log a_T–1000/T of PTMC3X20 (markers: experimental data; line: curve-fitting result). T_{ref} = 100 °C.

Table 2. Rheological properties of multiarm supramolecular polymers.

sample	$\overline{M}_{n\ PTMC}$ (g/mol)	HBM content[a] (mmol/g)	T_g[a] (°C)	$T_{crossover}$[a] (°C)	$\omega_{crossover}$[b] (rad/s)	τ_{rheo}[c] (s)	E_a[d] (kJ/mol)
PTMC3X20	2000	0	-19.7	98.4	2.27	2.77	231.9
PTMC3U20	2000	0.341	-16.1	151.5	6.08×10^{-6}	1.03×10^{6}	297.0
PTMC4U20	2000	0.364	-13.9	158.5	2.02×10^{-6}	3.11×10^{6}	313.5
PTMC3U10	1000	0.447	0.9	198.7	9.52×10^{-10}	1.05×10^{9}	-
PTMC3B20	2000	0.325	-9.5	147.0	1.37×10^{-4}	4.59×10^{4}	293.8
PTMC3B10	1000	0.482	2.2	178.7	1.22×10^{-8}	8.20×10^{7}	-

[a]Obtained from our previous work[41]. [b]Reduced frequency at G' and G'' crossover point at T_{ref} = 100 °C. [c]τ_{rheo} was obtained by the reciprocal of ω at T_{ref} = 100 °C. [d]E_a was obtained by the fitting of Arrhenius law.

3.2.4 Dynamic properties of multiarm supramolecular polymers with triuret and tetrauret HBMs

Thanks to the previous discussions, the dynamics of triuret and tetrauret HBMs can be isolated from the relaxations of PTMC chains (extremely short) and hydrogen bonding between urethane groups (2.77 s) in multiarm supramolecular polymers. The relaxation times of all supramolecular polymers containing HBMs (Table 2) were obtained from the crossover point of G' and G'' in frequency sweep curves followed by the application of horizontal shifts with a reference temperature of 100 °C. After the incorporation of HBMs, the relaxation times are all increased strikingly. For example, compared to PTMC3X20 (τ_{rheo} = 2.77 s), the τ_{rheo} of

PTMC3U20 containing triuret HBMs is increased to 1.03×10^6 s. For PTMC3U10 based on $PTMC_{1000}$ with shorter chain length, the τ_{rheo} is even higher (1.05×10^9 s). The same phenomena are also observed for samples containing tetrauret HBMs. Considering the relatively similar T_g for all these supramolecular polymers (Table 2), it indicates that it is the type and density of HBM not T_g that has significant effects on the big variation of τ_{rheo}. Then, the dynamic properties of triuret and tetrauret HBMs, in relation to the functionality and chain length, are discussed separately.

3.2.4.1 Dynamic properties of triuret HBMs

As seen in Figure 8 (A), the superposition of tan δ curves obtained at different temperatures fails for PTMC3U20 but with a greater overlay deviation extent for each curve as compared to PTMC3X20. Complex rheological behavior is again found which proves that triuret HBMs indeed have complex influence on the supramolecular structures relaxations. When vertical shifts are applied, the master curve of PTMC3U20 (Figure 8, B) fails to superpose with systematical upturns presented at the highest frequencies for each frequency sweep curve. It is related to the fact that segmental relaxation does not follow the same activation energy. Considering the significantly increased τ_{rheo} of PTMC3U20 (1.03×10^6 s) as compared to PTMC3X20 (2.77 s), it is then apparent that triuret HBMs could form stronger hydrogen bonding than urethane groups. These stronger associations also explain the several orders of magnitude higher G' and G'' modulus of PTMC3U20 than those of PTMC3X20 at low frequencies as well as the measured higher activation energy of PTMC3U20 (E_a = 297.0 kJ/mol, Figure 9).

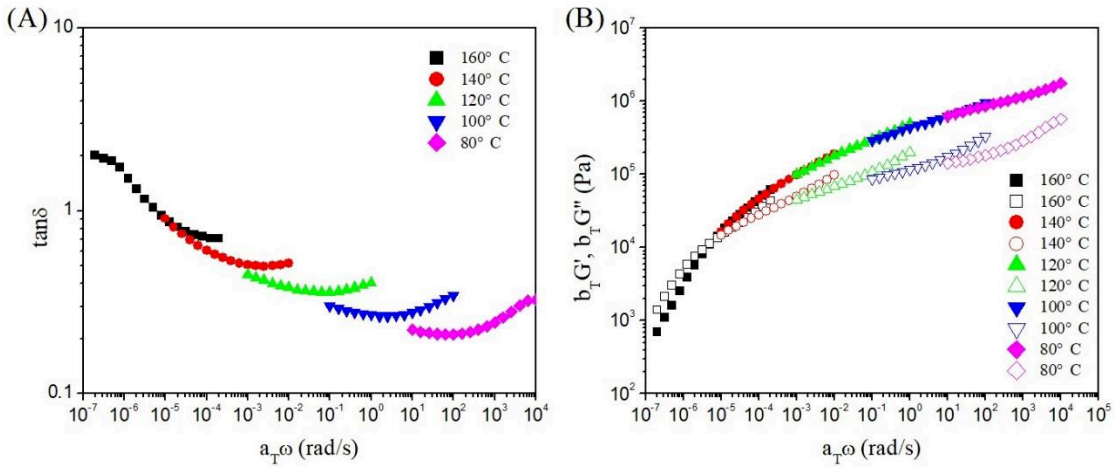

Figure 8. (A) Attempts to superpose tan δ (ω, T) curves for PTMC3U20; (B) Master curve of PTMC3U20 (G': filled markers; G'': void markers). T_{ref} = 100 °C.

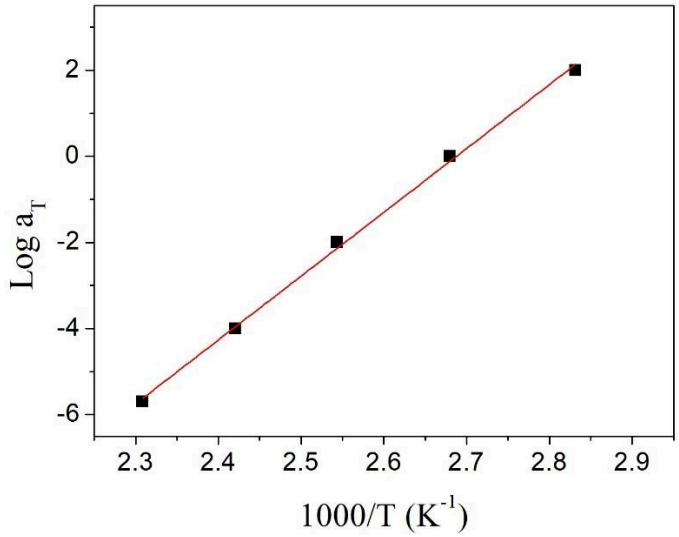

Figure 9. Log a_T–1000/T of PTMC3U20 (markers: experimental data; line: curve-fitting result).

As reported by Roy et al.[52], the tris-urea motifs -NH-C(=O)-NH-NH-C(=O)-NH-NH-C(=O)-NH- tend to form 6 hydrogen bonds with one other. However, due to the perpendicular orientation of N-N bonds, 4 hydrogen bonds are formed more or less in the same plane with 2 others in the second. In our case, it is reasonable to infer that triuret HBM -NH-C(=O)-NH-C(=O)-NH-C(=O)-NH-C(=O)-NH- could form 6 hydrogen bonds only if they are in the same plane, which is a relatively strict condition. In this context, the formation of 3D aggregates which contain more than 2 HBMs is postulated.

A schematic and global structure description of these supramolecular polymers at different temperatures is proposed in Figure 10. As seen, hydrogen bonds between both urethane groups and triuret HBMs in PTMC3U20 contribute to the formation of transient physical network structures at low temperature. With the increase of temperature, weaker hydrogen bonds between urethane groups are first broken but with the retention of strong HBM aggregates. At higher temperature, hydrogen bonds between triuret HBMs also begin to dissociate. However, due to the high number of HBMs participating in one microdomain, the dissociation of partial hydrogen bonds cannot lead to the total breakdown of aggregates. In this case, the material is still in the elastic state. At the highest temperature, all HBM microdomains are dislocated completely, which in turn causes the collapse of physical networks and a large degree of softening to show a terminal flow zone.

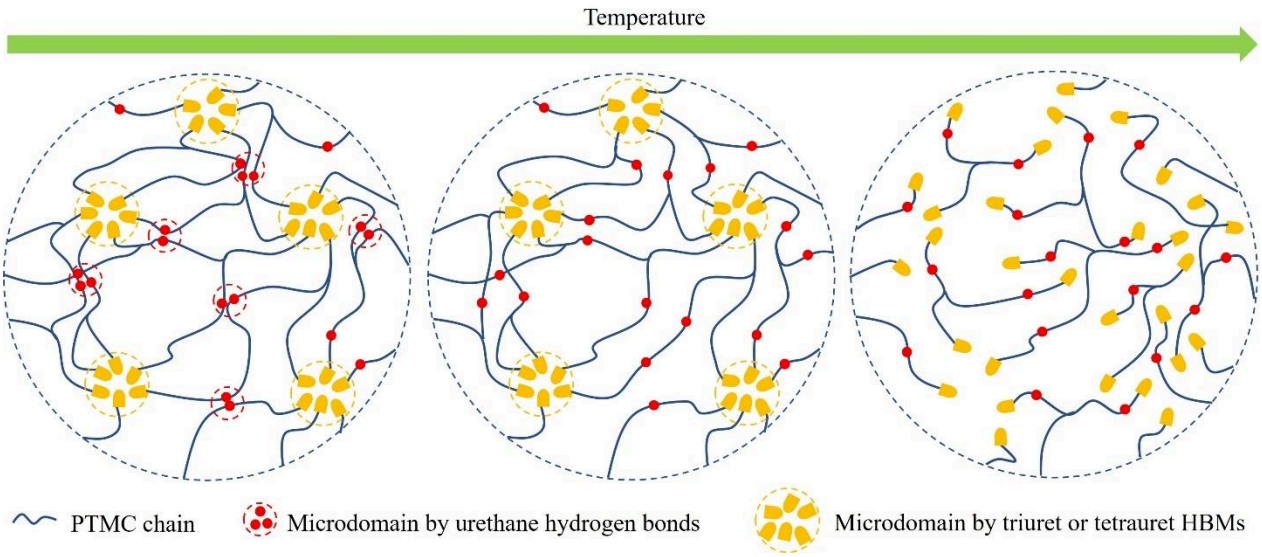

Figure 10. Schematic structures of multiarm supramolecular polymers at different temperatures.

The PTMC chain length was also found to have a great influence on the relaxations of these supramolecular structures. When PTMC molar mass is reduced from 2000 g/mol to 1000 g/mol, the triuret HBM concentration is increased correspondingly from 0.341 mmol/g for PTMC3U20 to 0.447 mmol/g for PTMC3U10.The relaxation time of PTMC3U10 is 3 orders of magnitude (1.05×10^{9} s) higher than PTMC3U20 (1.03×10^{6} s). As clarified previously, $PTMC_{1000}$ and $PTMC_{2000}$ have similar activation energies, excluding the effects of PTMC chain relaxation on this big τ_{rheo} discrepancy. It has already been described by Herbst et al.[35,40] that though the lifetime of hydrogen-bonding is hardly affected by the polymer chain length, the decrease of polymer molar mass can indeed lead to the increase of aggregate size and then the increase of relaxation time. In the present case, it can be speculated that the aggregate size is also the probable factor that affects the dynamics of PTMC3U10. Indeed, due to the higher triuret HBMs concentration in PTMC3U10 which imparts higher opportunities for hydrogen bonding moieties to contact, bigger and stronger aggregates could be formed. Consequently, more compact network structures were formed.

The superposition of tan δ curves for PTMC3U10 is shown in Figure 11 (A). Compared to the tan δ curves shown previously, a perfect superposition is not attainable as well. As seen in the Log a_T-1000/T curve (Figure 11, B), it is obvious that points cannot be linear fitted any more. Indeed, they can be relatively well fitted unconventionally by an increasing curve. The best fitting was obtained from the experimental points. By derivatives, two E_a at 80 °C and 200 °C were calculated at 506 and 186 kJ/mol respectively considering the uncertainty to the applied fitting. Thus, these variations of E_a with temperature may be induced by the existence of two

main kinds of relaxations, namely short relaxation of weak hydrogen bonds between urethane groups and long relaxation of strong triuret HBMs aggregates. At each temperature, the dynamics of supramolecular polymer are influenced by both relaxations, though with different levels. The hydrogen bonds between urethane groups have more impact on the relaxations of PTMC3U10 at low temperature while triuret HBM aggregates dominate at high temperature.

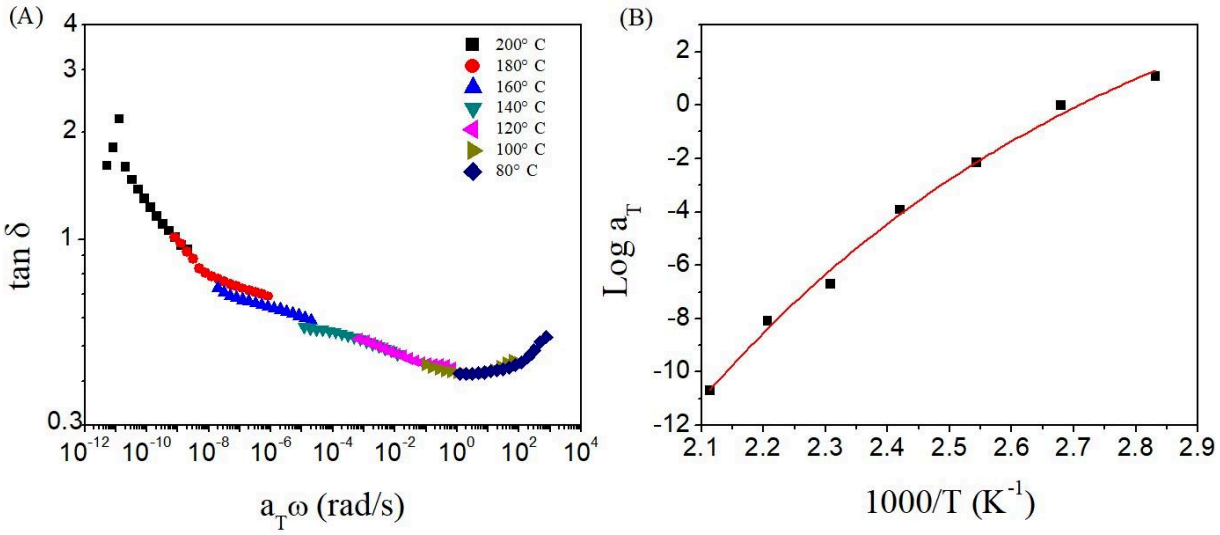

Figure 11. (A) Attempts to superpose tan δ (ω, T) curves for PTMC3U10; (B) Log a_T–1000/T of PTMC3U10 (markers: experimental data; line: curve-fitting result). T_{ref} = 100 °C.

Besides the PTMC chain length, the effects of functionality on supramolecular polymer dynamics are not negligible neither. Compared to PTMC3U20, the functionality (number of arms) of PTMC4U20 is increased from 3 to 4 while keeping the similar triuret HBM content (Table 2). In Figure 12 (A), the overlaid curves of tan δ show the same deviation tendency as PTMC3U20 but with slightly increased relaxation time of 3.11×10^6 s (Table 2). Given their nearly identical triuret HBM contents, the increased number of arms in PTMC4U20 might be an explanation. Due to the existence of one more arm in PTMC4U20, the possibility for each arm to participate in microdomains becomes higher than PTMC3U20, bringing about the formation of stronger aggregates which also contain more HBM numbers. Correspondently, the activation energy E_a = 313.5 kJ/mol of PTMC4U20 (Figure 12, B) is also higher than PTMC3U20.

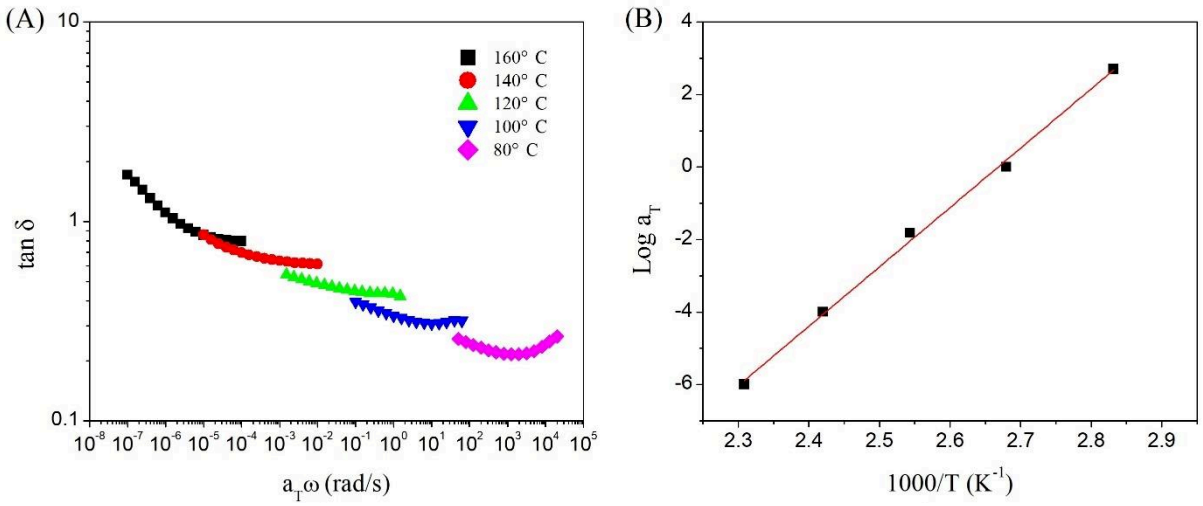

Figure 12. (A) Attempts to superpose the tan δ (ω, T) curves for PTMC4U20; (B) Log a_T–1000/T of PTMC4U20 (markers: experimental data; line: curve-fitting result). T_{ref} = 100 °C.

3.2.4.2 Dynamic properties of tetrauret HBMs

As studied previously[41], the NMR-calculated K_a of tetrauret HBM in $CDCl_3$ is 1.59 M^{-1}, higher than that of triuret HBM (0.32 M^{-1}). However, these supramolecular polymers with tetrauret HBMs have a lower crossover temperature ($T_{crossover}$) between G' and G'' and a higher creep than their triuret counterparts, which is in contradiction to the K_a order measured by NMR. In this case, the rheological properties of supramolecular polymers with triuret and tetrauret HBMs are prominent to compare here. As shown in Figure 13 (A), good superposition of tan δ is not achievable for PTMC3B20, just as PTMC3U20. However, the relaxation time of PTMC3B20 (4.59×10^4 s) is lower than that of PTMC3U20 (1.03×10^6 s). As reported by Herbst et al.[23] who compared the associations of thymine and 2,6-diaminotriazinein hydrogen-bonding moieties in solution and in the melt state, the order of association strength can be entirely different because of the probable formation of small domains in the melt state. It is then reasonable to infer that the different kinds of aggregates formed by triuret and tetrauret HBMs might be the main reason to have contrary properties in solution and in the melt state. A former study[53] has already reported that the tetrauret HBMs is potential to form intramolecular hydrogen bonds which can suspend the formation of intermolecular hydrogen bonds between HBMs. In this case, weaker tetrauret HBMs aggregates which contain less HBMs may be formed[35,40]. The calculated E_a of PTMC3B20 is 293.8 kJ/mol (Figure 13, B), which is a comparable value with 297.0 kJ/mol for PTMC3U20.

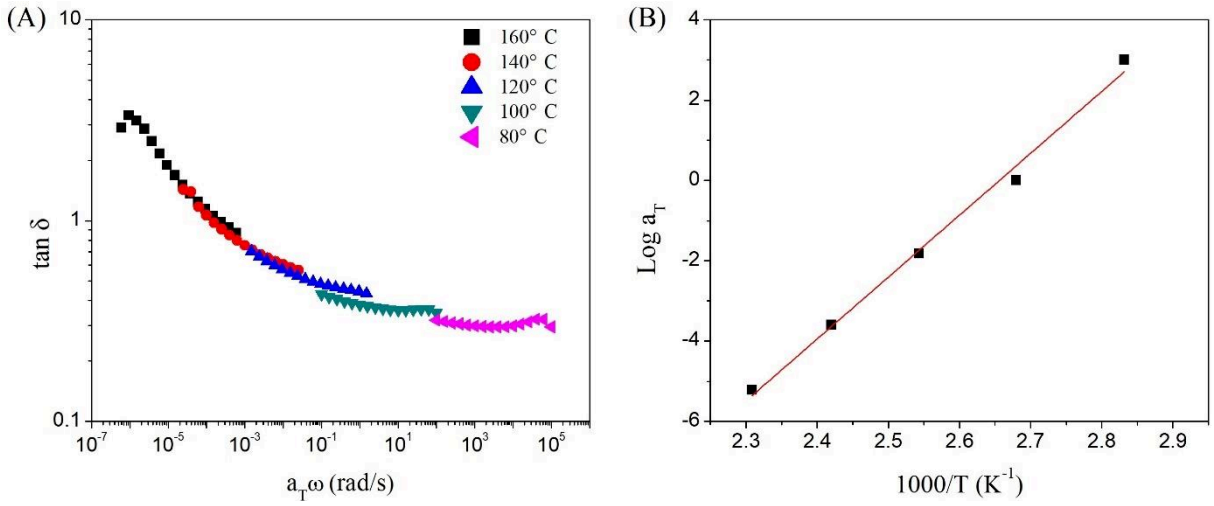

Figure 13. (A) Attempts to superpose tan δ (ω, T) curves for PTMC3B20; (B) Log a_T–1000/T of PTMC3B20 (markers: experimental data; line: curve-fitting result). T_{ref} = 100 °C.

The effect of PTMC chain length on the dynamics of supramolecular polymers with tetrauret HBM is similar to that for triuret system. As shown in Figure 14, the superposition of tan δ and linear fitting for points in Log a_T–1000/T plot also fail for PTMC3B10. Compared to PTMC3B20 (τ_{rheo} = 4.59×10^4 s), the rheological relaxation time of PTMC3B10 is increased with 3 orders of magnitude to 8.20×10^7 s. This strikingly increased τ_{rheo} can also be explained by the formation of bigger macrodomains induced by the higher tetrauret HBMs concentration as clarified previously. Meanwhile, the relaxation time of PTMC3B10 is shorter than PTMC3U10 (1.05×10^9 s), compatible to the τ_{rheo} order of $PTMC_{2000}$ based supramolecular polymers containing triuret and tetrauret HBMs as well. The E_a at 80 °C and 180 °C were calculated at 460 and 238 kJ/mol respectively using the same way as PTMC3U10.This phenomenon also indicates the formation of bigger and stronger aggregates by increasing the tetrauret HBM concentration. Besides, its lower E_a than PTMC3U10 at 80 °C (506 kJ/mol) indicates the effects of intramolecular hydrogen bonding in tetrauret HBMs. According to all the discussions above, it is obvious that the dynamics of supramolecular polymers are greatly dependent on the PTMC chain length. Nevertheless, the effect of HBM type, triuret or tetrauret, is relatively minor.

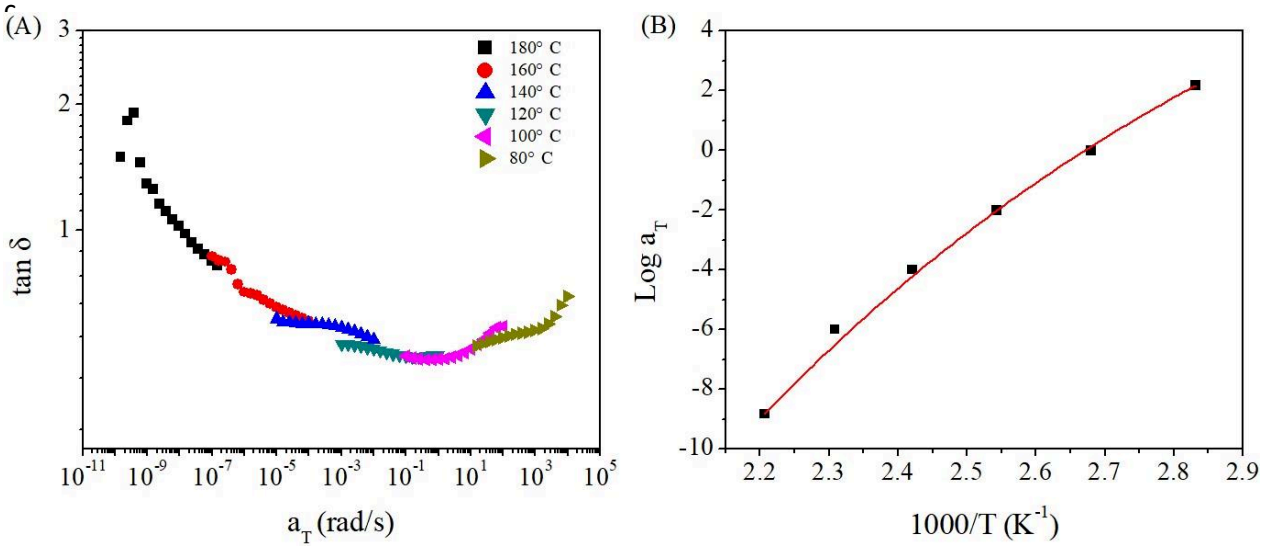

Figure 14. (A) Attempts to superpose tan δ (ω, T) curves for PTMC3B10; (B) Log a_T–1000/T of PTMC3B10 (markers: experimental data; line: curve-fitting result). T_{ref} = 100 °C.

4. Conclusion

The association and relaxation modes of triuret and tetrauret HBMs in PTMC-based multiarm supramolecular polymers in the melt state were clearly revealed by morphological studies and dynamic properties. All supramolecular polymers are amorphous. Hydrogen bonding by urethane groups and triuret/tetrauret HBMs can endow these materials with morphologies of microphase-separations. The average distances between microdomains are in the range of 8.0-12.3 nm, independent on HBM type and functionality but decrease with the shortening of PTMC chain length. The relaxation time of PTMC chains is extremely short while the hydrogen bonds between urethane groups have a relaxation time of 2.77 s. Either shortening PTMC chain length or increasing functionality can increase the size of triuret and tetrauret HBM aggregates, leading to the increased relaxation times and E_a. Though the ^{1}H-NMR-determined association constant of tetrauret HBM is higher than triuret HBM in $CDCl_3$, the intramolecular hydrogen bonds in tetrauret HBMs lead to the formation of smaller aggregates in the neat materials, making their relaxation times lower than triuret counterparts. When the temperature is increased, the weaker urethane hydrogen bonds will be broken first but the network structures can be maintained by stronger HBMs domains. At higher temperature, HBMs domains can also be dissociated and lead to the terminal flow for all these materials. This study provides the potentiality to use triuret or tetrauret HBMs to design supramolecular polymers with specific properties in the melt state.

Acknowledgments

The authors thank the financial support from China Scholarship Council (CSC). This work benefited from the international cooperation between Université Jean Monnet Saint-Etienne (France) and East China University of Science and Technology (China). The authors also acknowledge Isabelle Morfin (LIPhy, Grenoble, France) for her help with X-ray scattering measurements. The WOS (WAXS detector) was funded by the French National Research Agency (ANR) under the "Investissements d'avenir" program with the grant number: ANR-11-EQPX-0010.

References

[1] L. Yang, X. Tan, Z. Wang, X. Zhang, Supramolecular Polymers: Historical Development, Preparation, Characterization, and Functions, Chemical Reviews 115(15) (2015) 7196-7239.

[2] T.F.A. De Greef, M.M.J. Smulders, M. Wolffs, A.P.H.J. Schenning, R.P. Sijbesma, E.W. Meijer, Supramolecular Polymerization, Chemical Reviews 109(11) (2009) 5687-5754.

[3] H. Wang, J. Yu, H. Fang, H. Wei, X. Wang, Y. Ding, Largely improved mechanical properties of a biodegradable polyurethane elastomer via polylactide stereocomplexation, Polymer 137 (2018) 1-12.

[4] S. Chen, D. Döhler, W.H. Binder, Rheology of hydrogen-bonded dendritic supramolecular polymer networks in the melt state, Polymer 107 (2016) 466-473.

[5] Y. Takashima, Y. Sawa, K. Iwaso, M. Nakahata, H. Yamaguchi, A. Harada, Supramolecular Materials Cross-Linked by Host–Guest Inclusion Complexes: The Effect of Side Chain Molecules on Mechanical Properties, Macromolecules 50(8) (2017) 3254-3261.

[6] V. Schimpf, B. Heck, G. Reiter, R. Mülhaupt, Triple-Shape Memory Materials via Thermoresponsive Behavior of Nanocrystalline Non-Isocyanate Polyhydroxyurethanes, Macromolecules 50(9) (2017) 3598-3606.

[7] L.F. Scherz, S. Costanzo, Q. Huang, A.D. Schlüter, D. Vlassopoulos, Dendronized Polymers with Ureidopyrimidinone Groups: An Efficient Strategy To Tailor Intermolecular Interactions, Rheology, and Fracture, Macromolecules 50(13) (2017) 5176-5187.

[8] P.M. Lopez-Perez, R.M.P. da Silva, I. Strehin, P.H.J. Kouwer, S.C.G. Leeuwenburgh, P.B. Messersmith, Self-Healing Hydrogels Formed by Complexation between Calcium Ions and Bisphosphonate-Functionalized Star-Shaped Polymers, Macromolecules 50(21) (2017) 8698-8706.

[9] K. Xing, M. Tress, P. Cao, S. Cheng, T. Saito, V.N. Novikov, A.P. Sokolov, Hydrogen-bond strength changes network dynamics in associating telechelic PDMS, Soft Matter 14(7) (2018) 1235-1246.

[10] X. Yan, F. Wang, B. Zheng, F. Huang, Stimuli-responsive supramolecular polymeric materials, Chemical Society Reviews 41(18) (2012) 6042-6065.

[11] X. Ma, R. Sun, W. Li, H. Tian, Novel electrochemical and pH stimulus-responsive supramolecular polymer with disparate pseudorotaxanes as relevant unimers, Polymer Chemistry 2(5) (2011) 1068-1070.

[12] Y. Wang, X. Liu, S. Li, T. Li, Y. Song, Z. Li, W. Zhang, J. Sun, Transparent, Healable Elastomers with High Mechanical Strength and Elasticity Derived from Hydrogen-Bonded Polymer Complexes, ACS Applied Materials & Interfaces 9(34) (2017) 29120-29129.

[13] Y. Yang, X. Ding, M.W. Urban, Chemical and physical aspects of self-healing materials, Progress in Polymer Science 49–50 (2015) 34-59.
[14] M.D. Hager, S. Bode, C. Weber, U.S. Schubert, Shape memory polymers: Past, present and future developments, Progress in Polymer Science 49–50 (2015) 3-33.
[15] Z.-C. Jiang, Y.-Y. Xiao, Y. Kang, M. Pan, B.-J. Li, S. Zhang, Shape Memory Polymers Based on Supramolecular Interactions, ACS Applied Materials & Interfaces 9(24) (2017) 20276-20293.
[16] G. ten Brinke, J. Ruokolainen, O. Ikkala, Supramolecular Materials Based On Hydrogen-Bonded Polymers, in: Hydrogen bonded polymers, W. Binder (Ed.), Springer-Verlag, Berlin, Heidelberg, 2007, Vol. 207, pp. 113-177.
[17] Y.S. Kyung, Z.S. C., Hydrogen Bonding Modules for Use in Supramolecular Polymers, Israel Journal of Chemistry 53(8) (2013) 511-520.
[18] S. Seiffert, J. Sprakel, Physical chemistry of supramolecular polymer networks, Chemical Society Reviews 41(2) (2012) 909-930.
[19] W.C. Yount, D.M. Loveless, S.L. Craig, Strong Means Slow: Dynamic Contributions to the Bulk Mechanical Properties of Supramolecular Networks, Angewandte Chemie International Edition 44(18) (2005) 2746-2748.
[20] W.C. Yount, D.M. Loveless, S.L. Craig, Small-Molecule Dynamics and Mechanisms Underlying the Macroscopic Mechanical Properties of Coordinatively Cross-Linked Polymer Networks, Journal of the American Chemical Society 127(41) (2005) 14488-14496.
[21] D.M. Loveless, S.L. Jeon, S.L. Craig, Rational Control of Viscoelastic Properties in Multicomponent Associative Polymer Networks, Macromolecules 38(24) (2005) 10171-10177.
[22] G.G. Hammes, A.C. Park, Kinetic studies of hydrogen bonding. 1-Cyclohexyluracil and 9-ethyladenine, Journal of the American Chemical Society 90(15) (1968) 4151-4157.
[23] F. Herbst, W.H. Binder, Comparing solution and melt-state association of hydrogen bonds in supramolecular polymers, Polymer Chemistry 4(12) (2013) 3602-3609.
[24] T. Steiner, The Hydrogen Bond in the Solid State, Angewandte Chemie International Edition 41(1) (2002) 48-76.
[25] R.K. Bose, N. Hohlbein, S.J. Garcia, A.M. Schmidt, S. van der Zwaag, Relationship between the network dynamics, supramolecular relaxation time and healing kinetics of cobalt poly(butyl acrylate) ionomers, Polymer 69 (2015) 228-232.
[26] A. Embrechts, H. Schönherr, G.J. Vancso, Rupture Force of Single Supramolecular Bonds in Associative Polymers by AFM at Fixed Loading Rates, The Journal of Physical Chemistry B 112(25) (2008) 7359-7362.

[27] B.J. Gold, C.H. Hövelmann, N. Lühmann, N.K. Székely, W. Pyckhout-Hintzen, A. Wischnewski, D. Richter, Importance of Compact Random Walks for the Rheology of Transient Networks, ACS Macro Letters 6(2) (2017) 73-77.
[28] S. Hackelbusch, T. Rossow, P. van Assenbergh, S. Seiffert, Chain Dynamics in Supramolecular Polymer Networks, Macromolecules 46(15) (2013) 6273-6286.
[29] R.K. Bose, N. Hohlbein, S.J. Garcia, A.M. Schmidt, S. van der Zwaag, Connecting supramolecular bond lifetime and network mobility for scratch healing in poly(butyl acrylate) ionomers containing sodium, zinc and cobalt, Physical Chemistry Chemical Physics 17(3) (2015) 1697-1704.
[30] T. Aida, E.W. Meijer, S.I. Stupp, Functional Supramolecular Polymers, Science 335(6070) (2012) 813-817.
[31] C.L. Lewis, K. Stewart, M. Anthamatten, The Influence of Hydrogen Bonding Side-Groups on Viscoelastic Behavior of Linear and Network Polymers, Macromolecules 47(2) (2014) 729-740.
[32] K.E. Feldman, M.J. Kade, E.W. Meijer, C.J. Hawker, E.J. Kramer, Model Transient Networks from Strongly Hydrogen-Bonded Polymers, Macromolecules 42(22) (2009) 9072-9081.
[33] H. Goldansaz, D. Auhl, B. Goderis, Q. Voleppe, C.-A. Fustin, J.-F. Gohy, C. Bailly, E. van Ruymbeke, Transient Metallosupramolecular Networks Built from Entangled Melts of Poly(ethylene oxide), Macromolecules 48(11) (2015) 3746-3755.
[34] N.E. Botterhuis, D.J.M. van Beek, G.M.L. van Gemert, A.W. Bosman, R.P. Sijbesma, Self-assembly and morphology of polydimethylsiloxane supramolecular thermoplastic elastomers, Journal of Polymer Science Part A: Polymer Chemistry 46(12) (2008) 3877-3885.
[35] F. Herbst, K. Schröter, I. Gunkel, S. Gröger, T. Thurn-Albrecht, J. Balbach, W.H. Binder, Aggregation and Chain Dynamics in Supramolecular Polymers by Dynamic Rheology: Cluster Formation and Self-Aggregation, Macromolecules 43(23) (2010) 10006-10016.
[36] T. Yan, K. Schröter, F. Herbst, W.H. Binder, T. Thurn-Albrecht, Nanostructure and Rheology of Hydrogen-Bonding Telechelic Polymers in the Melt: From Micellar Liquids and Solids to Supramolecular Gels, Macromolecules 47(6) (2014) 2122-2130.
[37] S. Sivakova, D.A. Bohnsack, M.E. Mackay, P. Suwanmala, S.J. Rowan, Utilization of a Combination of Weak Hydrogen-Bonding Interactions and Phase Segregation to Yield Highly Thermosensitive Supramolecular Polymers, Journal of the American Chemical Society 127(51) (2005) 18202-18211.

[38] S. Chen, W.H. Binder, Dynamic Ordering and Phase Segregation in Hydrogen-Bonded Polymers, Accounts of Chemical Research 49(7) (2016) 1409-1420.
[39] H. Goldansaz, C.-A. Fustin, M. Wübbenhorst, E. van Ruymbeke, How Supramolecular Assemblies Control Dynamics of Associative Polymers: Toward a General Picture, Macromolecules 49(5) (2016) 1890-1902.
[40] F. Herbst, S. Seiffert, W.H. Binder, Dynamic supramolecular poly(isobutylene)s for self-healing materials, Polymer Chemistry 3(11) (2012) 3084-3092.
[41] X. Li, N. Mignard, M. Taha, F. Prochazka, J. Chen, S. Zhang, F. Becquart, Thermoreversible supramolecular networks from poly(trimethylene carbonate) synthesized by condensation with triuret and tetrauret, (2019).
[42] M.-C. Kuo, S.-M. Shau, J.-M. Su, R.-J. Jeng, T.-Y. Juang, S.A. Dai, Preparation of Supramolecular Extenders with Precise Chain Lengths via Iterative Synthesis and Their Applications in Polyurethane Elastomers, Macromolecules 45(13) (2012) 5358-5370.
[43] A. Pangon, G.P. Dillon, J. Runt, Influence of mixed soft segments on microphase separation of polyurea elastomers, Polymer 55(7) (2014) 1837-1844.
[44] A. Saralegi, A. Etxeberria, B. Fernández-d'Arlas, I. Mondragon, A. Eceiza, M.A. Corcuera, Effect of H12MDI isomer composition on mechanical and physico-chemical properties of polyurethanes based on amorphous and semicrystalline soft segments, Polymer Bulletin 70(8) (2013) 2193-2210.
[45] H.-Y. Tsi, C.-C. Chen, W.-C. Tsen, Y.-C. Shu, F.-S. Chuang, Characteristics of the phase transition of poly(siloxane/ether urethane) copolymers, Polymer Testing 30(1) (2011) 50-59.
[46] J.P. Sheth, A. Aneja, G.L. Wilkes, E. Yilgor, G.E. Atilla, I. Yilgor, F.L. Beyer, Influence of system variables on the morphological and dynamic mechanical behavior of polydimethylsiloxane based segmented polyurethane and polyurea copolymers: a comparative perspective, Polymer 45(20) (2004) 6919-6932.
[47] K.L. Kull, R.W. Bass, G. Craft, T. Julien, E. Marangon, C. Marrouat, J.P. Harmon, Synthesis and characterization of an ultra-soft poly(carbonate urethane), European Polymer Journal 71 (2015) 510-522.
[48] J. Dealy, D. Plazek, Time-Temperature Superposition-A Users Guide, Rheology Bulletin 78(2) (2009) 16.
[49] X. Callies, C. Fonteneau, C. Véchambre, S. Pensec, J.M. Chenal, L. Chazeau, L. Bouteiller, G. Ducouret, C. Creton, Linear rheology of bis-urea functionalized supramolecular poly(butylacrylate)s: Part I – weak stickers, Polymer 69 (2015) 233-240.

[50] X. Callies, C. Véchambre, C. Fonteneau, S. Pensec, J.M. Chenal, L. Chazeau, L. Bouteiller, G. Ducouret, C. Creton, Linear Rheology of Supramolecular Polymers Center-Functionalized with Strong Stickers, Macromolecules 48(19) (2015) 7320-7326.
[51] A.P. Pêgo, D.W. Grijpma, J. Feijen, Enhanced mechanical properties of 1,3-trimethylene carbonate polymers and networks, Polymer 44(21) (2003) 6495-6504.
[52] N. Roy, E. Buhler, J.-M. Lehn, The Tris-Urea Motif and Its Incorporation into Polydimethylsiloxane-Based Supramolecular Materials Presenting Self-Healing Features, Chemistry – A European Journal 19(27) (2013) 8814-8820.
[53] Y. Ni, F. Becquart, J. Chen, M. Taha, Polyurea–Urethane Supramolecular Thermo-Reversible Networks, Macromolecules 46(3) (2013) 1066-1074.

Chapter 5. Supramolecular poly(trimethylene carbonate) polycondensation by triuret : association constants determination in the melt state by rheology

Xiang Li[a,b,c], Jean-Charles Majesté[a,b,c], Nathalie Mignard[a,b,c], Jianding Chen[d], Shengmiao Zhang[d] and Frédéric Becquart[a,b,c,*]

[a]Université de Lyon, F-42023 Saint-Etienne, France

[b]CNRS, UMR 5223, Ingénierie des Matériaux Polymères, F-42023 Saint-Etienne, France

[c]Université Jean Monnet, F-42023 Saint-Etienne, France

[d]Laboratory of Advanced Materials Processing, East China University of Science and Technology, 200237 Shanghai, China

[*]Corresponding Author. E-mail: Frederic.Becquart@univ-st-etienne.fr

Abstract

In this work, the association dynamics of weak triuret hydrogen-bonding motifs (HBMs) in bifunctional linear supramolecular poly(trimethylene carbonate) (PTMC) was studied in the melt state. The material was heated at 150 °C firstly in order to remove the thermal history of hydrogen bonding followed by a rapid cooling process to study the associations and corresponding dynamics of triuret HBMs in this short cooling time. It was found that hydrogen bonds were formed between triuret HBMs as evidenced by the observed microdomains in SAXS. In rheological studies, the perfect applicability of time-temperature superposition (TTS) principle indicates the formation of only dimerization between triuret HBMs, leading to the linear chain extension. The association constants (K_a) of triuret HBMs at different temperatures were obtained ranging from 0.88 M^{-1} at 413 K to 3738.2 M^{-1} at 353 K. The activation energy of supramolecular polymer linear chain extension was measured to be 166.7 kJ/mol. After annealing for long time until the attainment of equilibrium, TTS principle failed for supramolecular polymer, induced by the formation of complex aggregates which act as transient physical crosslinkers in the material. This work presents an original method to calculate K_a and activation energy in solid state by rheology.

Keywords: supramolecular, hydrogen bond, dimer, association constant, rheology

1. Introduction

Since Jean-Marie Lehn et al.[1-3] proposed the concept of "supramolecular chemistry" in 1987, supramolecular polymer has become a rapidly developing interdisciplinary research field during the last several decades. Highly directional hydrogen bonding is the most widely used driving force to build supramolecular polymers among all noncovalent interactions[4,5]. Thanks to the development of multiple hydrogen-bonding motifs (HBMs)[6,7], the strength of hydrogen bonds is able to vary on a very large scale from weak and reversible interactions to strong and covalent-like bonds. Despite new evident opportunities are now offered to polymer materials science by applying supramolecular chemistry, understanding of these supramolecular polymer systems remain complex as well as their structure-properties relationships. Many challenges remain to be met to achieve a perfect control of this emerging chemistry. For example, as an illustration, the "supramolecular effect" in a polymer material is not necessarily only attributed to the own direct associations between HBMs. Indeed, other secondary interactions such as the formation of clusters may occur when a phase segregation is observed, driven by HBM groups[8-10]. For instance, Herbst et al.[8] studied in detail the chain dynamics of supramolecular polyisobutylenes (PIB) bearing to mono- and bifunctional chain ends with thymine (THY) and 2,6-diaminotriazine (DAT) moieties. Specific pairwise associations and more complex and stronger aggregates were evidenced by rheology. Later, Cortese et al.[11] synthesized telechelic supramolecular poly(propylene oxide) (PPO) by THY and DAT moieties as well. The material containing only weak self-complementary THY moieties ($K_{a,\ THY\text{-}THY}$ = 4.3 M^{-1}) was found to be a solid at room temperature due to the THY crystallization and a lamellar structuration. When both THY and DAT moieties were incorporated in PPO, though the THY-DAT interaction ($K_{a,\ Thy-DAT}$ = 890 M^{-1}) is stronger than THY-THY, a liquid was obtained in bulk at room temperature. The reason was attributed to the existence of DAT moieties which inhibited the microphase segregation by thymine-thymine interactions.

The strength of a reversible associated system, whether by single or multiple hydrogen-bonding motifs, can be evaluated indirectly by both its thermodynamic equilibrium and association constant (K_a). K_a is generally measured from titration experiments in solutions[12]. For example, ^{1}H NMR[13] is very commonly used with deuterated chloroform as a solvent. Besides, fluorescence[14], infrared[15], UV-vis[16], circular dichroism[17] or calorimetric measurements[18,19] were also used. If supramolecular polymers are elaborated directly in bulk, different aggregation modes of hydrogen-bonding interactions could occur comparatively to what generally happens in diluted solutions. As described previously, complex aggregates could

be formed by hydrogen bonds in bulk[8,9,11]. In this case, K_a measured by titration methods in solvents cannot be representative to describe the strength of associations in the neat materials. Herbst et al.[20] compared the associations of THY and DAT moieties in telechelic poly(n-butyl acrylate)s in solution and in the melt state. The association strength in solution followed the order of DAT–DAT < THY–THY << THY–DAT. While in the solid state, this order was redistributed with THY–THY < DAT–DAT ≤ THY–DAT, resulting from the polymer chains movement restriction in bulk and the small clusters formed by DAT–DAT interactions.

Considering this deficiency of using K_a measured in solution to evaluate the association strength, the determination of association energy or K_a in the solid state directly, have attracted the attention of researchers. For example, Cesteros et al.[21] succeeded to determine a relative low K_a (60 M^{-1}) between immiscible poly(vinylpyridine) and poly(vinyl alcohol-co-vinyl acetate) by FT-IR. Noro et al.[22] measured the hydrogen bonding energy between poly(2-vinylpyridine)-b-poly(ethyl acrylate)-b-poly(2-vinylpyridine) copolymer and poly(4-hydroxystyrene) crosslinker to be 13 kJ/mol by FT-IR as well. Recently, Staropoli et al.[23] measured the K_a between THY and DAT moieties which are attached to poly(butylene oxide) chains, to be 30 M^{-1} at 25 °C in the melt by means of small-angle neutron scattering (SANS). Krutyeva et al.[24] elaborated linear polymer chains by supramolecular associations between THY and DAT moieties which were located at telechelic poly(ethylene glycol) chain ends. They described their supramolecular polymerization by a polycondensation model associated to the Carothers theory and an isodesmic self-assembly. SANS was also used to detect the polymerization degree, namely aggregation numbers. Finally, a K_a of ~617 M^{-1} was calculated in the condensate state which is comparable to that measured in chloroform (1500 M^{-1}). From all these representative examples, the difference of supramolecular materials structuration in solution and in bulk is evident. Even if the direct interactions between HBMs always constitute the strong interactions, secondary interactions may greatly differ between the media by the presence of a solvent or not. Then, an association constant, which is determined in solution, by default, can only give an estimation of the association strength of the same supramolecular polymer applied in bulk.

In the present work, it is tried to determine association constants of a bulk thermoreversible supramolecular polymer. To this end, a bifunctional and linear supramolecular poly(trimethylene carbonate) (PTMC) bearing weak triuret HBMs is chosen as a model. This system is expected to follow a polycondensation model to get only linear chains in short cooling time from molten state. The material will be studied in the melt state within the thermoreversible

temperature range by morphological and rheological tests. WAXS and SAXS will be used first to show if hydrogen bonding between triuret HBMs can occur during fast cooling from the molten state to room temperature to finally lead to the own waited linear chain extension of the supramolecular polymer. The second step will be the determination of the material thermal stability at different temperatures in the melt state. Then, it could be highlighted if secondary chemical reactions or the dynamics of the system can affect the material in time. Consequently, the optimum conditions will be chosen to characterize the material in a state where only polycondensation can be considered to apply the corresponding theory and make K_a determinations. Thus, the supramolecular polymers molar masses will be directly connected with the thermodependent association constants. The applicability of time-temperature superposition (TTS) principle is expected to establish the relation between the average molar mass and the conversion by dimerization at different temperatures. The activation energy and association constants at different temperatures in bulk could be calculated. Finally, the measured K_a at different temperatures will be compared with the value determined previously at room temperature in $CDCl_3$ by ^1H NMR.

2. Experimental section

2.1 Materials

Glycerol (≥ 99.5%) and 1-pentanol (≥ 99%) were purchased from Sigma Aldrich and dried on 4 Å molecular sieves before use. Urea (98%), 4,4'-methylenebis(cyclohexyl isocyanate) (H_{12}MDI, 90%, mixture of isomers), dibutyltin dilaurate (DBTL, 95%) and N,N-dimethylformamide (DMF, anhydrous, 99.8%) were all purchased from Sigma Aldrich and used directly.

PTMC oligomers were synthesized by ring-opening polymerization with trimethylene carbonate (TMC) as monomer and 1,4-butanediol (BDO) as co-initiator. 1,5,7-triazabicyclo[4.4.0]dec-5-ene (TBD) was used as catalyst. The syntheses and characterizations were presented in detail in a recent study[25]. $PTMC_{2000}$ (number average molar mass $\overline{M}_n$ =2000 g/mol, $Đ_M$ = 1.60, T_g = -31.6 °C) oligomers were used in this work.

The strategy to synthesize the materials presented in this article is very similar to the one presented in another recent study[26]. The synthesis of the linear supramolecular polymer, called PTMC2U20, is shown in Scheme 1. In a three-neck flask, 0.201g 1,3-propanediol (2.639 mmol) and 10.556 g $PTMC_{2000}$ (5.278 mmol) were dissolved firstly in 60 mL anhydrous DMF at 80

°C under nitrogen atmosphere. After homogenization, 3.077 g 4,4'-methylenebis(cyclohexyl isocyanate) (H_{12}MDI) (10.556 mmol) and 0.010 g dibutyltin dilaurate catalyst (0.1 mol% of H_{12}MDI) were added. The reaction was kept until isocyanate carbonyl absorption (2260 cm^{-1}) became stable by FT-IR; In the second step, 0.317 g urea (5.300 mmol) and 1.539 g H_{12}MDI (5.278 mmol) were added after increasing the reaction temperature to 110 °C. When the absorption of isocyanate group at 2260 cm^{-1} became stable, 0.465 g 1-pentanol (5.300 mmol) was added and the reaction was stopped when the absorption at 2260 cm^{-1} disappeared in FT-IR spectrum. The obtained viscous solution was cooled to ambient temperature and precipitated with diethyl ether. The final material was dried at 80 °C for 24 hours at 0.2 mbar. (PTMC2U20: $\overline{M}_{n,\ NMR}$ = 6800 g/mol, T_g = -15.6 °C (heating rate at 10 °C/min by DSC), no melting endothermic peak was observed by DSC, TGA measured onset degradation temperature (5% of weight loss) is 228.7 °C, triuret HBM concentration [triuret] = 0.257 mmol/g).

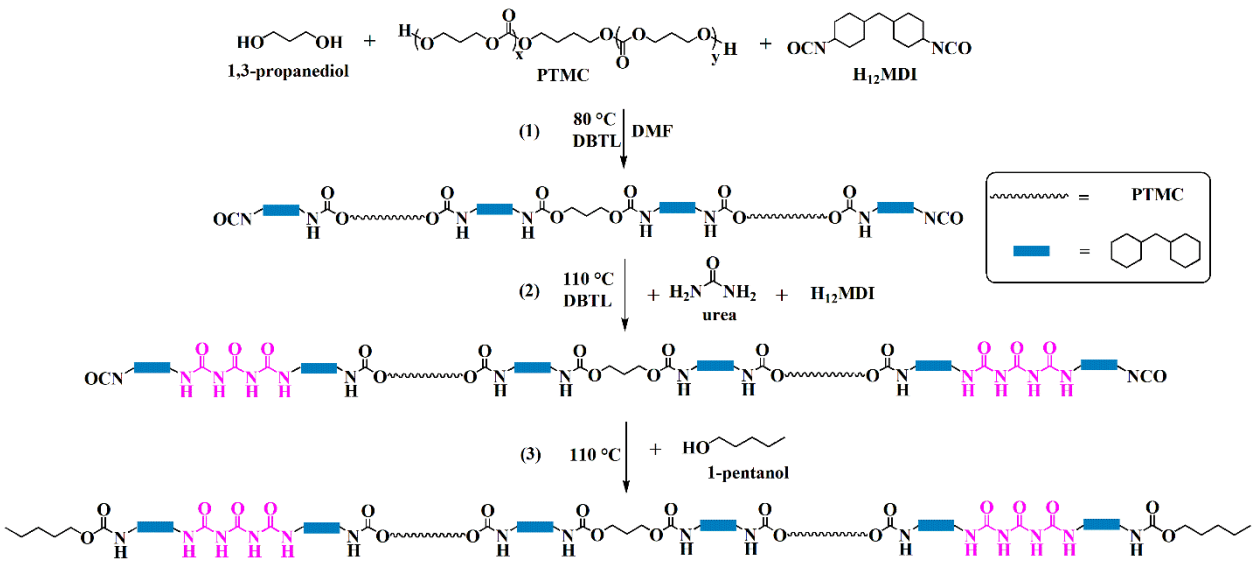

Scheme 1. Synthesis of supramolecular PTMC2U20 with triuret HBMs.

2.2 Characterization methods

2.2.1 Small-angle X-ray scattering (SAXS) and Wide-angle X-ray scattering (WAXS)

SAXS/WAXS experiments were carried out at the European Synchrotron Radiation Facility (ESRF) in Grenoble (France) on the BM2-D2AM beamline. The incident photon energy was set to 18 keV. Samples with a thickness between 800 and 1000 µm were directly placed in the beam path. The SAXS and the WAXS signals were detected simultaneously using two 2D XPad solid state detectors. For SAXS acquisition, the sample-to-detector distance was set at about

1.15 m and a beam stop with a diameter of 2 mm was used. For WAXS acquisition, the sample to detector distance was set at 10 cm. The q-calibration ($q = 4\pi\sin(\theta)/\lambda$; 2θ: scattering angle) was realized using a silver behenate powder standard for SAXS and a chromium(III) oxide (Cr_2O_3) powder standard for WAXS. The scattering contribution of air was subtracted from the scattering intensity of the samples. The image data treatments took into account the flat field response. The intensity was further normalized by the incident flux, and the sample thickness and I-calibration were realized with a glassy carbon standard. The scattering profiles of the intensity I as a function of the scattering vector q were obtained by azimuthally averaging the corrected images.

2.2.2 Oscillatory rheology tests

The rheology tests of supramolecular polymer were carried out with an ARES-G2 (TA Instruments) rheometer equipped with 8 mm diameter parallel plates. Strain sweep tests were performed firstly to obtain the linear viscoelastic region (LVR). Frequency sweep tests were performed at a constant strain of 1% in LVR with angular frequencies from 100 to 0.1 rad/s at different temperatures. A new sample was used for each temperature. Time-temperature superposition (TTS) principle was applied for the attempt to build master curves with frequency sweep data obtained at different temperatures with the reference temperature (T_{ref}) of 100 °C. Horizontal shift factors (a_T) were determined by the superposition of tan δ. Vertical shift factors (b_T) were obtained by the superposition of G' ($a_T\omega$, T) and G'' ($a_T\omega$, T) manually afterward.

2.3. Thermal treatments before characterizations

In order to remove the thermal history of triuret HBMs associations, PTMC2U20 was heated and molded between two steel plates under pressure at 150 °C for 10 min to get a thin film with the thickness around 1 mm. Afterwards, the film was cooled to room temperature rapidly (a few seconds). This preparation method was used for all the samples before following analyses or annealing by rheology.

3. Results and discussions

As clarified in a previous study[10], triuret HBMs are not only able to form pairwise hydrogen-bonding associations, more complex aggregates which may contain numerous HBMs can also be generated through the hydrogen bonding between different dimers. However, due to the high directionality of triuret HBMs, it is assumed that only dimers could be formed firstly during

short cooling in seconds because the formation of more complex aggregates always need longer time. In this case, PTMC2U20 was heated firstly at 150 °C in the molten state when complex hydrogen-bonding associates are broken and the material flows. Then, by the short cooling from 150 °C, a polycondensation mechanism is expected by the dimerization between triuret HBMs at the PTMC2U20 chain ends. Due to the low mobility of PTMC chains and HBM moieties at room temperature (T_g = -15.6 °C), it is assumed that the HBM moieties are "frozen". WAXS and SAXS experiments were conducted to verify if hydrogen bonding associations could be indeed limited, in particular the formation of complex aggregates during rapid cooling. From this systematical conditioning, the rheological properties of PTMC2U20 could be compared with short and long annealing to reveal if there are some evolutions of triuret HBMs association with time.

3.1 Morphology of linear supramolecular polymer

The morphology of PTMC2U20 with short cooling was studied firstly by both WAXS and SAXS. Though no crystalline structures were observed by DSC, it is still significant to confirm it by WAXS tests. A broad amorphous peak (Figure 1, A) was observed at the scattering vector q of 1.4 $Å^{-1}$. It suggests that the distribution of intersegment distance is random, namely, the material is indeed in an amorphous state[27]. Thereafter, SAXS spectrum was collected. As shown in Figure 1 (B), a single scattering peak at q around 0.05 $Å^{-1}$ is obvious, indicating a microphase-separated morphology. The scattering peak value is associated with the average interdomain distance (d-spacing), which can be calculated by

$$d = \frac{2\pi}{q^*} \qquad \text{Eq. (1)}$$

where q^* signifies the q value at the maximum intensity.

By this formula, the interdomain distance of PTMC2U20 was calculated to be 11.5 nm. According to a previous study[10], this d-spacing is certainly attributed to the microdomains formed by hydrogen bonding between triuret HBMs, at least by pairwise associations, even though the material was transformed from molten state to solid state rapidly. Due to the insufficient movement of chains and hydrogen-bonding moieties within short cooling time, the association between triuret HBMs are surely incomplete, making the material out of equilibrium.

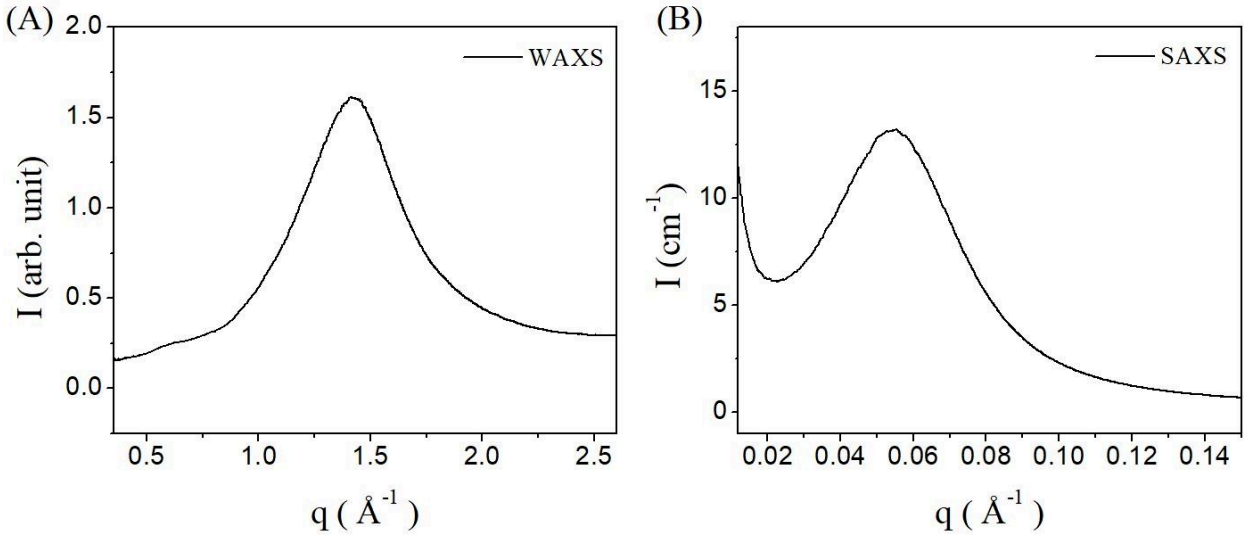

Figure 1. (A) WAXS spectrum of PTMC2U20. (B) SAXS spectrum of multiarm supramolecular structures (room temperature). I: intensity, q: scattering angle.

3.2 Thermal behavior of PTMC2U20 with time after a fast cooling

In order to highlight the evolution of triuret HBMs association with time, rheological properties of PTMC2U20 were studied by the storage and loss modulus evolutions at different temperatures. Then, the material was annealed at each chosen temperature between 25 h and 50 h. The time sweep curves at 80 °C, 100 °C, 120 °C and 140 °C are shown in Figure 2. It is clear to see that G' and G'' evolve with the annealing time and temperature. At 80 °C (Figure 2, A), both G' and G'' increase with time slowly before 20 hours, attributed to the association of hydrogen bonds. After 20 hours, the stable G' and G'' values suggest that the equilibrium is reached. However, the variation of modulus is different at other temperatures. At 100 °C (Figure 2, B), G' and G'' first increase during a relative short time, followed by an obvious decrease period. Later, G' and G'' increase again with the appearance of a crossover point. Finally, G' moduli get higher than G'' to keep the elastic solid state. Similar moduli tendency is also observed at 120 °C and 140 °C to get equilibrated states (Figure 2, C and D). All the decrease processes of modulus are possibly due to a secondary chemical reaction. Specifically, as already revealed in a recent study[25], the carbonate/carbonate exchange reactions between PTMC chains most probably account for this phenomenon.

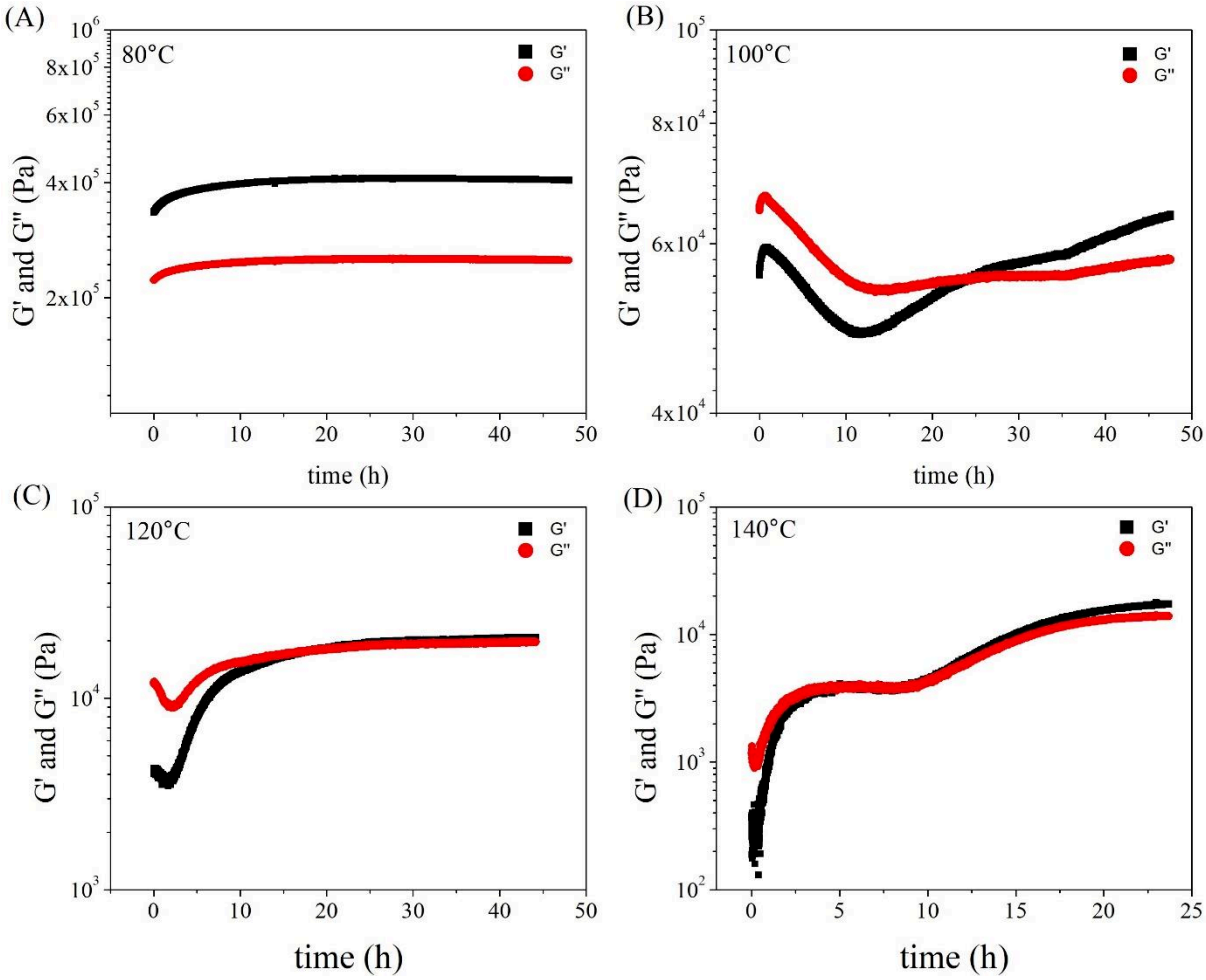

Figure 2. Time sweep tests of supramolecular polymer at different temperatures with (A) 80 °C, (B) 100 °C, (C) 120 °C and (D) 140 °C. frequency = 1 rad/s, strain = 1%.

In rheology, master curves are usually built to evidence viscoelastic properties over a large frequency range[28-31]. The master curve of PTMC2U20 at equilibrated state was tried to build with the frequency sweep curves obtained after the long time annealing at each temperature. The superposition of tan δ curves was conducted to obtain horizontal shift factors (a_T) at a reference temperature of 100 °C. As shown in Figure 3, superposing tan δ curves collected at different temperatures is obviously impossible, especially at high temperatures (120 °C and 140 °C). The breakdown of TTS principle could be an indication that triuret HBMs assemble to form complex aggregates, which have longer relaxation time than pairwise associations.

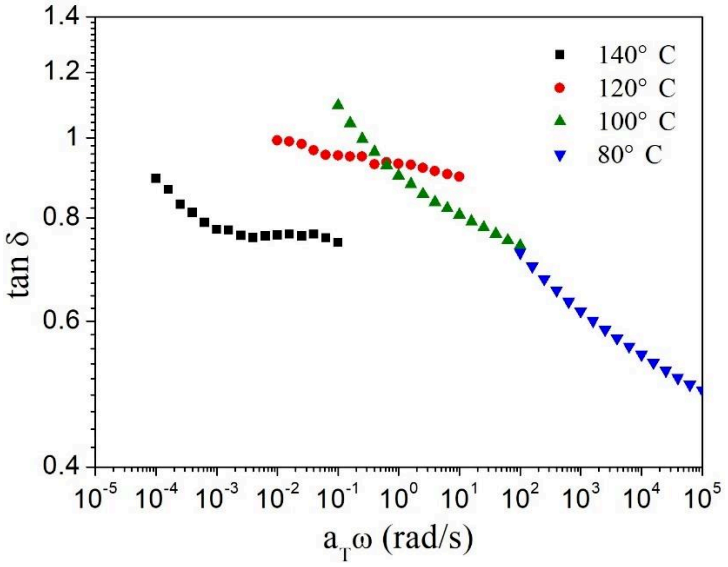

Figure 3. Attempts to superpose the tan δ curves for PTMC2U20. T_{ref} = 100 °C.

With the objective to determine the association constants of this supramolecular system bearing triuret HBMs, a polycondensation model can only be applied without other effects. It means that the material must be studied in conditions where no aggregates are formed. In consequence, for the rest of this study, the material will be analyzed by rheology in a "time window" as short as possible at the very beginning of chains association once the targeted temperature (80 °C, 100 °C, 120 °C and 140 °C) is reached from the cooling at 150°C.

3.3 Dynamics of supramolecular polymer with short cooling and quantitative characterizations by rheology

The master curve of PTMC2U20 with shorting cooling was tried to build with the same method as mentioned previously. The used frequency sweep curves were obtained from rheometer once the measurement temperatures were reached. As shown in Figure 4 (A), an almost perfect superposition of tan δ was obtained with the existence of hydrogen bonds evidenced by SAXS previously. Then, after applying these a_T to build master curves, it is impossible to perfectly superimpose G' and G'' versus frequency (Figure 4, B). However, once vertical shifts were applied, a nearly perfect master curve is attainable as shown in Figure 5. Abnormally, when the temperature is higher than T_{ref}, b_T is lower than 1, and vice versa. This phenomenon may come from the dilution effect of very short associated chains. According to a previous study[10], the triuret HBMs can associate to form complex aggregates which act as transient physical crosslinks and lead to the failure of TTS principle. Obviously, it is not equivalent to PTMC2U20 with short cooling time. These results seem to satisfy the assumption given previously that only pairwise associations are formed between triuret HBMs during

a rapid cooling process. In this case, the dimerization of triuret HBMs only results in the change of chain length but not the topological structures, namely, only linear chain extension happens. Furthermore, from the crossover point of b_TG' and b_TG'' (tan δ = 1) in the master curve, the rheological relaxation time τ_{rheo} was calculated to be 1.32 s by $\tau_{rheo} = 2\pi/\omega$[31-33]. The terminal zone in Figure 5 implies that there is a second relaxation in the material, which is most probably from the unbroken secondary effects at 150 °C. The characteristic time of this secondary relaxation process was measured to be 40000 s at 100 °C by the reciprocal of $a_T\omega$ where η" is the maximum in η"-$a_T\omega$ plot.

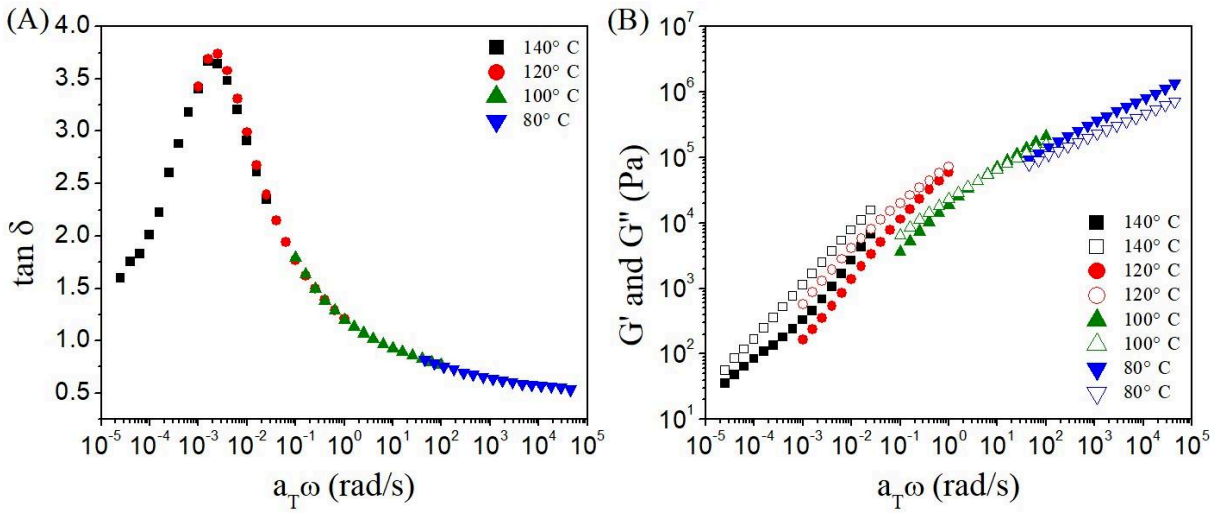

Figure 4. (A) Attempts to superpose tan δ curves for PTMC2U20. (B) G' and G'' of PTMC2U20 with only horizontal shifts (G': filled markers; G'': void markers). T_{ref} = 100 °C.

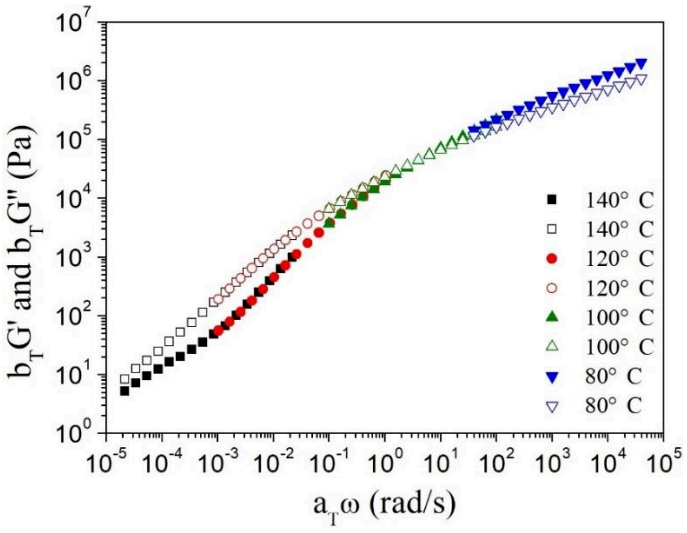

Figure 5. Master curve of PTMC2U20 (b_TG': filled markers; b_TG'': void markers). T_{ref} = 100 °C.

Due to the perfect fitness of TTS principle for PTMC2U20 with short cooling, a polycondensation theory can be applied to study the linear chain extension by triuret HBMs

dimerization. Since the chain structure is always linear, it is then assumed that the activation energy is constant for supramolecular polymer with different chain lengths.

According to Arrhenius equation, the real horizontal shift factors at temperature T can be defined as

$$a_{T\,real} = \frac{\eta_0(T)}{\eta_0(T_0)} = \frac{A(\overline{M}_T)\exp(\frac{E_a}{RT})}{A(\overline{M}_{T_0})\exp(\frac{E_a}{RT_0})} = \frac{A(\overline{M}_T)}{A(\overline{M}_{T_0})}\exp(\frac{E_a}{R}\times(\frac{1}{T}-\frac{1}{T_0})) \quad \text{Eq. (2)}$$

where T_0 is the reference temperature at 100 °C, E_a is the activation energy of the supramolecular polymer, R is the universal gas constant, $A(M)$ is the pre-exponential factor and M is the molar mass.

If the change of chain length has no contribution to the value of $A(M)$ and the activation energy of supramolecular polymer equals to PTMC, the expected horizontal shift factor $a_{T\,exp}$ will be described by

$$a_{T\,\exp} = \exp(\frac{E_{a\,PTMC}}{R}\times(\frac{1}{T}-\frac{1}{T_0})) \qquad \text{Eq. (3)}$$

where $E_{a\,PTMC}$ is the PTMC activation energy of 59.8 kJ/mol as calculated in a previous study[10].

In this case, the $a_{T\,exp}$–1/T and $a_{T\,real}$–1/T curves ($a_{T\,real}$ was obtained by master curve) of PTMC2U20 are compared in Figure 6. It is obvious that the expected and real horizontal shift factors are deviated. It then denies our assumption shown previously and $A(M)$ is indeed related to the chain length, namely molar mass.

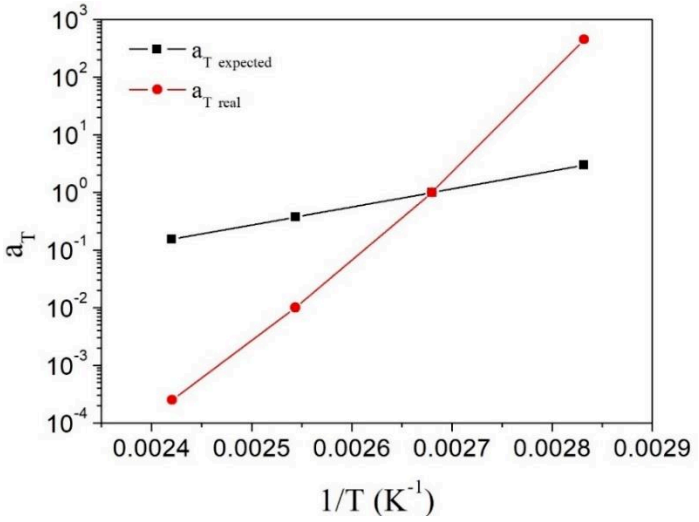

Figure 6. $a_{T\,exp}$–1/T and $a_{T\,real}$–1/T curves of PTMC2U20.

Then, according to Eq. (2) and Eq. (3), the ratio between real and expected horizontal shift factors are used to describe the change of molar mass with temperature by

$$\frac{a_{T\ real}}{a_{T\ exp}} = \frac{A(\overline{M}_T)}{A(\overline{M}_{T_0})} = \left(\frac{\overline{M}_T}{\overline{M}_{T_0}}\right)^{\alpha} \qquad \text{Eq. (4)}$$

Because the molar masses of all supramolecular chains are higher than the critical entanglement values for PTMC (M_e = 2700 g/mol[34]), the coefficient α equals to 3.4.

Then, the relation between M_T and M_{T0} is defined as

$$\frac{\overline{M}_T}{\overline{M}_{T_0}} = \left(\frac{a_{T\,real}}{a_{T\,\exp}}\right)^{\frac{1}{3.4}} \qquad \text{Eq. (5)}$$

If supramolecular polymer molar mass at T_0 can be obtained, its molar mass at temperature T will also be calculated by Eq. (5).

To gain the supramolecular polymer molar mass at T_0, it must be assumed firstly that a pure PTMC chain and a supramolecular PTMC chain have the same viscosity if their molecular weights are identical. In this case, the molar mass of supramolecular polymer poly(PTMC2U20) at T_0 ($\overline{M}_{T0}$) can be calculated by the molar mass and viscosity (at T_0) of pure PTMC.

$\overline{DP}_n$ of the linear PTMC2U20 chains at different temperatures is obtained according to Carothers equation with

$$\overline{DP}_{n,T} = \frac{1}{1-p_T} = \frac{\overline{M}_{n,T}}{\overline{M}_0} \qquad \text{Eq. (6)}$$

where $\overline{M}_0$ is the molar mass of unassociated PTMC2U20 chain, p_T is the conversion by dimerization at different temperature.

Moreover, in the linear chain extension, a statistical (Flory) molecular weight distribution is expected with $\overline{M}_w/\overline{M}_n = 2$. After applying this formula to Eq. (6), p_T is expressed by

$$p_T = 1 - \frac{2\overline{M}_0}{\overline{M}_{w,T}} \qquad \text{Eq. (7)}$$

The conversions p were calculated from the molecular weights of linear structures generated by the partial association of the HBMs by dimerization. To correlate a p value to a K_a of these HBMs, at each temperature, the equilibrium associated to the constant is here considered as corresponding to the association between HBM by dimerization independently of the location of their association in the formed poly(PTMC2U20) chain. Generally, such polymerization by supramolecular chemistry are considered by isodesmic or cooperative nucleated self-assembly mechanisms[35]. Their differentiation cannot be distinguished obviously without fundamental characterizations like molecular weight distributions at several stages of the polymerization. Systematically for such mechanisms, the considered species to express an association constant, are the polymer chain concentrations[35]. To simplify these theoretical approaches, we only consider the own HBM in the expression of K_a toward the equilibrium. As given by Eq. (8), A is the free associable HBM at the PTMC2U20 or a growing poly(PTMC2U20) chain end, A-A is a newly formed chain by the dimerization of HBMs which link two PTMC2U20 or poly(PTMC2U20) chain ends respectively. By this simple model, the reactivity of the HBM is considered as constant wherever its location, in a free PTMC2U20 chain or in a newly formed poly(PTMC2U20) chain whatever its polymerization degree. The association constant can then be expressed (Eq. 9) simply with $[A]_0$ and p, where p can be determined by the rheological analyses (Eq. (8)) and $[A]_0$ is the initial HBM concentration in the system.

$$A \quad + \quad A \quad \rightleftarrows \quad A-A \qquad \text{Eq. (8)}$$

$$K_a = \frac{[A-A]}{[A]\times[A]} = \frac{1}{[A]_0} \times \frac{p}{(1-p)^2} \qquad \text{Eq. (9)}$$

If the triuret HBM concentration [triuret] and the density of PTMC2U20 (ρ = 1.3 g/cm^3) are introduced, then the corresponding association constant K_a of the triuret HBMs at different temperatures can be determined by a polycondensation theory with Eq. (10):

$$K_{a,T} = \frac{\rho\times[triuret]\times p_T}{\left(\rho\times[triuret]\times(1-p_T)\right)^2} = \frac{p_T}{\rho\times[triuret]\times(1-p_T)^2} \qquad \text{Eq. (10)}$$

All the parameters in the quantitative characterizations of PTMC2U20 with short cooling are shown in Table 1. It is clear that at 140 °C (413 K), the $\overline{DP}_n$ is only 1.2 with a low p value of 0.191. In this case, only short chains are obtained. However, at 80 °C (353 K), the $\overline{DP}_n$ is much higher at 35.8 and with 97.2% of triuret HBMs participated in the dimerization. As compared to the K_a measured at 298 K in $CDCl_3$ by ^{1}H NMR (K_a = 0.32 M^{-1}), the K_a values calculated by rheology in bulk varies from 0.88 M^{-1} at 413 K to 3738.2 M^{-1} at 353 K. It seems obvious that the K_a measured in bulk by rheology is much higher than that measured in $CDCl_3$ by ^{1}H NMR at the same temperature.

Table 1. The parameters in the quantitative characterizations of PTMC2U20 with short cooling.

Temperature (K)	$a_{T\ real}$	$a_{T\ exp}$	$a_{T\ real}/a_{T\ exp}$	$\overline{M}_T/\overline{M}_{T0}$	$\overline{M}_w$ (g/mol)	$\overline{DP}_n$	p	K_a (M^{-1})
413	0.00025	0.155	0.00161	0.151	16819	1.2	0.191	0.88
393	0.01	0.375	0.0266	0.344	38363	2.8	0.645	15.37
373	1	1	1	1	111420	8.2	0.878	176.37
353	450	2.978	151.13	4.375	487473	35.8	0.972	3738.2

According to Arrhenius law, the activation energy of supramolecular linear chain extension is defined as

$$K_a = A\exp\left(\frac{E_a}{RT}\right) \qquad \text{Eq. (11)}$$

As shown in Figure 7, after the linear fitting of lnK_a-1/T, the E_a was calculated to be 166.7 kJ/mol. In a previous study[10], it was presented that E_a of triuret HBMs aggregates in multiarm supramolecular polymers varied from 297.0 kJ/mol to 511.9 kJ/mol, depending on their

functionalities and HBM concentrations. Thus, the much lower E_a obtained in PTMC2U20 indicates the much weaker associations of HBMs dimers than their complex aggregates.

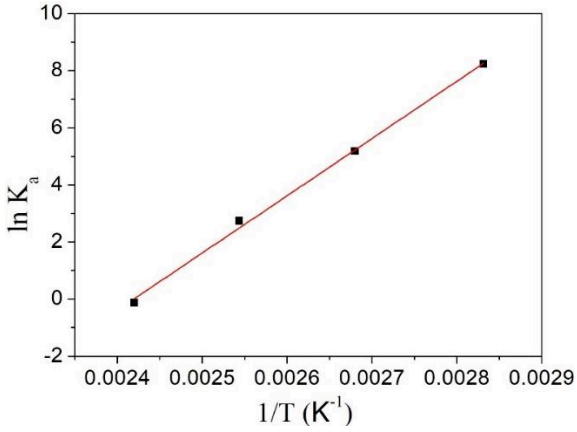

Figure 7. Ln K_a-1000/T of TMC2U20 (markers: calculated data; line: curve-fitting result).

3.4 Physical description of PTMC2U20 evolutions at different times and temperatures

After comparing the dynamic properties with short and long annealing, the association of triuret HBMs in PTMC2U20 with time can be proposed. A schematic structure of PTMC2U20 at different temperatures and times is shown in Figure 8. At 150 °C, almost all the triuret HBMs are dissociated, leading to the molten state for the material. After cooling the material from 150 °C to 80 °C in seconds, the isolated triuret HBMs tend to dimerize in this short cooling time, inducing the formation of only linear chain extensions. With prolonged time, these dimers can assemble gradually to form complex aggregates which have longer relaxation time than dimers. These complex aggregates act as transient physical crosslinks in the material. The dynamics of these aggregates have already discussed in a previous study[10].

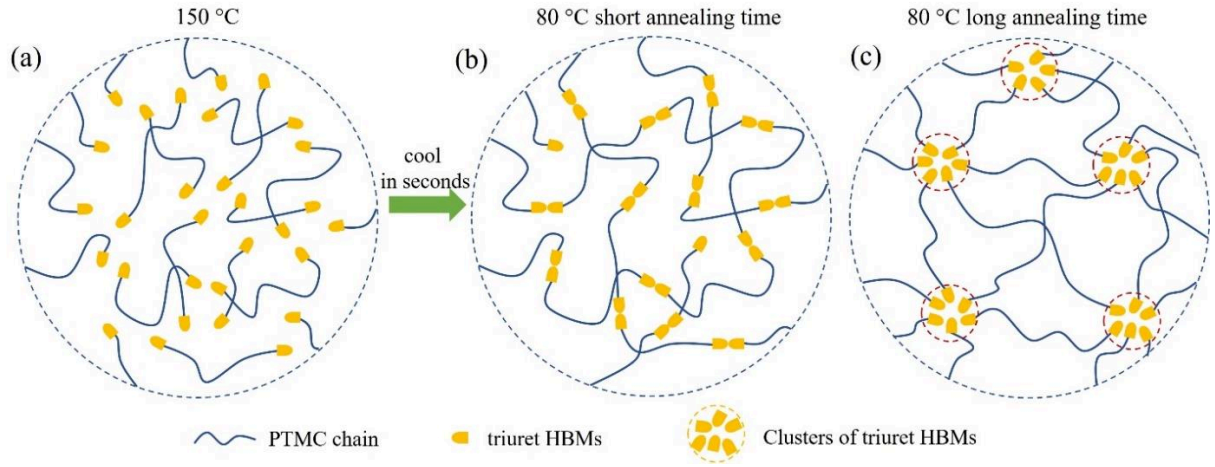

Figure 8. Schematic structures of PTMC2U20 (a) heated at 150 °C, (b) cooled at 80 °C in short time and (c) annealed at 80 °C for long time.

4. Conclusion

The association dynamics of triuret HBMs in bifunctional linear supramolecular PTMC was studied through the comparison of rheological properties at short cooling and long annealing time. When the material was heated to 150 °C, almost all the hydrogen bonds were dissociated. After cooling this material from 150 °C to room temperature in seconds, triuret HBMs tend to dimerize and lead to the linear chain extension. Their rheological properties fit with TTS principle and allow the quantitative characterizations by rheology. K_a was measured to be 3738.2 M^{-1} and 0.88 M^{-1} at 353 K and 413 K respectively, much higher than that measured in $CDCl_3$ at 298 K (K_a = 0.32 M^{-1}). The activation energy was calculated to be 166.7 kJ/mol. After annealing the material for long time to get equilibrium state at each temperature, both G' and G'' are increased, attributing to the association of triuret HBMs to form complex aggregates which can act as transient physical network crosslinkers in supramolecular polymer. Besides the revealing of triuret HBMs association dynamics in supramolecular polymer, this work also offers the viability to calculate K_a and activation energy of supramolecular interactions in bulk by rheology.

Acknowledgments

The authors thank the financial support from China Scholarship Council (CSC). This work benefited from the international cooperation between Université Jean Monnet Saint-Etienne (France) and East China University of Science and Technology (China). The authors also acknowledge Guillaume Sudre (IMP, Lyon, France) and Isabelle Morfin (LIPhy, Grenoble, France) for their help with X-ray scattering measurements. The WOS (WAXS detector) was funded by the French National Research Agency (ANR) under the "Investissements d'avenir" program with the grant number: ANR-11-EQPX-0010.

References

[1] J.-M. Lehn, Supramolecular Chemistry—Scope and Perspectives Molecules, Supermolecules, and Molecular Devices (Nobel Lecture), Angewandte Chemie International Edition in English 27(1) (1988) 89-112.

[2] D.J. Cram, The Design of Molecular Hosts, Guests, and Their Complexes (Nobel Lecture), Angewandte Chemie International Edition in English 27(8) (1988) 1009-1020.

[3] C.J. Pedersen, The Discovery of Crown Ethers (Noble Lecture), Angewandte Chemie International Edition in English 27(8) (1988) 1021-1027.

[4] L. Yang, X. Tan, Z. Wang, X. Zhang, Supramolecular Polymers: Historical Development, Preparation, Characterization, and Functions, Chemical Reviews 115(15) (2015) 7196-7239.

[5] L. Brunsveld, B.J.B. Folmer, E.W. Meijer, R.P. Sijbesma, Supramolecular Polymers, Chemical reviews 101(12) (2001) 4071-4098.

[6] D.C. Sherrington, K.A. Taskinen, Self-assembly in synthetic macromolecular systems multiple hydrogen bonding interactions, Chemical Society Reviews 30(2) (2001) 83-93.

[7] S.C. Zimmerman, P.S. Corbin, Heteroaromatic Modules for Self-Assembly Using Multiple Hydrogen Bonds, in: Molecular Self-Assembly Organic Versus Inorganic Approaches, M. Fuiita (Ed.), Springer Berlin Heidelberg, Berlin, Heidelberg, 2000, Vol., pp. 63-94.

[8] F. Herbst, K. Schröter, I. Gunkel, S. Gröger, T. Thurn-Albrecht, J. Balbach, W.H. Binder, Aggregation and Chain Dynamics in Supramolecular Polymers by Dynamic Rheology: Cluster Formation and Self-Aggregation, Macromolecules 43(23) (2010) 10006-10016.

[9] S. Chen, W.H. Binder, Dynamic Ordering and Phase Segregation in Hydrogen-Bonded Polymers, Accounts of Chemical Research 49(7) (2016) 1409-1420.

[10] X. Li, N. Mignard, J.-C. Majesté, G. Sudre, J. Chen, S. Zhang, F. Becquart, Microphase Separation Morphology and Chain Dynamics of PTMC-Based Hydrogen-bonded Supramolecular Networks in the Melt State, (2019).

[11] J. Cortese, C. Soulié-Ziakovic, S. Tencé-Girault, L. Leibler, Suppression of Mesoscopic Order by Complementary Interactions in Supramolecular Polymers, Journal of the American Chemical Society 134(8) (2012) 3671-3674.

[12] P. Thordarson, Determining association constants from titration experiments in supramolecular chemistry, Chemical Society Reviews 40(3) (2011) 1305-1323.

[13] L. Fielding, Determination of Association Constants (Ka) from Solution NMR Data, Tetrahedron 56(34) (2000) 6151-6170.

[14] K. Hirose, Quantitative Analysis of Binding Properties, in: Analytical Methods in Supramolecular Chemistry, C.A. Schalley (Ed.), Wiley-VCH, Weinheim, 2012, Vol., pp. 27-66.
[15] N.D. Coggeshall, E.L. Saier, Infrared Absorption Study of Hydrogen Bonding Equilibria, Journal of the American Chemical Society 73(11) (1951) 5414-5418.
[16] B.A. Blight, C.A. Hunter, D.A. Leigh, H. McNab, P.I.T. Thomson, An AAAA–DDDD quadruple hydrogen-bond array, Nature Chemistry 3(3) (2011) 244-248.
[17] T.J. Gilligan, G. Schwarz, The self-association of adenosine-5'-triphosphate studied by circular dichroism at low ionic strengths, Biophysical Chemistry 4(1) (1976) 55-63.
[18] A. Arnaud, L. Bouteiller, Isothermal Titration Calorimetry of Supramolecular Polymers, Langmuir 20(16) (2004) 6858-6863.
[19] P.R. Stoesser, S.J. Gill, Calorimetric study of self-association of 6-methyl-purine in water, The Journal of Physical Chemistry 71(3) (1967) 564-567.
[20] F. Herbst, W.H. Binder, Comparing solution and melt-state association of hydrogen bonds in supramolecular polymers, Polymer Chemistry 4(12) (2013) 3602-3609.
[21] L.C. Cesteros, J.R. Isasi, I. Katime, Hydrogen bonding in poly(4-vinylpyridine)/poly(vinyl acetate-co-vinyl alcohol) blends. An infrared study, Macromolecules 26(26) (1993) 7256-7262.
[22] A. Noro, Y. Matsushita, T.P. Lodge, Thermoreversible Supramacromolecular Ion Gels via Hydrogen Bonding, Macromolecules 41(15) (2008) 5839-5844.
[23] M. Staropoli, A. Raba, C.H. Hövelmann, M. Krutyeva, J. Allgaier, M.-S. Appavou, U. Keiderling, F.J. Stadler, W. Pyckhout-Hintzen, A. Wischnewski, D. Richter, Hydrogen Bonding in a Reversible Comb Polymer Architecture: A Microscopic and Macroscopic Investigation, Macromolecules 49(15) (2016) 5692-5703.
[24] M. Krutyeva, A.R. Brás, W. Antonius, C.H. Hövelmann, A.S. Poulos, J. Allgaier, A. Radulescu, P. Lindner, W. Pyckhout-Hintzen, A. Wischnewski, D. Richter, Association Behavior, Diffusion, and Viscosity of End-Functionalized Supramolecular Poly(ethylene glycol) in the Melt State, Macromolecules 48(24) (2015) 8933-8946.
[25] X. Li, N. Mignard, M. Taha, C. Fernandez-de-Alba, J. Chen, S. Zhang, F. Becquart, Synthesis of poly(trimethylene carbonate) (PTMC) oligomers by ring-opening polymerization in bulk (submitted), (2019).
[26] X. Li, N. Mignard, M. Taha, F. Prochazka, J. Chen, S. Zhang, F. Becquart, Thermoreversible supramolecular networks from poly(trimethylene carbonate) synthesized by condensation with triuret and tetrauret, (2019).

[27] A. Pangon, G.P. Dillon, J. Runt, Influence of mixed soft segments on microphase separation of polyurea elastomers, Polymer 55(7) (2014) 1837-1844.
[28] S. Seiffert, J. Sprakel, Physical chemistry of supramolecular polymer networks, Chemical Society Reviews 41(2) (2012) 909-930.
[29] X. Callies, C. Fonteneau, C. Véchambre, S. Pensec, J.M. Chenal, L. Chazeau, L. Bouteiller, G. Ducouret, C. Creton, Linear rheology of bis-urea functionalized supramolecular poly(butylacrylate)s: Part I – weak stickers, Polymer 69 (2015) 233-240.
[30] X. Callies, C. Véchambre, C. Fonteneau, S. Pensec, J.M. Chenal, L. Chazeau, L. Bouteiller, G. Ducouret, C. Creton, Linear Rheology of Supramolecular Polymers Center-Functionalized with Strong Stickers, Macromolecules 48(19) (2015) 7320-7326.
[31] S. Chen, D. Döhler, W.H. Binder, Rheology of hydrogen-bonded dendritic supramolecular polymer networks in the melt state, Polymer 107 (2016) 466-473.
[32] R.K. Bose, N. Hohlbein, S.J. Garcia, A.M. Schmidt, S. van der Zwaag, Relationship between the network dynamics, supramolecular relaxation time and healing kinetics of cobalt poly(butyl acrylate) ionomers, Polymer 69 (2015) 228-232.
[33] F. Herbst, S. Seiffert, W.H. Binder, Dynamic supramolecular poly(isobutylene)s for self-healing materials, Polymer Chemistry 3(11) (2012) 3084-3092.
[34] A.P. Pêgo, D.W. Grijpma, J. Feijen, Enhanced mechanical properties of 1,3-trimethylene carbonate polymers and networks, Polymer 44(21) (2003) 6495-6504.
[35] M.M.J. Smulders, M.M.L. Nieuwenhuizen, T.F.A. de Greef, P. van der Schoot, A.P.H.J. Schenning, E.W. Meijer, How to Distinguish Isodesmic from Cooperative Supramolecular Polymerisation, Chemistry – A European Journal 16(1) (2010) 362-367.

Chapter 6. Thermoreversible poly(trimethylene carbonate) based networks by Diels-Alder reaction

Xiang Li[a,b,c], Frédéric Becquart[a,b,c], Mohamed Taha[a,b,c], Jianding Chen[d], Shengmiao Zhang[d] and Nathalie Mignard[a,b,c*]

[a]Université de Lyon, F-42023 Saint-Etienne, France

[b]CNRS, UMR 5223, Ingénierie des Matériaux Polymères, F-42023 Saint-Etienne, France

[c]Université Jean Monnet, F-42023 Saint-Etienne, France

[d]Laboratory of Advanced Materials Processing, East China University of Science and Technology, 200237 Shanghai, China

[*]Corresponding Author: nathalie.mignard@univ-st-etienne.fr

Abstract

In this work, thermoreversible poly(trimethylene carbonate) (PTMC) based networks with different densities were obtained by Diels-Alder reaction between furan-functionalized PTMC and a bismaleimide. Furan-grafted PTMC with various functionalities determined by ^{1}H-NMR analyses were firstly prepared from telechelic PTMC oligomer, glycerol, 4,4'-methylenebis(cyclohexyl isocyanate) (H_{12}MDI) and furfuryl alcohol. Thermoreversible networks were obtained and then characterized by their swelling ratios, FT-IR, DSC, TGA, tensile tests and rheological analyses. Creep tests highlighted perfect network structures for all materials and the effect of furan functionality on network density and properties was evidenced. The thermoreversibility was proved by several methods and the disruption of networks was found to occur in high temperature ranges from 130 to 160 °C by DSC based on their density.

Keywords: PTMC, Diels-Alder reaction, thermoreversibility, networks

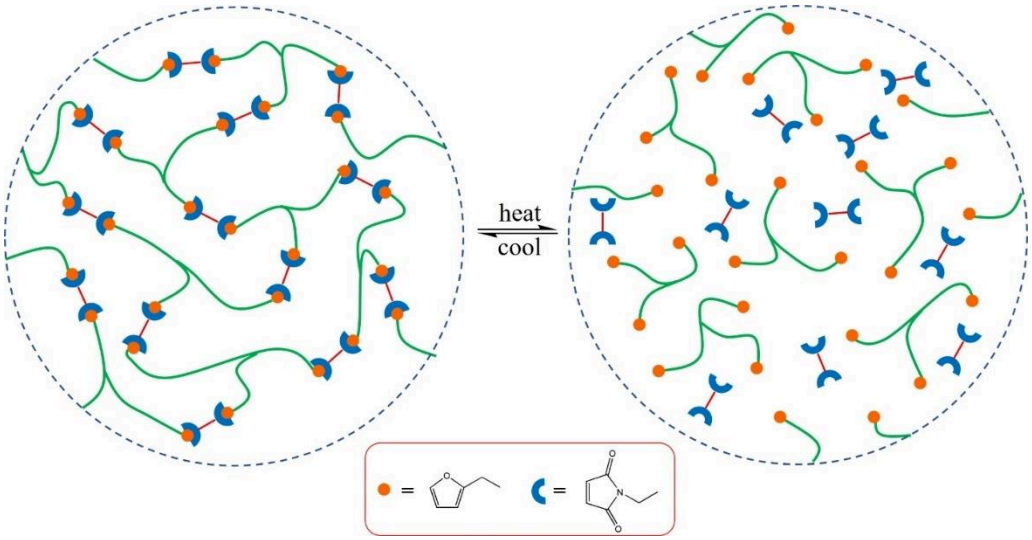

1. Introduction

Click chemistry has attracted great attention since Sharpless et al.[1] fully described this concept in 2001. Thanks to its benefits, including high yields, simple reaction conditions, high selectivity and fast reaction times[2], the applications of click chemistry have been extended in almost all fields, especially in bioconjugation, materials science and drug discovery[3]. Diels-Alder (DA) cycloaddition reaction, which occurs between a diene and a dienophile ([4+2] cycloaddition)[4], is one of the most attractive members of click chemistry not only because of its thermoreversibility but also because of the non-necessity of additives such as catalysts and the absence of by-products[5,6]. Due to this thermoreversibility, the formed covalent links, which can be broken with increasing temperature, can lead to the design of network structures while preserving the possibility of a further melt-processing. Therefore, these structures can be engineered with special properties such as self-healing[7-10] and shape memory[11,12]. Among all diene/dienophile couplings, furan/maleimide[13-15] is the most widely investigated one due to its relatively mild dissociation temperature, around 100 °C, providing a potential functionalization method, especially for polymers with low thermal degradation temperatures. Moreover, the renewable resources of furan derivatives also satisfy the more and more serious environmentally friendly requirements[13].

Over the last decades, biodegradable materials such as poly(ε-caprolactone) (PCL), polylactic acid (PLA) and polyglycolic acid (PGA) have gained much attention in the medical and medically-related domains[16]. However, the intrinsic defects of these materials usually limit their further applications. In this case, combining these biomaterials with thermoreversible Diels-Alder reactions has been an effective strategy not only to overcome their drawbacks such

as poor mechanical properties, but also to endow them with special properties such as shape memory or mendability. For example, Raquez et al.[17] reported the crosslinking of PCL by Diels-Alder reactions to obtain semicrystalline networks with shape memory properties. Defize et al.[18,19] obtained 4-arm star-shaped recyclable shape-memory PCL by the mixture of tetra-furan and tetra-maleimide functionalized PCLs with the most appropriate temperatures for DA and retro-Diels-Alder (rDA) reactions at 65 and 125 °C respectively. Thanks to DA reactions, Rivero et al.[20] synthesized PCL-based polyurethanes with healing capability at mild temperature conditions (50 °C). Furthermore, in our former studies, thermoreversible PLA[21] and PGA[22] based networks which could crosslink/de-crosslink via DA/rDA reactions over several cycles were also achieved.

Among all biomaterials, poly(trimethylene carbonate) (PTMC) is an extremely promising biodegradable and biocompatible biomaterial which is already used in scaffolds, drug delivery systems and antimicrobials[23,24]. However, considering its relatively poor dimensional stability and low tensile mechanical properties, functionalization or crosslinking is crucial in order to extend its applications[23]. Only a few and recent studies have been published about the use of DA chemistry with polycarbonates[25-27]. In 2009, Hu et al.[27] synthesized furan-grafted polycarbonates from CO_2 and furfuryl glycidyl ether (FGE) and the included DA reaction was used for the protection of furan functions only. Similarly, Hilf et al.[25] synthesized aliphatic polycarbonates from glycidyl methyl ether, CO_2 and FGE. Through the reaction between furfuryl side chains and maleimide derivatives, reversible networks were formed. Thongsomboon et al.[26] synthesized a biodegradable polycarbonate film bearing furan and maleimide side chains. Interestingly, due to the thermosensitivity of the DA reaction, this film could be used for nanoimprinting. However, to the best of our knowledge, no work has been published yet on the study of PTMC crosslinking/decrosslinking by DA and on the effect of network density on its reversibility.

This study reports the syntheses of PTMC-based thermoreversible networks with different densities. Firstly, furan-functionalized PTMC precursors (PTMC-F) with several functionalities will be synthesized in two steps from hydroxy telechelic PTMC oligomers through the simple reaction between hydroxyl and isocyanate groups. Then, small molecular bismaleimide, which acts as crosslinker, will be used to build the network structures. Physicochemical, thermal, rheological and tensile mechanical properties of the networks will be investigated as well as their thermoreversibility as a function of temperature. The influence of materials density, which is directly related to the furan functionality of PTMC-F, on the thermoreversibility property

will also be discussed. This work provides the first study regarding the combination of DA reactions and PTMC oligomers to produce thermoreversible crosslinked structures with tunable network density.

2. Experimental section

2.1 Materials

Trimethylene carbonate (TMC, Boehringer, Germany) was dissolved and refluxed in THF with CaH_2 as desiccant for two days and recrystallized twice before use. 1,4-butanediol (BDO) (≥99%), 1,5,7-triazabicyclo[4.4.0]dec-5-ene (TBD) (98%), furfuryl alcohol (FAL, 98%), glycerol (99.5%), 4,4'-methylenebis(cyclohexyl isocyanate) (H_{12}MDI, mixture of isomers, 90%), dibutyltin dilaurate (DBTL, 95%), maleic anhydride, acetic anhydride, nickel acetate, triethylamine, 1,6-diaminohexane and N,N-dimethylformamide (DMF, anhydrous, 99.8%) were all purchased from Sigma Aldrich. DMF and glycerol were dehydrated by 4Å molecular sieves for 48 h before use and all other reactants were employed as received.

2.2 Characterization techniques

FT-IR analyses

Fourier-transform infrared spectroscopy (FT-IR) spectra were recorded with a Nicolet Nexus FT-IR spectrometer using the ATR technique from 4000 cm^{-1} to 650 cm^{-1}. 64 scans were collected with a bandwidth set at 4 cm^{-1} at room temperature.

^{1}H NMR analyses

^{1}H NMR spectra were recorded by a Bruker Advance III spectrometer working at 400 MHz with a 5 mm multinuclear broad band probe (BBFO+) with z-gradient coil at 298 K with 128 scans. The samples (20-30 mg) were dissolved in DMSO-d_6 (0.7 mL). Tetramethylsilane (TMS) was used as reference with a chemical shift (δ) of 0 ppm.

Size-Exclusion Chromatography (SEC)

Number average molecular weight ($\overline{M}_n$) and molar-mass dispersity ($Đ_M = \overline{M}_n/\overline{M}_w$) of PTMC-F precursors were determined by size exclusion chromatography (SEC) equipped with a Waters 515 HPLC pump, a Waters 717 plus autosampler system, three columns of Shodex KF-801, KF-0802 and KF-804 and three detectors (a WATERS 2414 refractive index detector, a

WYATT ViscoStar viscometer and a WYATT miniDAWN TREOS multi-angle light scattering detector). Tetrahydrofuran (THF, Biosolve, GPC grade) was used as mobile phase with an elution rate of 1 mL/min. The refractive index increment *dn/dC* was calculated directly from the signal. Narrow dispersity polystyrene standards were used for universal calibration and all tests were conducted at 30 °C.

Thermal analysis

Differential scanning calorimetry (DSC) tests were performed by a TA Q10 Differential Scanning Calorimeter. All samples were tested in hermetically sealed pans under a heat-cool-heat process from -70 °C to 200 °C with heating and cooling rates at 10 °C.min^{-1} under nitrogen atmosphere (50 mL/min). The rDA of DA networks were visible in the first heating ramp. All the other data were collected from the second cycle.

A Mettler Toledo TGA/DSC 1 Star system was used to perform thermogravimetric analysis (TGA) for all samples under nitrogen atmosphere (80 mL/min) with a heating rate of 10 °C.min^{-1}. The weight of samples was fixed around 5 mg.

Swelling and soluble fraction of DA networks

The swelling behavior of DA networks was studied by a general gravimetric method. Dried DA networks (weight, m_i) were immersed in DMF solvent at room temperature for 48 h. The swollen samples were weighed (weight of swollen network, m_s) and then dried in an oven at 80 °C for 24 h at 0.2 mbar (weight of dried samples, m_d). The *gel fraction* (*GF*) and *swelling ratio* (*SR*) could be calculated as follows:

$$Gel\ fraction\ (GF) = \frac{m_d}{m_i} \times 100\% \qquad \text{Eq. (1)}$$

$$Swelling\ ratio\ (SR) = \frac{m_s - m_i}{m_i} \times 100\% \qquad \text{Eq. (2)}$$

Oscillatory rheology tests

Rheology properties of DA networks were assessed with an ARES-G2 (TA Instruments) rheometer with parallel geometry (25 mm diameter). All samples were annealed at 80 °C for approximately 24 h before rheology tests. Measurements were performed within the linear

viscoelastic regime (LVR) under oscillation mode. Temperature ramp tests were conducted from 70 to 200 °C with a strain of 1% and a heating/cooling rate at 5 °C/min. Frequency sweep tests were performed with a strain of 1% at 80 °C and 130 °C for all samples.

Creep tests

Creep tests were carried out with a stress-controlled Anton Parr MCR 301 rheometer with 25 mm diameter parallel geometry at a gap size between 0.5 and 0.8 mm at 80 °C or 130 °C. All tests were conducted under a controlled constant rotational stress of 100 Pa for 30 min followed by a relaxation process of 120 min. Samples were annealed at the measurement temperature for around 24 h in an oven before each test.

Tensile tests

Tensile measurements were performed by a universal tensile tester Shimadzu Autograph AGS-X with 500 N load cells. Dumbbell-shaped specimens were prepared with a dimension of 50 mm (L) × 4 mm (W) × 0.5 mm (H) (ISO 37:2005 standard, dumbbell: type 3) and submitted to maturation at 80 °C for 24 h prior to the tests. All tests were conducted at room temperature with a crosshead speed of 10 $mm \cdot min^{-1}$ to get stress–strain curves. Young's modulus E was measured from true stress versus true strain plots in the strain range of 0.2 to 0.6%.

2.3 Syntheses

2.3.1 Synthesis of hydroxy telechelic PTMC oligomers

The synthesis and characterization of PTMC oligomers with a molar mass of 2000 g/mol ($PTMC_{2000}$) have already been described in detail in our recent work[28]. PTMC oligomers were obtained from ring-opening polymerization with trimethylene carbonate as monomer, 1,4-butanediol as co-initiator, 1,5,7-triazabicyclo[4.4.0]dec-5-ene (TBD) as catalyst as follows:

In a 250 mL glass reactor equipped with a steel anchor, a cooler, nitrogen gas flow and an oil bath, 60.006 g TMC (0.588 mol) and 2.788 g BDO (0.031 mol) were firstly mixed in the reactor at 100 °C until a homogeneous state was reached. Then, 0.082 g TBD catalyst (0.588 mmol) were added. The reaction was maintained for 30 min to get a transparent viscous material in the molten state. The molar mass dispersity ($Đ_M = \overline{M}_n/\overline{M}_w$) of $PTMC_{2000}$ is 1.60. The T_g of $PTMC_{2000}$ is -31.6 °C.

2.3.2 Synthesis of furan-functionalized PTMC (PTMC-F) precursors

PTMC-F precursors were synthesized by the reaction between hydroxy and isocyanate groups with the same protocol in two steps. The synthesis of PTMC-F3 precursor is given as an example. In a three-necked flask, 0.243 g glycerol (2.639 mmol) and 15.834 g $PTMC_{2000}$ (7.917 mmol) were firstly dissolved in 80 mL DMF at 80 °C under nitrogen atmosphere. 4.154 g $H_{12}MDI$ (15.834 mmol) and 0.010 g DBTL (0.1 mol% of $H_{12}MDI$) catalyst were added after the homogenization of the system. The reaction was followed up by FTIR until the absorption band of the isocyanate groups at 2260 cm^{-1} remained stable. Then, 0.777 g furfuryl alcohol (7.917 mmol) were added and the reaction was maintained until the absorption of isocyanate groups totally disappeared. After cooling down to room temperature, the final product was precipitated by diethyl ether and dried in a vacuum oven at 80 °C for 24 h at 0.2 mbar. All the synthesis parameters of PTMC-F precursors are given in Table 1.

2.3.3 Synthesis of 1,1'-hexane-1,6-diylbis(1H-pyrrole-2,5-dione) bismaleimide

Bismaleimide was synthesized according to a previous work[22] with a yield of 85%. 1,6-diaminohexane and maleic anhydride were used as reagents in the presence of acetic anhydride, nickel acetate and triethylamine. ^1H NMR (400 MHz, DMSO-d_6, δ ppm): 7.05 (s, 4H), 3.38 (t, J = 7.1 Hz, 4H), 1.51 (m, J = 6.4 Hz, 4H), 1.26 (m, J = 3.4 Hz, 4H). FT-IR (cm^{-1}): 3087 ($\upsilon_{=C-H}$), 1690 ($\upsilon_{C=O}$), 840 ($\delta_{C=C}$), 698 ($\delta_{=C-H}$). M = 276.29 g/mol. Melting temperature T_m = 136 °C.

2.3.4 Synthesis of DA networks

DA networks were obtained from the mixture of PTMC-F precursors and bismaleimide based on the stoichiometry of furan and maleimide functions. The formation of DA-F3 network is given as an example. 10.000 g PTMC-F3 (1.329 mmol) was dissolved in DMF at room temperature. Then, 0.551 g bismaleimide (1.994 mmol) was added. When a homogeneous solution was obtained, the solvent was eliminated by evaporation in a vacuum oven at 80 °C for 24 h to give the final product.

Table 1. Synthesis parameters of PTMC-F precursors with different functionalities at 80 °C in DMF.

Sample name	Expected $\overline{f}_{furan}{}^a$	$H_{12}MDI$ (mol)	Glycerol (mol)	PTMC (mol)	FAL (mol)
PTMC-F3	3	6	1	3	3
PTMC-F4	4	9	2	4	4
PTMC-F5	5	12	3	5	5

[a]Functionality of furan.

3. Results and discussions

3.1 Synthesis and structure characterizations of PTMC-F precursors

The synthesis of PTMC-F precursors is based on the reaction between hydroxyl and isocyanate functions. However, due to the reactivity discrepancy of hydroxyl groups in furfuryl alcohol, glycerol and PTMC, the reaction must be conducted in 2 steps. As shown in Scheme 1, H_{12}MDI was used to react with glycerol and PTMC in order to gain an intermediate bearing free-NCO groups in the first step. Then, furfuryl alcohol was added to react with these remaining free -NCO groups to obtain the final product. The end of the first step was evaluated by FT-IR when the absorbance of -NCO groups around 2260 cm^{-1} became stable. At this time, all hydroxyl groups from glycerol and PTMC oligomers had reacted to form urethane groups. The remaining free -NCO groups were then reacted with furfuryl alcohol to obtain telechelic PTMC-F precursors.

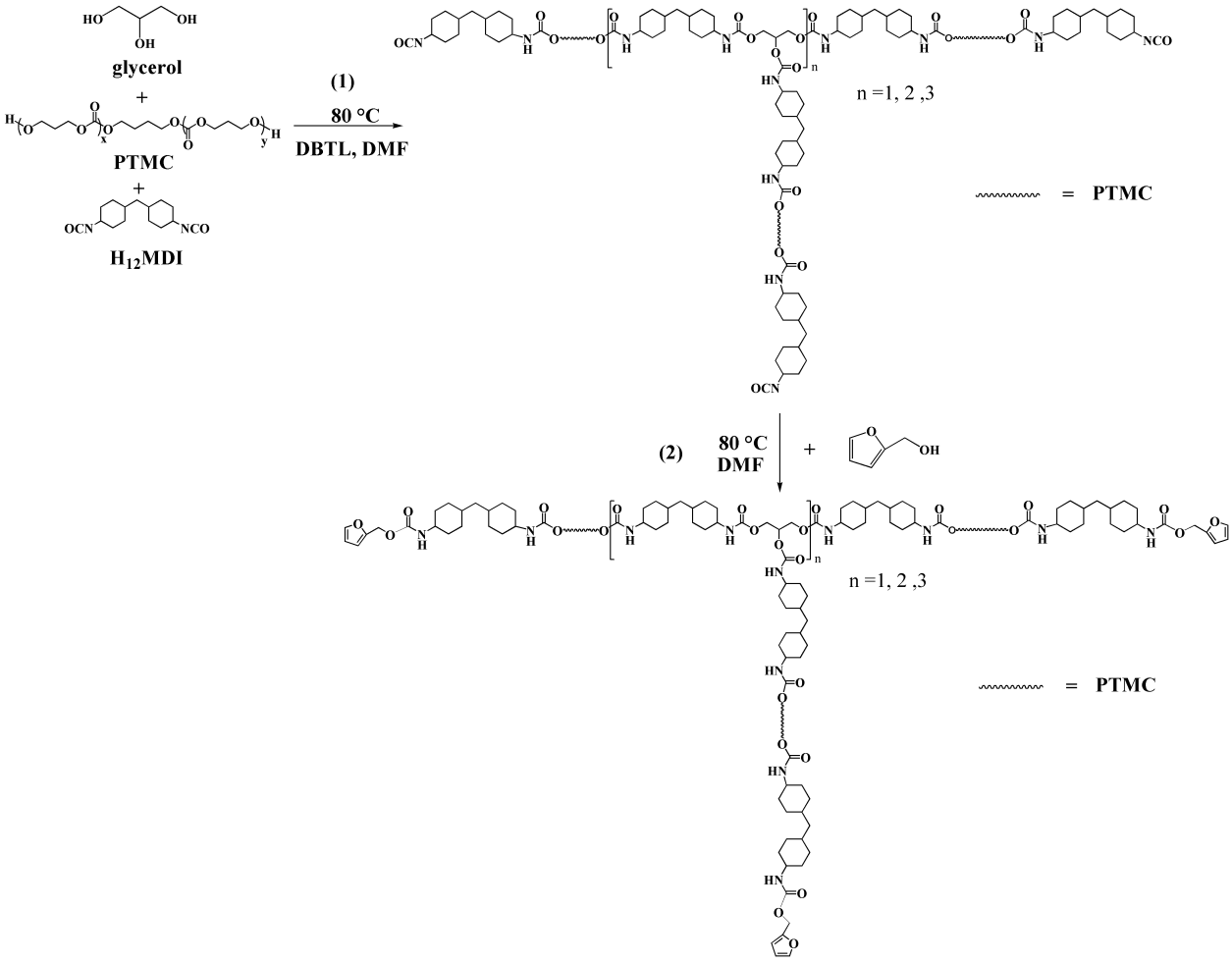

Scheme 1. Synthesis and structures of PTMC-F precursors.

The structure of PTMC-F precursors was characterized firstly by FT-IR. The FT-IR spectra of $PTMC_{2000}$ and PTMC-F3 are compared in Figure 1. As seen, the main absorbances at 1741 and 1238 cm^{-1} in $PTMC_{2000}$ belong to the absorption of carbonyl group C=O and C-O-C respectively. The absorbances at 1523 and 1696 cm^{-1} in PTMC-F3 belong to the bending vibration of >N-H groups and to the stretching vibration of carbonyl groups C=O in urethane bonds (-NH-(C=O)-O-), which were formed by the reaction between isocyanate and hydroxyl functions. The absorptions at 3087, 1150, 837 and 737 cm^{-1} in PTMC-F3 are ascribed to the characteristic absorption peaks of furan rings. These newly appeared signals compared to $PTMC_{2000}$ spectrum prove the formation of furan-functionalized PTMC.

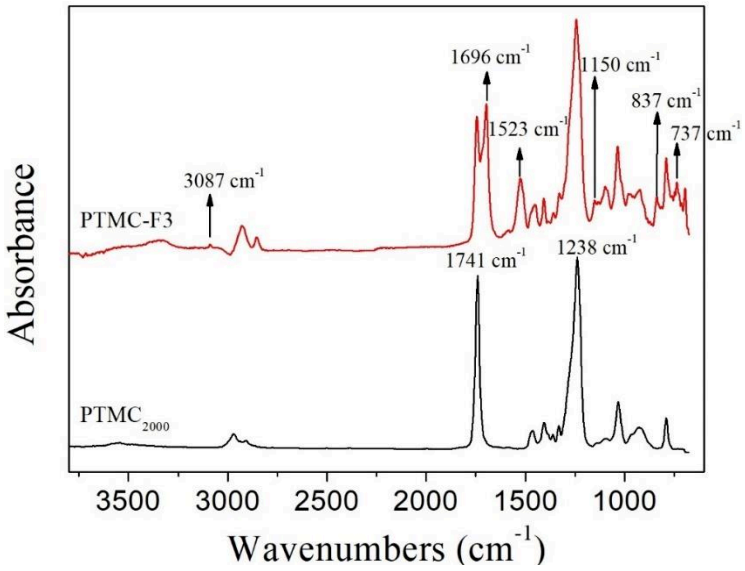

Figure 1. FT-IR spectra of $PTMC_{2000}$ and PTMC-F3.

Furthermore, the success in obtaining the expected structures was verified by ^1H NMR. All the PTMC-F precursors with different functionalities possess similar ^1H NMR spectra. In this case, the ^1H NMR spectrum of PTMC-F3 was given as an example. As seen in Figure 2, all protons of the pendant furfuryl moieties were observed. The resonances at 7.65 ppm, 6.47 ppm and 6.44 ppm are assigned to H_v, H_t and H_u in furan rings respectively[29]. Moreover, the resonances of methylene protons (H_r) linked to furan rings are at the position of 4.94 ppm[30]. The peaks group around 7.00 ppm characterize labile protons resonances from -NH- in urethane bonds (H_c, H_i and H_q)[31]. Protons H_p, H_l, H_k, $H_{k'}$, H_j and $H_{j'}$ belong to PTMC chains. The resonances of glycerol protons are at 5.03 ppm (H_a) and 3.65 ppm (H_b) respectively. After clarifying the attributions of all proton resonances in PTMC-F precursors, their structures can then be characterized precisely.

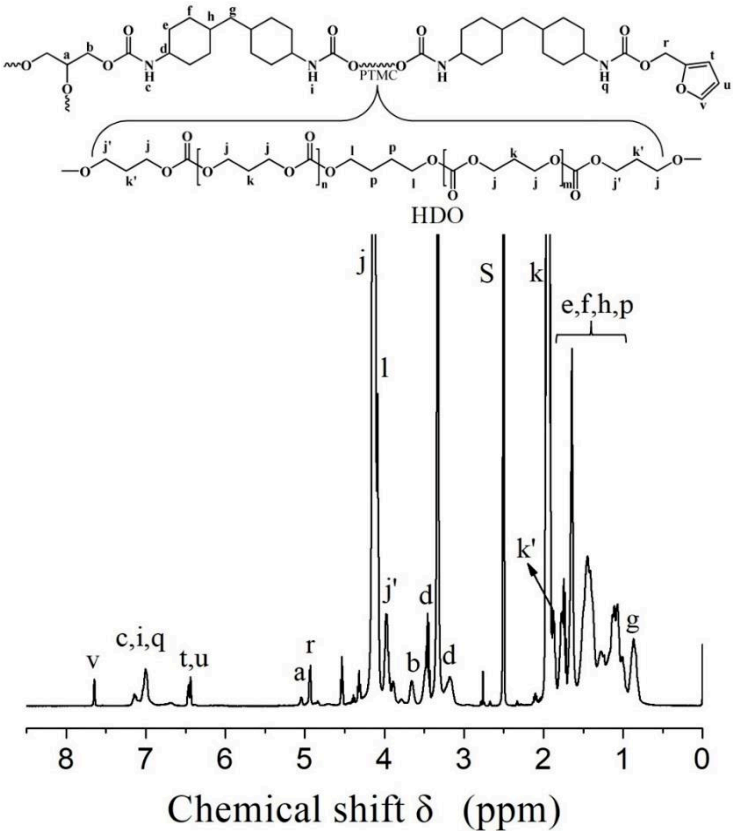

Figure 2. ^{1}H NMR spectrum of PTMC-F3 in DMSO-d_6 at 400 MHz and 298 K.

Based on the integration of H_g, H_a and H_b, the molar ratio of H_{12}MDI to glycerol can be calculated by the following equation:

$$\frac{n_{H_{12}MDI}}{n_{glycerol}} = \frac{\frac{I_g}{2}}{\frac{(I_a + I_b)}{5}} = \frac{5I_g}{2(I_a + I_b)} \qquad \text{Eq. (3)}$$

In addition, the molar ratios of FAL/glycerol and PTMC/glycerol can be calculated by the integration of $H_{t,u}$, $H_{j'}$, H_a and H_b with Eq. (4) and Eq. (5) shown below:

$$\frac{n_{FAL}}{n_{glycerol}} = \frac{\frac{I_{t,u}}{2}}{\frac{(I_a + I_b)}{5}} = \frac{5I_{t,u}}{2(I_a + I_b)} \qquad \text{Eq. (4)}$$

$$\frac{n_{PTMC}}{n_{glycerol}} = \frac{\frac{I_{j'}}{2}}{\frac{(I_a + I_b)}{5}} = \frac{5I_{j'}}{2(I_a + I_b)} \qquad \text{Eq. (5)}$$

Using the formulas given in Eq. (3), Eq. (4) and Eq. (5), the ratios of glycerol, H_{12}MDI, PTMC and FAL reagent segments in PTMC-F3 can then be calculated (Table 2). Likewise, the molar ratios of reagents for PTMC-F precursors with functionalities of 4 and 5 are also obtained. As compared to the designed ratios shown in Table 1, all these calculated ratios are accordant, indicating the attainment of the desired functionalities. The NMR-calculated $\overline{M}_n$ of all PTMC-F precursors are shown in Table 3. As expected, $\overline{M}_n$ values increase with functionality and are all close to theoretical ones.

Table 2. Structure parameters of PTMC-F precursors by ^{1}H NMR.

Sample	H_{12}MDI/glycerol (mol/mol)		PTMC/glycerol (mol/mol)		FAL/glycerol (mol/mol)	
	Theoretical values	Calculated values	Theoretical values	Calculated values	Theoretical values	Calculated values
PTMC-F3	6	6.31	3	2.75	3	2.70
PTMC-F4	4.5	4.62	2	1.81	2	1.84
PTMC-F5	4	4.16	1.67	1.44	1.67	1.56

SEC analyses allow the comparison of $\overline{M}_{n\ SEC}$ and dispersity $Đ_M$ values of the various furan-grafted PTMC. As seen in Figure 3, the chromatograms of all PTMC-F precursors display a pretty Gaussian distribution. Besides, a shift towards shorter retention times with the increase of functionality was observed. The obtained $\overline{M}_{n\ SEC}$ shown in Table 3 are also close to the theoretical values, indicating the success in obtaining the expected structures. The $Đ_M$ of PTMC-F precursors measured by SEC are in the range of 1.75 - 2.61.

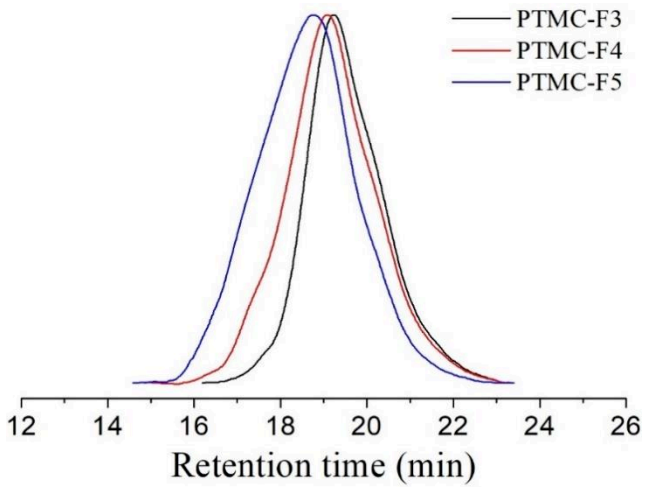

Figure 3. SEC chromatograms of PTMC-F precursors.

Table 3. Structure parameters of PTMC-F precursors by ^{1}H NMR.

Sample name	PTMC/glycerol (mol/mol)	H_{12}MDI/glycerol (mol/mol)	FAL/glycerol (mol/mol)	$\overline{f}_{furan\ theo}$[a]	$\overline{f}_{furan}$[b]	$\overline{M}_{n\ theo}$[c] (g/mol)	$\overline{M}_{n\ NMR}$[d] (g/mol)	$\overline{M}_{n\ SEC}$[e] (g/mol)	$Đ_M$	T_g (°C)
PTMC-F3	2.75	6.31	2.70	3	2.7	8000	7500	8600	1.75	-14.8
PTMC-F4	1.81	4.62	1.84	4	3.7	10900	10200	11200	2.37	-14.8
PTMC-F5	1.44	4.16	1.56	5	4.7	13900	12600	13300	2.61	-11.4

[a]Theoretical functionality of furan. [b]Furan functionality calculated by ^{1}H NMR. [c]Theoretical $\overline{M}_n$. [d]$\overline{M}_{n\ NMR}$ calculated by ^{1}H NMR. [e]$\overline{M}_{n\ SEC}$ calculated by SEC.

DSC studies proved the formation of amorphous polymers for PTMC-F precursors. Their unique glass transition temperatures T_g are given in Table 3. Compared to the T_g of $PTMC_{2000}$ which is -31.6 °C[28], all the T_g values of PTMC-F are higher. These increased T_g are induced not only by the new branched structure with higher molar masses but also by hydrogen bonds between urethane functions in the polymer[32], which limit the mobility of molecules. However, with values of -14.8, -14.8 and -11.4 °C for precursors whose functionalities are 3, 4 and 5 respectively, T_g are very close and seem to be irrelative to the functionality. This could be due to the similar branched structure of PTMC-F precursors.

3.2 Synthesis and characterizations of DA networks

3.2.1 Synthesis of DA networks

DA networks were obtained by the mixing of PTMC-F precursors and bismaleimide with stoichiometric quantities of furan and maleimide functions. The gel point, which represents the minimum molar conversion of reagents to get gelation, was determined according to the gel theory and the Macosko-Miller equation[33] shown as follows:

$$\overline{f}_{furan} = \frac{\sum n_{furan} f_{furan}^{\ 2}}{\sum n_{furan} f_{furan}} \qquad \text{Eq. (6)}$$

$$\overline{f}_{maleimide} = \frac{n_{maleimide} \times f_{maleimide}^{\ 2}}{n_{maleimide} \times f_{maleimide}} = 2 \qquad \text{Eq. (7)}$$

$$r = \frac{n_{furan} \times f_{furan}}{n_{maleimide} \times f_{maleimide}} \qquad \text{Eq. (8)}$$

$$P_{gel}^{\ 2} = \frac{1}{r(\overline{f}_{furan} - 1)(\overline{f}_{maleimide} - 1)} \qquad \text{Eq. (9)}$$

where $\overline{f}_{furan}$ and $\overline{f}_{maleimide}$ are the average degrees of functionality for furan and maleimide groups respectively, r is the stoichiometric ratio of furan/maleimide and P_{gel} is the gel conversion.

All the gel conversions of DA networks are given in Table 4. It is seen that with the increase of functionality, gel conversion decreases. For DA-F5, only 52.0% of reagent conversion is needed to reach gelation.

Table 4. Structure parameters of DA networks with different functionalities.

Sample name	Gel conversion (%)	C_{node} (mmol.cm^{-3})	*SR* (%)	*GF* (%)	T_g (°C)
DA-F3	76.7	0.165	660	72.8	-13.6
DA-F4	60.9	0.243	628	76.1	-13.8
DA-F5	52.0	0.295	573	85.8	-12.4

The various DA network structures are expected to have different properties. To link properties to structure, theoretical node concentration (C_{node})[21,22], which represents the mole of crosslinking points per cubic centimeter of network, was introduced to describe their structural characteristics. C_{node} was calculated by the following equation:

$$C_{node} = \frac{n_{multialcohol} \times \rho_{network}}{total\ mass} \qquad \text{Eq. (10)}$$

where $n_{multialcohol}$ is the molar number of glycerol and $\rho_{network}$ is the density of networks. C_{node} of all DA networks are given in Table 4.

3.2.2 Structure characterization

FT-IR was used to evidence the DA reaction between furan and maleimide groups. As shown in Figure 4, the absorption bands at 954 and 1192 cm^{-1} which belong to the vibration of C-O-C bonds in DA adduct[34,35] appear in the spectrum of DA-F5. These newly observed absorbances prove the occurrence of a DA reaction between furan and maleimide groups. Moreover, even if the decrease of the furan ring absorption band at 737 cm^{-1} is evident, the fact that this band it still visible confirms the remaining of free furan groups. In addition, absorbances observed at 845 and 1583 cm^{-1} belong to $\delta_{C=C}$ and $\upsilon_{C=C}$ respectively in maleimide. These absorbances

indicate that the DA reaction between furan and maleimide groups is incomplete. According to the gel conversion shown in Table 4, only 52.0 % of the reaction is needed to obtain the network structures for DA-F5, imparting the possibility to have unreacted furan and maleimide groups.

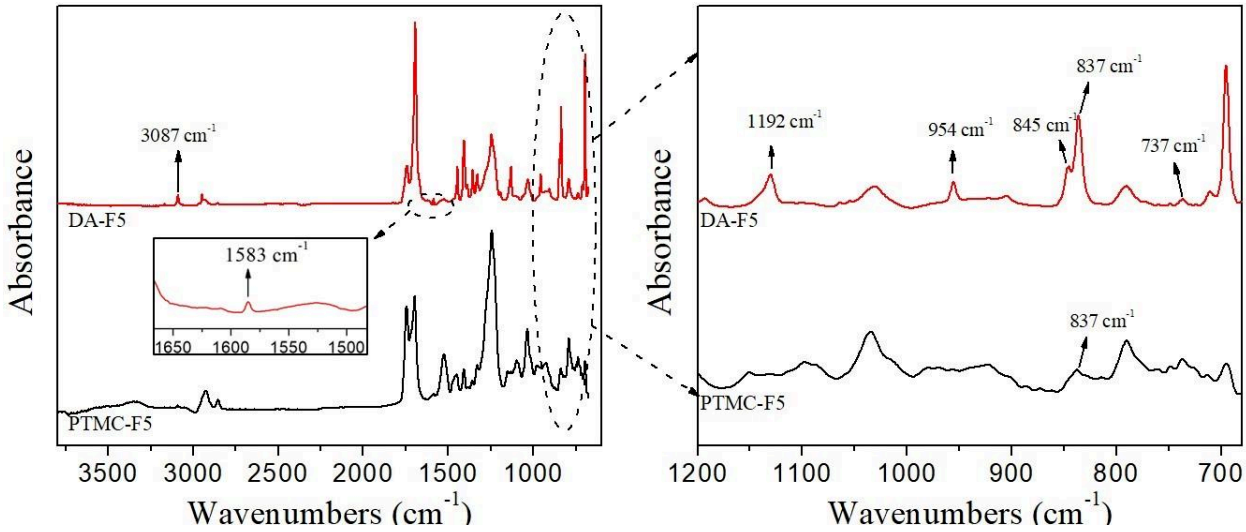

Figure 4. FT-IR spectra of PTMC-F5 and DA-F5.

To highlight crosslinking and compare network densities, swelling tests were investigated. In fact, the swelling ratio is expected to be higher for less dense -or less crosslinked- networks. Swelling behaviors of DA networks were studied quantitatively in DMF which is a good solvent for PTMC-F and bismaleimide at room temperature. The *gel fraction* (*GF*) and *swelling ratio* (*SR*) of DA networks are given in Table 4. As seen, *SR* decreases when the functionality is increased. For example, DA-F3 has a *SR* of 660% but DA-F5 bears the lowest *SR* of 573%, resulting from a more compact network structures with the highest C_{node} of 0.295 mmol.cm^{-3} for DA-F5. On the contrary, *GF* increases with functionality and DA-F5 has the highest *GF* at 85.8%. These observed phenomena are certainly due to the fact that the higher furan functionality in PTMC-F leads to the formation of more compact network structures with higher cross-linking node concentration.

T_g of amorphous DA networks were compared by DSC analyses. As can be seen in Table 4, T_g of DA networks are only slightly higher than their PTMC-F counterparts. This weak difference between T_g values indicates a structure not so far from PTMC-F branched structures in this study.

3.2.3 Tensile mechanical properties of DA networks

Mechanical properties of DA networks were studied by tensile tests. The true stress (σ_t) and true strain (ε_t) were calculated as follows:

$$\sigma_t = \lambda \sigma_e = \lambda \frac{P}{A_0} \qquad \text{Eq. (11)}$$

$$\varepsilon_t = \ln \lambda \qquad \text{Eq. (12)}$$

where σ_e is the engineering stress, λ is the extension ratio, P is the force and A_0 is the original specimen cross-sectional area.

The tensile curves recorded at room temperature are illustrated in Figure 5. The true stress at break (σ_b), true strain at break (ε_b) and Young's modulus (E) were all determined on the average of 5 samples with their data given in Table 5. Firstly, the tensile mechanical properties of PTMC-F precursors were studied. As shown, it is apparent that both σ_b and E increase with functionality. For example, σ_b and E increase from 5.3 MPa and 0.03 MPa for PTMC-F3 to 10.7 MPa and 0.10 MPa for PTMC-F5 respectively. However, ε_b decreases from 104% for PTMC-F3 to 90% for PTMC-F5. These phenomena can be attributed to the increased molecular weight as well as to the higher number of arms for PTMC-F precursors with higher functionality. However, tensile mechanical properties of DA materials are dramatically different from those of PTMC-F. All DA materials show higher σ_b and E and lower ε_b than their corresponding PTMC-F precursors. For all cases, ε_b decreases around 40%. For example, DA-F3 has σ_b and E values of 13.9 MPa and 0.19 MPa respectively, which are significantly higher than σ_b of 5.3 MPa and E of 0.03 MPa for PTMC-F3. This confirms a real structure modification corresponding to the restraints of polymer segments mobility by crosslinking. Moreover, DA networks have higher σ_b and E and lower ε_b when furan functionality increases. This is due to the higher DA crosslink concentration brought by higher furan functionality and number of arms in PTMC-F.

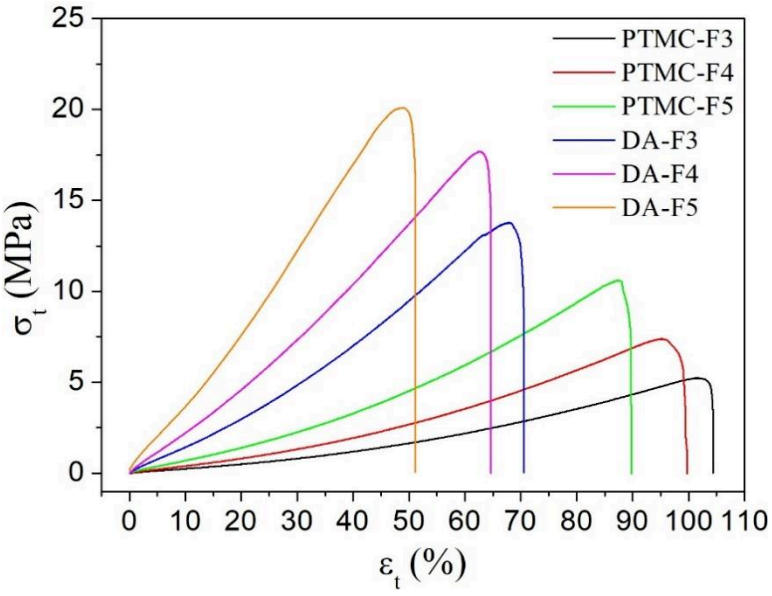

Figure 5. True stress-true strain curves of DA networks.

Table 5. Tensile mechanical properties of PTMC-F precursors and DA networks.

Sample	E[a] (MPa)	σ_b[b] (MPa)	ε_b[c] (%)
PTMC-F3	0.03	5.3 ± 0.3	104 ± 6
PTMC-F4	0.05	7.5 ± 0.4	99 ± 5
PTMC-F5	0.10	10.7 ± 1.3	90 ± 7
DA-F3	0.19	13.9 ± 1.1	71 ± 6
DA-F4	0.27	17.7 ± 1.9	65 ± 7
DA-F5	0.49	20.1 ± 1.5	52 ± 4

[a]Young's modulus. [b]Ultimate strength. [c]Elongation at break.

3.3 Thermal properties and decrosslinking of DA networks

The thermal properties of networks as well as the effects of network density were investigated in this part. Qualitative solubility tests at low and high temperatures were performed first. As they are indubitably not sufficient to prove the reversibility of the covalent DA links, analyses such as DSC, FT-IR, rheology and creep tests were performed at high temperature and compared to low temperature analyses.

3.3.1 Solubility tests

The thermoreversibility of DA networks was studied by solubility tests in DMF at 25°C and 150 °C. As shown in Figure 6 (A), after immersing DA-F3 in DMF at 25 °C for 24 h, the

material was only swelled but not dissolved. Once heating at 150 °C for 10 min, complete dissolution of DA-F3 was observed (Figure 6, B). Similar behavior was seen for all DA materials and can be attributed to the disruption of the networks thanks to the break of DA links at high temperature. By rDA, free bismaleimide and PTMC-F which are soluble in DMF are released, giving a pale yellow transparent solution. Once this solution was dried in a vacuum oven at 80 °C for 24 h, the obtained material was insoluble in DMF again at room temperature, proving the thermoreversibility of DA networks.

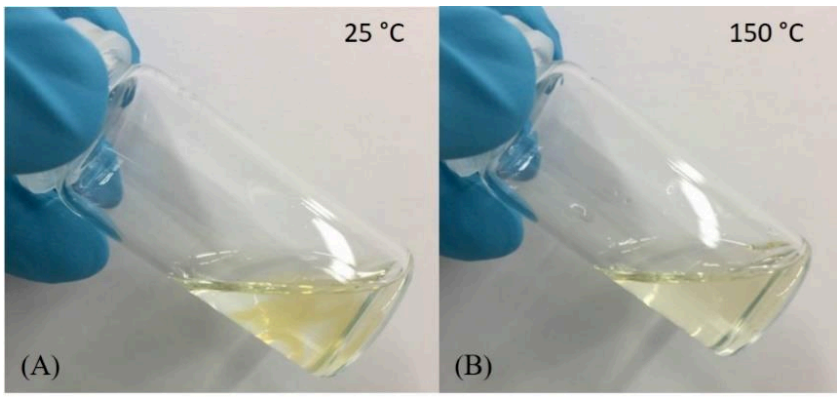

Figure 6. Solubility tests on DA networks in DMF at (A) 25 °C for 24 h and (B) 150 °C for 10 min.

3.3.2 DSC study

The thermoreversible properties of networks were then studied by DSC. During the first heating ramp of networks in DSC thermograms (Figure 7, A), broad endothermic peaks between 130 °C and 160 °C were observed for all materials. These peaks are absent in PTMC-F DSC curves and are attributed to the endothermic rDA reactions[29,36]. Generally, the DA reaction between furan and maleimide groups is known to lead to an adduct with two stereoisomeric forms, namely endo and exo[37-41], with the latter one being the thermodynamically more stable form. As revealed, the rDA temperature of endo DA adducts is 20-40 °C lower than that of exo DA adducts. Herein, all curves show a peak centered at 140-150°C depending on the network as well as a weak broad shoulder peak around 120°C, attributed to exo and endo forms respectively. However, the endo form, which is probably generated by the synthesis conditions at low temperature, remains as the minority form in the networks. Duval and co-workers[29] also obtained both endo and exo DA networks from furan-grafted tannins and a bismaleimide oligomer with similar rDA temperatures measured by DSC at the same heating rate. The measured enthalpy of the rDA reaction for DA-F3, DA-F4 and DA-F5 is 2.346 J/g, 3.328 J/g and 4.040 J/g respectively and increases with the content of DA adduct in the networks[29].

However, as shown in Figure 7 (B), these endothermic peaks became less obvious in the second heating ramp, indicating that the DA reaction is a slow process which cannot occur completely within the relatively short time scale of the DSC experiments during cooling at a rate of 10 °C/min[41].

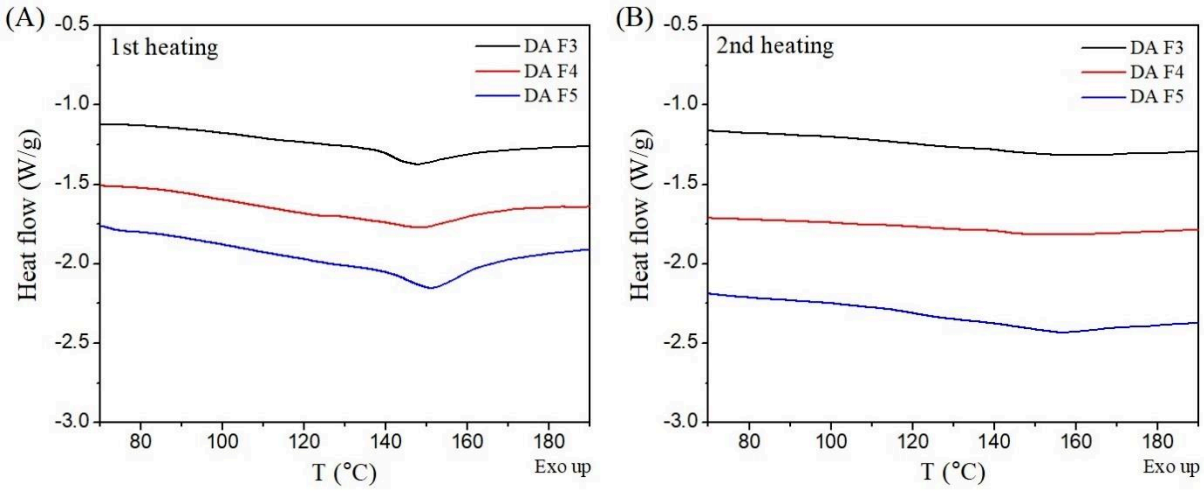

Figure 7. DSC curves of DA networks in (A) first heating ramp and (B) second heating ramp (10 °C/min).

3.3.3 FT-IR

To confirm the thermoreversibility of DA/rDA reactions, FT-IR analysis was then investigated. The FT-IR spectra of DA-F5 collected at different temperatures are shown in Figure 8. As revealed previously, the signals observed at 954 and 1192 cm^{-1} (Figure 8, a) are attributed to the DA adduct (C-O-C). However, when the material was heated at 150 °C for 10 min, these signals disappeared (Figure 8, b), resulting from the occurrence of a rDA reaction at high temperature. After keeping the same material at 80 °C for 12 h, these absorbances at 954 and 1192 cm^{-1} appeared again (Figure 8, c), indicating the formation of a DA adduct from furan and maleimide groups and the thermoreversibility of DA networks as well.

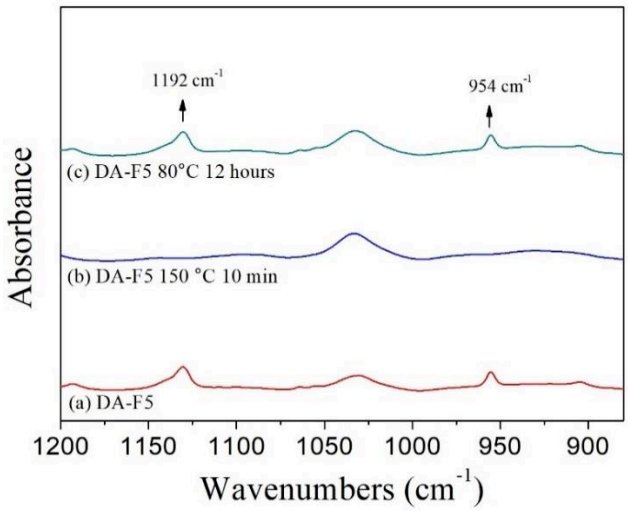

Figure 8. FT-IR spectra of (a) DA-F5, (b) DA-F5 heated at 150 °C for 10 min and (c) DA-F5 maturated at 80 °C for 12 h.

3.3.4 TGA analyses

The thermal weight losses of $PTMC_{2000}$, PTMC-F precursors and DA networks were evaluated and compared by TGA. The weight loss and derivative thermogravimetry (DTG) curves are displayed in Figure 9 (A) and (B) respectively. In this work, the onset decomposition temperature T_{onset} (5% of weight loss) and the fastest degradation temperature T_{max} are used to characterize the thermal degradation properties. All the data were gathered in Table 6. As seen, all the samples exhibit nearly 100% degradation before 500 °C except for DA networks which still have a little percentage of residues. Obviously, $PTMC_{2000}$ oligomers begin to degrade at lower temperature with a T_{onset} of 184.2 °C while T_{onset} raise strikingly for all PTMC-F precursors and DA networks. For PTMC-F precursors, when the functionality of furan increases, T_{onset} also increases from 270.2 °C to 274.5 °C and 278.7 °C for PTMC-F3, PTMC-F4 and PTMC-F5 respectively. DA networks degrade at slightly higher temperatures than PTMC-F. As seen, T_{onset} increase to 281.2, 284.2 and 285.0 °C for DA-F3, DA-F4 and DA-F5 respectively. The temperatures at maximum degradation rate T_{max} are directly obtained from DTG curves. It can be seen that the $PTMC_{2000}$ oligomer has the lowest T_{max} value at 237.4 °C whereas the T_{max} increases to above 290 °C for all PTMC-F precursors and DA networks. For PTMC-F precursors, the T_{max} seems to be weakly related to functionality with their values around 295 °C for all PTMC-F precursors. After introducing bismaleimide to form networks, the T_{max} all raise to values between 300 and 310 °C. Even if networks are more stable regarding their weight loss versus temperature than PTMC-F precursors, it is obvious that TGA analyses

do not allow the highlight of rDA reactions. No weight loss is observed around the rDA temperatures given by DSC analyses. In fact, at temperatures corresponding to the beginning of adduct degradation, the reverse DA reaction has already occured and only the thermal degradation of reactants is observed.

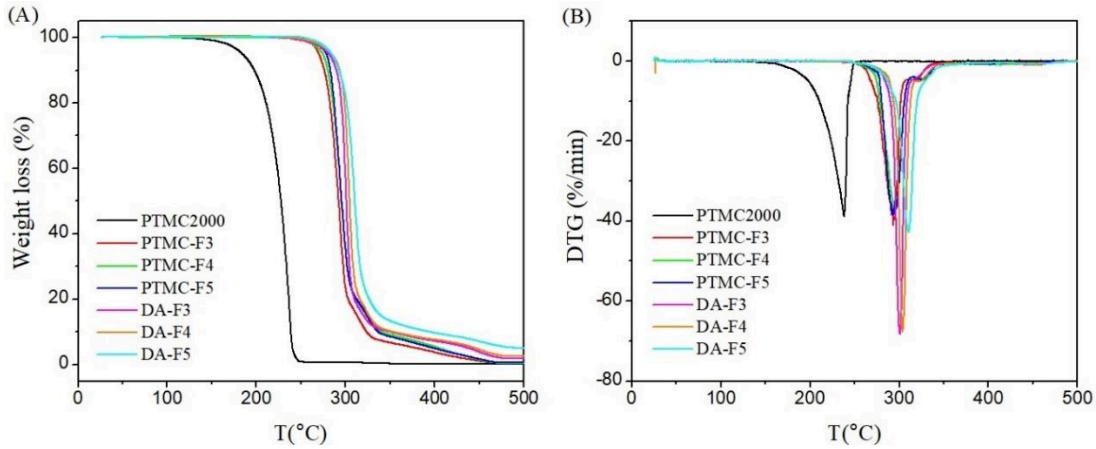

Figure 9. (A) TGA and (B) derivative thermogravimetry (DTG) curves of PTMC oligomers, PTMC-F precursors and DA networks.

Table 6. Thermal properties of PTMC oligomers, PTMC-F precursors and DA networks.

Sample name	C_{node} (mmol/cm^3)	T_{onset} (°C)	T_{max}[b] (°C)
PTMC2000[a]	-	184.2	237.4
PTMC-F3	-	270.2	293.3
PTMC-F4	-	274.5	293.8
PTMC-F5	-	278.7	296.6
DA-F3	0.165	281.2	301.1
DA-F4	0.243	284.2	303.6
DA-F5	0.295	285.0	310.2

[a]Thermal properties of the used PTMC oligomers. [b]T_{max} was obtained in DTG curves.

3.3.5 Rheological properties

3.3.5.1 Creep tests

The creep test under constant stress is a good method to prove the existence of network structures since perfect networks can prevent the creep phenomenon. In this case, creep tests were conducted for all PTMC-F precursors and DA networks to verify the formation of network structures. Strain-time curves collected at 80 °C and 130 °C for PTMC-F precursors are shown

in Figure 10 (A) and (B) with creep data given in Table 7. The recovery ratio was calculated by the ratio of final recovery strain to maximum strain. As seen, under the application of stress, the strains extend continuously. After the removal of stress, the extended strains recover slowly to reach stable values. At 80 °C, the recovery ratio increases with functionality from 51.2% for PTMC-F3 to 69.6% for PTMC-F5. The partial recovery of PTMC-F precursors refutes the network structure of these materials. In addition, the creep rate also decreases with functionality. For PTMC-F5, the creep rate is the lowest with 0.108%/h under 100 Pa stress. Once the temperature increased to 130 °C, the recovery ratio for all materials decreased and the creep rate increased. For example, the recovery ratio of PTMC-F3 reduces from 51.2% at 80 °C to 0% at 130 °C, indicating the absolute flow of this material at 130 °C. For PTMC-F5, the recovery ratio also reduces from 69.6% at 80 °C to only 9.9% at 130 °C.

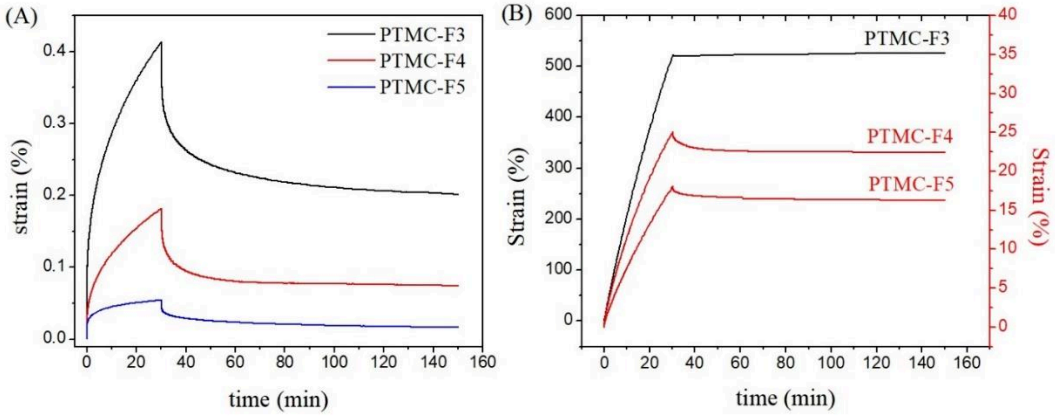

Figure 10. Creep curves of PTMC-F precursors at (A) 80 °C and (B) 130 °C with 30 min under 100 Pa and 90 min for relaxation.

Table 7. Creep properties of PTMC precursors and DA networks at 80 and 130 °C.

Temperature	80 °C				130 °C			
Sample name	Maximum strain[a] (%)	Final ratio[b] (%)	Recovery ratio (%)	Creep rate (%/h)	Maximum strain[a] (%)	Final ratio[b] (%)	Recovery ratio (%)	Creep rate (%/h)
PTMC-F3	0.414	0.202	51.2	0.828	524	524	0	1048
PTMC-F4	0.182	0.074	59.5	0.364	25.1	22.4	10.8	50.2
PTMC-F5	0.054	0.016	69.6	0.108	18.1	16.3	9.9	36.2
DA-F3	0.133	0.002	98.2	0.266	245	239	2.4	490
DA-F4	0.079	0.003	96.2	0.158	14.8	9.8	31.5	29.6
DA-F5	0.046	0	100	0.092	10.8	5.9	45.4	21.6

[a]Maximum strain: the strain after 30 min under stress of 100 Pa. [b]Final ratio: the final ratio after 120 min of recovery.

As shown in Figure 11 (A), all the DA networks bear 100% recovery at 80 °C after relaxation. This complete recovery means that perfect network structures were formed. Meanwhile, the creep rate decreases with functionality as well. For instance, when the functionality of DA networks increased from 3 to 5, the creep rate decreased from 0.266%/h to 0.092%/h, correlating the stiffer networks with higher functionality. When temperature increased to 130 °C, all the recovery ratios decreased (Figure 11, B). DA-F3 has a recovery ratio of only 2.4% after 2 h of relaxation, indicating the almost complete breaking of the network structure. For DA-F4 and DA-F5, the recovery ratios are relatively higher at 31.5 and 45.4% respectively. These values mean that a partial rDA reaction is still sufficient to induce the disruption of the network structures.

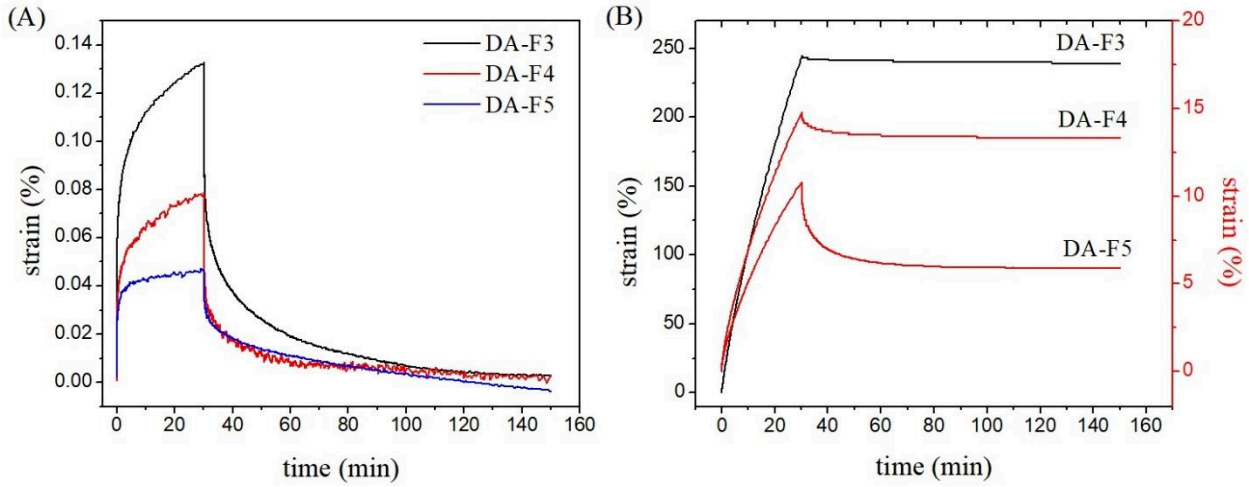

Figure 11. Creep curves of DA networks at (A) 80 °C and (B) 130 °C.

3.3.5.2 Frequency sweep tests

The frequency sweep curves of DA networks are shown in Figure 12. At 80 °C, all the DA networks have higher G' than G'', indicating a dominant elastic behavior for these materials. In addition, both G' and G'' increase with functionality or C_{node}, indicating the increased stiffness of networks with a higher crosslinking degree.

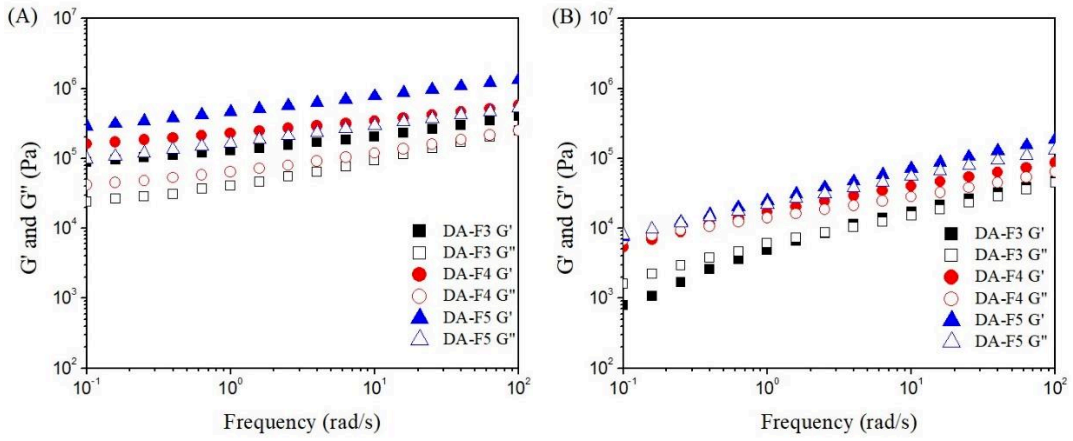

Figure 12. Frequency sweep tests of DA networks at (A) 80 °C and (B) 130 °C (strain = 1%).

According to the rubber elasticity theory[22,42], the molar mass between crosslinks ($\overline{M}_c$) which depicts the density of crosslinks can be calculated from the frequency sweep curves with the following formula:

$$\overline{M}_c = \left(\frac{G'}{\rho_{network} RT} \right)^{-1} \qquad \text{Eq. (13)}$$

where G' is the storage modulus at 1 rad/s at the temperature of T (Kelvin temperature), R is the ideal gas constant of 8.314 J.K^{-1}.mol^{-1} and $\rho_{network}$ is the density of the network. The calculated $\overline{M}_c$ values of all DA networks are reported in Table 8. As expected from swelling tests and tensile results, the increase of functionality can lead to the formation of more compact network structures. The $\overline{M}_c$ values measured here correspond exactly to these expectations. For DA-F5, which has the highest functionality, the measured $\overline{M}_c$ of 8.3 kg/mol is the lowest among all DA networks, verifying the formation of the densest network structure.

Table 8. Rheological parameters of DA networks.

Sample name	ω (rad/s)	τ (s)	$T_{crossover}$[c] (°C)	$\overline{M}_c$ (kg/mol)
PTMC-F3	-	-	118.7	-
PTMC-F4	-	-	121.0	-
PTMC-F5	-	-	122.3	-
DA-F3	2.62	2.40	123.2	29.8
DA-F4	0.32	19.63	138.1	16.8
DA-F5	0.18	34.89	139.1	8.3

According to the studies of Bowman et al.[43,44], when temperature is above gel point, the rDA reaction dominates and makes the materials exhibit a liquid-like behavior. To evidence the disruption of the networks, frequency sweep tests were also performed at high temperature. As seen in Figure 12 (B), when temperature increased to 130 °C, a drop-off in both G' and G'' was clearly observed. Compared to the curves at 80 °C, the newly appeared crossover between G' and G'' demonstrates the transition from solid to viscous state and the relaxation over long time scales, resulting from the retro reaction of DA adducts. The longest relaxation time τ can be obtained from the equation $\tau = 2\pi/\omega$[45]. As shown in Table 8, τ value is 2.40 s for DA-F3 and 34.89 s for DA-F5 respectively and increases with functionality or C_{node}.

3.3.5.3 Temperature ramp tests

Temperature ramp tests can be used to trace the evolution of G' and G'' with temperature. Before imparting the effect of DA reaction, temperature ramp tests of PTMC-F precursors were first conducted. As seen in Figure 13 (A) and Table 8, furan-grafted PTMC curves of G' and G'' vs T show a crossover, which indicates a nominal transition from elastic behavior to viscous state. Considering the relatively low T_g (below 0 °C) for all PTMC-F precursors, these $T_{crossover}$ are related to urethane hydrogen bonds. Both $T_{crossover}$ and modulus of PTMC-F precursors increase with functionality, which is certainly attributed to the higher molecular weights and arm numbers. The curves of temperature sweep experiments obtained for DA networks are gathered in Figure 13 (B). As can be seen, the G' and G'' of DA networks are all higher than their corresponding PTMC-F counterparts. This is attributed to the crosslinking by DA adducts, making the material stiffer. Furthermore, all DA networks exhibit a crossover for G' and G'' at a temperature higher than their PTMC-F counterparts, only ascribed to the addition of bismaleimide. The reason lies in the fact that DA adducts function as crosslinks between PTMC-F precursors. In this case, higher temperature or heat is needed to break the network and make the material flow. For example, the $T_{crossover}$ of DA-F5 (139.1 °C) is 16.8 °C higher compared to that of PTMC-F5 (122.3 °C). When temperature reaches 122.3 °C, the urethane hydrogen bonds in PTMC-F5 are broken. However, the remaining DA nodes can still maintain the elastic state. The material begins to flow at higher temperatures when sufficient DA adducts are broken to lead to the collapse of network frame structures. Furthermore, networks with higher functionality - or higher C_{node} – have higher $T_{crossover}$ and this shows the dependence of the thermal reversibility on the density of networks.

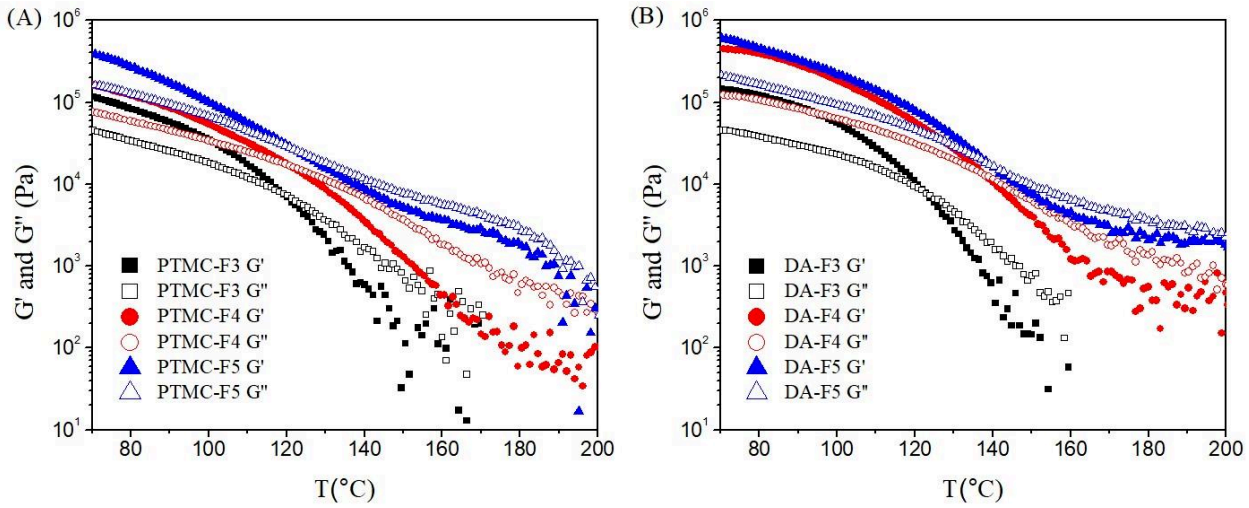

Figure 13. Temperature ramp tests of (A) PTMC precursors and (B) DA networks (5 °C/min, frequency = 1 rad/s, strain = 1%).

4. Conclusion

In this work, thermoreversible PTMC-based networks were built from synthesized and well-characterized furan-functionalized PTMC and a maleimide crosslinker via Diels-Alder reaction. The formation of network structures was proved by several analyses. DSC study evidenced both exo and endo adduct forms with the latter being the minority form. The increase of PTMC-F functionality lead to stiffer networks with higher crosslinking density. In creep tests, the recovery ratio of 100% at 80 °C for all DA networks proved the formation of perfect networks, while at 130 °C these networks could be partially broken and lost their creep resistance. This decrosslinking reaction occurred in the 130-160°C temperature range depending on the networks' density.

Acknowledgments

The authors thank the financial support from China Scholarship Council (CSC). This work benefited from the international cooperation between Université Jean Monnet Saint-Etienne (France) and East China University of Science and Technology (China).

References

[1] H.C. Kolb, M.G. Finn, K.B. Sharpless, Click Chemistry: Diverse Chemical Function from a Few Good Reactions, Angewandte Chemie International Edition 40(11) (2001) 2004-2021.

[2] W.H. Binder, R. Sachsenhofer, 'Click' Chemistry in Polymer and Materials Science, Macromolecular Rapid Communications 28(1) (2007) 15-54.

[3] J.E. Moses, A.D. Moorhouse, The growing applications of click chemistry, Chemical Society Reviews 36(8) (2007) 1249-1262.

[4] M.A. Tasdelen, Diels–Alder "click" reactions: recent applications in polymer and material science, Polymer Chemistry 2(10) (2011) 2133.

[5] M. Watanabe, N. Yoshie, Synthesis and properties of readily recyclable polymers from bisfuranic terminated poly(ethylene adipate) and multi-maleimide linkers, Polymer 47(14) (2006) 4946-4952.

[6] A.J. Inglis, L. Nebhani, O. Altintas, F.G. Schmidt, C. Barner-Kowollik, Rapid Bonding/Debonding on Demand: Reversibly Cross-Linked Functional Polymers via Diels−Alder Chemistry, Macromolecules 43(13) (2010) 5515-5520.

[7] J. Kötteritzsch, S. Stumpf, S. Hoeppener, J. Vitz, M.D. Hager, U.S. Schubert, One-Component Intrinsic Self-Healing Coatings Based on Reversible Crosslinking by Diels–Alder Cycloadditions, Macromolecular Chemistry and Physics 214(14) (2013) 1636-1649.

[8] L. Feng, Z. Yu, Y. Bian, J. Lu, X. Shi, C. Chai, Self-healing behavior of polyurethanes based on dual actions of thermo-reversible Diels-Alder reaction and thermal movement of molecular chains, Polymer 124 (2017) 48-59.

[9] P. Du, X. Liu, Z. Zheng, X. Wang, T. Joncheray, Y. Zhang, Synthesis and characterization of linear self-healing polyurethane based on thermally reversible Diels-Alder reaction, RSC Advances 3(35) (2013) 15475-15482.

[10] L. Yuan, Z. Wang, M.S. Ganewatta, M.A. Rahman, M.E. Lamm, C. Tang, A biomass approach to mendable bio-elastomers, Soft Matter 13(6) (2017) 1306-1313.

[11] G. Zhang, Q. Zhao, L. Yang, W. Zou, X. Xi, T. Xie, Exploring Dynamic Equilibrium of Diels–Alder Reaction for Solid State Plasticity in Remoldable Shape Memory Polymer Network, ACS Macro Letters 5(7) (2016) 805-808.

[12] X. Kuang, G. Liu, X. Dong, D. Wang, Triple-shape memory epoxy based on Diels–Alder adduct molecular switch, Polymer 84 (2016) 1-9.

[13] A. Gandini, The furan/maleimide Diels–Alder reaction: A versatile click–unclick tool in macromolecular synthesis, Progress in Polymer Science 38(1) (2013) 1-29.

[14] Y.N. Yuksekdag, T.N. Gevrek, A. Sanyal, Diels-Alder "Clickable" Polymer Brushes: A Versatile Catalyst-Free Conjugation Platform, ACS Macro Letters 6(4) (2017) 415-420.
[15] A. Duval, H. Lange, M. Lawoko, C. Crestini, Reversible crosslinking of lignin via the furan-maleimide Diels-Alder reaction, Green Chemistry 17(11) (2015) 4991-5000.
[16] L.S. Nair, C.T. Laurencin, Biodegradable polymers as biomaterials, Progress in Polymer Science 32(8–9) (2007) 762-798.
[17] J.M. Raquez, S. Vanderstappen, F. Meyer, P. Verge, M. Alexandre, J.M. Thomassin, C. Jérôme, P. Dubois, Design of Cross-Linked Semicrystalline Poly(ε-caprolactone)-Based Networks with One-Way and Two-Way Shape-Memory Properties through Diels–Alder Reactions, Chemistry – A European Journal 17(36) (2011) 10135-10143.
[18] T. Defize, R. Riva, J.-M. Raquez, P. Dubois, C. Jérôme, M. Alexandre, Thermoreversibly Crosslinked Poly(ε-caprolactone) as Recyclable Shape-Memory Polymer Network, Macromolecular Rapid Communications 32(16) (2011) 1264-1269.
[19] T. Defize, J.-M. Thomassin, M. Alexandre, B. Gilbert, R. Riva, C. Jérôme, Comprehensive study of the thermo-reversibility of Diels–Alder based PCL polymer networks, Polymer 84 (2016) 234-242.
[20] G. Rivero, L.-T.T. Nguyen, X.K.D. Hillewaere, F.E. Du Prez, One-Pot Thermo-Remendable Shape Memory Polyurethanes, Macromolecules 47(6) (2014) 2010-2018.
[21] D. Djidi, N. Mignard, M. Taha, Thermosensitive polylactic-acid-based networks, Industrial Crops and Products 72 (2015) 220-230.
[22] S. Mhiri, N. Mignard, M. Abid, F. Prochazka, J.-C. Majeste, M. Taha, Thermally reversible and biodegradable polyglycolic-acid-based networks, European Polymer Journal 88 (2017) 292-310.
[23] K. Fukushima, Poly(trimethylene carbonate)-based polymers engineered for biodegradable functional biomaterials, Biomaterials science 4(1) (2016) 9-24.
[24] K. Fukushima, Biodegradable functional biomaterials exploiting substituted trimethylene carbonates and organocatalytic transesterification, Polym J 48(12) (2016) 1103-1114.
[25] J. Hilf, M. Scharfenberg, J. Poon, C. Moers, H. Frey, Aliphatic Polycarbonates Based on Carbon Dioxide, Furfuryl Glycidyl Ether, and Glycidyl Methyl Ether: Reversible Functionalization and Cross-Linking, Macromolecular Rapid Communications 36(2) (2015) 174-179.
[26] W. Thongsomboon, M. Sherwood, N. Arellano, A. Nelson, Thermally Induced Nanoimprinting of Biodegradable Polycarbonates Using Dynamic Covalent Cross-Links, ACS Macro Letters 2(1) (2013) 19-22.

[27] Y. Hu, L. Qiao, Y. Qin, X. Zhao, X. Chen, X. Wang, F. Wang, Synthesis and Stabilization of Novel Aliphatic Polycarbonate from Renewable Resource, Macromolecules 42(23) (2009) 9251-9254.
[28] X. Li, N. Mignard, M. Taha, C. Fernandez-de-Alba, J. Chen, S. Zhang, F. Becquart, Synthesis of poly(trimethylene carbonate) (PTMC) oligomers by ring-opening polymerization in bulk (submitted), (2019).
[29] A. Duval, G. Couture, S. Caillol, L. Avérous, Biobased and Aromatic Reversible Thermoset Networks from Condensed Tannins via the Diels−Alder Reaction, ACS Sustainable Chemistry & Engineering 5(1) (2017) 1199-1207.
[30] K. Roos, E. Dolci, S. Carlotti, S. Caillol, Activated anionic ring-opening polymerization for the synthesis of reversibly cross-linkable poly(propylene oxide) based on furan/maleimide chemistry, Polymer Chemistry 7(8) (2016) 1612-1622.
[31] L.H. Chan-Chan, G. González-García, R.F. Vargas-Coronado, J.M. Cervantes-Uc, F. Hernández-Sánchez, A. Marcos-Fernandez, J.V. Cauich-Rodríguez, Characterization of model compounds and poly(amide-urea) urethanes based on amino acids by FTIR, NMR and other analytical techniques, European Polymer Journal 92 (2017) 27-39.
[32] K.A. Houton, A.J. Wilson, Hydrogen-bonded supramolecular polyurethanes, Polymer International 64(2) (2015) 165-173.
[33] D.R. Bauer, Calculating Network Structure Using Miller—Macosko Theory, in: Computer Applications in Applied Polymer Science II, American Chemical Society1989, Vol. 404, pp. 190-212.
[34] J. Bai, H. Li, Z. Shi, M. Tian, J. Yin, Dynamic crosslinked poly(styrene-block-butadiene-block-styrene) via Diels-Alder chemistry: an ideal method to improve solvent resistance and mechanical properties without losing its thermal plastic behavior, RSC Advances 5(56) (2015) 45376-45383.
[35] Y. Zhang, A.A. Broekhuis, F. Picchioni, Thermally Self-Healing Polymeric Materials: The Next Step to Recycling Thermoset Polymers?, Macromolecules 42(6) (2009) 1906-1912.
[36] C. Gaina, O. Ursache, V. Gaina, D. Ionita, Investigation on the thermal properties of new thermo-reversible networks based on poly(vinyl furfural) and multifunctional maleimide compounds, eXPRESS Polymer Letters 6 (2011) 129-141.
[37] E.H. Discekici, A.H. St. Amant, S.N. Nguyen, I.-H. Lee, C.J. Hawker, J. Read de Alaniz, Endo and Exo Diels–Alder Adducts: Temperature-Tunable Building Blocks for Selective Chemical Functionalization, Journal of the American Chemical Society 140(15) (2018) 5009-5013.

[38] J.R. McElhanon, D.R. Wheeler, Thermally Responsive Dendrons and Dendrimers Based on Reversible Furan-Maleimide Diels−Alder Adducts, Organic Letters 3(17) (2001) 2681-2683.
[39] A. Gandini, D. Coelho, A.J.D. Silvestre, Reversible click chemistry at the service of macromolecular materials. Part 1: Kinetics of the Diels–Alder reaction applied to furan–maleimide model compounds and linear polymerizations, European Polymer Journal 44(12) (2008) 4029-4036.
[40] C. Judit, F. Hartmut, D.W. Gijsbertus, v.B.R.A.T. M., Stereoisomeric effects in thermo-remendable polymer networks based on Diels–Alder crosslink reactions, Journal of Polymer Science Part A: Polymer Chemistry 48(15) (2010) 3456-3467.
[41] A. Cuvellier, R. Verhelle, J. Brancart, B. Vanderborght, G. Van Assche, H. Rahier, The influence of stereochemistry on the reactivity of the Diels–Alder cycloaddition and the implications for reversible network polymerization, Polymer Chemistry 10(4) (2019) 473-485.
[42] M. Marref, N. Mignard, C. Jegat, M. Taha, M. Belbachir, R. Meghabar, Epoxy-amine based thermoresponsive networks designed by Diels–Alder reactions, Polymer International 62(1) (2013) 87-98.
[43] B.J. Adzima, H.A. Aguirre, C.J. Kloxin, T.F. Scott, C.N. Bowman, Rheological and Chemical Analysis of Reverse Gelation in a Covalently Cross-Linked Diels−Alder Polymer Network, Macromolecules 41(23) (2008) 9112-9117.
[44] C.J. Kloxin, C.N. Bowman, Covalent adaptable networks: smart, reconfigurable and responsive network systems, Chemical Society Reviews 42(17) (2013) 7161-7173.
[45] R.J. Sheridan, C.N. Bowman, A Simple Relationship Relating Linear Viscoelastic Properties and Chemical Structure in a Model Diels–Alder Polymer Network, Macromolecules 45(18) (2012) 7634-7641.

Appendix

Thermoreversible networks by furan/maleimide functionalized PTMC precursors and stickers

The preparation of thermoreversible networks by the mixture of furan and maleimide functionalized PTMCs (PTMC-F and PTMC-M, equimolar mixture of furan and maleimide functions) were also studied. The furan and maleimide grafted polyurethanes (PU-F and PU-M) stickers were designed to change the DA concentrations in the networks. Their syntheses were conducted with one-shot processes (Table 1) with expected structures shown in Scheme 1.

Table 1. Synthesis parameters of PTMC-F, PTMC-M precursors and DA stickers with different functionalities with one-shot process at 80 °C in DMF.

Sample name	Expected functionalities	H_{12}MDI (mol)	Glycerol (mol)	PTMC (mol)	FAL (mol)
PTMC-F5	5	14	3	7	5
PTMC-F4	4	10	2	5	4
PTMC-F3	3	6	1	3	3
PU-F sticker	3	3	1	0	3.05
	Average functionalities	H_{12}MDI (mol)	Glycerol (mol)	PTMC (mol)	p-HMM (mol)
PTMC-M5	5	14	3	7	5
PTMC-M4	4	10	2	5	4
PTMC-M3	3	6	1	3	3
PU-M sticker	3	3	1	0	3.05

However, the structures of PTMC-F/PTMC-M precursors and PU-F/PU-M are not expected by the analysis of ^{1}H NMR. Meanwhile, due to the complexity of ^{1}H NMR spectra, their structures cannot be characterized precisely.

The temperature ramp curves of these networks with different average functionalities are shown in Figure 1. Abnormal phenomena were observed. When the functionality of PTMC networks is increased from 3 to 5, the crossover temperature ($T_{crossover}$) decrease. The possible reason is that the reactivity of hydroxyl groups in furfuryl alcohol are higher than those in glycerol and PTMC oligomers to react with isocyanate functions. As a result, small molecules with

bifunctional furfuryl groups were synthesized, leading to the real functionalities lower than expected ones.

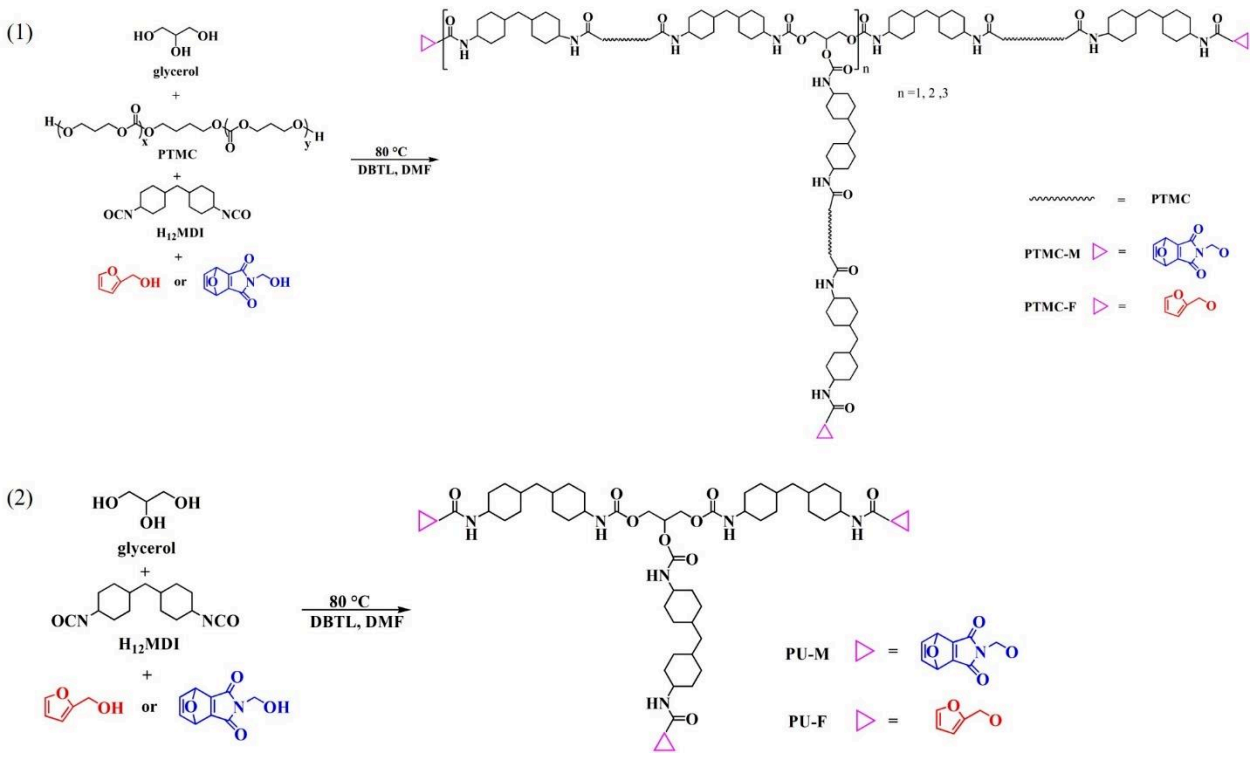

Scheme 1. Synthesis and structures of (1) PTMC-F and PTMC-M precursors; (2) PU-F and PU-M stickers.

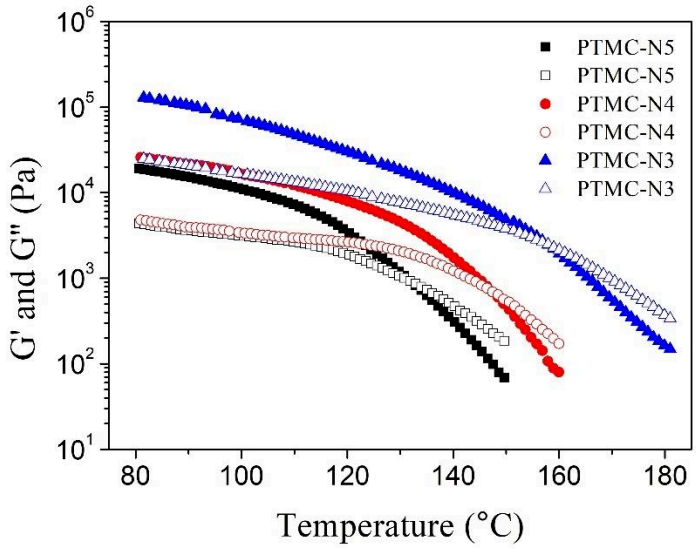

Figure 1. Temperature ramp tests of PTMC networks with different average functionalities (5 °C/min, frequency = 1 rad/s, strain = 1%).

General conclusion

Noncovalent interactions and dynamic covalent bonds are attractive associations which can be used to elaborate new class of materials. Their dynamic properties enable the possibility to obtain reprocessable or recyclable networks with good mechanical properties and creep resistance. With the objective to understand the structure-property relationships of thermoreversible networks, a biodegradable and biocompatible polymer poly(trimethylene carbonate) (PTMC) was selected to elaborate with triuret/tetrauret hydrogen-bonding motifs (HBMs) and Diels-Alder (DA) stickers to prepare networks.

In this aim, chapter 2 was devoted to the synthesis and precise structural control of telechelic PTMC oligomers. PTMC oligomers were successfully synthesized in bulk at 100 °C by ring-opening polymerization with trimethylene carbonate (TMC) as monomer and 1,4-butanediol (BDO) as co-initiator. Due to the low TMC/BDO ratios, not both alcohol functions in BDO are able to initiate the PTMC chains growing. No decarboxylation was observed at 100 °C but exchange reactions between carbonate and alcohol functions are intense, leading to the formation of new PTMC structures. The increase of TMC/BDO feed ratios leads to less exchange reactions. In contrast, with the prolongation of reaction time, more violent exchange reactions occur. As a result, longer chains are formed and mass distributions are also broadened. 1,5,7-triazabicyclo[4.4.0]dec-5-ene (TBD) is a more efficient catalyst than tin(II) bis(2-ethylhexanoate) ($Sn(Oct)_2$) and a total monomer conversion is obtained after 30 min at 100 °C. TBD can also induce closer $\overline{M}_n$ to theoretical values and lower $Đ_M$ than $Sn(Oct)_2$. The PTMC T_g increase with $\overline{M}_n$ and stabilize at -22 °C when $\overline{M}_n$ exceeds 5070 g/mol. Rheological tests proved that no chain entanglements exist when $\overline{M}_n$ is below 5070 g/mol.

Thermoreversible networks were synthesized based on the synthesized PTMC oligomers. Chapter 3 focuses on triuret and tetrauret HBMs functionalized PTMC-based multiarm supramolecular networks. The relationships between their structures (functionality, HBM type and HBM concentration) and thermal properties, dimensional stability, tensile mechanical properties and aerobic biodegradability were studied. Their T_g was found to increase by decreasing PTMC chain length but with minor relation to functionality or HBM type. Tetrauret HBMs endow supramolecular polymers with higher thermal stability than triuret HBMs. Supramolecular polymers are thermoreversible as verified by FT-IR tests at variable temperatures. The K_a of triuret and tetrauret HBMs in supramolecular polymers were

determined to be 0.32 M^{-1} and 1.59 M^{-1} respectively in $CDCl_3$ by ^1H NMR. Compared to the K_a of triuret HBMs (95 M^{-1}) in supramolecular polymers without PTMC, the PTMC chains reduce the triuret HBMs K_a by nearly 300 times. Increasing the functionality or shortening PTMC chain length increases $T_{crossover}$, creep resistance and Young's modulus in tensile tests. The highest $T_{crossover}$ and 100% recovery ratio were only obtained for triuret and tetrauret HBMs with $PTMC_{1000}$, caused by the formation of denser transient physical crosslinks by hydrogen bonds. Abnormally, although tetrauret HBMs has higher K_a than triuret HBMs, the supramolecular polymers bearing tetrauret HBMs has lower $T_{crossover}$, worse creep resistance and lower Young's modulus in tensile tests.

Chapter 4 aims at the study of triuret and tetrauret HBMs dynamics in supramolecular polymers in the melt state and tries to find explanations for abnormal phenomena observed in Chapter 3. WAXS and SAXS proved that all supramolecular polymers are amorphous but with microphase-separation morphologies, induced by hydrogen bonding between urethane groups and triuret/tetrauret HBMs. The d-spacings between microdomains are from 8.0 mm to 12.3 nm, which are independent of HBM type and functionality but decrease with the shortening of PTMC chain length. PTMC chains relax in extremely short time while the hydrogen bonding between urethane groups prolongs the relaxation time of multiarm structures to 2.77 s. Supramolecular polymers with shorter PTMC chain length and lower functionality have longer relaxation time and higher E_a, resulting from the formation of bigger aggregates by triuret and tetrauret HBMs. Due to the existence of intramolecular hydrogen bonds in tetrauret HBMs, the formed aggregates are smaller than those formed by triuret HBMs. As a result, the supramolecular polymers containing tetrauret HBMs have lower relaxation times than their triuret counterparts. These smaller aggregates of tetrauret HBMs may also account for the abnormal phenomena observed in Chapter 3. When the temperature is increased, the weaker urethane hydrogen bonds will be broken firstly but the network structures can still be maintained by stronger HBMs domains. At higher temperature, HBMs domains are dissociated, leading to the terminal flow for multiarm supramolecular networks.

Chapter 5 studied the association dynamics of triuret HBMs in bifunctional linear supramolecular PTMC in bulk. It was found that only dimers were formed by triuret HBMs in the short annealing time. In this case, the supramolecular chains bear linear chain extension just as a traditional polycondensation. The perfect applicability of time-temperature superposition (TTS) principle allows the calculation of K_a of triuret HBMs at different temperatures, ranging from 0.88 M^{-1} at 413 K to 3738.2 M^{-1} at 353 K. The activation energy of supramolecular

polymer linear chain extension was measured to be 166.7 kJ/mol. At equilibrium state after long annealing time, complex aggregates which act as transient physical crosslinkers in the material are formed, leading to the failure of TTS principle. This work presents an original method to calculate K_a and activation energy in solid state by rheology as well.

Chapter 6 synthesized thermoreversible PTMC-based networks by Diels-Alder reactions. The networks were obtained by the mixture of furan-functionalized PTMC and a maleimide crosslinker. Both exo and endo adduct were generated in the networks with the latter being the minority form. Increasing PTMC-F functionality brings about stiffer networks with higher crosslinking density. The recovery ratios of all DA networks are 100% at 80 °C in creep tests, proving the formation of perfect networks. However, these networks could be partially broken and then lose their creep resistance at 130 °C due to the rDA reactions. This decrosslinking reaction occurs between 130 °C and 160 °C, depending on the density of networks.

The intensive studies of triuret and tetrauret HBMs allow a well understanding of their associations and the corresponding dynamics in bulk and validate the potentiality of their usage to design supramolecular systems with specific properties. The thermoreversible PTMC-based networks prepared in this work could have potential applications in the medical field.

Conclusion générale

Les interactions non covalentes et les liaisons covalentes dynamiques sont des modes d'association attrayants qui peuvent être utilisées pour élaborer une nouvelle classe de matériaux. Leurs propriétés dynamiques permettent l'obtention de réseaux thermoréversibles, recyclables avec plusieurs cycles de vie et de mise en œuvre, tout en conservant de bonnes propriétés mécaniques sans fluage possible dans les conditions d'usage.

Dans l'objectif d'établir des relations structure-propriétés, souvent complexes pour ces deux types de réseaux thermosensibles, des structures polyfonctionnelles branchées ont été élaborées à partir de glycérol, d'un diisocyanate et d'un polymère biodégradable et biocompatible, du poly(trimethylene carbonate) (PTMC) et en y associant à différentes fonctionnalités soit des motifs auto-associatifs à liaisons hydrogène multiples de type triuret ou tetrauret (HBM), soit des groupements réactifs à base de cycle furane et de maléimide permettant la réaction de Diels-Alder (DA). Par ces deux approches, des réseaux tridimensionnels ont été créés avec des températures seuil autorisant la réversibilité des associations.

Dans cet objectif, le chapitre 2 a été consacré à la synthèse de structures téléchéliques contrôlées d'oligomères de PTMC. Ces structures ont été obtenues en quelques minutes avec succès en masse à 100 °C par polymérisation de cycles de triméthylène carbonate (TMC) avec du butane-1,4-diol (BDO) comme co-amorceur. En raison des rapports molaires faibles TMC/BDO, les deux fonctions alcool du BDO n'ont pas été forcément capables d'amorcer des croissances de chaînes PTMC. Aucune réaction de décarboxylation n'a été observée à 100 °C mais des réactions d'échange entre fonctions carbonate et alcool se sont avérées intenses, menant à la formation de nouvelles structures de PTMC avec un ou plusieurs radicaux BDO par chaîne, voire aucun. L'augmentation du rapport molaire TMC/BDO réduit les réactions d'échange secondaires. En revanche, des temps longs de réaction dépassant le temps nécessaire à la conversion totale du monomère favorisent ces réactions d'échange. En conséquence, des chaînes de PTMC plus longues ont pu être observées aux temps longs avec des distributions de masse élargies. Parmi les deux catalyseurs/amorceurs utilisés, le [4.4.0] dec-5-ene 1,5,7-triazabicyclo (TBD) s'est avéré plus efficace que le bis (2- éthyle hexanoate) d'étain où des conversions totales en monomère ont pu être obtenues qu'après 30 minutes de réaction à 100 °C. Le TBD s'est montré plus performant pour un meilleur contrôle des masses en relation avec le rapport théorique TMC/BDO accompagné de distributions de masse plus étroites. Les températures de transition vitreuse des PTMC synthétisés se sont montrées dépendantes des

masses molaires moyennes en nombre pour atteindre une valeur limite à -22 °C lorsque M_n atteint 5070 g/mol. Des études rhéologiques ont montré qu'aucun enchevêtrement de chaînes n'était observable en deçà de cette masse molaire moyenne critique. De ce fait, pour la suite de l'étude, tous les réseaux thermoréversibles ont été mis au point à partir des oligomères de PTMC synthétisés avec des masses molaires moyennes en nombre de 1000 et 2000 g/mol, inférieures à la masse critique.

Le chapitre 3 est centré sur la synthèse de réseaux supramoléculaires à partir de structures multi-bras de PTMC fonctionnalisés en bout de chaîne par des motifs de type triuret ou tétrauret (HBM). Les relations entre les structures élaborées, (déterminées par la fonctionnalité en HMB, le type de HBM et la concentration en HBM) et les propriétés thermiques, la stabilité dimensionnelle, les propriétés mécaniques et la biodégradabilité aérobie ont été étudiées. Ainsi, les Tg augmentent avec une diminution de la longueur des chaînes de PTMC, mais sans influence majeure du type de HBM ou de la fonctionnalité. Les tétrauret sont les motifs ayant permis d'avoir la meilleure stabilité thermique des matériaux. La thermoréversibilité a pu être vérifiée par spectroscopie IR-TF à différentes températures. Les constantes d'association K_a des motifs triuret et tétrauret des structures supramoléculaires ont été déterminées à des valeurs de 0.32 M^{-1} et 1.59 M^{-1} dans le $CDCl_3$ par RMN du proton. En comparaison avec la constante K_a des motifs triuret (95 M^{-1}) de polymères supramoléculaires à base d'acrylates précédemment étudiés, les chaînes de PTMC réduisent la constante d'association de presque 300 fois. Augmenter la fonctionnalité, ou raccourcir la longueur des chaînes de PTMC, augmente la température de croisement des modules de perte et de conservation, tout en diminuant le fluage et augmentant le module d'Young lors d'essais de traction. Les points de croisement des modules les plus hauts, accompagnés de taux de recouvrement de 100% des tests de fluage, n'ont été obtenus que pour des structures avec triuret ou tétrauret synthétisées à partir de chaînes de PTMC de masse molaire moyenne en nombre de 1000 g/mol. Cela a pu être expliqué par une densité plus élevée en liaisons d'hydrogène. Anormalement, bien que les HBM de tétrauret aient une K_a plus élevée que les HBM de triuret, les réseaux supramoléculaires portant des HBM de tétrauret ont une plus faible résistance au fluage et un module de Young, obtenu par des essais de traction, inférieur.

Le chapitre 4 a consisté en l'étude des motifs triuret et tétrauret et de leur dynamique dans les réseaux supramoléculaires à l'état fondu pour tenter de comprendre et expliquer les phénomènes anormaux observés dans le Chapitre 3. Les analyses WAXS et SAXS ont prouvé que tous les matériaux synthétisés étaient amorphes mais présentaient des morphologies avec une séparation

microphasée induite par les liaisons hydrogène entre les fonctions uréthane présentes mais aussi par les associations par liaisons hydrogène entre motifs triuret ou tétrauret. Les distances séparant ces microdomaines ont pu être calculées et sont comprises entre 8.0 nm et 12.3 nm indépendamment du type de motif et de la fonctionnalité en motifs des structures. A nouveau, la longueur des chaînes de PTMC s'est avérée être le seul facteur impactant, modifiant la concentration en motif dans les matériaux. Il a pu être montré que les chaînes de PTMC relaxaient en des temps extrêmement courts tandis qu'en présence de liaisons hydrogène dues aux groupes uréthane, ces temps augmentent jusqu'à 2.77 s.

Les structures synthétisées avec des PTMC de masses plus faibles ou de fonctionnalité plus élevées ont les temps de relaxation les plus longs et les énergies d'activation E_a les plus élevées, s'expliquant par la formation d'agrégats composés de motifs triuret ou tétrauret. En raison de l'existence de liaisons hydrogène intramoléculaires entre tétrauret, les agrégats formés sont apparus plus petits que ceux formés en présence de triuret. En conséquence, les réseaux supramoléculaires formés par association de tétrauret, ont des temps de relaxation inférieurs à ceux de leurs homologues triuret. Ces agrégats plus petits de tétrauret peuvent aussi expliquer les phénomènes anormaux observés dans le Chapitre 3. Quand la température est augmentée, les liaisons hydrogènes les plus faibles, liées aux fonctions uréthane présentes, ont été cassées en premier mais les réseaux formés se sont maintenus grâce aux domaines composés d'agrégats de triuret ou tétrauret, plus forts. À de températures plus hautes, ces domaines se dissocient, ce qui provoque l'écoulement du matériau.

Le chapitre 5 a étudié la dynamique d'association des motifs triuret incorporés dans des structures linéaires bifonctionnelles à base d'oligomères de PTMC. Des études rhéologiques en régime isotherme et à différentes températures ont pu montrer que ces motifs triuret étaient capables de s'associer en dimères en des temps très courts. Dans ce cas, les structures formées par associations supramoléculaires s'apparentent à des chaînes linéaires formées selon un modèle de polycondensation traditionnel. Les superpositions parfaites obtenues pour obtenir des courbes maîtresse, par équivalence temps-température, ont permis de remonter aux calculs de constantes d'association K_a des motifs triuret dans les matériaux en masse, de 0.88 M^{-1} à 413 K jusque 3738 M^{-1} à 353 K. L'énergie d'activation d'extension des chaînes linéaires supramoléculaires a été calculée à 166.7 kJ/mol. Lors d'isotherme sur de longues durées, jusque 48 h, des évolutions significatives complexes des matériaux ont montré qu'il devenait impossible d'envisager d'établir des courbes maîtresse correctes. Enfin, ce chapitre a au final permis de présenter une méthode originale de calcul de constante d'association

supramoléculaire K_a et d'énergie d'activation directement dans le matériau par rhéologie à l'état fondu sans utiliser un traditionnel solvant lorsque cette constante est déterminée usuellement par RMN. Cette différence dans les conditions d'analyse a montré que la constante d'association pouvait prendre des valeurs significativement différentes.

Le chapitre 6 a repris la même stratégie de synthèse de réseaux à partir de structures formées d'oligomères de PTMC mais en utilisant un système d'association covalent thermoréversible par la réaction de Diels-Alder. Des structures branchées de PTMC ayant des fonctionnalités différentes en furane ont été synthétisées et les réseaux obtenus par le mélange de ces structures de PTMC greffé et d'un agent réticulant de type bismaléimide. Les formes exo et endo ont été observées lors de la formation des réseaux, l'endo étant la forme minoritaire. L'augmentation de la fonctionnalité en furane a conduit à la formation de structures réticulées de densités plus fortes. Les taux de recouvrement lors de tests de fluage, de tous les réseaux de DA, sont de 100% à 80° C, ce qui prouve la formation de réseaux parfaits. A 130 °C, leur comportement est différent et les taux de recouvrement chutent en raison des réactions de rétro Diels-Alder qui se produisent à cette température. Pour des densités de réseau plus élevée, tous les liens de DA ne sont pas ouverts mais suffisamment pour détruire la structure réticulée. Cette réaction de déréticulation se produit entre 130 et 160 °C, en fonction de la densité des réseaux.

Les études approfondies des comportements des motifs supramoléculaires triuret et tétrauret et de leurs effets pour former des réseaux tridimensionnels, ont permis de mieux comprendre leurs façons de s'associer et leur dynamique globale. Les réseaux thermoréversibles à base de PTMC préparés dans le cadre de ce travail pourraient trouver de possibles applications dans le domaine médical.